University of Reading

# Developing mucoadhesive and mucus-penetrating nanoparticles for drug delivery: Silica and chitosan models

Submitted as partial fulfilment for the degree of Doctor of Philosophy in Pharmaceutics

**School of Pharmacy**

Twana Mohammed M. Ways

**March 2019**

**Acknowledgements**

I would like to thank my supervisors Prof Vitaliy Khutoryanskiy and Dr Wing Man Lau for their continuous help, support, guidance and encouragement during my PhD study. Special thanks to Dr Keng Wooi Ng; always been supportive during this study.

I warmly thank all my colleagues and friends at University of Reading, especially, the members of LG3 lab for their help, patience and support. I really enjoyed been a part of this great group for the academic environment, regular meetings and the group day-out activities.

I would like to express my gratitude to our collaborators Prof Richard Hoogenboom research group at University of Ghent, Belgium; for their contribution to the synthesis of some materials for my project.

I would also like to thank my sponsor HCED-Iraq for funding my PhD project and MHE-Kurdistan Regional Government for their support.

I would like to thank everyone else who helped and supported me over the 4 years of my study.

Thanks to my parents, brothers and sisters, relatives and friends in back home.

Last but definitely not least, thanks to my lovely wife Sazan, my daughter Zhwlya and my son Sina for their spiritual support and patience throughout all these years.

Twana Mohammed M. Ways

March 2019

**Declaration of original authorship**

I confirm that this is my own work and the use of all materials from other sources has been properly and fully acknowledged.

Twana Mohammed M. Ways

March 2019

## Abstract

Mucosal drug delivery is often limited by the presence of several barriers including mucus, the harsh pH and enzymatic activity on the mucosal surfaces. Nanoparticles have shown some potential to overcome these barriers. The aim of this thesis was to investigative how functionalisation of nanoparticles with non-ionic hydrophilic polymers (polyethylene glycol (PEG), polyhydroxyethyl acrylate (PHEA), poly-2-ethyl-2-oxazoline (POZ) and polyvinyl pyrrolidone (PVP)) affects their physicochemical and mucoadhesive properties, diffusion in mucin solution as well as ability to penetrate into mucosal tissues. Silica and chitosan nanoparticles were chosen. Thiolated silica nanoparticles were functionalised with PEG and POZ and therefore three types of silica nanoparticles were obtained; thiolated, PEGylated and POZylated. After the synthesis, the effect of the pH on the size of the silica nanoparticles was studied. No significant change in the size of PEGylated silica nanoparticles over the pH range of 1.5–9 was observed. A significant increase in the size of thiolated and POZylated silica nanoparticles at pH $\leq 2$ was observed. Fluorescently labelled thiolated, PEGylated and POZylated silica nanoparticles were incubated with freshly excised rat intestinal mucosae. Then, the mucosae with the nanoparticles were washed with phosphate buffer solution for several cycles and their fluorescent images were taken. It was found that PEGylated and POZylated silica nanoparticles were less mucoadhesive compared to the thiolated counterpart. This was evident by the lower fluorescence signal of the PEGylated and POZylated silica nanoparticles compared to the thiolated counterpart.

Four chitosan derivatives (PEG-, PHEA-, POZ- and PVP-chitosan) were synthesised, which showed complete solubility over a broad pH range (3-9). Unmodified and modified chitosan nanoparticles were prepared using ionic gelation with sodium tripolyphosphate. Modified chitosan nanoparticles diffused faster in bovine submaxillary mucin solution measured by nanoparticle tracking analysis. The penetration of chitosan nanoparticles was evaluated using fluorescence microscopy and demonstrated that modified chitosan nanoparticles penetrated deeper into sheep nasal mucosa compared to unmodified chitosan nanoparticles.

The possibilities of incorporating psychoactive drugs (haloperidol and phenobarbital) into unmodified and PVP-chitosan nanoparticles were investigated. Haloperidol-unmodified chitosan nanoparticles showed a relatively low loading capacity. However, phenobarbital-unmodified and PVP-chitosan nanoparticles showed a high loading capacity and provided a sustained drug release.

These findings illustrate how the functionalisation of nanoparticles affect their physicochemical properties, which in turn determine their mucoadhesive properties and ability to penetrate mucus. They provide an important contribution to the field of mucosal drug delivery.

## List of publications

M. Ways, T.M., Lau, W.M., Hoogenboom, R., Maji S., Glassner, M., Cegłowski M., Filippov S. K. & Khutoryanskiy, V.V., Developing mucus-penetrating chitosan nanoparticles for nasal drug delivery. To be published in Nanoscale.

M. Ways, T.M., Lau, W.M., Ng, K.W., & Khutoryanskiy, V.V., 2018. Synthesis of thiolated, PEGylated and POZylated silica nanoparticles and evaluation of their retention on rat intestinal mucosa *in vitro*. Eur. J. Pharm. Sci. 122, 230-238.

M. Ways, T.M., Lau, W.M., & Khutoryanskiy, V.V., 2018. Chitosan and its derivatives for application in mucoadhesive drug delivery systems. Polymers 10, 267.

## List of conferences

- 4th London Polymer Group Symposium, King's College London, UK, November 14 2018. PEGylated chitosan nanoparticles for nasal drug delivery- Poster
- APS Nanomedicines for the Delivery of Biologics, University of Reading, UK, July 18 2018. Attendance
- 4th Annual Nanopharmaceutics Symposium, Keele University, UK, June 29 2018. PEGylated chitosan nanoparticles for nasal drug delivery- Poster
- Reading School of Pharmacy Research Day, University of Reading, UK, April 10 2018. Development of nanomaterials for mucosal drug delivery: Silica and chitosan models-Talk
- UKICRS Symposium, University of Strathclyde, UK, May 30-31 2017. Mucoadhesion study of silica nanoparticles in rat model-Talk
- Reading School of Pharmacy PhD Research Day, University of Reading, UK, March 31 2017. Organosilica nanoparticles: Synthesis and *ex vivo* mucoadhesion study in rat model-Talk
- 10th International Conference and Exhibition on Pharmaceutics and Novel Drug Delivery Systems, London, UK, March 13-15 2017. Attendance
- Secrets of Formulations IV, Society of Chemical Industry, London, UK, January 10 2017. Attendance
- 6th Annual Postgraduate Symposium on Nanoscience and Nanotechnology, University of Birmingham, UK, December 13 2016. Development of silica nanoparticles for mucosal delivery-Flash presentation
- Doctoral Research Conference, University of Reading, UK, June 23 2016. Attendance

## Table of contents

## List of figures

## List of tables

## List of abbreviations

| | |
|---|---|
| 6, 6′-DTNA | 6, 6′-Dithionicotinamide |
| 6-MNA | 6-Mercaptonicotinamide |
| BSA | Bovine serum albumin |
| BSM | Bovine submaxillary mucin |
| Chi-C | Chitosan-catechol |
| CLSM | Confocal laser scanning microscopy |
| $C_{max}$ | Maximum concentration |
| CNS | Central nervous system |
| CPP | Cell penetrating peptide |
| CTAB | Cetyltrimethylammonium bromide |
| CTAC | Cetyltrimethylammonium chloride |
| CVM | Cervicovaginal mucus |
| DA | Degree of acetylation |
| DAPI | 4′,6-Diamidino-2-phenylindole dihydrochloride |
| $D_c$ | Diffusion coefficient |
| DLS | Dynamic light scattering |
| DMF | Dimethylformamide |
| DMSO | Dimethyl sulfoxide |
| DS | Degree of substitution |
| DTNB | 5,5′-Dithiobis (2-nitrobenzoic acid) |
| EDAC | 1-Ethyl-3-(3-dimethylaminopropyl)-carbodiimide hydrochloride |
| EDTA | Ethylenediaminetetraacetic acid |
| ELISA | Enzyme-linked immunosorbent assay |

| | |
|---|---|
| FDA | Food and drug administration |
| FITC | Fluorescein isothiocyanate |
| FMA | Fluorescein-*O*-methacrylate |
| FTIR | Fourier-transform infrared spectroscopy |
| GIT | Gastrointestinal tract |
| h | Hour |
| HPLC | High performance liquid chromatography |
| MDDS | Mucosal drug delivery systems |
| min | Minute |
| MPTS | 3-Mercaptopropyltrimethoxysilane |
| NHS | *N*-Hydroxysuccinimide |
| NMR | Nuclear magnetic resonance |
| NPs | Nanoparticles |
| NTA | Nanoparticle tracking analaysis |
| PBS | Phosphate buffer solution |
| PDI | Polydispersity index |
| pDMAEMA | Poly(2-dimethylaminoethyl) methacrylate |
| PEG | Polyethylene glycol |
| PEGDA | Poly(ethylene glycol) diacrylate |
| PEI | Polyethylene imine |
| PGM | Porcine gastric mucin |
| PHEA | Polyhydroxyethyl acrylate |
| pHPMA | *N*-(2-Hydroxypropyl) methacrylamide |
| PHPMA | Poly-*N*-2-hydroxypropyl methacrylamide |

| | |
|---|---|
| PLA | Polylactide |
| PLGA | Polylactide-co-glycolide |
| POZ | Poly-2-ethyl-2-oxazoline |
| PVP | Polyvinyl pyrrolidone |
| TBA | Thiobutylamidine |
| TEA | Triethyl amine |
| TEER | Transepithelial electrical resistance |
| TEM | Transmission electron microscopy |
| TEOS | Tetraethylorthosilicate |
| TFA | Trifluoroacetic acid |
| TGA | Thioglycolic acid |
| TMC | Trimethyl chitosan |
| TMOS | Tetramethoxysilane |
| TPP | Sodium tripolyphosphate |
| TRITC | Tetramethyl-rhodamine isothiocyanate |
| UPS | Undecylenic acid modified thermally hydrocarbonized porous silica |

# Chapter 1: Chitosan and its derivatives for application in mucoadhesive drug delivery systems

This chapter is published as:

M. Ways, T.M., Lau, W.M., & Khutoryanskiy, V.V., 2018. Chitosan and its derivatives for application in mucoadhesive drug delivery systems. Polymers 10, 267.

## Graphical abstract

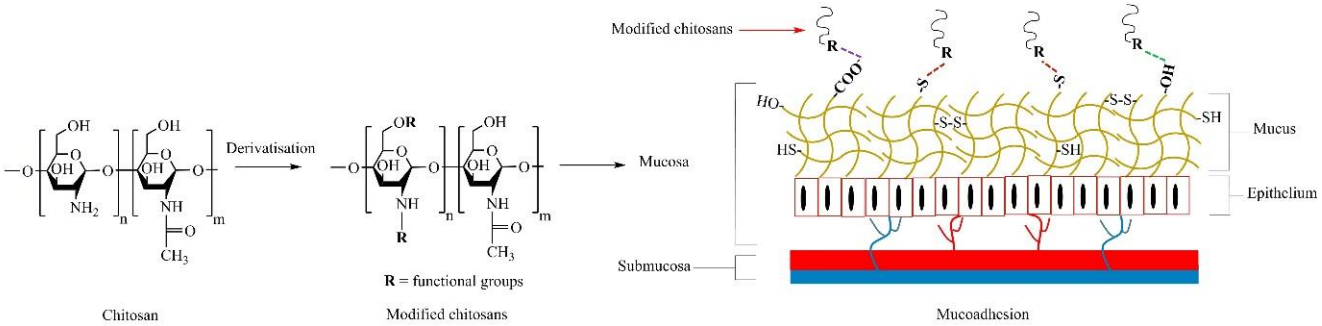



## Abstract

Mucoadhesive drug delivery systems are desirable as they can increase the residence time of drugs at the site of absorption/action, provide sustained drug release and minimize the degradation of drugs in various body sites. Chitosan is a cationic polysaccharide that exhibits mucoadhesive properties and it has been widely used in the design of mucoadhesive dosage forms. However, its limited mucoadhesive strength and limited water-solubility at neutral and basic pH are considered as two major drawbacks of its use. Chemical modification of chitosan has been exploited to tackle these two issues. In this review, we highlight the up-to-date studies involving the synthetic approaches and description of mucoadhesive properties of chitosan and chitosan derivatives. These derivatives include trimethyl chitosan, carboxymethyl chitosan, thiolated chitosan, chitosan-enzyme inhibitors, chitosan-ethylenediaminetetraacetic acid (chitosan-EDTA), half-acetylated chitosan, acrylated chitosan, glycol chitosan, chitosan-catechol, methyl pyrrolidinone-chitosan, cyclodextrin-chitosan and oleoyl-quaternised chitosan. We have particularly focused on the effect of chemical derivatization on the mucoadhesive properties of chitosan. Additionally, other important properties including water-solubility, stability, controlled release, permeation enhancing effect, and *in vivo* performance are also described.

## 1.1 Introduction

Mucus is a viscoelastic gel lining the mucosal tissues exposed to the external environment including gastrointestinal, respiratory, and reproductive tracts and the eyes (Lai et al., 2009a; Khutoryanskiy, 2011). It is mainly composed of water (~ 90-98% w/w), mucins (0.2-5% w/v), salts (~ 0.5-1.0% w/w), proteins (~ 0.5% w/v), cells and cellular debris, DNA, bacteria and lipids (Peppas & Huang, 2004; Bansil & Turner, 2006; Lai et al., 2009a; Lai et al., 2009b; Khutoryanskiy, 2011; Boegh & Nielsen, 2015; Leal et al., 2017). Mucins are the main component of the mucus, which are glycoproteins responsible for its gel-like characteristics. These glycoproteins are made of protein core to which carbohydrate side chains are covalently attached via O-glycosidic linkages (Peppas & Buri, 1985; Serra et al., 2009).

Conventional (non-mucoadhesive) formulations lack the ability to withstand the strong involuntary muscular movement as well as the extensive washing effect by certain body fluids available, e.g., in the gastrointestinal lumen, ocular surface, urinary bladder and other mucosal surfaces. This limitation leads to the loss of a substantial amount of the administered drugs at the site of application/absorption. This may not only result in the overall increased cost of the treatment courses; it can also lead to the failure of therapy as effective drug concentration cannot be reached. This is especially more important in case of drugs such as antibiotics as amount lower than minimum inhibitory concentration probably leads to intractable complications including bacterial resistance. Mucoadhesive drug delivery systems are advantageous as they can adhere to the mucus layer of the mucous membrane. The adhesion of the delivery systems to mucosa (defined as mucoadhesion) increases the residence time of drugs, increases the concentration gradient, and protects the vulnerable small molecular weight drugs as well as peptide-based drugs. The overall effects could lead to controlled drug release, prolongation of therapeutic effects, enhancement in the bioavailability, cost-effective treatment, and improved patient compliance (Serra et al., 2009; Gullberg et al., 2011; Khutoryanskiy, 2011; Lee et al., 2013; Date et al., 2016). However, transmucosal drug delivery systems often have poor residence on mucosal surfaces, which justifies the need for novel mucoadhesive materials.

Various polymers have been used in the formulation of mucoadhesive delivery systems. Among them, chitosan and its derivatives are listed at the top (Bernkop-Schnürch et al., 1997; Bernkop-Schnürch et al., 2004b; Peppas & Huang, 2004; Sogias et al., 2008; Khutoryanskiy, 2011; Kulkarni et al., 2017). Chitosan is a polysaccharide composed of N-

acetyl-D-glucosamine and D-glucosamine and its units linked by 1-4-β-glycosidic bonds (Figure 1.1). It can be prepared by deacetylation of chitin in basic media (Hejazi & Amiji, 2003; Sogias et al., 2010). Chitin is the second most abundant polysaccharide in nature, while cellulose is the most abundant (Hejazi & Amiji, 2003). Crustaceans produce chitin in their shells and plants produce cellulose in their cell walls. Therefore, these two polysaccharides impart structural integrity and protection to animals and plants (Pillai et al., 2009).

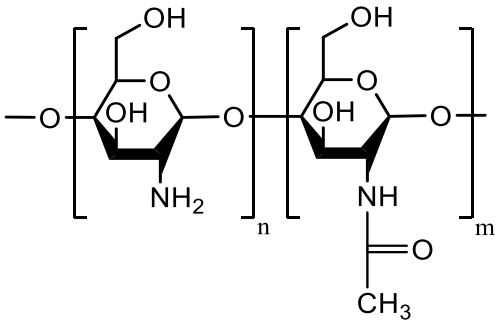


Figure 1.1 Chemical structure of chitosan.

Chitosan has –OH and $–NH_2$ groups leading to the capability of forming hydrogen and covalent bonding. This characteristic results in the possibilities of various chitosan chemical derivatization. These functional groups also play an essential role in the solubility character of chitosan macromolecules. At low pH, the amino groups undergo protonation, which makes chitosan macromolecules positively charged. This cationic nature provides strong electrostatic interaction with negatively charged components of mucus including sialic acid as well as epithelial surfaces (Smart et al., 1984; Peppas & Buri, 1985; Robinson et al., 1987; Robinson & Mlynek, 1995; Sogias et al., 2008; Khutoryanskiy, 2011; Casettari et al., 2012). Hydrogen bonding and hydrophobic interaction also play important role in the mucoadhesion of chitosan (Sogias et al., 2008).

The derivatization of chitosan to improve its mucoadhesive properties has been considered in several publications (Figure 1.2). Some chitosan and its derivatives have shown potential in preclinical and clinical investigations for applications in transmucosal drug delivery (e.g., ChiSys® as a platform for nasal vaccination (Watts et al., 2014) and Lacrimera® eye drops (Bonengel & Bernkop-Schnürch, 2014)). However, there is still lack of review articles analyzing recent studies on the mucoadhesive applications of chitosan derivatives. In this review, we report various chitosan derivatives with potential applications as mucoadhesive

materials. This review, however, does not consider any physical mixtures of chitosan or salt forms, which are discussed in several previous publications (Ganguly & Dash, 2004; Bonferoni et al., 2009).

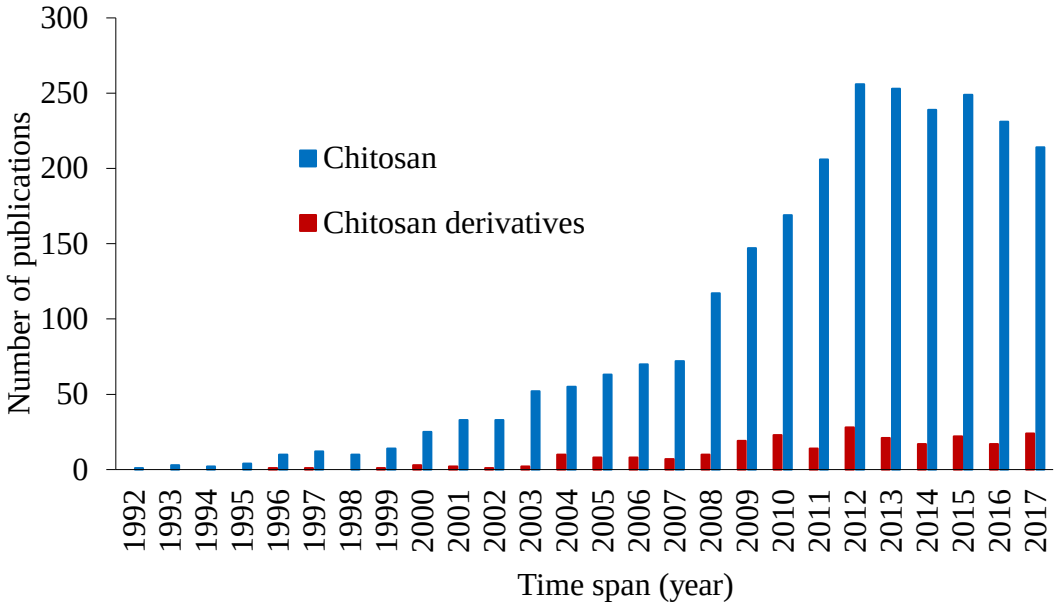


Figure 1.2 Number of publications related to mucoadhesive properties of chitosan and chitosan derivatives, source: SciFinder, keywords: chitosan or chitosan derivatives and mucoadhesion, retrieved on 24 November 2017.

## 1.2 Chitosan as a mucoadhesive material

Chitosan has been widely used in various biomedical and drug delivery areas because of its low toxicity, biocompatibility, antimicrobial activity, mucoadhesive properties and permeation enhancing effects (Illum et al., 1994; Illum et al., 2001; Hejazi & Amiji, 2003; Rabea et al., 2003; Agnihotri et al., 2004; Peppas & Huang, 2004; Issa et al., 2005; Sogias et al., 2008). It has been extensively studied as a potential excipient for the oral delivery of peptides (Bernkop-Schnürch et al., 2000). Alonso and co-workers found that chitosan nanocapsules enhanced and prolonged intestinal absorption of salmon calcitonin because of their mucoadhesive properties and strong interactions with the intestinal barrier (Prego et al., 2006).

Our group has demonstrated the mucoadhesive character of chitosan in several studies. We have used a range of techniques including mucin-particle interaction (Sogias et al., 2008), tensile strength (Sogias et al., 2012) and most recently flow-through technique coupled with fluorescence microscopy (Irmukhametova et al., 2011; Mun et al., 2016). In the latest case,

fluorescein isothiocyanate-chitosan (FITC-chitosan) was used as a positive control and compared to other materials as well as FITC-dextran (non-mucoadhesive or negative control). Fluorescent samples were deposited onto *ex vivo* mucosal tissues (e.g., porcine urinary bladder or bovine eyes) and washed with bio-relevant fluids. Fluorescence images were taken after several wash cycles and the fluorescence intensity was used to compare the retention of each material on the mucosal tissues. We observed excellent mucoadhesive properties of chitosan in all cases, although some differences in the extent of its mucoadhesive potential in different mucosal tissues were noticed (Mun et al., 2016; Tonglairoum et al., 2016; Kaldybekov et al., 2018). Figure 1.3 shows the result of mucoadhesion study of different silica nanoparticles in porcine urinary bladder *ex vivo*. The fluorescence signal of chitosan after washing was more intense compared to other materials and this indicated its excellent mucoadhesive properties. The rank of retention of materials was as follows: FITC-chitosan > thiolated silica nanoparticles > PEGylated (polyethylene glycol, 750 Da) silica nanoparticles > PEGylated (5000 Da) silica nanoparticles > FITC-dextran (Mun et al., 2016).

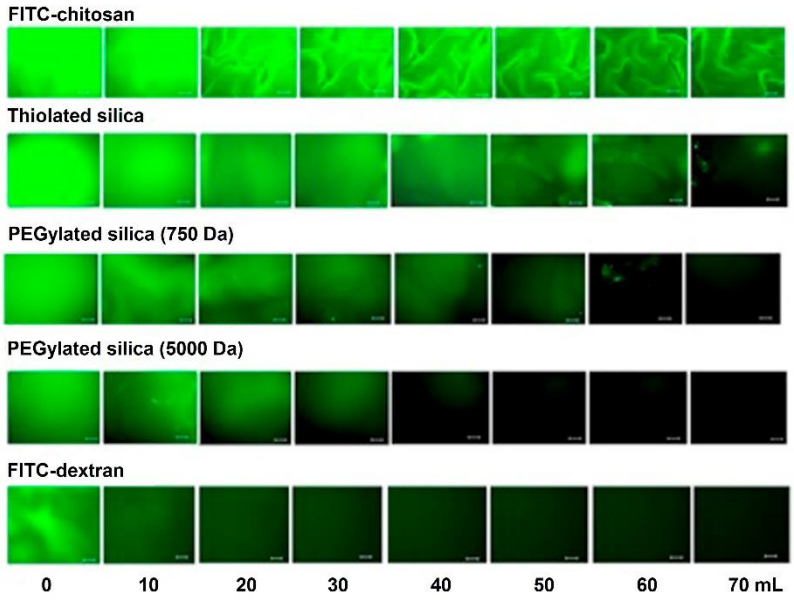


Figure 1.3 Representative microscopic fluorescence images of *ex vivo* porcine urinary bladder mucosa incubated with FITC-chitosan, thiolated silica, PEGylated silica (750 Da), PEGylated silica (5000 Da) and FITC-dextran and washed with different volumes of artificial urine solution. Scale bars are 200 µm. (Mun et al., 2016).

Behrens et al. (2002) studied interactions of polystyrene, chitosan and polylactide (PLA)-PEG nanoparticles with two types of human intestinal cell lines, the enterocyte-like Caco-2

and mucus-secreting MTX-E12 cells. They revealed that the nanoparticles associated with Caco2 cells in the following order: polystyrene > chitosan > PEG-PLA. On the other hand, chitosan nanoparticles strongly bound to the mucus secreting cells and the binding of polystyrene nanoparticles was significantly decreased. PEG-PLA did not show any association with the mucus secreting cells. Intraduodenal administration of chitosan nanoparticles demonstrated that they could be internalized in both epithelial cells and Peyer's patches. The mechanism of the transport of chitosan and polystyrene nanoparticles was studied using Caco2 cells. It was found that chitosan nanoparticles were internalized by adsorptive endocytosis, whereas non-adsorptive endocytosis could be involved with polystyrene nanoparticles. Decreasing the temperature of incubation (4 °C) significantly decreased the transport of both types of nanoparticles. Addition of 1 mM protamine sulfate (inhibitor of active transport process) and pre-treatment of the cells with 10 U/mL heparinase II or 35 mM sodium chlorate (led to de-sulfation and the removal of anionic sites of mucus and cell membranes) significantly reduced the cellular transport of chitosan nanoparticles. However, the transport of polystyrene nanoparticles did not change with these factors. Chitosan endocytosis was saturable, i.e., cellular association increased linearly with concentration (31.25–1000 µg/mL) and reached a steady state at some point. Other studies have also reported the cellular uptake enhancing effect of chitosan, which could occur by adsorptive endocytosis, where a positively-charged coated nanoparticles adhere strongly to the negatively charged components of the cell membranes (Kim et al., 2008).

Thongborisute et al. (2006) investigated the mucoadhesion and muco-penetration of chitosan solution, liposomes and chitosan-coated liposomes in rat small intestine in *ex vivo* and *in vivo* models. The systems were fluorescently labelled with FITC and administered orally to male Wistar rats or in the *ex vivo* model rats were sacrificed and the samples were incubated to interact with the mucosal tissues for 1 h at 37 °C. To visualize the penetration of these materials, cross-sections of 3 different regions of the small intestine (duodenum, jejunum, and ileum) were obtained and examined with confocal laser scanning microscopy (CLSM). They showed that chitosan, non-coated liposomes, and chitosan-coated liposomes could adhere and penetrate the mucosal tissues. However, the extent of adhesion and penetration of chitosan-coated liposomes was greater than for non-coated liposomes. The authors related this behaviour to firstly, the mucoadhesive properties of chitosan. Secondly, the presence of chitosan on the surface of liposomes could result in the formation of large aggregates due to the interactions of chitosan macromolecules leading to the large network of chitosan-coated

liposomes adhering to the mucus layer. This phenomenon is not observed in the case of non-coated liposomes and only individual particles disperse in the suspension. Interestingly, although the authors did not discriminate the mucoadhesion and the mucosal penetration, they observed more mucosal penetration in the ileum region compared to both duodenum and jejunum, which they believe was due to the thicker nature of the ileum, which is also supported by other studies (Atuma et al., 2001; Varum et al., 2010, 2012). Deacona et al. (1999) also revealed the difference in the mucoadhesive interactions of chitosan in different regions of porcine stomach by sedimentation velocity technique using analytical ultracentrifuge equipped with conventional Philpott-Svensson Schlieren optical systems and coupled on-line to a charge-coupled device (CCD) camera. The cardiac region displayed the strongest interaction with chitosan compared to corpus and antrum.

### 1.3 Problems of chitosan in mucosal drug delivery

Being a basic polymer, chitosan is mucoadhesive only at limited pH and is only soluble at acidic pH (pH < 6) (Caramella et al., 2010; Sogias et al., 2010). The requirement of decreasing the pH of chitosan vehicles limits its applications in drug and gene delivery as many biomolecules including DNA, proteins and peptide-based drugs are not stable at low pH (Jeong et al., 2008). Additionally, even acidic chitosan formulations will encounter neutral to basic pH once they administered into the human body either topically or systemically. High pH environment results in the precipitation of chitosan and can affect the performance of the carrier systems (Sogias et al., 2010).

Chitosan-based mucosal drug delivery systems have been investigated to increase the residence time of drugs on the application/absorption sites (Illum et al., 1994; Bernkop-Schnürch et al., 2000; Sogias et al., 2012). The increase in the residence time is advantageous as it may prolong the action of drugs and provides sustained drug release. However, with unmodified chitosan, this is only possible to a certain degree. Therefore, there is an obvious need for further controlled drug release with subsequent prolongation of drug action (Bernkop-Schnürch, 2000).

Several modifications of chitosan have been investigated to enhance its mucoadhesive properties. In the next sections, we will discuss various chitosan derivatives with potential applications in transmucosal drug delivery.

## 1.4 Mucoadhesive chitosan derivatives

### 1.4.1 Trimethyl chitosan (TMC)

TMC is a chitosan derivative which is always positively charged. This persistent cationic nature makes it one of the strongest mucoadhesive polymers. It has a much wider pH solubility range than unmodified chitosan due the presence of protonated groups (–$N^+(CH_3)_3$) (Kulkarni et al., 2017). TMC can be synthesized by three general methods: indirect trimethylation (Muzzarelli & Tanfani, 1985; Verheul et al., 2008), direct trimethylation (Sieval et al., 1998; de Britto & Assis, 2007) and protection of chitosan hydroxyl groups (at C-3 and C-6 positions) by O-silylation (Benediktsdóttir et al., 2011). The first method is usually a two-step process including the formation of an intermediate product (N,N-dimethyl chitosan) and can be conducted using two different reaction conditions. Whereas, the second method is a one-step process and does not contain any intermediate product, but it can also be conducted using two different reaction conditions. Using either indirect or direct trimethylation can often result in the formation of O-methylated TMC. However, using hydroxyl protection method by O-silylation, e.g., by employing tert-butyldimethylsilyl chloride, O-methylation can be avoided (Muzzarelli & Tanfani, 1985; Sieval et al., 1998; de Britto & Assis, 2007; Verheul et al., 2008; Benediktsdóttir et al., 2011; Wu et al., 2016; Kulkarni et al., 2017). Verheul et al. (2008) also claimed that their synthetic approach can result in O-methyl free TMC. The synthetic pathway for each method is illustrated in Figure 1.4, Figure 1.5 and Figure 1.6. For the details of the experimental methods of TMC synthesis, readers are referred to two recent reviews by Wu et al. (2016) and Kulkarni et al. (2017).

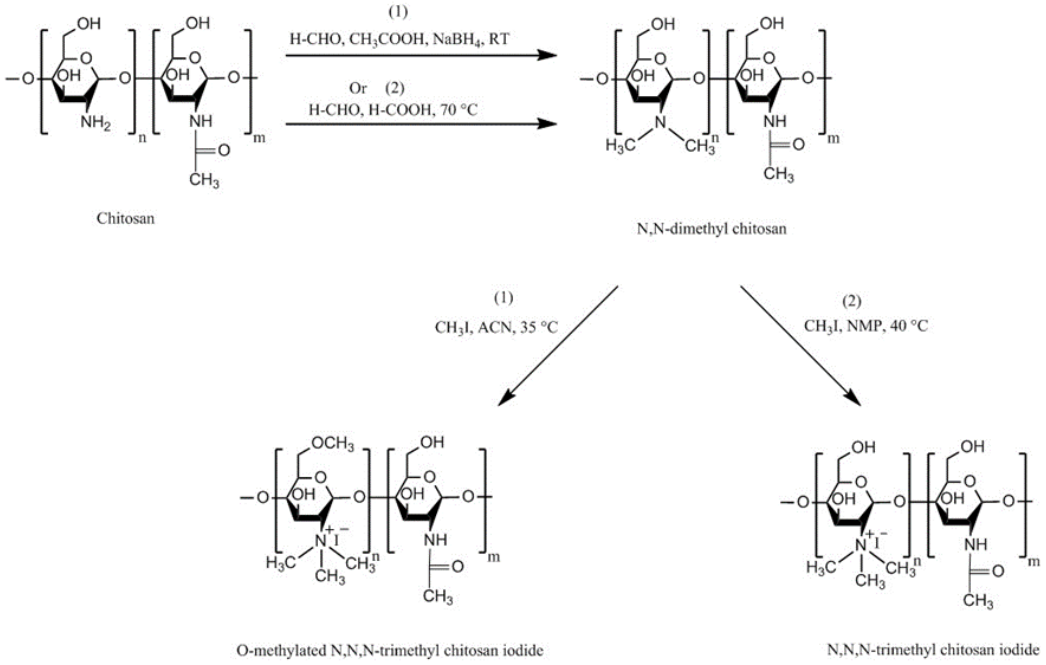


Figure 1.4 Synthetic pathway for preparation of TMC using indirect trimethylation approach according to (1) Muzzarelli and Tanfani (1985), ACN = acetonitrile and (2) Verheul et al. (2008) avoiding O-methylation, NMP = N-methyl-2-pyrrolidinone.

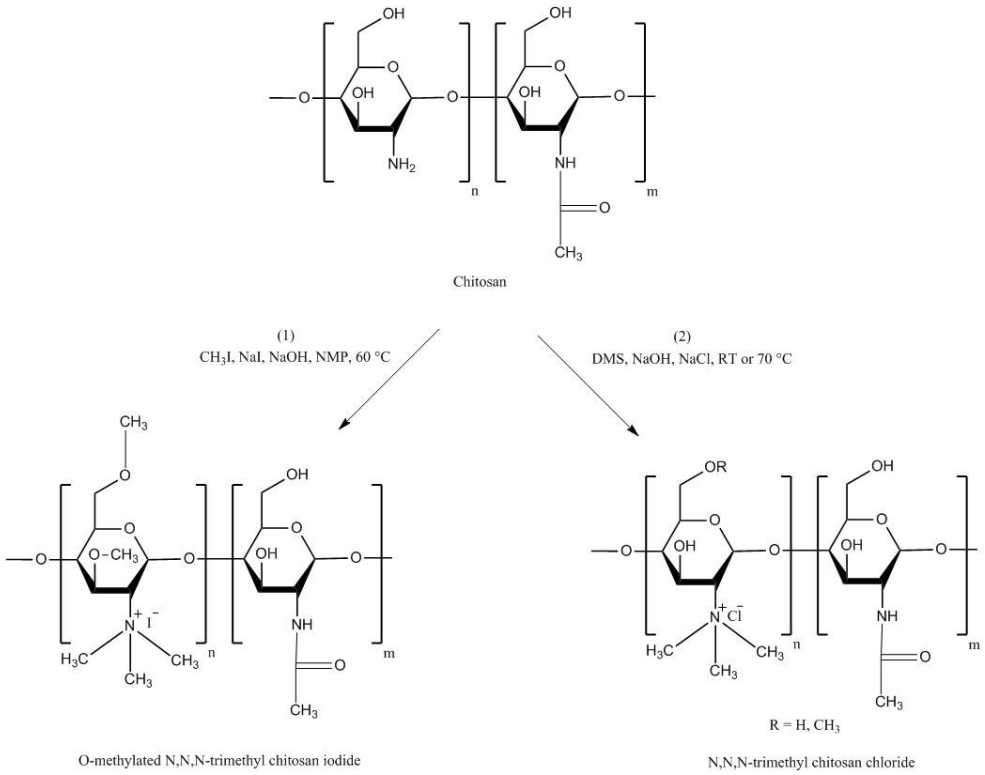


Figure 1.5 Synthetic pathway for preparation of TMC using direct trimethylation approach according to (1) Sieval et al. (1998), NMP = N-methyl-2-pyrrolidinone and (2) de Britto and Assis (2007), DMS = dimethyl sulfate.

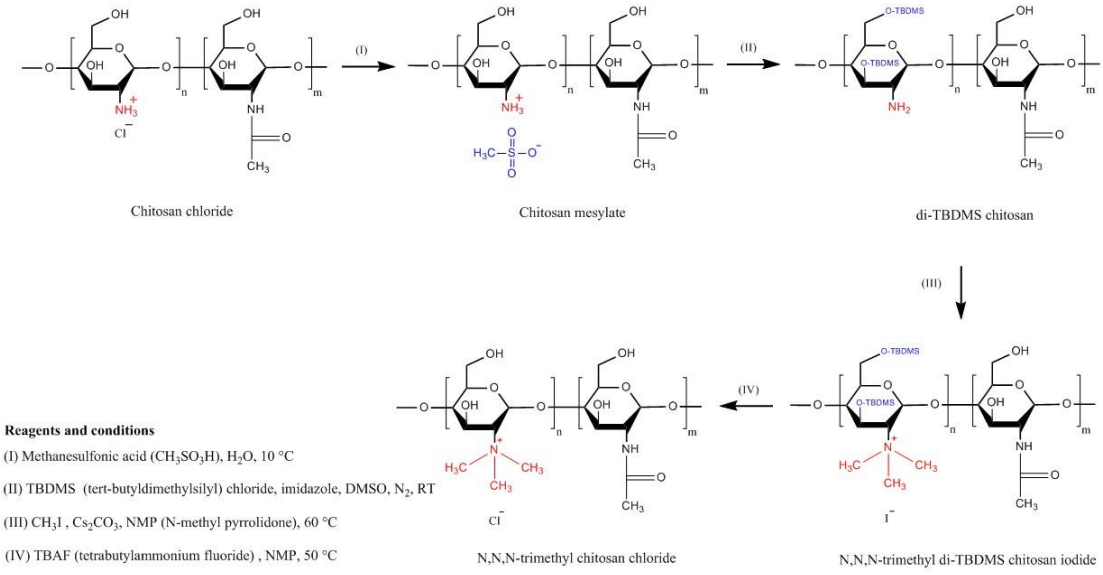


Figure 1.6 Synthetic pathway for preparation of TMC using hydroxyl groups protection approach by O-silylation according to Benediktsdóttir et al. (2011).

TMC has been synthesized so as to enhance the water-solubility of chitosan with wider applications in drug delivery (Dung et al., 1994). Subsequently, Sieval et al. (1998) studied

the effect of a few variables including the number of reaction steps, the duration of each reaction step and the amount of methyl iodide as a reagent. It was found that 2-step reaction resulted in products with high degree of substitution (40–80%). However, 3-step reaction led to even greater degree of substitution but at the same time water-solubility of the resulting product decreased.

Jintapattanakit et al. (2009) synthesized TMC by reductive methylation of chitosan. TMC was then PEGylated. Both polymers were then fluorescently labelled using tetramethyl-rhodamine isothiocyanate (TRITC) and Oregon Green carboxylic acid succinimidyl ester (Oregon Green 448). The insulin-loaded nanoparticles were synthesized using self-assembly technique. The influence of TMC PEGylation and its positive charge density on mucoadhesive properties were assessed using a mucin assay and mucus-secreting HT29-MTX-E12 (E12) monolayers. It was found that introduction of PEG improved the mucoadhesive effect of TMC. This could be due to the interpenetration of PEG with mucus. In some other studies, PEGylation of chitosan also shown reduced toxicity and significantly increased the cellular permeation of hydrophilic macromolecules including FITC-dextran (Casettari et al., 2010; Casettari et al., 2012).

Hauptstein et al. (2014) also studied the effect of PEGylation as well as thiolation (will be discussed in the next section) on adhesion of chitosan's compressed discs to porcine intestinal mucosa. They synthesized PEG-bearing thiolated chitosan by conjugating thiol-bearing polyoxyethylene ligand [O-(3-carboxylpropyl)-O′-[2- [3-mercaptopropionylamino)ethyl]-polyethyleneglycol] to amino groups of chitosan. The reaction was mediated by 1-ethyl-3-(3-dimethylaminopropyl)-carbodiimide hydrochloride (EDAC)/N-hydroxysuccinimide (NHS). In addition to its solubility in basic media, PEG-bearing thiolated chitosan showed greater mucoadhesive strength compared to unmodified chitosan. However, it was equally mucoadhesive as thiolated chitosan. Moreover, PEG-bearing thiolated chitosan enhanced the permeation of FITC-dextran through rat intestinal mucosa and Caco2 cells monolayer. The enhancement in mucoadhesion is based on the formation of disulfide bridges with mucus glycoproteins. The permeation enhancing effect could be due to the interaction of thiol groups of the thiolated chitosans with protein tyrosine phosphatase enzyme, which modulates the tight junction by a glutathione-dependent process.

Sayın et al. (2009) demonstrated a novel approach for formation of nanoparticles via complexation between cationic TMC and polyampholytic N-carboxymethylchitosan without a crosslinker. The nanoparticles were loaded with FITC-BSA (bovine serum albumin) and their cellular uptake was studied. A significant number of the nanoparticles was taken up by murine macrophage J774A.1 within 30 min of incubation. The authors believed that the mucoadhesive effect of TMC plays a major role in the enhancement of the cellular uptake. The nasal administration of tetanium toxiod-loaded 283 nm nanoparticles in mice, induced the mucosal and systemic immune responses.

Sajomsang et al. (2009) synthesized two methylated N-aryl chitosan derivatives, methylated N-(4-N,N-dimethylaminocinnamyl) chitosan chloride and methylated N-(4-pyridylmethyl) chitosan chloride by reductive amination and methylation of chitosan. It was found that increasing the degree of quaternization led to a stronger mucin-particle interaction. Moreover, the cytotoxicity was dependent on the polymer structure, the location of the positive charge and the molecular weight after methylation.

On the other hand, some studies showed that TMC has greater potential to adhere to the epithelial tissue than to the mucin. For instance, Keely et al. (2005) evaluated the adhesion of coumarin-labelled-poly(2-dimethylaminoethyl) methacrylate (pDMAEMA) with different levels of quaternization (0, 10, 24 and 32%) and TMC to human mucus-secreting and non-mucus-secreting intestinal cell monolayers (E12 and HT29, respectively) as well as freshly excised rat intestinal mucosa using non-everted intestinal sacs model. CLSM, light and fluorescence microscopy were used to quantify either mucoadhesion (adhesion to the mucus layer) or bioadhesion (adhesion to the epithelial tissue rather than mucosal surface). It was found that pDMAEMA, regardless of the degree of quaternization, was more mucoadhesive than bioadhesive, whereas TMC was found to be more bioadhesive and as mucoadhesive as unquaternized pDMAEMA and 24% quaternized pDMAEMA. When E12 cells and intestinal sacs were treated with mucolytic agent, N-acetylcysteine, for 15 min, the mucoadhesion of pDMAEMA polymers was significantly decreased, while the bioadhesion of TMC had not changed following this treatment. Additionally, the permeability of FITC-dextran through both E12 cells monolayer and intestinal sacs was significantly decreased in the presence of pDMAEMA, whereas the use of TMC led to a significant increase in the permeability. Although they did not study the interactions between the polymers and the mucus, the authors claimed that pDMAEMA perhaps increased the viscosity of the mucus gel as in case of carbopol (Foster et al., 1994) and thus impede the diffusion of FITC-dextran.

However, chitosan and its derivatives can open the tight junctions (Jonker et al., 2002; Hamman et al., 2003; Smith et al., 2004) that could enhance the paracellular diffusion of FITC-dextran.

Liu et al. (2016) developed core-shell nanoparticles based on TMC. The nanoparticles were coated with dissociable layer of N-(2-hydroxypropyl) methacrylamide copolymer (pHPMA). The diffusion of coated and uncoated nanoparticles in human cervicovaginal mucus was evaluated using multiple particle tracking technique and Ussing chamber. Cellular internalization and transport were evaluated using E12 cells. It was found that pHPMA coating could enhance the diffusion of TMC nanoparticles through both mucus and epithelial layer. Non-coated TMC nanoparticles were found to be less diffusive in both mucus and the cells. Liu et al. (2016) indirectly demonstrated the mucoadhesive properties of TMC.

Generally, mucoadhesive properties of chitosan could be affected by both the degree of quaternization and its molecular weight. Nazar et al. (2011) prepared TMC thermosensitive nasal gel from low, medium, and high molecular weight chitosan with quaternization of 25.6 to 61.3%. It was found that gels made from lower quaternization and medium molecular weight TMC had the greatest work of adhesion (252 ± 14 μJ) and the shortest sol-gel transition time (7 min) at 32.5 °C. This could be due to their great capacity to hydrate and absorb large amounts of water. Partially quaternized TMC has the advantage of having a better water solubility profile in neutral and basic environment than the native chitosan (van der Merwe et al., 2004). This is important since absorption of most drugs happens at slightly basic or neutral part of the gastrointestinal tract (DeSesso & Jacobson, 2001).

TMC has been used as an absorption enhancer for the delivery of buserelin and insulin across Caco-2 cells monolayers. Although at low concentrations TMC is a less active absorption enhancer than both chitosan hydrochloride and chitosan glutamate, increasing its concentration could increase its activity. Since it is more soluble than both chitosan salts, increasing TMC concentration is very unlikely to cause precipitation, however, it resulted in an increase in the transport rate of both buserelin and insulin across Caco-2 cell monolayers, which might be due to the decrease in transepithelial electrical resistance (TEER) (Kotzé et al., 1997). TEER is a parameter, which determines the intercellular ion flux and indicates the tightness of paracellular “junctional complexes” of biological membranes (Deli, 2009).

### 1.4.2 Carboxymethyl chitosans

Carboxymethyl chitosan is another derivative of chitosan with amphoteric properties, acting as both acid and base depending on the pH of its solution. The amphoteric properties originate from the presence of both amino (basic) and carboxylic (acidic) groups in its chemical structure (Jayakumar et al., 2010; Upadhyaya et al., 2014; Thanou et al., 2001). The amino groups undergo protonation in acidic media and make carboxymethyl chitosan positively charged. On the other hand, in basic media carboxylic groups dissociate and impart carboxymethyl chitosan negative charged.

Chen and Park (2003) studied the pH-solubility profile of various O-carboxymethyl chitosans synthesized at different reaction conditions (temperature and ratio of water/isopropanol). The resultant chitosans showed a pH-dependent water-solubility character. Based on the degree of substitution, carboxymethyl chitosans (0.2 mg/mL) were insoluble at pH ranges close to neutral. However, at highly acidic and basic pHs, they demonstrated complete water-solubility. It was found that using low temperature (0 and 10 °C, during the synthesis) resulted in completely water-soluble products but with low yield. Increasing the temperature and decreasing the water/isopropanol ratio resulted in more carboxymethylation, which subsequently shifted the region of insolubility towards the lower pH (~3). Vikhoreva and Gal'braikh (1997) also reported that carboxymethyl chitosan was insoluble at pH range of 3.5–6.5, whereas it showed complete solubility at pH < 3.5 and > 6.5. The insolubility at those pH ranges could be due to the fact that the isoelectric point of carboxymethyl chitosan is 4.1 and therefore when the pH of the solution is near the isoelectric point, precipitation and aggregation could happen (Thanou et al., 2001).

Generally, carboxymethyl chitosans can be prepared using two different approaches, which are reductive alkylation and direct alkylation. In case of reductive alkylation, the amino groups of chitosan react with aldehyde groups of glyoxylic acid to form an intermediate imine product, which then is hydrogenated using sodium borohydride or sodium cyanoborohydride. The ratio of glyoxylic acid to chitosan is important in determining whether mono- or di-carboxymethyl chitosan is formed. Direct alkylation can be performed by reacting chitosan with some alkyl halides, such as monochloroacetic acid, in the presence of inorganic bases including sodium bicarbonate and sodium carbonate to raise the pH to 8.0–8.5. The pH of the reaction mixture is considered to be one of the important factors in determining whether O-, N- or O, N-substitution takes place (An et al., 2008; An et al., 2009; Upadhyaya et al., 2013, 2014). Also, the higher pH resulted in a greater degree of substitution

(Ge & Luo, 2005). Figure 1.7 shows the pathways for the synthesis of carboxymethyl chitosans.

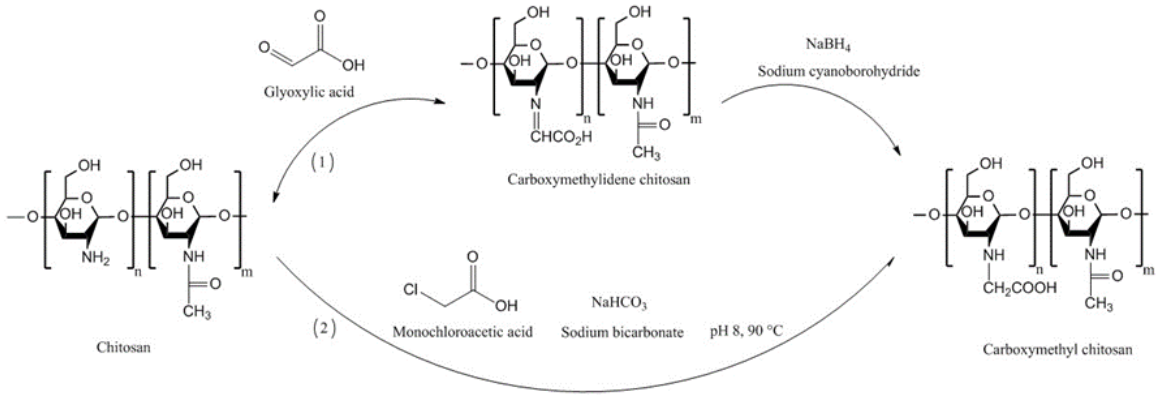


Figure 1.7 Schematic representation of the synthesis of carboxymethyl chitosans using reductive (1) (Thanou et al., 2001) and direct (2) alkylation (An et al., 2009) methods.

Di Colo et al. (2004) studied the effect of chitosan and N-carboxymethyl chitosan on the ocular pharmacokinetics of ofloxacin in rabbits. Chitosan enhanced the penetration of the drug through the ocular tissue and its maximum concentration ($C_{max}$) in the aqueous humor was greater than in the case when conventional eye drops (Exocin® eye drops) and reference formulation (polyvinyl alcohol-based ofloxacin solution) were used. This may be due to the tight junction opening effect of chitosan. N-carboxymethyl chitosan did not significantly enhance the $C_{max}$ of the drug in the aqueous humor. However, it resulted in a steady state drug concentration from 30–150 min post-ocular administration. The authors measured the viscosity of the three formulations and found that they were approximately similar. However, they still claimed that the viscosity enhancement is one of the reasons for the enhancement of pre-ocular drug residence time compared to the reference formulation. The binding of ofloxacin to N-carboxymethyl chitosan due to hydrogen bonding between amino groups of the drug and hydroxyl groups of the polymer, is also a reason for both the decrease in the ocular drug penetration and the increase in the residence time (Di Colo et al., 2004). Although they did not evaluate the mucoadhesive properties of these polymers, they hypothesized that it could have an impact on the increased residence time in the ocular tissues. Clearly, the residence time of a formulation on the ocular tissues will be related to their mucoadhesive properties.

N-carboxymethyl chitosan has also been used as an intestinal absorption enhancer and proved to increase the *in vitro* and *in vivo* transmucosal absorption of low molecular weight heparin (Thanou et al., 2001). It has also showed potential in the oral delivery of small molecules. Prabaharan and Gong (2008) synthesized thiolated carboxymethyl chitosan-g-β-cyclodextrin and showed its potential for the oral delivery of lipophilic drug ketoprofen. The modified chitosan resulted in 5-fold improvement in the adhesion to mouse intestinal mucosa and slower drug release.

### 1.4.3 Thiolated chitosans

Thiolation is one of the techniques used to functionalize various polymers including chitosan using thiolating agents bearing thiol groups. These include cysteine (Bernkop-Schnürch et al., 1999a), thioglycolic acid (TGA) (Kast et al., 2003), 2-iminothiolane or 4-thiobutylamidine (TBA) (Bernkop-Schnürch et al., 2003), N-acetyl cysteine (Schmitz et al., 2008), isopropyl-S-acetylthioacetimidate (Kafedjiiski et al., 2005b) and glutathione (Kafedjiiski et al., 2005a). This technique has been pioneered by Bernkop-Schnürch and co-workers (Bernkop-Schnürch et al., 1999b) to enhance the mucoadhesion of polymers for pharmaceutical and biomedical applications. Thiolated chitosans are now one of the extensively studied mucoadhesive materials. In addition to their superior mucoadhesive properties, they also have some permeation enhancing effects, ability to inhibit efflux pumps and in situ gelling properties (Bonengel & Bernkop-Schnürch, 2014). Figure 1.8 shows the synthetic pathways to different thiolated chitosans.

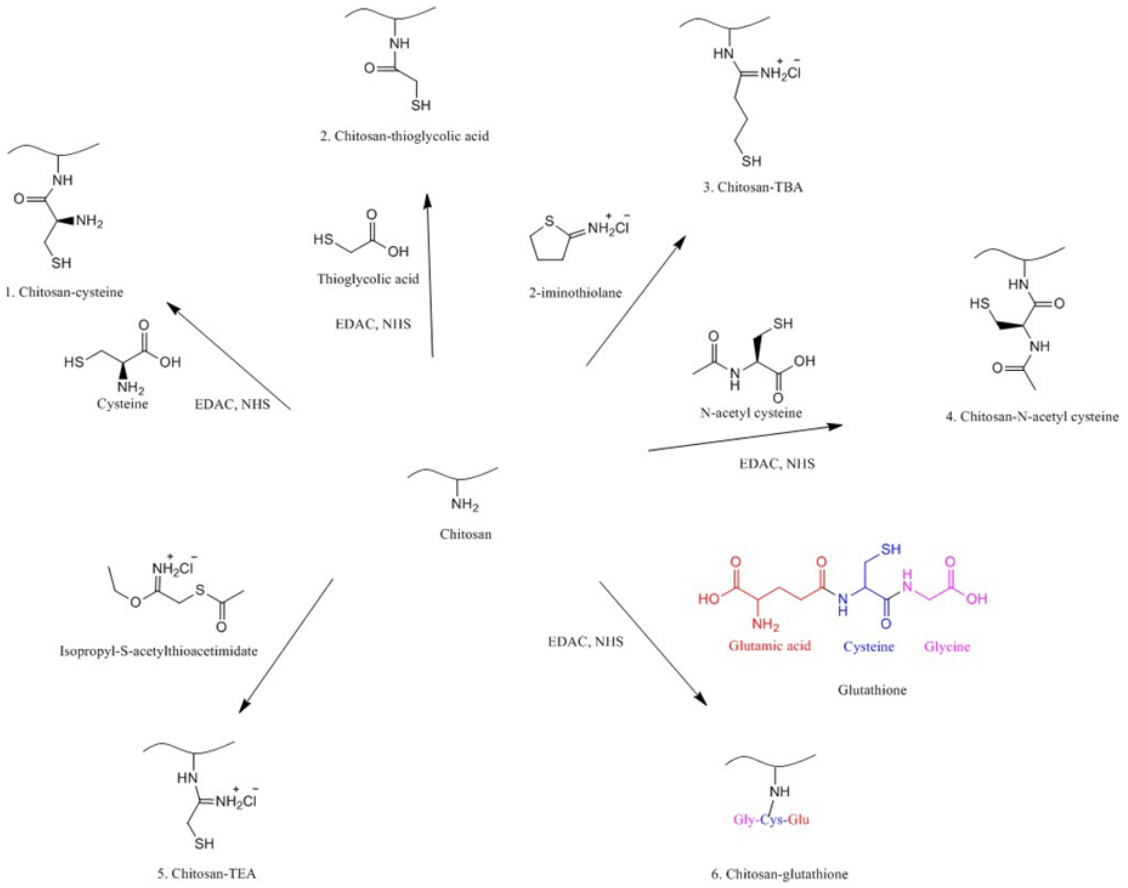


Figure 1.8 Synthetic pathways to different thiolated chitosan derivatives (Bernkop-Schnürch et al., 1999a; Bernkop-Schnürch et al., 2003; Kast et al., 2003; Bernkop-Schnürch et al., 2004b; Kafedjiiski et al., 2005a; Kafedjiiski et al., 2005b; Schmitz et al., 2008; Li et al., 2013).

### 1.4.3.1 Chitosan-cysteine

In 1999, Bernkop-Schnürch et al. (1999a) synthesized chitosan-cysteine conjugate by covalent attachment of cysteine to chitosan mediated by carbodiimide, where the amount of bound-cysteine was increased with an increase in the amount of the mediator reaching 1.2%. Subsequent mucoadhesion study revealed no significant difference between chitosan and thiolated chitosan. However, thiolated chitosan tablets showed superior cohesion over the chitosan tablets which could be due to the formation of intra/intermolecular disulfide bonds as a result of the oxidation of the thiol groups in thiolated chitosan. This improved cohesion is desirable not only for the mucoadhesion but also for the design of controlled release dosage forms (Bernkop-Schnürch et al., 1999a; Bernkop-Schnürch et al., 2004b).

TMC has also been thiolated by reacting with cysteine mediated with EDAC/NHS. Insulin-loaded nanoparticles were prepared using polyelectrolyte complexation method. The resultant TMC-cysteine showed significantly greater mucoadhesion capacity compared to unmodified TMC in both rat ileal loop and mucin adsorption models. This might be due firstly to the electrostatic interaction between positively charged chitosan and negatively charged sialic acid of mucin glycoproteins leads to the interpenetration of the polymer and mucin. Secondly, at neutral pH (pH of small intestine) the thiol groups of TMC-cysteine could be oxidized by reacting with cysteine-rich domains of mucin leads to the formation of disulfide bonds, which finally may immobilize more thiolated polymeric particles in the mucus layer than the unmodified polymer (Yin et al., 2009). TMC-cysteine nanoparticles also showed greater permeability enhancement effect compared to unmodified TMC, which can be linked to the inhibition of protein tyrosine phosphatase which facilitates opening of tight junctions (Bernkop-Schnürch et al., 2004b). It might also be due to the greater mucoadhesion of TMC-cysteine than the native chitosan. Third possible reason is the inhibition of protease activities on insulin via shielding of enzymatic cutting sites after formation of self-assembled nanoparticles (Yin et al., 2009).

#### 1.4.3.2 Chitosan-N-acetyl-cysteine

Schmitz et al. (2008) synthesized chitosan-N-acetyl-cysteine conjugate via covalent attachment of N-acetyl-cysteine to chitosan using two different concentrations of EDAC as a mediator. They observed that this modification resulted in 50-fold increase in the retention of chitosan compressed discs on *ex vivo* porcine intestinal mucosa. The total work of adhesion required to detach the chitosan-N-acetyl-cysteine discs from the intestinal mucosa was 8.3-fold greater than unmodified chitosan. This may be due to the increase in the number of disulfide bonds between the polymers and the cysteine-rich domains of mucosa. They also revealed that increasing the concentration of EDAC resulted in products with greater amount of thiol groups. This is due to the activation of carboxylic groups of N-acetyl-cysteine, which resulted in immobilization of more thiol groups on the polymer. This eventually increased its mucoadhesive strength.

1.4.3.3 Chitosan-thioglycolic acid (Chitosan-TGA)

Chitosan-TGA has been synthesized by introducing TGA to chitosan using EDAC as a mediator. The resulting thiolated chitosan showed 4.3-fold increase in the viscosity, which is desirable for mucosal drug and gene delivery and scaffold materials in tissue engineering. This improvement in the viscosity may be related to the formation of disulfide bonds within the polymeric matrix (Kast et al., 2003). The viscosity of this thiolated chitosan can be further improved by using different oxidizing agents including hydrogen peroxide, sodium periodate, ammonium persulfate and sodium hypochlorite. These agents accelerated the sol-gel transition to take place only within few min, while without them this transition requires 40 min. 25 nmol/L hydrogen peroxide has increased the dynamic viscosity of 1% chitosan-TGA solution by up to 16,500-fold. This may be due to the formation of more inter- and intra-chain disulfide bonds (Sakloetsakun et al., 2009). To assess the potential of chitosan-TGA for non-viral oral gene delivery, 100–200 nm nanoparticles with zeta potential of 5-6 mV have been formed by complex coacervation of plasmid DNA and the thiolated chitosan. These particles showed acceptable stability toward DNase and thus resulted in a 5-fold increase in the rate of transfection (Martien et al., 2007) .

In another study, Barthelmes et al. (2011) synthesized mucoadhesive nanoparticles based on chitosan-TGA using ionic gelation with sodium tripolyphosphate (TPP) for intravesical drug delivery. Two types of partially oxidized (different in their disulfide content, -SH groups oxidized to form -S-S- bonds) chitosan-TGA-TPP nanoparticles were also synthesized by the addition of $H_2O_2$ solution (0.5% v/v) to chitosan-TGA-TPP nanoparticles. Either fluorescein diacetate or trimethoprim were then loaded into the nanoparticles. Then, using a flow through technique, the amount of fluorescein diacetate adhered to the bladder mucosa was quantified using fluorescence spectrophotometry. It was found that using chitosan-TGA-TPP nanoparticles, 14.2 ± 7.2% of fluorescein diacetate remained on the surface of the mucosal tissues but in the case of unmodified chitosan-TPP nanoparticles, only 1.1 ± 0.1% fluorescein diacetate remained after washing with simulated artificial urine for 3 h with a flow rate of 2 mL/min. This improvement in the mucoadhesion was due to the covalent bonds formed between the thiol groups of the polymers and the cysteine-rich domains of the glycosaminoglycan layer of the mucus which is composed of proteoglycans and glycoproteins as in the case of adhesion to the intestinal mucosa (Soler et al., 2008; Barthelmes et al., 2011). To prove the concept, a quantitative analysis of free thiol groups of intestinal and urinary bladder mucus was performed and revealed no significant difference

between the thiol contents of the two mucosal tissues. Interestingly, release study using artificial urine as a dissolution media shown that covalently crosslinked chitosan-TGA-TPP nanoparticles resulted in a slower and more controlled release of trimethoprim compared to ionically crosslinked chitosan-TGA-TPP and unmodified chitosan-TPP nanoparticles. The nanoparticles with greater content of disulfide bonds released the drug significantly slower than the nanoparticles with fewer disulfide bonds. The authors suggested that covalent crosslinking resulted in harder nanoparticles due to the formation of disulfide bridges within the matrix of the nanoparticles. This then increased the mechanical strength of the nanoparticles and thus made the artificial urine diffuse slowly into the nanoparticles. Consequently the dissolution of trimethoprim decreased and the nanoparticles released the drug slowly (Barthelmes et al., 2011).

#### 1.4.3.4 Chitosan-4-thiobutylamidine

Chitosan-4-thiobutylamidine (chitosan-TBA) is another type of thiolated chitosan with mucoadhesive properties (Grabovac et al., 2005). It remained on porcine small intestinal mucosa for 161 ± 7 h when tested using rotating cylinder method. In addition, the total work of adhesion was 740 ± 147 µJ. It has been reported that the mucoadhesive property of thiolated chitosans is pH dependent, and this point should be considered in the design of thiolated chitosan-based mucosal drug delivery systems (Grabovac et al., 2005).

Langoth et al. (2006) designed mucoadhesive buccal delivery system of pituitary adenylate cyclase-activating polypeptide using chitosan-TBA as a promising treatment for type-2 diabetes mellitus. The *in vivo* buccal administration through porcine buccal mucosa resulted in a continuous rise in the plasma level of the enzyme over 6 h.

Dünnhaupt et al. (2011) synthesized fluorescently-labelled nanoparticles of chitosan-TBA and polyacrylic acid-cysteine conjugate using ionotropic gelation technique. For the mucoadhesion study, fresh jejunum of rats was cut into 2 cm segments and filled with 0.1 mL nanoparticles. After fixation, the mucosal tissues were examined by fluorescence microscopy. The penetration study was performed using fresh “mucus-filled silicon tube” technique. It was found that nanoparticles of both modified chitosan (Figure 1.9) and polyacrylic acid exhibit greater mucoadhesive strength than unmodified nanoparticles. Chitosan particles showed 2-fold greater mucoadhesive property than polyacrylic acid particles. On the contrary, the muco-penetration ability of unmodified nanoparticles was greater than the thiolated nanoparticles.

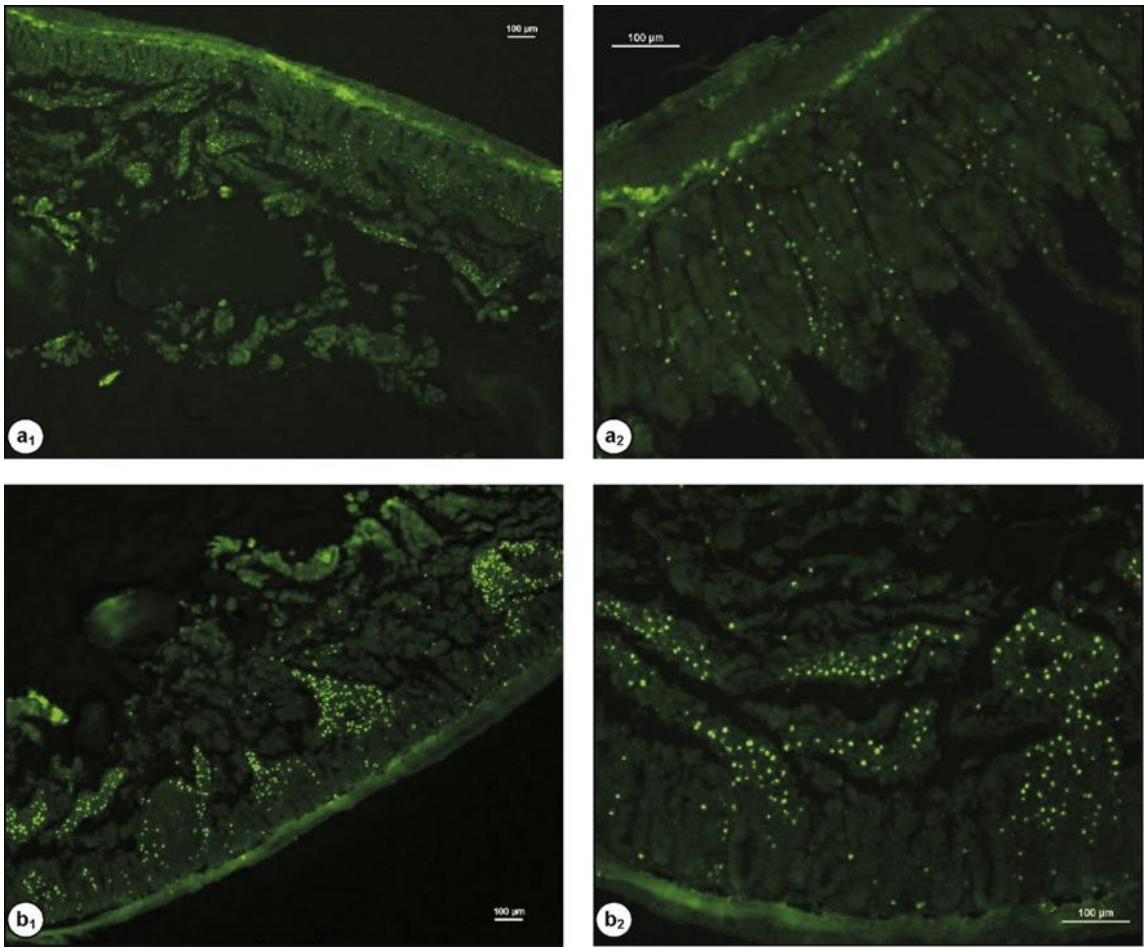


Figure 1.9 Fluorescent images of rat intestinal tissues after 2 h incubation with 100 µL 0.5% w/v (a) chitosan and (b) chitosan-TBA nanoparticles labelled with Alexa Fluor 488, ($a_1$ and $b_1$,40×; $a_2$ and $b_2$, 100× magnification). The scale bars are 100 µm. Reprinted from (Dünnhaupt et al., 2011) with permission of Elsevier.

The combination of chitosan-TBA and chitosan-Bowman-Birk inhibitor in the design of 2 mg enteric coated microtablets showed a significant enhancement in the effect of oral salmon calcitonin on the level of plasma calcium when tested in rats (Guggi et al., 2003). The derivatization of chitosan with enzyme inhibitors will be discussed in a separate section.

1.4.3.5 Chitosan-thioethylamidine

The use of 2-iminothiolane to synthesize thiolated chitosan resulted in a marked increase in the mucoadhesion. However, the resultant thiolated chitosan lacks sufficient stability leading to the reduction in the number of free thiol groups. One of the reasons for the instability could be the formation of N-chitosanyl-substituted 2-iminothiolane structures, which happens after modification of some amines using 2-iminothiolane. This intermediate product loses ammonia and results in the formation of re-cyclized N-substituted 2-iminothiolanes.

To avoid this side reaction, Kafedjiiski et al. (2005b) synthesized thiolated chitosan using isopropyl-S-acetylthioacetimidate as a thiolating agent and an alternative to 2-iminothiolane. In contrast to chitosan-TBA (higher than unmodified chitosan) (Krauland et al., 2006), the swelling property of chitosan-thioethylamidine was not significantly different from unmodified chitosan. However, the mucoadhesion was significantly improved. Using chitosan-thioethylamidine, the release of FITC-dextran was sustained over 3 h, which could be due to the presence of disulfide bonds in the structure of chitosan, which can slow the diffusion of FITC-dextran macromolecules down.

1.4.3.6 Chitosan-glutathione

Several studies reported the use of glutathione for the synthesis of chitosan-glutathione conjugates (Kafedjiiski et al., 2005a; Moghaddam et al., 2009; Koo et al., 2011; Li et al., 2013). Due to its permeation-enhancing effect, redox potential and safe toxicological profile, glutathione is a suitable thiolating agent for biomedical applications. Due to the presence of thiol groups in the cysteine part of glutathione, it has strong electron donating property, acting as a reducing agent. Additionally, the stability of glutathione against cellular aminopeptidase is provided by the presence of ɤ-peptidic bond between glutamic acid and cysteine. Also, its conformational flexibility, makes glutathione a highly reactive ligand (Kafedjiiski et al., 2005a).

Similar to other thiolated chitosans, the synthetic approach is based on the formation of amide bonds between glycine carboxylic acid groups of glutathione and amino groups of chitosan. The reaction can be mediated by EDAC/NHS. The method was developed by Kafedjiiski et al. (2005a). The resultant chitosan-glutathione exhibited acceptable cohesive properties and did not disintegrate in physiological solution (0.1 M phosphate buffer solution pH 6.8) for 48 h. However, unmodified chitosan was only stable for 9 h. Interestingly, both polymers showed the same swelling behaviour, whereas chitosan glutathione had greater mucoadhesive properties (expressed as the total work of adhesion and tablets-porcine intestinal detachment time) than unmodified chitosan. The apparent permeability of rhodamine 123 across rat duodenum using chitosan-glutathione and unmodified chitosan were $2.06 \times 10^{-7}$, and $0.66 \times 10^{-7}$ cm/s, respectively.

Jin et al. (2011) demonstrated the application of chitosan-glutathione in the oral delivery of thymopentin (a synthetic pentapeptide with immune-regulatory action). They synthesized thymopentin-loaded poly(butyl cyanoacrylate) nanoparticles using emulsion polymerization

technique. The particles were subsequently coated with either chitosan or chitosan-glutathione and orally administered to immunosuppressed rats. It was found that chitosan-glutathione-coated nanoparticles were able to normalize the immune function of rats, which is probably due to the enhanced mucoadhesive properties of chitosan-glutathione.

Chitosan-glutathione hydrogel was also found to be more effective in the reduction of oxidative stress in neonatal rat cardiomyocytes than unmodified chitosan hydrogel. The action possibly related to better cellular adhesion potential of chitosan-glutathione compared to unmodified chitosan as a result of the availability of the biocompatible glutathione promoting the cells survival (Li et al., 2013).

1.4.3.7 Comparison of chitosan, trimethyl chitosan and thiolated chitosan

In a comparative study, Mei et al. (2008) investigated the mucoadhesion as well as the nasal absorption enhancing effect of chitosan, thiolated chitosan and trimethyl chitosan. Chitosans of different molecular weights were synthesized by depolymerization then the depolymerized samples were either trimethylated as reported in (Mao et al., 2005) or thiolated by reacting with cysteine using EDAC/NHS chemistry according to Bernkop-Schnürch and Steininger (2000) with slight modification. The mucoadhesion of chitosan and thiolated chitosan was evaluated and the detachment time of 5 mm discs of the polymers from freshly excised porcine intestinal mucosa was evaluated. Discs of thiolated chitosan with greater degree of substitution (152 µmol/g) detached in a significantly longer time (about 12 h) than unmodified chitosan. The bioavailability of 2,3,5,6-tetramethylpyrazine phosphate through nasal route after its formulation with different chitosans was investigated. It was found that the use of any type of chitosan (unmodified, thiolated and trimethyl chitosan) resulted in a significantly improved absorption of 2,3,5,6-tetramethylpyrazine, however, no significant difference between thiolated chitosans (two different degrees of substitution) with unmodified chitosan was observed. The authors claimed that the permeation-enhancing effect is dose- and molecular weight-dependent and 100 kDa resulted in maximal absorption enhancement. On the other hand, trimethyl chitosan led to a significant enhancement in the nasal absorption of the drug. These results contradict those studies reporting the absorption enhancing effect of thiolated chitosan through intestinal mucosa. For example, Krauland et al. (2004; 2006) demonstrated that chitosan-4-thiobulyamidine resulted in an increase in the oral and nasal absorption of insulin compared to unmodified chitosan. In Krauland et al. studies (2004; 2006), the absorption enhancement

could also be due to the inhibition of protein tyrosinase and P-glycoprotein efflux pump in the mucosal membranes (Föger et al., 2006; Krauland et al., 2006).

1.4.3.8 Pre-activated (S-protected) thiolated chitosans

Vulnerability of thiolated chitosans to oxidation can be considered as one of the major limitations of their use as mucoadhesive polymers. Thiolated chitosans are generally stable in dry state. However, in solutions, they undergo rapid oxidation especially in the presence of oxidants such as oxygen and particularly at pH > 5 (Bernkop-Schnürch et al., 2003). This, will not only lead to the formation of intra- and inter-molecular disulfide bonds, but also results in the reduction of the free thiol groups necessary for the formation of disulfide bridges with the cysteine-rich domains of the mucin. This will then lead to a significant reduction in the mucoadhesive potential of thiolated chitosans under physiological conditions of the gastrointestinal tract (Bernkop-Schnürch et al., 2003). To prevent the unwanted oxidation of thiolated chitosans, pre-activated or S-protected thiolated chitosans have been developed by Bernkop-Schnürch and co-workers.

Generally, pre-activated thiolated chitosan can be synthesized by two steps. Firstly, thiolated chitosan is prepared using a thiolating agent and secondly thiol groups are protected by disulfide bond formation using ligands with mercaptopyridine substructure including mercaptonicotinamide, mercaptonicotinic acid and mercaptopyridine. Due to its toxicity profile mercaptopyridine is less commonly used (Bonengel & Bernkop-Schnürch, 2014). Despite improvement of mucoadhesive properties, S-protection can also enhance the intestinal permeability of hydrophilic molecules such as FITC-dextran. In addition, S-protected thiolated chitosans have shown less cellular toxicity than the unprotected chitosans (Dünnhaupt et al., 2012b).

Dünnhaupt et al. (2012c) synthesized S-protected thiolated chitosan using a two-steps approach (Figure 1.10). First, thioglycolic acid was covalently attached to chitosan and resulted in the formation of amide bonds between the amino groups of chitosan and the carboxylic groups of thioglycolic acid. Secondly, aromatic ligand 6-mercaptonicotinamide (6-MNA) was synthesized by reacting 6-chloro-nicotinamide with thiourea, which was then oxidized using hydrogen peroxide to form 6, 6′-dithionicotinamide (6, 6′-DTNA). Both 6-MNA and 6, 6′-DTNA were then reacted with thiolated chitosan to obtain S-protected thiolated chitosan. Tablets of unmodified, thiolated and S-protected thiolated chitosans were prepared. Using rotating cylinder method, it was found that S-protected thiolated chitosan

with 660 µmol/g thiol groups remained attached to the intestinal mucosa for 90 h, whereas unprotected thiolated chitosan were only attached for 45 h. However, it seemed there was no significant difference between unprotected and S-protected thiolated chitosan with more thiol groups (980 µmol/g). Unmodified chitosan detached after only 10 h. Rheological studies also indicated that mixing S-protected thiolated chitosan with mucin resulted in a significant increase in the apparent viscosity of the mixture compared to both unmodified and unprotected thiolated chitosan. The authors believed that S-protected thiolated chitosan interacts more rapidly and quantitatively with mucus by thiol-disulfide exchange reaction between the thiol groups of mucus-cysteine and the pyridyl-thiol moiety of the S-protected thiolated chitosan. In the mucus, the amount of free thiol groups (-SH) is approximately two times greater than their oxidized form (-S-S-) (Barthelmes et al., 2011) and this is in favour of thiol-disulfide exchange. Thus, more bonding between S-protected thiolated chitosan and the mucus can be achieved compared to unprotected thiolated chitosan (Dünnhaupt et al., 2012c).

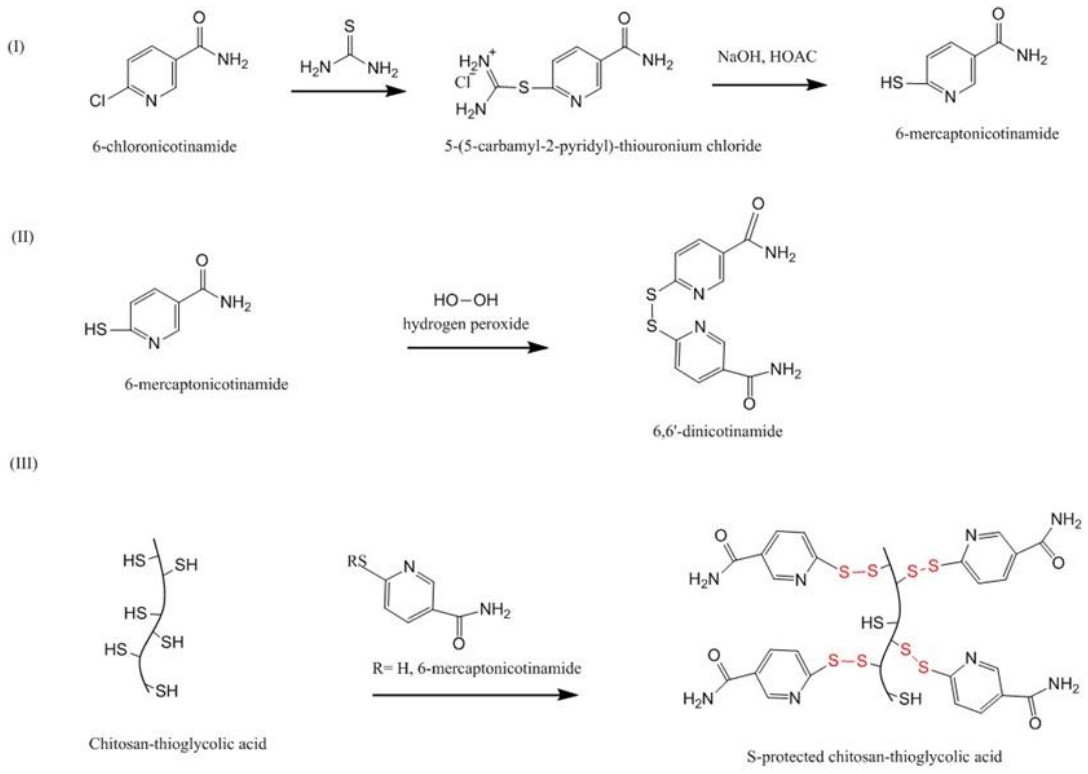


Figure 1.10 Synthetic pathway to S-protected chitosan-thioglycolic acid (Dünnhaupt et al., 2012c).

In another study, Dünnhaupt et al. (2012a) demonstrated the application of S-protected chitosan-TGA (chitosan-TGA-MNA) in the oral delivery of antide as tablets dosages forms. It was shown that hardness of chitosan-TGA-MNA tablets was significantly increased due to introduction of 6-MNA ligand and the presence of disulfide bonds within the polymeric network. Chitosan tablets swelled quickly and reached maximum within 2 h. However, chitosan-TGA tablets swelled slowly and continuously with greater extent than the unmodified chitosan. The presence of disulfide bonds might explain the enhanced water absorbing capacity of chitosan-TGA. On the other hand, chitosan-TGA-MNA tablets swelled to a lesser extent (1.5-fold) than chitosan-TGA tablets, which could be due to the presence of hydrophobic 6-MNA ligand. Additionally, chitosan-TGA-MNA resulted in a constant sustained release of antide and after 8 h, only 65% released. However, the % of antide released from chitosan-TGA and unmodified chitosan were 77 and 100%, respectively. The *in vivo* study in male Sprague Dawley rats, however, indicated only a slightly higher plasma concentration of antide, but not statistically significant ($p > 0.05$) using chitosan-TGA-MNA compared to chitosan-TGA. The authors claimed that this compromise in the oral bioavailability of antide could be due to the enhanced cohesiveness and controlled release of chitosan-TGA-MNA tablets. These two properties are essentially important in the design of mucoadhesive formulations as if the polymer is not cohesive enough it might collapse and therefore the peptide might not be protected and rapidly released into the lumen of the gastrointestinal tract and degraded and no longer contributes to the concentration gradient (Dünnhaupt et al., 2012a).

#### 1.4.3.9 Other thiolated chitosans

Thiolated methylated dimethylaminobenzyl chitosan has been synthesized by Hakimi et al. (2017). Although the authors claimed that the modified chitosan had better water-solubility profile and potential for drug delivery, in their work, apart from cytotoxicity, they did not perform any studies related to the application of this type of thiolated chitosan as a mucoadhesive polymer. Clearly, this chitosan derivative will be of interest for evaluation of its mucoadhesive properties.

### 1.4.4 Acrylated chitosan

The use of acrylate groups in the development of mucoadhesive materials was pioneered by Davidovich-Pinhas and Bianco-Peled (2010). The mechanism of mucoadhesion is believed to be due to Michael-type addition reaction between the acrylate vinyl groups of the polymers and the sulfhydryl groups of mucus glycoproteins. The nature of this interaction

was proved by $^{1}$H-NMR study, where the intensity of the peaks related to the vinyl groups of polyethylene glycol diacrylate hydrogels was decreased after their reactions with mucin dispersion (Davidovich-Pinhas & Bianco-Peled, 2010). Thus, the presence of covalent interactions with mucus is a common feature of acrylated and thiolated mucoadhesive materials (Bernkop-Schnürch et al., 2003; Davidovich-Pinhas & Bianco-Peled, 2010, 2011; Irmukhametova et al., 2011; Štorha et al., 2013; Bonengel & Bernkop-Schnürch, 2014; Eshel-Green & Bianco-Peled, 2016; Mun et al., 2016). The idea of acrylated chitosan synthesis was developed by Ma et al. (2009). However, they did not demonstrate any application in the mucosal drug delivery. This chitosan derivative is water-soluble, can be cross-linked under ultraviolet light using photoinitiator 2959 and has less antimicrobial activity compared to parent chitosan (Ma et al., 2009).

Shitrit and Bianco-Peled (2017) synthesized acrylated chitosan by reacting chitosan solution (1% w/v in 2% v/v acetic acid, molecular weight 207 kDa, degree of deacetylation 77.6%) with poly(ethylene glycol) diacrylate (PEGDA) via Michael-type reaction (Figure 1.11). Two different molecular weight PEGDA (0.7 and 10 kDa) were used. The acrylated chitosan was characterized using $^{1}$H-NMR spectroscopy and ninhydrin test. It was found that using smaller molecular weight (0.7 kDa PEGDA) at chitosan/PEGDA ratio of 1:4 resulted in more acrylation (98%) than using higher molecular weight PEGDA (10 kDa, 30%). The authors believed that this could be due the presence of greater molar amount of acrylate groups leading to a more efficient reaction. However, using chitosan/PEGDA 1:2 molar ratio led to the formation of a product with a lower degree of acrylation (45%).

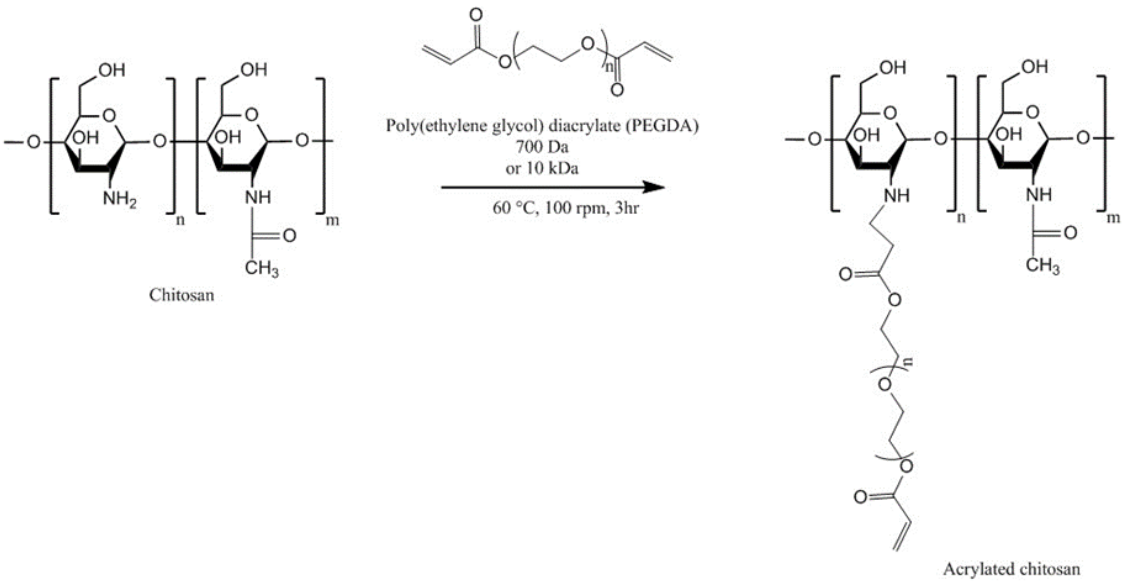


Figure 1.11 Synthetic pathway to acrylated chitosan (Shitrit & Bianco-Peled, 2017).

The mucoadhesion was evaluated using tensile strength and rotating cylinder method using tablets of chitosan, thiolated and acrylated chitosan on porcine intestinal mucosa. The order of detachment force was the following: chitosan-PEGAc (10 kDa) > thiolated chitosan > chitosan = chitosan-PEGAc (0.7 kDa). Unexpectedly, the maximum detachment force of chitosan-PEGAc (0.7 kDa) was not significantly different from chitosan tablets. Both chitosan-PEGAc (10 kDa) and thiolated chitosan remained attached to the intestinal mucosa for more than 6 h, whereas chitosan-PEGAc (0.7 kDa) detached after 1 min. Chitosan tablets detached after 1.1 ± 0.2 h. The authors claimed that chitosan-PEGAc (0.7 kDa) has greater degree of acrylation than chitosan-PEGAc (10 kDa) and this means higher grafting density of PEG, which could result in the steric hindrance and preventing the covalent bonding with the cysteine-rich domain of mucus (Shitrit & Bianco-Peled, 2017). Similar trend with polyacrylic acid was observed; 450 kDa showed a stronger interaction with porcine gastric mucin whereas 2 kDa did not exert any effect (Albarkah et al., 2015). Additionally, shorter PEG (smaller molecular weight) cannot deeply penetrate the mucosal tissues and results in a lower mucoadhesive strength, since mucoadhesive properties of polymers are proportional to the molecular weight (Shitrit & Bianco-Peled, 2017). Other studies reported that an optimum molecular weight of polymers is required to achieve maximal mucoadhesion. Small molecular weight polymers form weak gels and easily dissolve whereas high molecular weight polymers do not readily hydrate, thus the free binding groups are not

available to interact with the mucus components. Therefore, in both cases, weak mucoadhesion can be observed (Smart, 2005).

### 1.4.5 Half-acetylated chitosan

Half-acetylated chitosan is another type of chitosan derivatives, which can be prepared by reacting chitosan with acetic anhydride. Several studies explored the solubility of half-acetylated chitosan and its subsequent effect on the antimicrobial and mucoadhesive properties of chitosan (Qin et al., 2006; Sogias et al., 2008; Sogias et al., 2010; Sogias et al., 2012). Qin et al. (2006) found that half-acetylated chitosan had no antimicrobial activity against Staphylococcus aureus, Escherichia coli and Candida albicans. However, unmodified chitosan had antimicrobial effects against these microorganisms. They claimed that chitosan can interact with the components of the microorganism surfaces and thus be absorbed on their surfaces. Since the pH of bacterial and fungal cells is around 7, unmodified chitosan precipitates and forms an impermeable layer around the cells. This layer blocks the channels, which are essential for the cells survival. However, half-acetylated chitosan fully dissolved at neutral pH, thus did not form an impermeable layer, and led to a better survival of cells compared to unmodified chitosan.

Sogias et al. (2010) demonstrated that half-acetylated chitosan (the degree of acetylation = 52 ± 4 mol%) was soluble over a broad pH range and did not precipitate below pH 7.4. This improved solubility profile of half-acetylated chitosan over unmodified chitosan was related to the reduced crystallinity (caused by disruption of inter- and intra-molecular hydrogen bonds) upon N-acetylation (Sogias et al., 2008; Sogias et al., 2010). In another study, Sogias et al. (2008) found that, at pH 2, half-acetylated chitosan interacted with porcine gastric mucin particles at a higher polymer/mucin ratio than unmodified chitosan, which was due to the decrease in the number of free amino groups in half-acetylated chitosan. At this pH, the amino groups undergone protonation and were responsible for the electrostatic interaction between chitosan macromolecules and mucin. They also revealed that at pH 7, where unmodified chitosan precipitates, half-acetylated chitosan was still able to interact with mucin particles. To explore the mechanisms of mucoadhesion, the polymer-mucin interaction was studied in the presence of sodium chloride (0.2 M), urea (8 M) and ethanol (10% v/v). These agents are known to disrupt the electrostatic interaction, hydrogen bonding and hydrophobic effects, respectively. The results indicated that all these forces were involved in the mucoadhesion of chitosan and half-acetylated chitosan. In case of half-acetylated chitosan, at pH 7, the electrostatic interaction was the major contributing force in

the mucoadhesive interactions. This may be due to the higher negative charge density of mucin particles at pH 7 compared to pH 2 (Sogias et al., 2008). However, the mucoadhesive properties of unmodified chitosan at pH 7 were not evaluated, which could be due to its insolubility at this pH.

Sogias et al. (2012) prepared microparticles containing ibuprofen and either chitosan or half-acetylated chitosan by two different techniques; spray-drying and co-grinding. 65 mg tablets were prepared from spray-dried chitosan and half-acetylated chitosan, spray-dried mixtures of chitosan or half-acetylated chitosan with ibuprofen and co-ground mixtures of the polymers and the drug. It was found that tablets of half-acetylated chitosan significantly enhanced ibuprofen release at pH 7. The force of detachment between unmodified chitosan tablets and porcine gastric mucosa was decreased when measured at very acidic (pH 1) and neutral (pH 7) media (Figure 1.12). However, the mucoadhesion of half-acetylated chitosan tablets was only decreased at low pH and increased linearly up to pH 7. Half-acetylated chitosan tablets were generally less mucoadhesive than chitosan tablets. This could be due to the reduction of cationic charge density upon acetylation, which diminished the electrostatic interaction with mucin (Sogias et al., 2012). Incorporation of ibuprofen in chitosans tablets resulted in a significant drop of mucoadhesion (Figure 1.12).

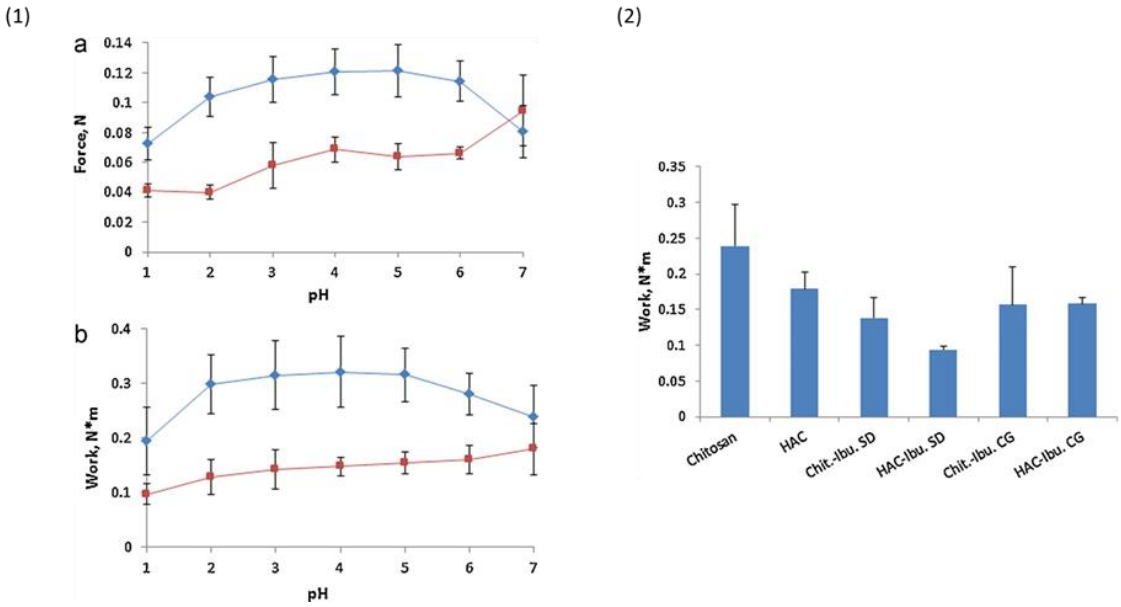


Figure 1.12 (1) Detachment force (a) and work of adhesion (b) for chitosan (◆) and half-acetylated chitosan (HACHI) (■) tablets as a function of pH on porcine gastric mucosal tissues at 37 ± 0.1 °C. Mean ± SD, *n* = 3. (2) Work of adhesion of tablets on porcine gastric mucosa at pH 7.0 and 37 ± 0.1 °C. Chit.: chitosan, Ibu.: ibuprofen, SD: spray-dried, CG: co-ground. Mean ± SD, *n* = 3. Reprinted from (Sogias et al., 2012) with permission of Elsevier.

### 1.4.6 Glycol chitosan

Glycol chitosan is a hydrophilic chitosan derivative, which can be prepared by adding ethylene glycol groups to chitosan backbone. It is soluble in water at any pHs (Trapani et al., 2009; Palazzo et al., 2017). It is commercially available from Sigma-Aldrich.

Glycol chitosan has been used in the design of nanoparticles for the delivery of poorly water-soluble drugs. Trapani et al. (2009) prepared 6-coumarin-loaded glycol chitosan-TPP nanoparticles using ionic gelation method. Different cyclodextrins were used to form an inclusion complex with this dye. It was found that nanoparticles containing (2,6-di-O-methyl)-ß-cyclodextrin could be internalized by Caco2 cells, which could be due to the mucoadhesive nature of chitosan.

Glycol chitosan has been modified to prepare amphiphilic chitosan derivatives. Below, we will discuss two examples of these amphiphilic glycol chitosan derivatives.

#### 1.4.6.1 Palmitoyl glycol chitosan

Palmitoyl glycol chitosan is a hydrophobically-modified glycol chitosan. Its use in drug delivery started since the 1990s.The presence of both of hydrophilic and hydrophobic groups

imparts it an amphiphilic character (Uchegbu et al., 1998; Uchegbu et al., 2014). It has ability to self-assemble into vesicles suitable for delivery of water-soluble drugs such as bleomycin (Uchegbu et al., 1998). Its quaternized form (quaternary ammonium palmitoyl glycol chitosan) can self-assemble into micelles with a high drug loading capacity. It also facilitated transport of hydrophobic drugs including griseofulvin and propofol and hydrophilic drugs (but to a lower degree) including ranitidine through biological barriers such as intestinal and blood brain barriers, respectively, led to enhanced bioavailability (Qu et al., 2006; Siew et al., 2012). It is conceivable that, the hydrophilic groups (–OH and $–NH_2$) of glycol chitosan located in the external shell of the micelles and the hydrophobic groups in the cores. Thus, the mucoadhesive property of glycol chitosan should be well maintained upon self-assembly as these groups are mainly responsible for the mucoadhesive nature of chitosan and its derivatives (Sogias et al., 2008; Bonferoni et al., 2010).

The hydrophobicity is one of the important factors affecting the mucoadhesive character of materials. Martin et al. (2002) investigated this by synthesizing palmitoyl glycol chitosan with various degrees of palmitoylation (a hydrophobic group). First, glycol chitosan was dissolved in water before sodium bicarbonate and absolute ethanol were added. To this, ethanolic solution of palmitoyl-N-hydroxysuccinimide was added and then the mixture was stirred for 72 h in the dark (Figure 1.13). This was followed by dialysis and recovery of the product. The physically crosslinked gels were prepared by freeze drying the products and evaluated for their bioadhesive strength by measuring the force necessary to detach the gels from porcine buccal mucosa. It was found that by increasing the hydrophobicity (represented by the degree of palmitoylation), the hydration and erosion of the gels decreased. On the other hand, bioadhesion could be enhanced by increasing the hydrophobicity. Although no comparison with chitosan has been shown, palmitoyl glycol chitosans were found to be less bioadhesive than hydroxypropylmethyl cellulose/carbopol control. The most hydrophobic palmitoyl glycol chitosan gel (20.31 ± 2.22 mol% palmitoylation) resulted in the slowest controlled release of the model hydrophilic drug (FITC-dextran).

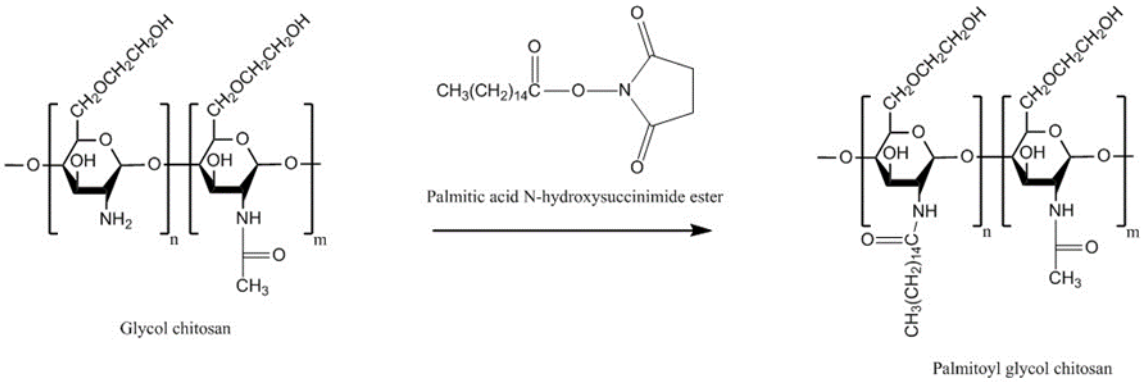


Figure 1.13 Synthetic pathway to palmitoyl glycol chitosan (Martin et al., 2002).

Siew et al. (2012) developed nanoparticles based on quaternary ammonium palmitoyl glycol chitosan, which enhanced the oral absorption of both hydrophilic (ranitidine) and lipophilic drugs (griseofulvin and cyclosporine A). The bioavailability enhancement was believed to be due to a combination of increased drug dissolution rate (as a result of a great surface area of drug-loaded nanoparticles) and the mucoadhesive nature of chitosan, which increased the intestinal residence time of the nanoparticles, bringing them in close contact with the absorptive epithelial cells and thereby reducing the absorption barrier of the mucosal membrane (Siew et al., 2012). This is because the established adhesion of the nanoparticles to the mucus layer provides some degree of penetration into the mucosal membranes (Khutoryanskiy, 2011).

1.4.6.2 Hexanoyl glycol chitosan

Cho et al. (2016b) synthesized hexanoyl glycol chitosan by N-acylation of glycol chitosan (Figure 1.14). To do that, glycol chitosan was dissolved in water and then diluted with methanol. Then, various amounts of hexanoic anhydride were added and the reaction mixture was continuously stirred for 24 h. The hexanoyl-glycol chitosan was precipitated by acetone and the product was recovered by lyophilization after been dialyzed against water.

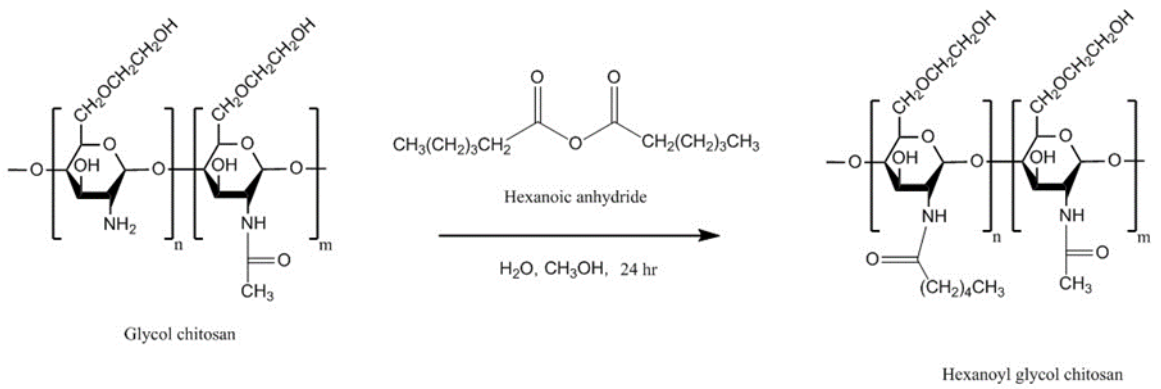


Figure 1.14 Synthetic pathway to hexanoyl glycol chitosan (Cho et al., 2016b).

Interestingly, hexanoyl glycol chitosan with 39.5 ± 0.4% degree of hexanoylation had a thermosensitive gelling property as it underwent gelation at 37 °C. The *in vitro* release study showed no significant difference between brimonidine-loaded hexanoyl glycol chitosan-based formulation and the marketed eye drops (Alphagan P). However, the *in vivo* pre-ocular (inferior fornix of the eyes) retention study in rabbits revealed that hexanoyl glycol chitosan enhanced the retention of rhodamine in the pre-ocular tissues (Figure 1.15). The fluorescence signal from rhodamine was still strong after 60 min post administration, and became weak after 90 min. On the other hand, weak fluorescence signal was observed after only 10 min (and become weaker after 60 min) when both PBS (negative control) and unmodified glycol chitosan were used indicating their poor retention in pre-ocular tissues (Figure 1.15). Additionally, the intra-ocular pressure was significantly dropped and the therapeutic action was prolonged compared to unmodified glycol chitosan as well as conventional eye drops (Cho et al., 2016b).

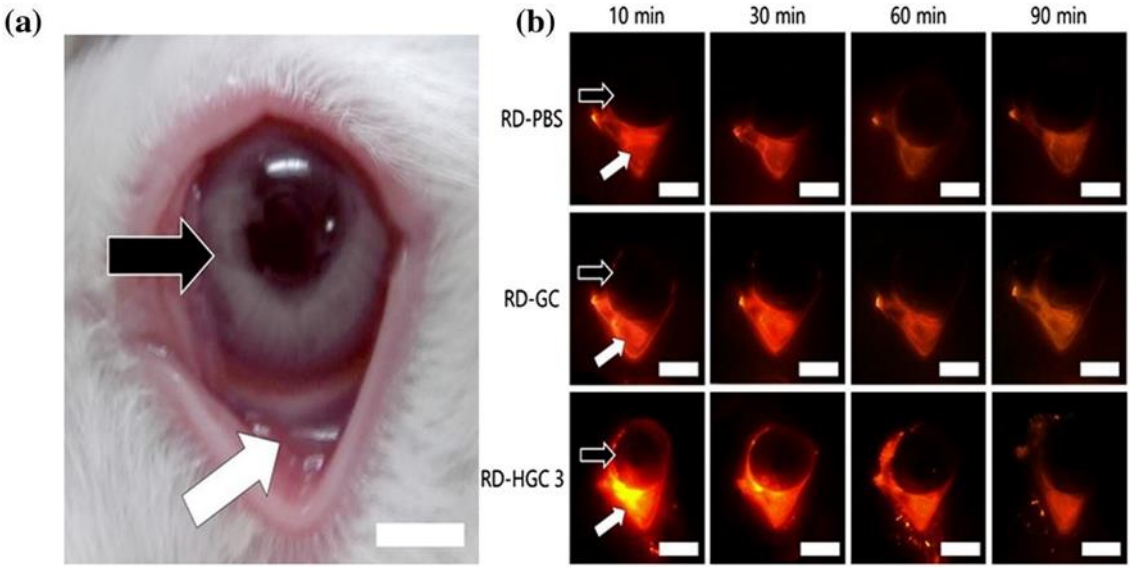


Figure 1.15 (a) Photograph of rabbit eyes showing the eyeball and the inferior fornix. (b) The fluorescence images of rabbit eyes at different time intervals after ocular administration of rhodamine-loaded PBS (RD-PBS), glycol chitosan (RD-GC) and hexanoyl glycol chitosan with 39.5 ± 0.4% degree of hexanoylation (RD-HGC 3). The eyeball and the inferior fornix (into which the formulations were administered) were shown by the black and white arrows, respectively. Scale bars are 5 mm. Reprinted from (Cho et al., 2016b) with permission of Elsevier.

Subsequently, Cho et al. (2016a) have further modified hexanoyl glycol chitosan by reacting it with glycidyl methacrylate (Figure 1.16) to form methacrylated hexanoyl glycol chitosan, which demonstrated a thermo-reversible sol–gel transition behaviour in aqueous solutions. Moreover, the thermally-induced hydrogels could be chemically crosslinked by photo-crosslinking under UV-radiation. Although no studies, to our knowledge, reported the mucoadhesive potential of methacrylated hexanoyl glycol chitosan, the presence of a methacrylated part within this polymer can potentially lead to a strong interaction with the mucin because of the covalent bonding between methacrylate part of methacrylated hexanoyl glycol chitosan and the thiol groups of the mucin components.

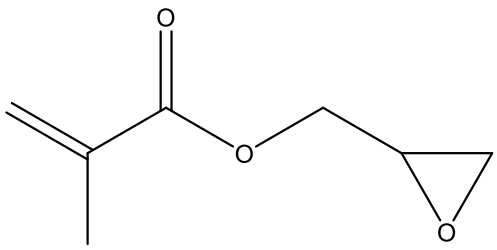


Figure 1.16 Chemical structure of glycidyl methacrylate.

### 1.4.7 Chitosan conjugates

#### 1.4.7.1 Chitosan-enzyme inhibitors

These systems have been developed to protect orally administered peptide-based drugs from enzymatic degradation in the gastrointestinal lumen. Some mucoadhesive polymers including carbomer could also act as weak enzyme inhibitors (Akiyama et al., 1996), however, chitosan lacks this property. Examples of enzyme inhibitors include antipain, chymostatin, elastatinal and Bowman–Birk inhibitor (Bernkop-Schnürch & Kast, 2001). It has been shown that enzyme inhibitors are toxic to certain types of cells. They also could induce pancreatic secretion of secretin and cholecystokinin in rats (Watanabe et al., 1992). These characters could limit the application of free enzyme inhibitors in the formulation of peptide-based drugs. However, covalent attachment of enzyme inhibitors to mucoadhesive polymers such as chitosan could reduce the unwanted effects as their absorption can be reduced. Bernkop-Schnürch et al. (1997) synthesized chitosan-antipain conjugate. The synthetic approach based on the formation of amide bond between carboxylic acid groups of enzyme inhibitors and the primary amino groups of chitosan which was mediated with EDAC and sulfo-N-hydroxysuccinimide. Chitosan-antipain conjugate not only showed mucoadhesive properties similar to unmodified chitosan, it also inhibited the action of trypsin. Tablets containing 5% chitosan-antipain conjugate protected insulin from trypsin inactivating effect. A sustained insulin release for 6 h was also achieved.

#### 1.4.7.2 Chitosan-complexing agent

Ethylenediaminetetraacetic acid (EDTA) is a potent chelating agent and has US FDA approval for the treatment of heavy metal poisoning since 1950s (Song et al., 2014). Removal of ions has been shown to enhance the permeation of antiviral drugs such as dolutegravir across Caco2 cells monolayer and rat intestinal mucosa *ex vivo* (Grießinger et al., 2016). EDTA is also able to decrease pre-systemic metabolism of peptide-based drugs by inhibiting brush border membrane bound enzymes by their deprivation of ions such as $Zn^{2+}$ in the mucous membrane (Bernkop-Schnürch & Kast, 2001; Netsomboon et al., 2017). However, the rapid biodistribution of EDTA limits this application. Thus, chitosan-based EDTA system has been developed which has mucoadhesive properties on one side and metal chelating ability on the other side (Bernkop-Schnürch & Scerbe-Saiko, 1998 ; Netsomboon et al., 2017).

Compared to unmodified chitosan, chitosan-EDTA tablets showed better retention on porcine intestinal mucosa. The mucoadhesive strength decreased with the reduction of the % of EDTA attached to chitosan. It also inhibited Zn- and Co-dependent proteases including carboxypeptidase A and aminopeptidase N. This is because chitosan-EDTA conjugate strongly bound to Zn and Co. (Bernkop-Schnürch & Krajicek, 1998).

S-protected thiolated chitosan-EDTA has also been synthesized to combine the advantages of EDTA, thiolation and pre-activation or protection of thiol groups. The synthetic pathway is shown in Figure 1.17 (Netsomboon et al., 2017). The multifunctional thiolated chitosan exhibited 5.6- and 3.6-fold longer residence time on porcine intestinal mucosa compared to chitosan-EDTA and chitosan-EDTA-cysteine, respectively (Figure 1.18).

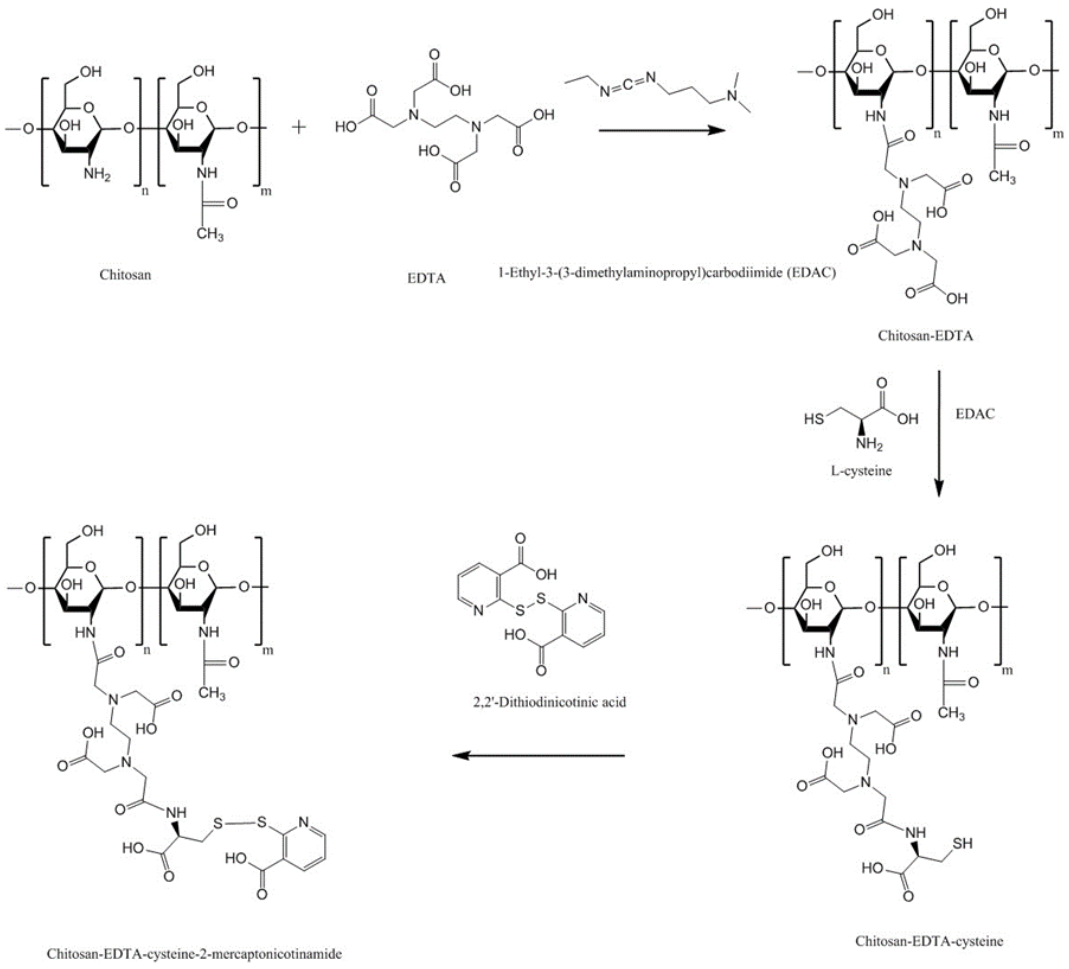


Figure 1.17 Synthetic pathway to chitosan-EDTA-cysteine-2-mercaptonicotinamide (Netsomboon et al., 2017).

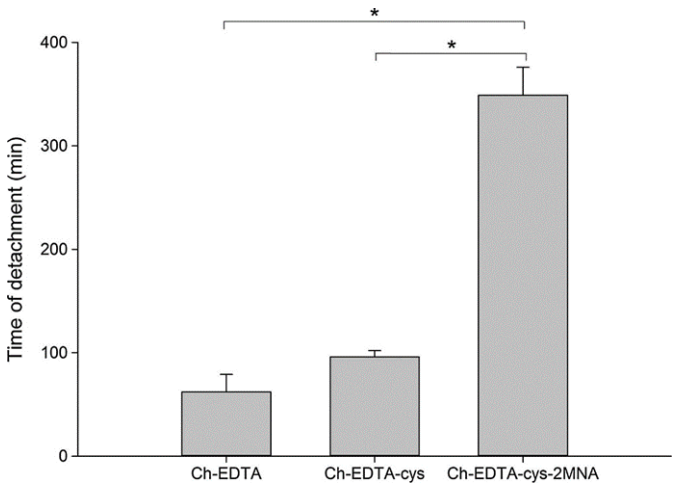


Figure 1.18 Mucoadhesion time of mini-tablets containing 30 mg of Ch-EDTA, Ch-EDTA-cys or Ch-EDTA-cys-2MNA studied by rotating cylinder method using porcine intestinal mucosa. Ch: chitosan, cys: cysteine, 2MNA: 2-mercaptonicotinamide. (Mean ± SD, $n = 5$, * denotes statistical significant difference at $p < 0.05$). Reprinted from (Netsomboon et al., 2017) with permission of Elsevier.

### 1.4.7.3 Chitosan-EDTA-enzyme inhibitors

By combining enzyme inhibitors and complexing agents coupled with chitosan, the degradation of peptide-based drugs by the gut luminal enzymes could be significantly minimized (Bernkop-Schnürch & Scerbe-Saiko, 1998 ). Additionally, as EDTA could bind to ions such as $Zn^{2+}$ and $Ca^{2+}$, the concentration of free forms of these ions can be reduced. This decreases the formation of non-absorbable complexes between some drugs and these ions leading to enhanced drug permeation (Song et al., 2014; Grießinger et al., 2016). Thus, chitosan-EDTA-serine protease inhibitors were synthesized using a two-step approach. First, to form chitosan-serine protease inhibitors, covalent attachment of antipain, chymostatin and elastatinal to chitosan was performed. Second, chitosan-enzyme inhibitors were bound to EDTA. Tensile study using porcine intestinal mucosa demonstrated that the mucoadhesive strength of the chitosan-EDTA-serine inhibitor was lower than both chitosan-EDTA and chitosan. The reduction of the mucoadhesion of chitosan-EDTA-serine protease inhibitors could be due to the substitution of the free amino groups of chitosan or chitosan-EDTA upon covalent attachment to the enzyme inhibitors (Bernkop-Schnürch & Scerbe-Saiko, 1998 ).

### 1.4.8 Chitosan-catechol (Chi-C)

Catechol is a naturally occurring compound. It is an essential component of L-3,4-dihydroxyphenylalanine (L-DOPA), which is an amino acid secreted by certain marine mussels (e.g., Mytilus edulis), which have ability to adhere to various substrates under wet conditions (Kim et al., 2015). This adhesive property is mainly linked to the ability of catechol to form covalent and non-covalent bonds to different organic, inorganic, and metallic surfaces (Ryu et al., 2011; Kim et al., 2013). Generally, chitosan-catechol can be synthesized by chemical, electrochemical and enzymatic methods. The chemical method includes three main approaches: amide bond formation using carbodiimide chemistry (Figure 1.19), reductive amination using aldehyde-terminated catechol and reducing agents such as $NaCNBH_3$ or $NaBH_4$, and formation of catechol-amine adducts using oxidizing agents such as $NaIO_4$ (Kim et al., 2015; Ryu et al., 2015).

Inspired by mussel adhesion to surfaces, Kim et al. (2015) synthesized chitosan-catechol conjugate by reacting chitosan with 3,4-dihydroxy hydrocinnamic acid mediated with EDAC (Figure 1.19). Mucoadhesion was evaluated *in vitro* using mucin-particle interaction, turbidimetry, surface plasmon resonance (SPR) spectroscopy and rheological characterization as well as *in vivo* fluorescence imaging technique and fluorescence measurement in various organs of mice. Chitosan-catechol conjugate showed superior mucoadhesion than both unmodified chitosan and polyacrylic acid. The *in vivo* study explored the difference in the retention of different polymers in different body sites. No fluorescence was detected in organs lacking mucosal tissues including liver, spleen, and kidney (Figure 1.20). However, at 3 h post-oral administration, strong fluorescence signal from chitosan-catechol conjugate in intestinal tissues was observed (Figure 1.20). This could be due to the formation of strong covalent bonds via Michael-type addition reaction upon the reaction of oxidized form of catechol (quinone) and amine or thiol functionalities of mucins or Schiff base formation reaction (Kim et al., 2015). The electrostatic attractive interaction between the positively charged groups of chitosan and negatively charged carboxyl and sulfate groups of mucin could lead to an initial contact stage and the adsorption of chitosan-catechol macromolecules on the mucosal surfaces. This was then followed by an established consolidation stage via the covalent interaction (Smart, 2005; Kim et al., 2015). Unmodified chitosan and polyacrylic acid showed poor fluorescence signal. The retention of chitosan-catechol conjugate decreased significantly in both stomach and esophagus. The authors claimed that chitosan-catechol conjugate-mucin interaction was stronger when the

pH of mucin solution was 7 compared to pH 2 (Kim et al., 2015). This might explain better retention in small intestine, where pH is near neutral compared to poor retention in stomach (highly acidic) and esophagus (slightly acidic, pH 4–6) (Kim et al., 2015). The oxidation of catechol to quinone in alkaline environment is more likely than in acidic environment, which could provide additional adhesive interactions (Lee et al., 2006; Ryu et al., 2011; Kim et al., 2015). On the other hand, polyacrylic acid showed slightly greater mucoadhesion to esophagus than stomach and intestine (Figure 1.20-C). The difference in the pH of these organs might explain this observation as it may affect the structures of both polyacrylic acid and the mucus layer resulting in a different nature and extent of mucoadhesive interactions at different pHs (Patel et al., 2003). Some studies reported that the mucoadhesive nature of polyacrylic acid may be due to its ability to form hydrogen bonds with the mucus components (Riley et al., 2001; Patel et al., 2003; Albarkah et al., 2015; Kim et al., 2015), which is strongest at slightly acidic pHs, depending on the type of the polymer (Mortazavi et al., 1993; Riley et al., 2001). However, Kim et al. (2015) suggested further studies to investigate the organ-specific mucoadhesive properties of chitosan, chitosan-catechol and polyacrylic acid. Chitosan-catechol conjugate also enhanced the oral bioavailability of insulin and $C_{max}$ reached after 2 h compared to unmodified chitosan which was 30 min (Figure 1.20-D).

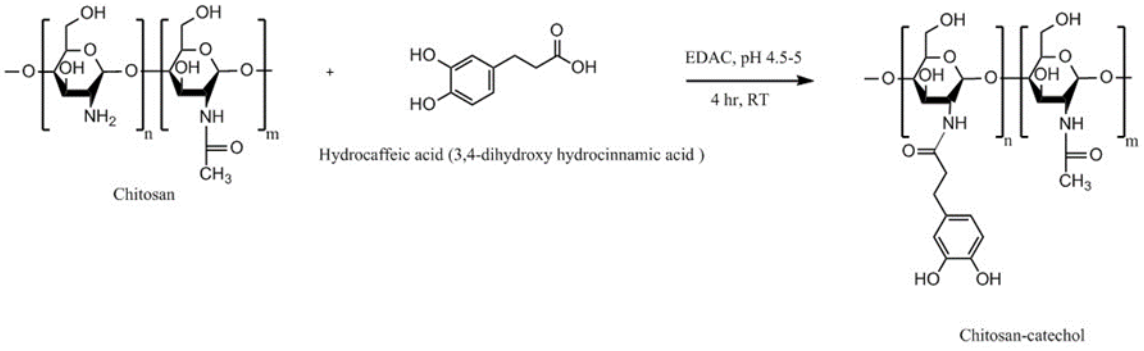


Figure 1.19 Synthetic pathway to chitosan-catechol using carbodiimide chemistry (Kim et al., 2015).

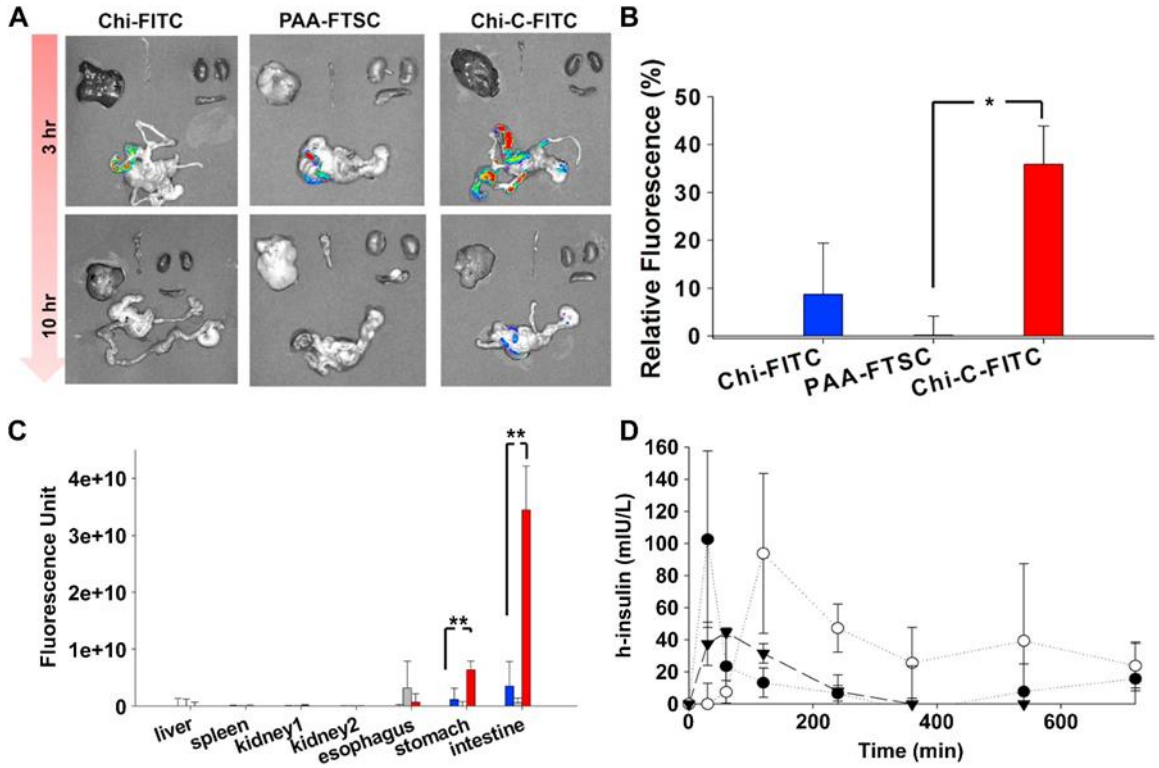


Figure 1.20 Chitosan-fluorescein isothiocyanate (Chi-FITC), polyacrylic acid-fluorescein-5-thiosemicarbazide (PAA-FTSC) and chitosan-catechol-fluorescein isothiocyanate (Chi-C-FITC) were orally administered to BALB/c mice and the animals were euthanized after 3 or 10 h. (A) The extracted organs were imaged using *in vivo* imaging system. (B) The relative fluorescence intensity of Chi-FITC, PAA-FTSC and Chi-C-FITC in the gastrointestinal tract (esophagus, stomach and intestine) at 10 h after administration. (C) The fluorescence in the liver, spleen, kidneys, esophagus, stomach, and small/large intestine at 10 h after administration are shown (mean ± SD, n = 3 mice/time point). (* denotes statistical significant difference at $p < 0.05$, ** indicates $p < 0.005$). (D) The human-insulin (closed triangle), h-insulin/chitosan (closed circle) and h-insulin/chitosan-catechol (open circle) were orally administered to Wistar rats and blood insulin concentration was measured using enzyme-linked immunosorbent assay (ELISA) ($n$ = 4 rats/time point). Reprinted from (Kim et al., 2015) with permission of Elsevier.

### 1.4.9 Methyl Pyrrolidinone Chitosan

Methyl pyrrolidinone chitosan can be synthesized by reacting chitosan with levulinic acid (Figure 1.21) (Muzzarelli, 1992; Muzzarelli et al., 1993). Specific experimental conditions including pH of the reaction mixture, type and the rate of addition of reducing agents ($NaCNBH_3$ or $NaBH_4$), molar ratio of levulinic acid/chitosan/reducing agents are required to obtain methyl pyrrolidinone chitosan and not *N*-carboxybutylchitosan derivatives

(Rinaudo et al., 2001; Kurita & Isogai, 2010). Sandri et al. (2004) studied the mucoadhesive and penetration enhancing properties of various chitosans including 5-methyl pyrrolidinone chitosan, low molecular weight chitosan, a partially re-acetylated chitosan and chitosan HCl using buccal or submaxillary bovine mucin dispersion, vaginal mucosa or porcine gastric mucin dispersion. It was found that different chitosans behaved differently in different substrates. In submaxillary mucin dispersion, chitosan HCl was the most mucoadhesive. However, 5-methyl pyrrolidinone chitosan showed the greatest mucoadhesion among other polymers in all other studied substrates and provided the greatest permeation of acyclovir through porcine cheek mucosa and deepest penetration into the vaginal mucosa. This could be due to the penetration enhancing effect of 5-methyl pyrrolidinone, which has been demonstrated in other studies (Sasaki et al., 1991; Kim et al., 1993).

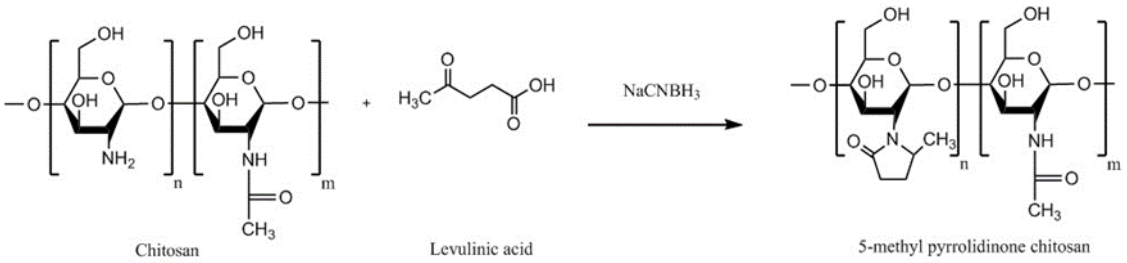


Figure 1.21 Synthetic pathway to 5-methyl pyrrolidinone chitosan.

### 1.4.10 Cyclodextrin-chitosan

Cyclodextrins can enhance solubility and dissolution of poorly water-soluble drugs by forming inclusion complexes. In 2001, the idea of grafting cyclodextrin to chitosan was adopted by Auzély-Velty and Rinaudo (2001), who used a reductive amination approach, where a solution of chitosan in acetic acid/methanol was reacted with aldehyde-containing cyclodextrin derivative in the presence of sodium cyanoborohydride ($NaCNBH_3$). The reaction was mediated with EDAC. The inclusion ability of the grafted-cyclodextrin was studied using NMR spectroscopy and found that it could form inclusion complexes with two model compounds tert-butylbenzoic acid and (+)-catechin.

In 2006, Venter et al. (2006) studied the mucoadhesion of this cyclodextrin-chitosan derivative by tensile separation test (microbalance method) using partially purified porcine gastric mucin type III (Sigma, UK) as a substrate. Figure 1.22 shows the experimental set-up for the mucoadhesion study. Briefly, the aluminum plates of the apparatus were coated with the polymer solution (1% w/v) and left to dry until polymeric films formed. Mucin

solution (30% w/v) was prepared and placed in a water bath (25 °C). The polymer-coated plate was lowered to contact with the mucin solution for 2 min. Then, the maximum detachment force to separate the polymeric films from the mucin solution was measured using a computerized system. It was found that upon derivatization, chitosan lost its mucoadhesive properties by 13.5%, but, it was 12% stronger than pectin.

In another study, Chaleawlert-umpon et al. (2011) synthesized citrated cyclodextrin-g-chitosan. In this study, citric acid was used to facilitate cyclodextrin mobility. Glycidyl trimethylammonium chloride was also used to quaternize chitosan. The mucoadhesion study using mucin-particle interaction method and SPR revealed that combination of quaternization and citrate modification led to a significant enhancement in the mucoadhesive interactions. This could be due to an increase in the cationic charge of chitosan as well as hydrogen bonding between carboxyl and hydroxyl groups of the spacer and the mucus components.

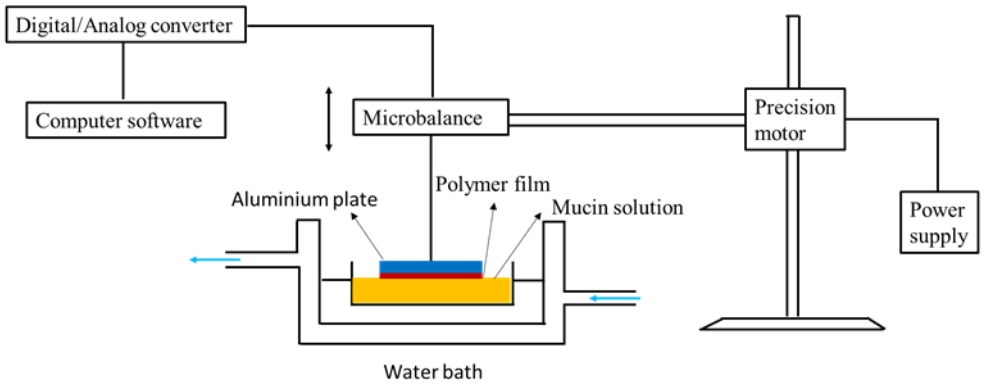


Figure 1.22 Experimental set-up for evaluation of mucoadhesion using microbalance method according to Venter et al. (2006) with some modifications.

### 1.4.11 Oleoyl-quaternised chitosan

Yostawonkul et al. (2017) developed a nanostructure lipid carrier for the delivery of lipophilic drug molecules using high-pressure homogenization technique. They found coating of these carriers with oleoyl-quaternised chitosan enhanced carcinoma Caco-2 cellular uptake of the model drug (alpha-mangostin). This enhancement could be due to the mucoadhesive properties of oleoyl-quaternised chitosan, which was evaluated by mucin-particle interaction method. However, cytotoxicity of the carriers was also increased and thus the authors suggested careful optimization of the drug loading to target cancer cells for chemotherapy.

## 1.5 Comparison of different chitosan derivatives

Table 1 illustrates the advantages and disadvantages of different chitosan-based systems reported in the literature together with the drug model, administration routes and mucus substrates types that were used to evaluate them.

Table 1.1 A summary of chitosan derivatives properties with examples of drug candidates used in the mucoadhesive drug delivery evaluation.

| Chitosan Derivatives | Advantages | Disadvantages | Drug | Route of Administration/ Substrate | References |
|---|---|---|---|---|---|
| Trimethyl chitosan | Soluble at broad range of pHs (2-12), strong mucoadhesion; decreased TEER; increased paracellular permeability of basic or neutral macromolecules | Strong aggregation with anionic macromolecules such as heparin | Buserelin, ropinirol HCl | Oral, small intestine, cattle nasal mucosa | (Sieval et al., 1998; Thanou et al., 2000; Pardeshi & Belgamwar, 2016) |
| N-carboxymethyl chitosan | Decreased TEER; increased paracellular permeability of anionic macromolecules | Insoluble at pH 3-7 (depending on the degree of substitution) due to its polyampholytic character | Low molecular weight heparin; Ofloxacin | Oral, rat small intestine; Ocular, rabbit eyes, in vivo | (Chen & Park, 2003; Di Colo et al., 2004; Thanou et al., 2001) |
| Chitosan-cysteine | Same mucoadhesion as unmodified chitosan, improved cohesion compared to unmodified chitosan, permeation enhancing effect | Susceptible to premature oxidation, undesirable side reactions led to the formation of (chitosan-cysteine-cysteine)$_n$ side chains | - | Oral, porcine intestinal mucosa | (Bernkop-Schnürch et al., 1999a; Bonengel & Bernkop-Schnürch, 2014) |
| Chitosan-N-acetylcysteine | 50-fold longer retention time than unmodified chitosan, biodegradability as indicated by the reduction of its solution viscosity after addition of hen white egg | Susceptible to premature oxidation | - | Oral, flat faced-discs, porcine intestinal mucosa | (Schmitz et al., 2008) |
| Chitosan-TGA | Controlled drug release, longer disintegration time (up to 100-fold) and 26-fold longer mucoadhesion time against unmodified chitosan | Need of mediator such as EDAC | Clotrimazole | Vaginal, tablets, bovine vaginal mucosa | (Kast et al., 2002) |

| | | | | | |
|---|---|---|---|---|---|
| Chitosan-TBA | Strong mucoadhesion, permeation enhancing effect, controlled release, no need for mediator | Prone to oxidation. In addition, unintended cyclisation side reactions | Insulin, cefadroxil | Oral, tablets, porcine and rat intestinal mucosa | (Bernkop-Schnürch et al., 2004a; Krauland et al., 2004) |
| chitosan–thioethylamidine | Much quicker synthetic reaction rate than chitosan-TBA (1.5 h vs 24 h), 8.9-fold longer mucosal detachment time than unmodified chitosan, controlled release, no cyclisation side reactions as in chitosan-TBA | Stability issues | FITC-dextran | Oral, tablets, porcine intestinal mucosa | (Kafedjiiski et al., 2005b) |
| Chitosan-glutathione | Improved stability compared to unmodified chitosan, enhanced mucoadhesion (9.9-fold increased adhesion force and 55-fold longer adhesion time), 4.9-fold higher permeation-enhancing effect against unmodified chitosan, used as oxidative stress suppressant | Stability issues | Thymopentin | Oral, tablets, *in vitro* porcine rat intestinal mucosa; Oral nanoparticles, *in vivo* rats; Injectable hydrogels | (Kafedjiiski et al., 2005a; Jin et al., 2011; Li et al., 2013) |
| Pre-activated (S-protected) thiolated chitosan | Improved stability and mucoadhesion compared to unmodified chitosan and unprotected thiolated chitosan | 2-fold less swelling than unmodified chitosan | Leuprolide; Antide | Oral, tablets, porcine intestinal mucosa; Oral, rat intestinal mucosa | (Dünnhaupt et al., 2012a; Dünnhaupt et al., 2012c) |
| Acrylated chitosan | Strong mucoadhesion, water-soluble | Use of low molecular weight PEGDA results in a weaker mucoadhesion | - | Oral, porcine intestinal mucosa | (Shitrit & Bianco-Peled, 2017) |
| Half-acetylated chitosan | Better solubility at higher pH (up to 7.4) compared to unmodified chitosan, sustained drug release | Less mucoadhesive compared to unmodified chitosan | Ibuprofen | Oral, porcine gastric mucosa | (Sogias et al., 2012) |
| Palmitoyl glycol chitosan | Amphiphilic property, diminished erosion and slow hydration led to controlled release, control bioadhesive strength by changing the degree of palmitoylation | Potential problems with reproducibility with the degrees of substitution related to insolubility of the final product | FITC-dextran | Buccal/disc shaped gels, porcine buccal mucosa | (Martin et al., 2002) |

| | | | | | |
|---|---|---|---|---|---|
| Hexanoyl glycol chitosan | In situ gelling property, *in vivo* ocular retention, longer duration of action | - | Rhodamine, brimonidine | Ocular, rabbit, *in vivo* ocular tissues | (Cho et al., 2016b) |
| Chitosan-enzyme inhibitors | Protects drugs from enzymatic degradation. Controlled antipain release over 6 h, mucoadhesive properties preserved | Potential stability issues | Insulin | Oral, flat-faced discs, porcine intestinal mucosa | (Bernkop-Schnürch et al., 1997) |
| Chitosan-EDTA | Better mucoadhesion than unmodified chitosan<br>Inhibits Zn and Co-dependent proteases including carboxypeptidase A and aminopeptidase N | No Ca-dependent serine proteases inhibition | - | Oral, flat-faced discs, porcine intestinal mucosa | (Bernkop-Schnürch & Krajicek, 1998) |
| Chitosan-enzyme inhibitors-EDTA | Strong inhibitory action against serine proteases, Zn-dependent exopeptidases including carboxypeptidase A and B, aminopeptidase N | Less mucoadhesive than unmodified chitosan and chitosan-EDTA | - | Oral, flat-faced discs, porcine intestinal mucosa | (Bernkop-Schnürch & Scerbe-Saiko, 1998 ) |
| Chitosan-catechol conjugate | Strong mucoadhesion, higher solubility at neutral pH, sustained drug release, improved therapeutic effect *in vivo* compared to unmodified chitosan | Poor mucoadhesion in acidic environment, optimum degree of substitution (7.2%) is required to achieve water-soluble product and formation of large gel-like aggregates has been observed for greater degree of substitution (12.7%) | Lidocaine; Sulfasalazine | Oral, mice gastrointestinal tract, porcine gastric mucin type II; Buccal, hydrogels, porcine and rabbit buccal mucosa; Rectal, hydrogels, mice rectal mucosa *in vivo* | (Kim et al., 2013; Kim et al., 2015; Xu et al., 2015; Xu et al., 2017) |
| Methyl pyrrolidinone chitosan | Greater mucoadhesion and penetration enhancing effect than unmodified chitosan | - | Acyclovir | Buccal and vaginal, porcine cheek or submaxillary bovine mucin, vaginal mucosa, or porcine gastric mucin | (Sandri et al., 2004) |

| | | | | | |
|---|---|---|---|---|---|
| Chitosan-cyclodextrin | Inclusion ability, sustained release | Weaker mucoadhesion than the parent chitosan | - | Porcine gastric mucin | (Auzély-Velty & Rinaudo, 2001; Venter et al., 2006) |

## 1.6 Conclusions

In this review, general methods of synthesis of potential mucoadhesive chitosan derivatives have been highlighted. Some properties of chitosan and chitosan derivatives have been discussed. These include solubility profile, stability, mucoadhesive and permeation enhancing effects. The mucoadhesive properties of the derivatives have been particularly considered. It was shown that the mucoadhesive properties of some derivatives have been significantly increased compared to unmodified chitosan. In the majority of cases, this resulted in an enhancement in the bioavailability and a significant improvement of the therapeutic efficacy of several candidate drugs compared to unmodified chitosan. In some others, the mucoadhesive character either did not change or slightly decreased. This however, was compensated with an improvement of other important chitosan properties including solubility in physiological pH and cohesiveness, which are crucial parameters in mucoadhesion. Therefore, improvement in the properties of chitosan derivatives discussed in this review clearly demonstrate that its chemical modification could potentially lead to further advances in transmucosal drug delivery. However, chemical modification of chitosan has limitations. These include low reproducibility, especially with hydrophobically-modified chitosans, poor solubility of chitosan in organic solvents used for the synthesis and changes with the degree of acetylation during chemical modification.

## 1.7 Acknowledgments

We are thankful to HCED-Iraq for funding this research.

## 1.8 References

Agnihotri, S.A., Mallikarjuna, N.N., & Aminabhavi, T.M., 2004. Recent advances on chitosan-based micro- and nanoparticles in drug delivery. J. Control. Release 100, 5-28.

Akiyama, Y., Lueβen, H.L., de Boer, A.G., Verhoef, J.C., & Junginger, H.E., 1996. Novel peroral dosage forms with protease inhibitory activities. II. Design of fast dissolving poly(acrylate) and controlled drug-releasing capsule formulations with trypsin inhibiting properties. Int. J. Pharm. 138, 13-23.

Albarkah, Y.A., Green, R.J., & Khutoryanskiy, V.V., 2015. Probing the mucoadhesive interactions between porcine gastric mucin and some water-soluble polymers. Macromol. Biosci. 15, 1546-1553.

An, N.T., Dung, P.L., Thien, D.T., Dong, N.T., & Nhi, T.T.Y., 2008. An improved method for synthesizing N,N′-dicarboxymethylchitosan. Carbohydr. Polym. 73, 261-264.

An, N.T., Thien, D.T., Dong, N.T., & Dung, P.L., 2009. Water-soluble N-carboxymethylchitosan derivatives: Preparation, characteristics and its application. Carbohydr. Polym. 75, 489-497.

Atuma, C., Strugala, V., Allen, A., & Holm, L., 2001. The adherent gastrointestinal mucus gel layer: Thickness and physical state *in vivo*. Am J Physiol Gastrointest Liver Physiol 280, G922-G929.

Auzély-Velty, R., & Rinaudo, M., 2001. Chitosan derivatives bearing pendant cyclodextrin cavities: Synthesis and inclusion performance. Macromolecules 34, 3574-3580.

Bansil, R., & Turner, B.S., 2006. Mucin structure, aggregation, physiological functions and biomedical applications. Curr. Opin. Colloid Interface Sci. 11, 164-170.

Barthelmes, J., Perera, G., Hombach, J., Dünnhaupt, S., & Bernkop-Schnürch, A., 2011. Development of a mucoadhesive nanoparticulate drug delivery system for a targeted drug release in the bladder. Int. J. Pharm. 416, 339-345.

Behrens, I., Pena, A.I., Alonso, M.J., & Kissel, T., 2002. Comparative uptake studies of bioadhesive and non-bioadhesive nanoparticles in human intestinal cell lines and rats: The effect of mucus on particle adsorption and transport. Pharm. Res. 19, 1185-1193.

Benediktsdóttir, B.E., Gaware, V.S., Rúnarsson, Ö.V., Jónsdóttir, S., Jensen, K.J., & Másson, M., 2011. Synthesis of N,N,N-trimethyl chitosan homopolymer and highly substituted N-alkyl-N,N-dimethyl chitosan derivatives with the aid of di-tert-butyldimethylsilyl chitosan. Carbohydr. Polym. 86, 1451-1460.

Bernkop-Schnürch, A., 2000. Chitosan and its derivatives: Potential excipients for peroral peptide delivery systems. Int. J. Pharm. 194, 1–13.

Bernkop-Schnürch, A., Brandt, U.M., & Clausen, A.E., 1999a. Synthesis and *in vitro* evaluation of chitosan-cysteine conjugates Sci. Pharm. 67, 196–208.

Bernkop-Schnürch, A., Bratengeyer, I., & Valenta, C., 1997. Development and *in vitro* evaluation of a drug delivery system protecting from trypsinic degradation. Int. J. Pharm. 157, 17–25.

Bernkop-Schnürch, A., Guggi, D., & Pinter, Y., 2004a. Thiolated chitosans: Development and *in vitro* evaluation of a mucoadhesive, permeation enhancing oral drug delivery system. J. Control. Release 94, 177–186.

Bernkop-Schnürch, A., Hornof, M., & Guggi, D., 2004b. Thiolated chitosans. Eur. J. Pharm. Biopharm. 57, 9-17.

Bernkop-Schnürch, A., Hornof, M., & Zoidl, T., 2003. Thiolated polymers—thiomers: Synthesis and *in vitro* evaluation of chitosan–2-iminothiolane conjugates. Int. J. Pharm. 260, 229-237.

Bernkop-Schnürch , A., & Kast, C.E., 2001. Chemically modified chitosans as enzyme inhibitors. Adv. Drug Del. Rev. 52, 127–137.

Bernkop-Schnürch, A., & Krajicek, M.E., 1998. Mucoadhesive polymers as platforms for peroral peptide delivery and absorption: Synthesis and evaluation of different chitosan–EDTA conjugates. J. Control. Release 50, 215–223.

Bernkop-Schnürch, A., & Scerbe-Saiko, A., 1998 Synthesis and *in vitro* evaluation of chitosan-EDTA-protease-inhibitor conjugates which might be useful in oral delivery of peptides and proteins. Pharmceutical Research 15, 263-269.

Bernkop-Schnürch, A., Scholler, S., & Biebel, R.G., 2000. Development of controlled drug release systems based on thiolated polymers. J. Control. Release 66, 39–48.

Bernkop-Schnürch, A., Schwarz, V., & Steininger, S., 1999b. Polymers with thiol groups: A new generation of mucoadhesive polymers. Pharm. Res. 16, 876-881.

Bernkop-Schnürch, A., & Steininger, S., 2000. Synthesis and characterisation of mucoadhesive thiolated polymers. Int. J. Pharm. 194, 239–247.

Boegh, M., & Nielsen, H.M., 2015. Mucus as a barrier to drug delivery – Understanding and mimicking the barrier properties. Basic Clin. Pharmacol. Toxicol. 116, 179–186.

Bonengel, S., & Bernkop-Schnürch, A., 2014. Thiomers-from bench to market. J. Control. Release 195, 120-129.

Bonferoni, M.C., Sandri, G., Ferrari, F., Rossi, S., Larghi, V., Zambito, Y., & Caramella, C., 2010. Comparison of different *in vitro* and *ex vivo* methods to evaluate mucoadhesion of glycol-palmitoyl chitosan micelles. J. Drug Deliv. Sci. Technol. 20, 419-424.

Bonferoni, M.C., Sandri, G., Rossi, S., Ferrari, F., & Caramella, C., 2009. Chitosan and its salts for mucosal and transmucosal delivery. Expert Opinion on Drug Delivery 6, 923-939.

Caramella, C., Ferrari, F., Bonferoni, M.C., Rossi, S., & Sandri, G., 2010. Chitosan and its derivatives as drug penetration enhancers. J. Drug Deliv. Sci. Technol. 20, 5-13.

Casettari, L., Vllasaliu, D., Castagnino, E., Stolnik, S., Howdle, S., & Illum, L., 2012. PEGylated chitosan derivatives: Synthesis, characterisations and pharmaceutical applications. Prog. Polym. Sci. 37, 659-685.

Casettari, L., Vllasaliu, D., Mantovani, G., Howdle, S.M., Stolnik, S., & Illum, L., 2010. Effect of PEGylation on the toxicity and permeability enhancement of chitosan. Biomacromolecules 11, 2854–2865.

Chaleawlert-umpon, S., Nuchuchua, O., Saesoo, S., Gonil, P., Ruktanonchai, U.R., Sajomsang, W., & Pimpha, N., 2011. Effect of citrate spacer on mucoadhesive properties of a novel water-soluble cationic β-cyclodextrin-conjugated chitosan. Carbohydr. Polym. 84, 186-194.

Chen, X.-G., & Park, H.-J., 2003. Chemical characteristics of O-carboxymethyl chitosans related to the preparation conditions. Carbohydr. Polym. 53, 355-359.

Cho, I.S., Cho, M.O., Li, Z., Nurunnabi, M., Park, S.Y., Kang, S.-W., & Huh, K.M., 2016a. Synthesis and characterization of a new photo-crosslinkable glycol chitosan thermogel for biomedical applications. Carbohydr. Polym. 144, 59-67.

Cho, I.S., Park, C.G., Huh, B.K., Cho, M.O., Khatun, Z., Li, Z., Kang, S.-W., Choy, Y.B., & Huh, K.M., 2016b. Thermosensitive hexanoyl glycol chitosan-based ocular delivery system for glaucoma therapy. Acta Biomater. 39, 124-132.

Date, A.A., Hanes, J., & Ensign, L.M., 2016. Nanoparticles for oral delivery: Design, evaluation and state-of-the-art. J. Control. Release 240, 504-526.

Davidovich-Pinhas, M., & Bianco-Peled, H., 2010. Novel mucoadhesive system based on sulfhydryl-acrylate interactions. J. Mater. Sci.: Mater. Med. 21, 2027-2034.

Davidovich-Pinhas, M., & Bianco-Peled, H., 2011. Alginate-PEGAc: A new mucoadhesive polymer. Acta Biomater. 7, 625-633.

de Britto, D., & Assis, O.B.G., 2007. A novel method for obtaining a quaternary salt of chitosan. Carbohydr. Polym. 69, 305-310.

Deacona, M.P., Davis, S.S., White, R.J., Nordman, H., Carlstedt, I., Errington, N., Rowe, A.J., & Harding, S.E., 1999. Are chitosan–mucin interactions specific to different regions of the stomach? Velocity ultracentrifugation offers a clue. Carbohydr. Polym. 38, 235–238.

Deli, M.A., 2009. Potential use of tight junction modulators to reversibly open membranous barriers and improve drug delivery. Biochim. Biophys. Acta, Biomembr. 1788, 892-910.

DeSesso, J.M., & Jacobson, C.F., 2001. Anatomical and physiological parameters affecting gastrointestinal absorption in humans and rats. Food Chem. Toxicol. 39, 209-228.

Di Colo, G., Zambito, Y., Burgalassi, S., Nardini, I., & Saettone, M.F., 2004. Effect of chitosan and N-carboxymethylchitosan on intraocular penetration of topically applied ofloxacin. Int. J. Pharm. 273, 37-44.

Dung, P.L., Milas, M., Rinaudo, M., & Desbrières, J., 1994. Water soluble derivatives obtained by controlled chemical modifications of chitosan. Carbohydr. Polym. 24, 209-214.

Dünnhaupt, S., Barthelmes, J., Hombach, J., Sakloetsakun, D., Arkhipova, V., & Bernkop-Schnürch, A., 2011. Distribution of thiolated mucoadhesive nanoparticles on intestinal mucosa. Int. J. Pharm. 408, 191-199.

Dünnhaupt, S., Barthelmes, J., Iqbal, J., Perera, G., Thurner, C.C., Friedl, H., & Bernkop-Schnürch, A., 2012a. *In vivo* evaluation of an oral drug delivery system for peptides based on S-protected thiolated chitosan. J. Control. Release 160, 477-485.

Dünnhaupt, S., Barthelmes, J., Rahmat, D., Leithner, K., Thurner, C.C., Friedl, H., & Bernkop-Schnürch, A., 2012b. S-protected thiolated chitosan for oral delivery of hydrophilic macromolecules: Evaluation of permeation enhancing and efflux pump inhibitory properties. Mol. Pharm. 9, 1331-1341.

Dünnhaupt, S., Barthelmes, J., Thurner, C.C., Waldner, C., Sakloetsakun, D., & Bernkop-Schnürch, A., 2012c. S-protected thiolated chitosan: Synthesis and *in vitro* characterization. Carbohydr. Polym. 90, 765-772.

Eshel-Green, T., & Bianco-Peled, H., 2016. Mucoadhesive acrylated block copolymers micelles for the delivery of hydrophobic drugs. Colloids Surf. B. Biointerfaces 139, 42-51.

Föger, F., Schmitz, T., & Bernkop-Schnürch, A., 2006. *In vivo* evaluation of an oral delivery system for P-gp substrates based on thiolated chitosan. Biomaterials 27, 4250-4255.

Foster, S.N.E., Pearson, J.P., Huton, D.A., Allen, A., & Detmar, P.W., 1994. Interaction of polyacrylates with porcine pepsin and the gastric mucus barrier: A mechanism for mucosal protection. Clin. Sci. 87, 719-726.

Ganguly, S., & Dash, A.K., 2004. A novel in situ gel for sustained drug delivery and targeting. Int. J. Pharm. 276, 83-92.

Ge, H.-C., & Luo, D.-K., 2005. Preparation of carboxymethyl chitosan in aqueous solution under microwave irradiation. Carbohydr. Res. 340, 1351-1356.

Grabovac, V., Guggi, D., & Bernkop-Schnürch, A., 2005. Comparison of the mucoadhesive properties of various polymers. Adv. Drug Del. Rev. 57, 1713-1723.

Grießinger, J.A., Hauptstein, S., Laffleur, F., Netsomboon, K., & Bernkop-Schnürch, A., 2016. Evaluation of the impact of multivalent metal ions on the permeation behavior of Dolutegravir sodium. Drug Dev. Ind. Pharm. 42, 1118-1126.

Guggi, D., Kast, C.E., & Bernkop-Schnürch, A., 2003. *In vivo* evaluation of an oral salmon calcitonin-delivery system based on a thiolated chitosan carrier matrix. Pharm. Res. 20, 1989-1994.

Gullberg, E., Cao, S., Berg, O.G., Ilback, C., Sandegren, L., Hughes, D., & Andersson, D.I., 2011. Selection of resistant bacteria at very low antibiotic concentrations. PLoS Pathog. 7, e1002158.

Hakimi, S., Mortazavian, E., Mohammadi, Z., Samadi, F.Y., Samadikhah, H., Taheritarigh, S., Tehrani, N.R., & Rafiee-Tehrani, M., 2017. Thiolated methylated dimethylaminobenzyl chitosan: A novel chitosan derivative as a potential delivery vehicle. Int. J. Biol. Macromol. 95, 574-581.

Hamman, J.H., Schultz, C.M., & Kotzé, A.F., 2003. N-trimethyl chitosan chloride: Optimum degree of quaternization for drug absorption enhancement across epithelial cells. Drug Dev. Ind. Pharm. 29, 161-172.

Hauptstein, S., Boengel, S., Griessinger, J., & Bernkop-Schnürch, A., 2014. Synthesis and characterization of pH tolerant and mucoadhesive (thiol–polyethylene glycol) chitosan graft polymer for drug delivery. J. Pharm. Sci. 103, 594–601.

Hejazi, R., & Amiji, M., 2003. Chitosan-based gastrointestinal delivery systems. J. Control. Release 89, 151-165.

Illum, L., Farraj, N.F., & Davis, S.S., 1994. Chitosan as a novel nasal delivery system for peptide drugs. Pharm. Res. 11, 1186-1189.

Illum, L., Jabbal-Gill, I., Hinchcliffe, M., Fisher, A.N., & Davis, S.S., 2001. Chitosan as a novel nasal delivery system for vaccines. Adv. Drug Del. Rev. 51, 81-96.

Irmukhametova, G.S., Mun, G.A., & Khutoryanskiy, V.V., 2011. Thiolated mucoadhesive and PEGylated nonmucoadhesive organosilica nanoparticles from 3-mercaptopropyltrimethoxysilane. Langmuir 27, 9551-9556.

Issa, M.M., Köping-Höggård, M., & Artursson, P., 2005. Chitosan and the mucosal delivery of biotechnology drugs. Drug Discovery Today: Technol. 2, 1-6.

Jayakumar, R., Prabaharan, M., Nair, S.V., Tokura, S., Tamura, H., & Selvamurugan, N., 2010. Novel carboxymethyl derivatives of chitin and chitosan materials and their biomedical applications. Prog. Mater Sci. 55, 675-709.

Jeong, Y.-I., Kim, D.-G., Jang, M.-K., & Nah, J.-W., 2008. Preparation and spectroscopic characterization of methoxy poly(ethylene glycol)-grafted water-soluble chitosan. Carbohydr. Res. 343, 282–289.

Jin, X., Xu, Y., Shen, J., Ping, Q., Su, Z., & You, W., 2011. Chitosan–glutathione conjugate-coated poly(butyl cyanoacrylate) nanoparticles: Promising carriers for oral thymopentin delivery. Carbohydr. Polym. 86, 51-57.

Jintapattanakit, A., Junyaprasert, V.B., & Kissel, T., 2009. The role of mucoadhesion of trimethyl chitosan and PEGylated trimethyl chitosan nanocomplexes in insulin uptake. J. Pharm. Sci. 98, 4818-4830.

Jonker, C., Hamman, J.H., & Kotzé, A.F., 2002. Intestinal paracellular permeation enhancement with quaternised chitosan: In situ and *in vitro* evaluation. Int. J. Pharm. 238, 205–213.

Kafedjiiski, K., Föger, F., Werle, M., & Bernkop-Schnürch, A., 2005a. Synthesis and *in vitro* evaluation of a novel chitosan-glutathione conjugate. Pharm. Res. 22, 1480-1488.

Kafedjiiski, K., Krauland, A.H., Hoffer, M.H., & Bernkop-Schnürch, A., 2005b. Synthesis and *in vitro* evaluation of a novel thiolated chitosan. Biomaterials 26, 819-826.

Kaldybekov, D.B., Tonglairoum, P., Opanasopit, P., & Khutoryanskiy, V.V., 2018. Mucoadhesive maleimide-functionalised liposomes for drug delivery to urinary bladder. Eur. J. Pharm. Sci. 111, 83-90.

Kast, C.E., Frick, W., Losert, U., & Bernkop-Schnürch, A., 2003. Chitosan-thioglycolic acid conjugate: A new scaffold material for tissue engineering? Int. J. Pharm. 256, 183-189.

Kast, C.E., Valenta, C., Leopold, M., & Bernkop-Schnürch, A., 2002. Design and *in vitro* evaluation of a novel bioadhesive vaginal drug delivery system for clotrimazole. J. Control. Release 81, 347-354.

Keely, S., Rullay, A., Wilson, C., Carmichael, A., Carrington, S., Corfield, A., Haddleton, D.M., & Brayden, D.J., 2005. *In vitro* and *ex vivo* intestinal tissue models to measure mucoadhesion of poly (methacrylate) and N-trimethylated chitosan polymers. Pharm. Res. 22, 38-49.

Khutoryanskiy, V.V., 2011. Advances in mucoadhesion and mucoadhesive polymers. Macromol. Biosci. 11, 748-764.

Kim, B.-S., Kim, C.-S., & Lee, K.-M., 2008. The intracellular uptake ability of chitosan-coated Poly (D,L-lactide-co-glycolide) nanoparticles. Arch. Pharmacal Res. 31, 1050-1054.

Kim, C.-K., Hong, M.-S., Kim, Y.-B., & Han, S.-K., 1993. Effect of penetration enhancers (pyrrolidone derivatives) on multilamellar liposomes of stratum corneum lipid: A study by UV spectroscopy and differential scanning calorimetry. Int. J. Pharm. 95, 43-50.

Kim, K., Kim, K., Ryu, J.H., & Lee, H., 2015. Chitosan-catechol: A polymer with long-lasting mucoadhesive properties. Biomaterials 52, 161-170.

Kim, K., Ryu, J.H., Lee, D.Y., & Lee, H., 2013. Bio-inspired catechol conjugation converts water-insoluble chitosan into a highly water-soluble, adhesive chitosan derivative for hydrogels and LbL assembly. Biomaterials Science 1, 783-790.

Koo, S.H., Lee, J.-S., Kim, G.-H., & Lee, H.G., 2011. Preparation, characteristics, and stability of glutathione-loaded nanoparticles. J. Agric. Food Chem. 59, 11264-11269.

Kotzé, A.F., de Leeuw, B.J., Lueßen, H.L., de Boer, A.G., Verhoef, J.C., & Junginger, H.E., 1997. Chitosans for enhanced delivery of therapeutic peptides across intestinal epithelia: *In vitro* evaluation in Caco-2 cell monolayers. Int. J. Pharm. 159, 243–253.

Krauland, A.H., Guggi, D., & Bernkop-Schnürch, A., 2004. Oral insulin delivery: The potential of thiolated chitosan-insulin tablets on non-diabetic rats. J. Control. Release 95, 547–555.

Krauland, A.H., Leitner, V.M., Grabovac, V., & Bernkop-Schnürch, A., 2006. *In vivo* evaluation of a nasal insulin delivery system based on thiolated chitosan. J. Pharm. Sci. 95, 2463-2472.

Kulkarni, A.D., Patel, H.M., Surana, S.J., Vanjari, Y.H., Belgamwar, V.S., & Pardeshi, C.V., 2017. N,N,N-Trimethyl chitosan: An advanced polymer with myriad of opportunities in nanomedicine. Carbohydr. Polym. 157, 875-902.

Kurita, Y., & Isogai, A., 2010. Reductive N-alkylation of chitosan with acetone and levulinic acid in aqueous media. Int. J. Biol. Macromol. 47, 184-189.

Lai, S.K., Wang, Y.Y., & Hanes, J., 2009a. Mucus-penetrating nanoparticles for drug and gene delivery to mucosal tissues. Adv. Drug Del. Rev. 61, 158-171.

Lai, S.K., Wang, Y.Y., Wirtz, D., & Hanes, J., 2009b. Micro- and macrorheology of mucus. Adv. Drug Del. Rev. 61, 86-100.

Langoth, N., Kahlbacher, H., Schöffmann, G., Schmerold, I., Schuh, M., Franz, S., Kurka, P., & Bernkop-Schnürch, A., 2006. Thiolated chitosans: Design and *in vivo* evaluation of a mucoadhesive buccal peptide drug delivery system. Pharm. Res. 23, 573-579.

Leal, J., Smyth, H.D.C., & Ghosh, D., 2017. Physicochemical properties of mucus and their impact on transmucosal drug delivery. Int. J. Pharm. 532, 555-572.

Lee, C.R., Cho, I.H., Jeong, B.C., & Lee, S.H., 2013. Strategies to minimize antibiotic resistance. Int. J. Environ. Res. Public Health 10, 4274-4305.

Lee, H., Scherer, N.F., & Messersmith, P.B., 2006. Single-molecule mechanics of mussel adhesion. Proceedings of the National Academy of Sciences 103, 12999-13003.

Li, J., Shu, Y., Hao, T., Wang, Y., Qian, Y., Duan, C., Sun, H., Lin, Q., & Wang, C., 2013. A chitosan–glutathione based injectable hydrogel for suppression of oxidative stress damage in cardiomyocytes. Biomaterials 34, 9071-9081.

Liu, M., Zhang, J., Zhu, X., Shan, W., Li, L., Zhong, J., Zhang, Z., & Huang, Y., 2016. Efficient mucus permeation and tight junction opening by dissociable "mucus-inert" agent coated trimethyl chitosan nanoparticles for oral insulin delivery. J. Control. Release 222, 67-77.

Ma, G., Zhang, X., Han, J., Song, G., & Nie, J., 2009. Photo-polymeriable chitosan derivative prepared by Michael reaction of chitosan and polyethylene glycol diacrylate (PEGDA). Int. J. Biol. Macromol. 45, 499-503.

Mao, S., Shuai, X., Unger, F., Wittmar, M., Xie, X., & Kissel, T., 2005. Synthesis, characterization and cytotoxicity of poly(ethylene glycol)-graft-trimethyl chitosan block copolymers. Biomaterials 26, 6343–6356.

Martien, R., Loretz, B., Thaler, M., Majzoob, S., & Bernkop-Schnürch, A., 2007. Chitosan–thioglycolic acid conjugate: An alternative carrier for oral nonviral gene delivery? J. Biomed. Mater. Res., Part A 82A, 1-9.

Martin, L., Wilson, C.G., Koosha, F., Tetley, L., Gray, A.I., Senel, S., & Uchegbu, I.F., 2002. The release of model macromolecules may be controlled by the hydrophobicity of palmitoyl glycol chitosan hydrogels. J. Control. Release 80, 87-100.

Mei, D., Mao, S., Sun, W., Wang, Y., & Kissel, T., 2008. Effect of chitosan structure properties and molecular weight on the intranasal absorption of tetramethylpyrazine phosphate in rats. Eur. J. Pharm. Biopharm. 70, 874-881.

Moghaddam, F.A., Atyabi, F., & Dinarvand, R., 2009. Preparation and *in vitro* evaluation of mucoadhesion and permeation enhancement of thiolated chitosan-pHEMA core-shell nanoparticles. Nanomedicine 5, 208-215.

Mortazavi, S.A., Carpenter, B.G., & Smart, J.D., 1993. A comparative study on the role played by mucus glycoproteins in the rheological behaviour of the mucoadhesive/mucosal interface. Int. J. Pharm. 94, 195-201.

Mun, E.A., Williams, A.C., & Khutoryanskiy, V.V., 2016. Adhesion of thiolated silica nanoparticles to urinary bladder mucosa: Effects of PEGylation, thiol content and particle size. Int. J. Pharm. 512, 32-38.

Muzzarelli, R. (1992). Italy Patent No. WO1992009635 A1.

Muzzarelli, R.A.A., llari, P., & Tomasetti, M., 1993. Preparation and characteristic properties of 5-methyl pyrrolidinone chitosan. Carbohydr. Polym. 20, 99-105.

Muzzarelli, R.A.A., & Tanfani, F., 1985. The N-permethylation of chitosan and the preparation of N-trimethyl chitosan iodide. Carbohydr. Polym. 5, 297-307.

Nazar, H., Fatouros, D.G., van der Merwe, S.M., Bouropoulos, N., Avgouropoulos, G., Tsibouklis, J., & Roldo, M., 2011. Thermosensitive hydrogels for nasal drug delivery: The formulation and characterisation of systems based on N-trimethyl chitosan chloride. Eur. J. Pharm. Biopharm. 77, 225-232.

Netsomboon, K., Suchaoin, W., Laffleur, F., Prüfert, F., & Bernkop-Schnürch, A., 2017. Multifunctional adhesive polymers: Preactivated thiolated chitosan-EDTA conjugates. Eur. J. Pharm. Biopharm. 111, 26-32.

Palazzo, C., Trapani, G., Ponchel, G., Trapani, A., & Vauthier, C., 2017. Mucoadhesive properties of low molecular weight chitosan- or glycol chitosan- and corresponding thiomer-coated poly(isobutylcyanoacrylate) core-shell nanoparticles. Eur. J. Pharm. Biopharm. 117, 315-323.

Pardeshi, C.V., & Belgamwar, V.S., 2016. Controlled synthesis of N,N,N-trimethyl chitosan for modulated bioadhesion and nasal membrane permeability. Int. J. Biol. Macromol. 82, 933-944.

Patel, M.M., Smart, J.D., Nevell, T.G., Ewen, R.J., Eaton, P.J., & Tsibouklis, J., 2003. Mucin/poly(acrylic acid) interactions: A spectroscopic investigation of mucoadhesion. Biomacromolecules 4, 1184-1190.

Peppas, N.A., & Buri, P.A., 1985. Surface, interfacial and molecular aspects of polymer bioadhesion on soft tissues. J. Control. Release 2, 257-275.

Peppas, N.A., & Huang, Y., 2004. Nanoscale technology of mucoadhesive interactions. Adv. Drug Del. Rev. 56, 1675-1687.

Pillai, C.K.S., Paul, W., & Sharma, C.P., 2009. Chitin and chitosan polymers: Chemistry, solubility and fiber formation. Prog. Polym. Sci. 34, 641-678.

Prabaharan, M., & Gong, S., 2008. Novel thiolated carboxymethyl chitosan-g-β-cyclodextrin as mucoadhesive hydrophobic drug delivery carriers. Carbohydr. Polym. 73, 117-125.

Prego, C., Fabre, M., Torres, D., & Alonso, M.J., 2006. Efficacy and mechanism of action of chitosan nanocapsules for oral peptide delivery. Pharm. Res. 23, 549-556.

Qin, C., Li, H., Xiao, Q., Liu, Y., Zhu, J., & Du, Y., 2006. Water-solubility of chitosan and its antimicrobial activity. Carbohydr. Polym. 63, 367-374.

Qu, X., Khutoryanskiy, V.V., Stewart, A., Rahman, S., Papahadjopoulos-Sternberg, B., Dufes, C., McCarthy, D., Wilson, C.G., Lyons, R., Carter, K.C., Schätzlein, A., & Uchegbu, I.F., 2006. Carbohydrate-based micelle clusters which enhance hydrophobic drug bioavailability by up to 1 order of magnitude. Biomacromolecules 7, 3452-3459.

Rabea, E.I., Badawy, M.E.-T., Stevens, C.V., Smagghe, G., & Steurbaut, W., 2003. Chitosan as antimicrobial agent: Applications and mode of action. Biomacromolecules 4, 1457-1465.

Riley, R.G., Smart, J.D., Tsibouklis, J., Dettmar, P.W., Hampson, F., Davis, J.A., Kelly, G., & Wilber, W.R., 2001. An investigation of mucus/polymer rheological synergism using synthesised and characterised poly(acrylic acid)s. Int. J. Pharm. 217, 87-100.

Rinaudo, M., Desbrières, J., Le Dung, P., Thuy Binh, P., & Dong, N.T., 2001. NMR investigation of chitosan derivatives formed by the reaction of chitosan with levulinic acid. Carbohydr. Polym. 46, 339-348.

Robinson, J.R., Longer, M.A., & Veillard, M., 1987. Bioadhesive polymers for controlled drug delivery. Ann. N. Y. Acad. Sci. 507, 307-314.

Robinson, J.R., & Mlynek, G.M., 1995. Bioadhesive and phase-change polymers for ocular drug delivery. Adv. Drug Del. Rev. 16, 45-50.

Ryu, J.H., Hong, S., & Lee, H., 2015. Bio-inspired adhesive catechol-conjugated chitosan for biomedical applications: A mini review. Acta Biomater. 27, 101-115.

Ryu, J.H., Lee, Y., Kong, W.H., Kim, T.G., Park, T.G., & Lee, H., 2011. Catechol-functionalized chitosan/pluronic hydrogels for tissue adhesives and hemostatic materials. Biomacromolecules 12, 2653-2659.

Sajomsang, W., Ruktanonchai, U.R., Gonil, P., & Nuchuchua, O., 2009. Mucoadhesive property and biocompatibility of methylated N-aryl chitosan derivatives. Carbohydr. Polym. 78, 945-952.

Sakloetsakun, D., Hombach, J.M.R., & Bernkop-Schnürch, A., 2009. In situ gelling properties of chitosan-thioglycolic acid conjugate in the presence of oxidizing agents. Biomaterials 30, 6151-6157.

Sandri, G., Rossi, S., Ferrari, F., Bonferoni, M.C., Muzzarelli, C., & Caramella, C., 2004. Assessment of chitosan derivatives as buccal and vaginal penetration enhancers. Eur. J. Pharm. Sci. 21, 351-359.

Sasaki, H., Kojima, M., Mori, Y., Nakamura, J., & Shibasaki, J., 1991. Enhancing effect of pyrrolidone derivatives on transdermal penetration of 5-fluorouracil, triamcinolone acetonide, indomethacin, and flurbiprofen. J. Pharm. Sci. 80, 533-538.

Sayin, B., Somavarapu, S., Li, X.W., Sesardic, D., Şenel, S., & Alpar, O.H., 2009. TMC-MCC (N-trimethyl chitosan-mono-N-carboxymethyl chitosan) nanocomplexes for mucosal delivery of vaccines. Eur. J. Pharm. Sci. 38, 362-369.

Schmitz, T., Grabovac, V., Palmberger, T.F., Hoffer, M.H., & Bernkop-Schnürch, A., 2008. Synthesis and characterization of a chitosan-N-acetyl cysteine conjugate. Int. J. Pharm. 347, 79-85.

Serra, L., Domenech, J., & Peppas, N.A., 2009. Engineering design and molecular dynamics of mucoadhesive drug delivery systems as targeting agents. Eur. J. Pharm. Biopharm. 71, 519-528.

Shitrit, Y., & Bianco-Peled, H., 2017. Acrylated chitosan for mucoadhesive drug delivery systems. Int. J. Pharm. 517, 247-255.

Sieval, A.B., Thanou, M., Kotzé, A.F., Verhoef, J.C., Brussee, J., & Junginger, H.E., 1998. Preparation and NMR characterization of highly substituted N-trimethyl chitosan chloride. Carbohydr. Polym. 36, 157-165.

Siew, A., Le, H., Thiovolet, M., Gellert, P., Schatzlein, A., & Uchegbu, I., 2012. Enhanced oral absorption of hydrophobic and hydrophilic drugs using quaternary ammonium palmitoyl glycol chitosan nanoparticles. Mol. Pharm. 9, 14-28.

Smart, J.D., 2005. The basics and underlying mechanisms of mucoadhesion. Adv. Drug Del. Rev. 57, 1556-1568.

Smart, J.D., Kellaway, I.W., & Worthington, H.E.C., 1984. An *in-vitro* investigation of mucosa-adhesive materials for use in controlled drug delivery. J. Pharm. Pharmacol. 36, 295-299.

Smith, J., Wood, E., & Dornish, M., 2004. Effect of chitosan on epithelial cell tight junctions. Pharm. Res. 21, 43-49.

Sogias, I.A., Khutoryanskiy, V.V., & Williams, A.C., 2010. Exploring the factors affecting the solubility of chitosan in water. Macromol. Chem. Phys. 211, 426-433.

Sogias, I.A., Williams, A.C., & Khutoryanskiy, V.V., 2008. Why is chitosan mucoadhesive? Biomacromolecules 9, 1837–1842.

Sogias, I.A., Williams, A.C., & Khutoryanskiy, V.V., 2012. Chitosan-based mucoadhesive tablets for oral delivery of ibuprofen. Int. J. Pharm. 436, 602-610.

Soler, R., Bruschini, H., Martins, J.R., Dreyfuss, J.L., Camara, N.O., Alves, M.T., Leite, K.R., Truzzi, J.C., Nader, H.B., Srougi, M., & Ortiz, V., 2008. Urinary glycosaminoglycans as biomarker for urothelial injury: Is it possible to discriminate damage from recovery? Urology 72, 937-942.

Song, Y., Huang, Z., Song, Y., Tian, Q., Liu, X., She, Z., Jiao, J., Lu, E., & Deng, Y., 2014. The application of EDTA in drug delivery systems: Doxorubicin liposomes loaded via $NH_4$EDTA gradient. International Journal of Nanomedicine 9, 3611-3621.

Štorha, A., Mun, E.A., & Khutoryanskiy, V.V., 2013. Synthesis of thiolated and acrylated nanoparticles using thiol-ene click chemistry: Towards novel mucoadhesive materials for drug delivery. RSC Adv. 3, 12275–12279.

Thanou, M., Florea, B.I., Langemeÿer, M.W.E., Verhoef, J.C., & Junginger, H.E., 2000. N-trimethylated chitosan chloride (TMC) improves the intestinal permeation of the peptide drug buserelin *in vitro* (Caco-2 Cells) and *in vivo* (rats). Pharm. Res. 17, 27-31.

Thanou, M., Nihot, M.T., Jansen, M., Verhoef, J.C., & Junginger, H.E., 2001. Mono-N-carboxymethyl chitosan (MCC), a polyampholytic chitosan derivative, enhances the intestinal absorption of low molecular weight heparin across intestinal epithelia *in vitro* and *in vivo*. J. Pharm. Sci. 90, 38-46.

Thongborisute, J., Takeuchi, H., Yamamoto, H., & Kawashima, Y., 2006. Visualization of the penetrative and mucoadhesive properties of chitosan and chitosan-coated liposomes through the rat intestine. J. Liposome Res. 16, 127-141.

Tonglairoum, P., Brannigan, R.P., Opanasopit, P., & Khutoryanskiy, V.V., 2016. Maleimide-bearing nanogels as novel mucoadhesive materials for drug delivery. J. Mater. Chem. B 4, 6581-6587.

Trapani, A., Sitterberg, J., Bakowsky, U., & Kissel, T., 2009. The potential of glycol chitosan nanoparticles as carrier for low water soluble drugs. Int. J. Pharm. 375, 97-106.

Uchegbu, I.F., Andreas, G.S., Laurence, T., Alexander, I.G., Julieann, S., Soryia, S., & Erasto, M., 1998. Polymeric chitosan-based vesicles for drug delivery. J. Pharm. Pharmacol. 50, 453-458.

Uchegbu, I.F., Carlos, M., McKay, C., Hou, X., & Schätzlein, A.G., 2014. Chitosan amphiphiles provide new drug delivery opportunities. Polym. Int. 63, 1145-1153.

Upadhyaya, L., Singh, J., Agarwal, V., & Tewari, R.P., 2013. Biomedical applications of carboxymethyl chitosans. Carbohydr. Polym. 91, 452-466.

Upadhyaya, L., Singh, J., Agarwal, V., & Tewari, R.P., 2014. The implications of recent advances in carboxymethyl chitosan based targeted drug delivery and tissue engineering applications. J. Control. Release 186, 54-87.

van der Merwe, S.M., Verhoef, J.C., Verheijden, J.H.M., Kotzé, A.F., & Junginger, H.E., 2004. Trimethylated chitosan as polymeric absorption enhancer for improved peroral delivery of peptide drugs. Eur. J. Pharm. Biopharm. 58, 225-235.

Varum, F.J.O., Veiga, F., Sousa, J.S., & Basit, A.W., 2010. An investigation into the role of mucus thickness on mucoadhesion in the gastrointestinal tract of pig. Eur. J. Pharm. Sci. 40, 335-341.

Varum, F.J.O., Veiga, F., Sousa, J.S., & Basit, A.W., 2012. Mucus thickness in the gastrointestinal tract of laboratory animals. J. Pharm. Pharmacol. 64, 218-227.

Venter, J.P., Kotzé, A.F., Auzély-Velty, R., & Rinaudo, M., 2006. Synthesis and evaluation of the mucoadhesivity of a CD-chitosan derivative. Int. J. Pharm. 313, 36-42.

Verheul, R.J., Amidi, M., van der Wal, S., van Riet, E., Jiskoot, W., & Hennink, W.E., 2008. Synthesis, characterization and *in vitro* biological properties of O-methyl free N,N,N-trimethylated chitosan. Biomaterials 29, 3642-3649.

Vikhoreva, G.A., & Galʹbraikh, L.S., 1997. Rheological properties of solutions of chitosan and carboxymethylchitin. Fibre Chemistry 29, 287-291.

Watanabe, S.-I., Takeuchi, T., & Chey, W.Y., 1992. Mediation of trypsin inhibitor-induced pancreatic hypersecretion by secretin and cholecystokinin in rats. Gastroenterology 102, 621-628.

Watts, P., Smith, A., & Hinchcliffe, M. (2014). ChiSys® as a chitosan-based delivery platform for nasal vaccination, in: J. das Neves & B. Sarmento (Eds.), Mucosal Delivery of Biopharmaceuticals: Biology, Challenges and Strategies. Springer US, Boston, MA, pp. 499-516.

Wu, M., Long, Z., Xiao, H., & Dong, C., 2016. Recent research progress on preparation and application of N, N, N-trimethyl chitosan. Carbohydr. Res. 434, 27-32.

Xu, J., Strandman, S., Zhu, J.X.X., Barralet, J., & Cerruti, M., 2015. Genipin-crosslinked catechol-chitosan mucoadhesive hydrogels for buccal drug delivery. Biomaterials 37, 395-404.

Xu, J., Tam, M., Samaei, S., Lerouge, S., Barralet, J., Stevenson, M.M., & Cerruti, M., 2017. Mucoadhesive chitosan hydrogels as rectal drug delivery vessels to treat ulcerative colitis. Acta Biomater. 48, 247-257.

Yin, L., Ding, J., He, C., Cui, L., Tang, C., & Yin, C., 2009. Drug permeability and mucoadhesion properties of thiolated trimethyl chitosan nanoparticles in oral insulin delivery. Biomaterials 30, 5691-5700.

Yostawonkul, J., Surassmo, S., Iempridee, T., Pimtong, W., Suktham, K., Sajomsang, W., Gonil, P., & Ruktanonchai, U.R., 2017. Surface modification of nanostructure lipid carrier (NLC) by oleoyl-quaternized-chitosan as a mucoadhesive nanocarrier. Colloids Surf. B. Biointerfaces 149, 301-311.

# Chapter 2: Potential of silica nanoparticles in mucosal drug delivery

**Abstract**

This chapter outlines the aims and the objectives of this thesis. Then, it provides an introduction to the silica nanoparticles, a brief explanation of the common methods of preparation of silica nanoparticles and highlights their potential in mucosal drug delivery. Also, some safety concerns and biodistribution of silica nanoparticles have been discussed.

## 2.1 Aims and objectives of this thesis

The aim of this thesis was to develop mucoadhesive and mucus-penetrating nanoparticles for oral and nasal mucosal drug delivery. The objectives were as follows:

1. To test the hypothesis that thiolated silica nanoparticles are mucoadhesive in the rat intestinal mucosal model and functionalisation of these nanoparticles with hydrophilic polymers reduces their mucoadhesiveness. Therefore, three types of silica nanoparticles with different surface functionalities (thiolated, PEGylated and POZylated) were synthesised. The mucoadhesive properties of these nanoparticles were evaluated using rat intestinal mucosa *in vitro*.
2. To test the hypothesis that nanoparticles prepared from a more hydrophilic chitosan (modified chitosan) diffuse faster in bovine submaxillary mucin (BSM) solution and penetrate deeper into nasal mucosa compared to the nanoparticles prepared from unmodified chitosan. To this end, different chitosan nanoparticles were prepared using ionic gelation between unmodified or four different modified chitosan (polyethylene glycol (PEG)-, polyhydroxyethyl acrylate (PHEA)-, poly-2-ethyl-2-oxazoline (POZ)- and polyvinyl pyrrolidone (PVP)-chitosan) and TPP. The diffusion of chitosan nanoparticles in BSM solution was evaluated using nanoparticle tracking analysis. Their ability to penetrate into sheep nasal mucosa was evaluated using fluorescence microscopy.
3. To explore the possibilities of loading centrally acting drugs (haloperidol and phenobarbital) into the prepared unmodified chitosan and PVP-chitosan nanoparticles.

## 2.2 Introduction

Among inorganic nanomaterials, silica nanoparticles have attracted a particular attention in nanomedicine. Basically, silica nanoparticles can be classified into nonporous (solid) and mesoporous (with 2-50 nm pore size) both with amorphous silica structure (Tang & Cheng, 2013). Mobil Crystalline Materials-41 (MCM-41) is a type of mesoporous silica nanoparticles which has been extensively used in drug delivery (Slowing et al., 2008; Tang et al., 2012; Manzano & Vallet-Regí, 2018; Narayan et al., 2018). Figure 2.1 shows the transmission electron microscopy image of nonporous and mesoporous (MCM-41) silica nanoparticles.

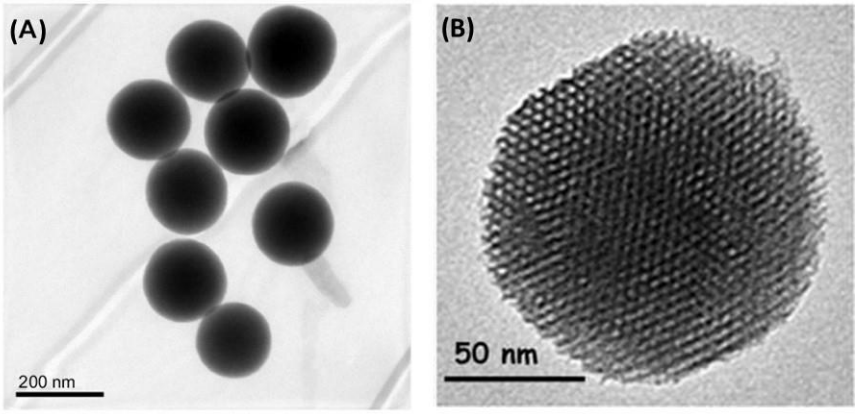


Figure 2.1 Transmission electron microscopy image of (A) nonporous and (B) mesoporous (MCM-41) silica nanoparticles. Reprinted from (Liu et al., 2015) and (Manzano & Vallet-Regí, 2018) with permission of Dove Medical Press and Springer US, respectively.

Generally, both types of silica nanoparticles have similar composition, however, mesoporous silica nanoparticles have a porous structure, lower density and a larger effective surface area compared to the nonporous counterpart (Tang et al., 2012). Due to these unique features, silica nanoparticles provide high loading efficiency and are considered as promising nanocarriers for various agents including, small molecules, macromolecules and vaccines (Wang et al., 2012). Depending on the silica source, silica nanoparticles can also be categorised into inorganic (prepared from pure alkoxysilanes typically tetraethylorthosilicate (TEOS)) and organosilica (from substituted alkoxysilanes, R-$Si(OR')_3$) nanoparticles (Du et al., 2009). Silica exists in nature abundantly and is generally regarded as safe and thus is approved by FDA as an excipient in cosmetics and food (Tang

et al., 2012). Additionally, silica nanoparticles are biocompatible, can be prepared by relatively simple methods using basic laboratory equipment, and can be functionalised using varieties of polymers and fluorescent dyes.

Due to the insolubility of silica and its stability in the harsh gastrointestinal environment (gastric acid and proteases), silica nanoparticles can potentially be used to protect molecules such as enzymes, DNAs and RNAs that are liable to degrade in such environment, and can potentially control their release (Slowing et al., 2008; Wang et al., 2012). This can be an advantage over the biodegradable nanocarriers including polymeric nanoparticles and liposomes, due to their "soft" unstable structure, the drugs would leak out of the carriers once they become in contact with the physiological environment resulting in a premature drug release. This, in most cases, will lead to ineffective therapeutic outcomes and the failure of the site-specific delivery of the drugs (Slowing et al., 2008).

### 2.3 Common methods of preparation of silica nanoparticles

Traditionally, silica nanoparticles are prepared using the Stöber method (Stöber et al., 1968) in which TEOS is used as a silica source, water and ethanol as solvent and ammonia as a catalyst (Figure 2.2).

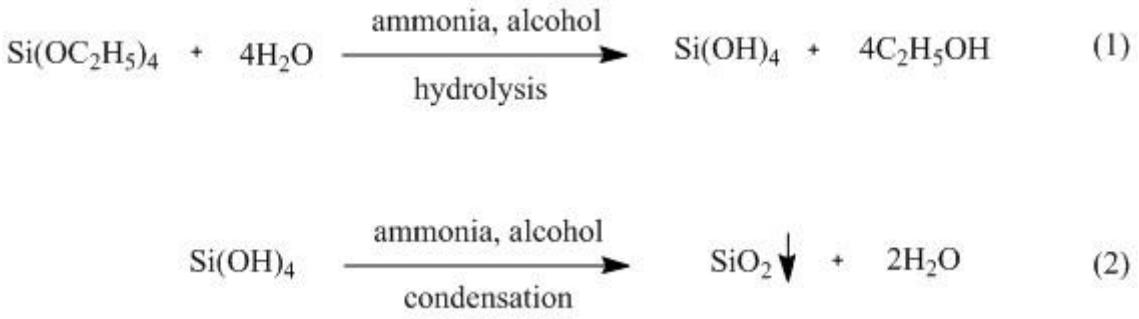


Figure 2.2 A reaction scheme showing the synthesis of silica nanoparticles from TEOS.

Other silica source such as tetramethoxysilane (TMOS), tetrakis-2-hydroxyethylorthosilicate and trimethoxyvinylsilane have been used in the synthesis of silica nanoparticles (Narayan et al., 2018). Several modifications of the Stöber method have been made in order to obtain particles with specific physicochemical properties for example size, polydispersity index, shape and surface functionalities (Rao et al., 2005; Guo et al., 2018). The size and shape of the prepared silica nanoparticles can be controlled by tuning the

concentration of the precursor, the type of the solvent and the catalyst and the reaction temperature (Rao et al., 2005; Tang et al., 2012; Gao et al., 2016; Guo et al., 2018). To prepare mesoporous silica nanoparticles surfactants as structure directing agents including cetyltrimethylammonium bromide (CTAB) and cetyltrimethylammonium chloride (CTAC) are added to the reaction mixture allowing the condensation of the silica precursors in these templates. At the final step, the surfactants will be removed leaving a porous silica nanostructure (Qiao et al., 2009; Lin & Haynes, 2010). Also, pore-expanding agents including alkanes are used to increase the size of the pore as a method to enhance the loading efficiency of the particles (Kao & Mou, 2013). The morphology of the mesoporous silica nanoparticles can be tailored by changing the ratio of the reactants, for instance, doubling the concentration of TEOS, CTAB and NaOH, kept the pore structure and pore size while resulted in the formation of tubes instead of regular sphere silica nanoparticles (Huh et al., 2003).

Nakamura and Ishimura (2007) synthesised thiolated organosilica nanoparticles from organosilicate (3-mercaptopropyltrimethoxysilane, MPTS) using the Stöber method. Later, they reported the possibilities of formation of silica nanoparticles using other organosilicates (3-mercaptopropyltriethoxysilane and 3-mercaptopropylmethyldimethoxysilane) using the Stöber method (with ethanol) and a complete aqueous synthetic technique (without ethanol) (Nakamura & Ishimura, 2008a). These types of the nanoparticles have abundant internal and surface thiol groups enabling their modification with fluorescent dyes and various biomolecules via thiol-maleimide chemistry (Nakamura & Ishimura, 2008b). However, they observed that all these types of organosilica nanoparticles had a wide size distribution (Nakamura & Ishimura, 2007, 2008a). In 2010, they found that performing the synthetic reaction at high temperature (100 °C) instead of room temperature could narrow the size distribution of the MPTS silica nanoparticles (Nakamura et al., 2010).

Silica nanoparticles can also be synthesised using reverse microemulsion method where the silica source (TEOS or TMOS) is added to a preformed water-in-oil emulsion (Osseo-Asare & Arriagada, 1990). Again here, the size of the nanoparticles can be tuned by the composition and the pH of the aqueous phase, changing the type of emulsifier, water to emulsifier ratio, amount of TEOS and the type of organic solvent comprising the organic phase of the emulsion (Finnie et al., 2007; Jin et al., 2008).

## 2.4 Applications of silica nanoparticles in mucosal drug delivery

Silica nanoparticles have a range of potential applications including drug delivery (mucosal and controlled delivery) (Wani et al., 2012; Florek et al., 2017; Maleki et al., 2017; Watermann & Brieger, 2017; M. Ways et al., 2018), diagnostics (Cha & Kim, 2019) and tissue engineering (mainly for bone) (Rosenholm et al., 2016; Yang et al., 2018). This section highlights some of the studies involving silica nanoparticles for mucosal drug delivery. There are several obstacles in mucosal drug delivery, which include luminal (pH and enzymes), mucus and epithelial barriers. The use of nanoparticles have been studied as an approach to overcome these barriers (Laffleur & Bernkop-Schnürch, 2013; Florek et al., 2017). Among these, silica nanoparticles have been studied as a potential nanocarrier for mucosal drug delivery.

Thiolated silica nanoparticles with the size of ~ 50 nm were synthesised by our group using MPTS as a silica source, NaOH as a basic catalyst and DMSO as a solvent (Irmukhametova et al., 2011). The size of these nanoparticles can be tuned by changing the synthetic conditions (Al Mahrooqi et al., 2018). The particles can be functionalised with polyethylene glycol (PEG) (Irmukhametova et al., 2011), poly-2-ethyl-2-oxazoline (POZ) (Mansfield et al., 2015) and hydroxyethylcellulose (Mansfield et al., 2018). These nanoparticles exhibited mucoadhesive properties *in vitro* on bovine cornea (Irmukhametova et al., 2011), porcine bladder mucosa (Mun et al., 2016) and rat intestinal mucosa model (M. Ways et al., 2018). Their mucoadhesiveness was decreased upon their PEGylation (Irmukhametova et al., 2011; Mun et al., 2016) and POZylation (M. Ways et al., 2018), however, these resulted in an enhancement of their diffusion in porcine gastric mucin dispersion and penetration into porcine gastric mucosa (Mansfield et al., 2015). Mun et al. (2014) showed that neither thiolated nor PEGylated (with 750 and 5000 Da PEG) silica nanoparticles penetrated the intact bovine cornea. They also revealed that thiolated silica nanoparticles did not penetrate the de-epithelialised cornea which could be due to the interactions of their thiol groups with the cysteine domains of the corneal stroma. Also, PEGylated (with 750 Da PEG) silica nanoparticles did not penetrate the de-epithelialised cornea as they contained some remaining thiol groups available for binding with the cysteine domains of the stroma. However, PEGylated (with 5000 Da PEG) silica nanoparticles penetrated the de-epithelialised cornea, which could be due to the substitution of a larger number of thiol groups with PEG (compared to PEGylated nanoparticles with 750 Da PEG), decreasing the nanoparticles-cysteine interactions.

Zhang et al. (2014) synthesised β-cyclodextrin modified mesoporous silica nanoparticles with three different surface functionalities namely hydroxyl, amino and thiol groups. They investigated the mucoadhesive properties of these nanoparticles using particle-mucin interaction (the size of the mixture of mucin suspension and the nanoparticles suspension measured by dynamic light scattering). This was also supported by confocal microscopic study of porcine bladder mucosa exposed to the fluorescein isothiocyanate-labelled nanoparticles followed by washing with artificial urine. They found that the thiol-functionalised silica nanoparticles had a superior mucoadhesiveness compared to both amine- and hydroxyl-functionalised counterparts. This was evident from a higher change in the size of the thiol-functionalised silica nanoparticles compared to amine- and hydroxyl-functionalised nanoparticles upon mixing with mucin suspension. Also, the mucoadhesion study showed a stronger fluorescence signal (only images without quantitative analysis are provided in their paper) from thiol-functionalised silica nanoparticles compared to amine- and hydroxyl-functionalised counterparts. Additionally, the thiol-functionalised silica nanoparticles provided a sustained doxorubicin release, and shown to be slower at the pH of artificial urine (6.1) compared to the pH of phosphate buffer solution (7.4) (~ 13% and 63% cumulative release after 48 hours, respectively) (Zhang et al., 2014).

Several studies demonstrated that uncoated undecylenic acid modified thermally hydrocarbonized porous silica (UPS) nanoparticles interact weakly with Caco-2/HT29-MTX (mono- and co-culture) cells, possibly due to the negatively charged surfaces of the nanoparticles. However, this interaction was enhanced when UPS nanopartilces were coated with chitosan either with physical adsorption or chemical conjugation, which they related to the fact that chitosan can adhere to the mucus secreted by HT29-MTX cells (Araújo et al., 2014; Shrestha et al., 2015). Shrestha et al. (2016) modified UPS nanoparticles with chitosan and then these were further modified with either cysteine or cell penetrating peptide (CPP) to generate cysteine-functionalised (cysteine-UPS) or CPP-functionalised (CPP-UPS) nanoparticles, respectively. They showed that both types of cysteine-UPS and CPP-UPS nanoparticles enhanced the intestinal permeation of insulin through triple coculture of Caco-2, HT29-MTX and Raji B cells monolayers. In case of cysteine-UPS nanoparticles, this was due to the presence of thiol groups in the structure of the nanoparticles, which form disulfide bonds with cysteine rich domain of the mucus glycoproteins. However, in case of CPP-UPS nanoparticles, the cell penetrating ability of CPP was the major reason for the enhanced insulin permeation through the cells. On the other hand, only cysteine-UPS nanoparticles,

enhanced the insulin oral bioavailability in a type 1 diabetic rat model, which they related to the possible degradation of the peptide layer of CPP-UPS nanoparticles by the rats gastrointestinal tract (GIT) luminal enzymes or the different nature of the mucus barrier of the *in vivo* model compared to the *in vitro* cells model (Shrestha et al., 2016).

Sarparanta et al. (2012) showed the strong mucoadhesion of hydrophobin-functionalised porous silica nanoparticles in an *in vitro* model of human adenocarcinoma cells, possibly due to the electrostatic and hydrophobic interactions between specific amino acid residues of hydrophobin and the mucus components of the cells. Additionally, the authors suggest the formation of disulfide bonds between the cysteine residue of hydrophobin and the thiol groups of mucus glycoprotein. The *in vivo* study in rats showed that these nanoparticles could actually retain in the glandular part of the stomach for up to 3 hours, due to their adhesion to the loosely bound mucus layer, followed by their transit into the small intestine. The organ-specific affinity of functionalised silica nanoparticles was also shown by other researchers. For example, in an *in vivo* study in mice, Desai et al. (2016) showed that polyethylene imine (PEI)-functionalised silica nanoparticles had a greater affinity to the small intestine whereas combined PEG-PEI-functionalised silica nanoparticles to the colon. Such types of nanoparticles have the potential applications in the design of targeted drug delivery systems for drugs like antibiotics and anticancer used for the treatment of various GIT diseases including infections and cancers.

The effect of hydrophilic polymers on the interaction of silica nanoparticles with mucin was also investigated by other researchers. Andreani et al. (2015) revealed that both alginate and chitosan coated silica nanoparticles interact strongly with mucin particles (evident by the reduction of the zeta potential of the nanoparticles after dispersing them in mucin solution), whereas both non-coated and PEG coated nanoparticles showed a weak interaction. This may indicate the ability of non-coated and PEG coated silica nanoparticles to diffuse into the mucus network.

Liu et al. (2013) studied mesoporous silica nanoparticles as a dual-drug loaded carrier for a hydrophobic (indomethacin) and a hydrophilic (human peptide, PYY3-36) compound. They found that the presence of PYY3-36 in the indomethacin /PYY3-36 loaded silica nanoparticles increased the permeation of both indomethacin and PYY3-36 through co-cultured Caco-2/HT29 cells monolayers. They related this to the presence of mucus secreted

by HT29 cells, leading to the cell-silica nanoparticles interactions resulting in a high local drug concentration close to the cells monolayers.

Several other studies demonstrated the potential of silica nanoparticles in mucosal drug delivery. Few examples are illustrated in Table 2.1.

Table 2.1 Some examples of mucosal drug delivery using silica nanoparticles in the literature.

| Drugs | Potential treatments | Routes of administration | Models | Advantages | References |
|---|---|---|---|---|---|
| 5-amino salicylic acid | Inflammatory bowel disease | Oral | *In vivo* mice | Delayed drug release and targeted delivery to the inflamed tissues | (Moulari et al., 2008) |
| Glucagon like peptide-1 | Type 2 diabetes mellitus | Oral | *In vitro* intestinal cells | Chitosan coated silica nanoparticles provided high drug loading capacity, sustained drug release and enhanced drug permeation | (Araújo et al., 2014) |
| Curcumin | Neurodegenerative diseases | Nasal | *In vitro* olfactory neuroblastoma cells | Bypassing blood brain barrier, better chemical stability of the loaded drug | (Lungare et al., 2016) |

## 2.5 Safety concerns and biodistribution of silica nanoparticles

The safety and biodistribution of silica nanoparticles are controversial and found to be highly dependent on the size, shape, surface properties, the types of cells or animals, the dose and the methods of administration. Using the everted gut sac method, Yoshida et al. (2014) demonstrated that silica nanoparticles with various sizes (70, 300 and 1000 nm) and surface functionalities (carboxyl or amine groups) were absorbed by the rat small intestine. However, they observed no abnormalities in mice after 28-days oral exposure to these nanoparticles indicated by blood biomarkers, histopathology examination of the liver, kidney, brain, lung, spleen, heart, stomach and intestine and hematological analysis. Using transmission electron microscopy, Yoshida et al. (2013) found that following nasal administration of silica nanoparticles in mice (20 μL, at a concentration of 500 μg/mouse daily for 7 days), the particles with a size of 30, 70 and 100 nm were absorbed by the nasal mucosa and were detected in the nasal cavity, lung and liver. 1000 nm particles were

detected in the nasal cavity and lung, however, 300 nm particles were only detected in the lung. Both 300 and 1000 nm particles were not detected the liver. Yoshida et al. (2013) did not provide any explanation on the difference observed with the biodistribution of these nanoparticles, but suggested that the transmission electron microscopy is only a qualitative method and thus no quantitative data can be obtained. They also hypothesised the possibilities of degradation of the larger nanoparticles (300 nm and 1000 nm) in the biological environment, leading to a smaller size nanoparticles compared to the size of the administered nanoparticles (Yoshida et al., 2013), which could be a reason for the inability to detect these nanoparticles in the liver. Only 30 and 70 nm nanoparticles prolonged the bleeding time of mice compared to the control, whereas no adverse biological effects was observed with the other nanoparticles (Yoshida et al., 2013).

In rats, subcutaneous injection of mesoporous silica particles (150-4000 nm) had no toxicity, however, intravenous and intraperitoneal injections in mice led to the death of the animals possibly due to pulmonary thrombosis (Hudson et al., 2008). The oral and ocular administration of nonporous silica nanoparticles to rats for 12 weeks was found to be safe (Kim et al., 2017).

Li et al. (2015) observed possible renal impairment with sphere-like mesoporous silica nanoparticles but not with rod-like mesoporous silica nanoparticles when orally administered to mice. They also reported that the silica nanorods were mainly accumulated in the liver and spleen of the mice, whereas the silica nanospheres were mainly found in the spleen. Some other investigators revealed the impact of silica nanoparticles shape on their toxicity, biodistribution and biocompatibility (Huang et al., 2011; Yu et al., 2011; Zhao et al., 2017)

## 2.6 Conclusion

Silica nanoparticles are promising drug nanocarriers for mucosal drug delivery. They have several advantages including their relatively simple methods of preparation, surface functionalisation, controlling the size and shape, high drug loading and controlled drug delivery. Silica nanoparticles were generally found to be relatively safe, however, some studies have pointed out some safety concerns, suggesting further investigation is needed before any clinical trials with these nanoparticles.

## 2.7 References

Al Mahrooqi, J.H., Mun, E.A., Williams, A.C., & Khutoryanskiy, V.V., 2018. Controlling the size of thiolated organosilica nanoparticles. Langmuir 34, 8347-8354.

Andreani, T., Miziara, L., Lorenzon, E.N., de Souza, A.L., Kiill, C.P., Fangueiro, J.F., Garcia, M.L., Gremiao, P.D., Silva, A.M., & Souto, E.B., 2015. Effect of mucoadhesive polymers on the *in vitro* performance of insulin-loaded silica nanoparticles: Interactions with mucin and biomembrane models. Eur. J. Pharm. Biopharm. 93, 118-126.

Araújo, F., Shrestha, N., Shahbazi, M.-A., Fonte, P., Mäkilä, E.M., Salonen, J.J., Hirvonen, J.T., Granja, P.L., Santos, H.A., & Sarmento, B., 2014. The impact of nanoparticles on the mucosal translocation and transport of GLP-1 across the intestinal epithelium. Biomaterials 35, 9199-9207.

Cha, B.G., & Kim, J., 2019. Functional mesoporous silica nanoparticles for bio-imaging applications. Wiley Interdisciplinary Reviews: Nanomedicine and Nanobiotechnology 11, e1515.

Desai, D., Prabhakar, N., Mamaeva, V., Karaman, D.Ş., Lähdeniemi, I.A.K., Sahlgren, C., Rosenholm, J.M., & Toivola, D.M., 2016. Targeted modulation of cell differentiation in distinct regions of the gastrointestinal tract via oral administration of differently PEG-PEI functionalized mesoporous silica nanoparticles. International journal of nanomedicine 11, 299-313.

Du, H., Hamilton, P.D., Reilly, M.A., d'Avignon, A., Biswas, P., & Ravi, N., 2009. A facile synthesis of highly water-soluble, core–shell organo-silica nanoparticles with controllable size via sol–gel process. J. Colloid Interface Sci. 340, 202-208.

Finnie, K.S., Bartlett, J.R., Barbé, C.J.A., & Kong, L., 2007. Formation of silica nanoparticles in microemulsions. Langmuir 23, 3017-3024.

Florek, J., Caillard, R., & Kleitz, F., 2017. Evaluation of mesoporous silica nanoparticles for oral drug delivery – current status and perspective of MSNs drug carriers. Nanoscale 9, 15252-15277.

Gao, W., Rigout, M., & Owens, H., 2016. Facile control of silica nanoparticles using a novel solvent varying method for the fabrication of artificial opal photonic crystals. J. Nanopart. Res. 18, 387.

Guo, Q., Yang, G., Huang, D., Cao, W., Ge, L., & Li, L., 2018. Synthesis and characterization of spherical silica nanoparticles by modified Stöber process assisted by slow-hydrolysis catalyst. Colloid. Polym. Sci. 296, 379-384.

Huang, X., Li, L., Liu, T., Hao, N., Liu, H., Chen, D., & Tang, F., 2011. The shape effect of mesoporous silica nanoparticles on biodistribution, clearance, and biocompatibility *in vivo*. ACS Nano 5, 5390-5399.

Hudson, S.P., Padera, R.F., Langer, R., & Kohane, D.S., 2008. The biocompatibility of mesoporous silicates. Biomaterials 29, 4045-4055.

Huh, S., Wiench, J.W., Trewyn, B.G., Song, S., Pruski, M., & Lin, V.S.Y., 2003. Tuning of particle morphology and pore properties in mesoporous silicas with multiple organic functional groups. Chem. Commun., 2364-2365.

Irmukhametova, G.S., Mun, G.A., & Khutoryanskiy, V.V., 2011. Thiolated mucoadhesive and PEGylated nonmucoadhesive organosilica nanoparticles from 3-mercaptopropyltrimethoxysilane. Langmuir 27, 9551-9556.

Jin, Y., Lohstreter, S., Pierce, D.T., Parisien, J., Wu, M., Hall, C., & Zhao, J.X., 2008. Silica nanoparticles with continuously tunable sizes: Synthesis and size effects on cellular contrast imaging. Chem. Mater. 20, 4411-4419.

Kao, K.-C., & Mou, C.-Y., 2013. Pore-expanded mesoporous silica nanoparticles with alkanes/ethanol as pore expanding agent. Microporous Mesoporous Mater. 169, 7-15.

Kim, M., Park, J.-H., Jeong, H., Hong, J., Choi, W.S., Lee, B.-H., & Park, C.Y., 2017. An evaluation of the *in vivo* safety of nonporous silica nanoparticles: Ocular topical administration versus oral administration. Sci. Rep. 7, 8238.

Laffleur, F., & Bernkop-Schnürch, A., 2013. Strategies for improving mucosal drug delivery. Nanomedicine 8, 2061-2075.

Li, L., Liu, T., Fu, C., Tan, L., Meng, X., & Liu, H., 2015. Biodistribution, excretion, and toxicity of mesoporous silica nanoparticles after oral administration depend on their shape. Nanomedicine: Nanotechnology, Biology and Medicine 11, 1915-1924.

Lin, Y.-S., & Haynes, C.L., 2010. Impacts of mesoporous silica nanoparticle size, pore ordering, and pore integrity on hemolytic activity. J. Am. Chem. Soc. 132, 4834-4842.

Liu, D., Bimbo, L.M., Mäkilä, E., Villanova, F., Kaasalainen, M., Herranz-Blanco, B., Caramella, C.M., Lehto, V.-P., Salonen, J., Herzig, K.-H., Hirvonen, J., & Santos, H.A., 2013. Co-delivery of a hydrophobic small molecule and a hydrophilic peptide by porous silicon nanoparticles. J. Control. Release 170, 268-278.

Liu, Y., Chen, Q., Xu, M., Guan, G., Hu, W., Liang, Y., Zhao, X., Qiao, M., Chen, D., & Liu, H., 2015. Single peptide ligand-functionalized uniform hollow mesoporous silica nanoparticles achieving dual-targeting drug delivery to tumor cells and angiogenic blood vessel cells. International journal of nanomedicine 10, 1855-1867.

Lungare, S., Hallam, K., & Badhan, R.K.S., 2016. Phytochemical-loaded mesoporous silica nanoparticles for nose-to-brain olfactory drug delivery. Int. J. Pharm. 513, 280-293.

M. Ways, T.M., Lau, W.M., Ng, K.W., & Khutoryanskiy, V.V., 2018. Synthesis of thiolated, PEGylated and POZylated silica nanoparticles and evaluation of their retention on rat intestinal mucosa *in vitro*. Eur. J. Pharm. Sci. 122, 230-238.

Maleki, A., Kettiger, H., Schoubben, A., Rosenholm, J.M., Ambrogi, V., & Hamidi, M., 2017. Mesoporous silica materials: From physico-chemical properties to enhanced dissolution of poorly water-soluble drugs. J. Control. Release 262, 329-347.

Mansfield, E.D., Sillence, K., Hole, P., Williams, A.C., & Khutoryanskiy, V.V., 2015. POZylation: A new approach to enhance nanoparticle diffusion through mucosal barriers. Nanoscale 7, 13671-13679.

Mansfield, E.D.H., Pandya, Y., Mun, E.A., Rogers, S.E., Abutbul-Ionita, I., Danino, D., Williams, A.C., & Khutoryanskiy, V.V., 2018. Structure and characterisation of hydroxyethylcellulose–silica nanoparticles. RSC Adv. 8, 6471-6478.

Manzano, M., & Vallet-Regí, M., 2018. Mesoporous silica nanoparticles in nanomedicine applications. J. Mater. Sci.: Mater. Med. 29, 65.

Moulari, B., Pertuit, D., Pellequer, Y., & Lamprecht, A., 2008. The targeting of surface modified silica nanoparticles to inflamed tissue in experimental colitis. Biomaterials 29, 4554-4560.

Mun, E.A., Morrison, P.W., Williams, A.C., & Khutoryanskiy, V.V., 2014. On the barrier properties of the cornea: A microscopy study of the penetration of fluorescently labeled nanoparticles, polymers, and sodium fluorescein. Mol. Pharm. 11, 3556-3564.

Mun, E.A., Williams, A.C., & Khutoryanskiy, V.V., 2016. Adhesion of thiolated silica nanoparticles to urinary bladder mucosa: Effects of PEGylation, thiol content and particle size. Int. J. Pharm. 512, 32-38.

Nakamura, M., & Ishimura, K., 2007. Synthesis and characterization of organosilica nanoparticles prepared from 3-mercaptopropyltrimethoxysilane as the single silica source. The Journal of Physical Chemistry C 111, 18892-18898.

Nakamura, M., & Ishimura, K., 2008a. One-pot synthesis and characterization of three kinds of thiol−organosilica nanoparticles. Langmuir 24, 5099-5108.

Nakamura, M., & Ishimura, K., 2008b. Size-controlled, one-pot synthesis, characterisation, and biological applications of epoxy-organosilica particles possessing positive zeta potential. Langmuir 24, 12228-12234.

Nakamura, M., Ozaki, S., Abe, M., Doi, H., Matsumoto, T., & Ishimura, K., 2010. Size-controlled synthesis, surface functionalization, and biological applications of thiol-organosilica particles. Colloids Surf. B. Biointerfaces 79, 19-26.

Narayan, R., Nayak, U.Y., Raichur, A.M., & Garg, S., 2018. Mesoporous Silica Nanoparticles: A Comprehensive Review on Synthesis and Recent Advances. Pharmaceutics 10, 118.

Osseo-Asare, K., & Arriagada, F.J., 1990. Preparation of $SiO_2$ nanoparticles in a non-ionic reverse micellar system. ColSu 50, 321-339.

Qiao, Z.-A., Zhang, L., Guo, M., Liu, Y., & Huo, Q., 2009. Synthesis of mesoporous silica nanoparticles via controlled hydrolysis and condensation of silicon alkoxide. Chem. Mater. 21, 3823-3829.

Rao, K.S., El-Hami, K., Kodaki, T., Matsushige, K., & Makino, K., 2005. A novel method for synthesis of silica nanoparticles. J. Colloid Interface Sci. 289, 125-131.

Rosenholm, J.M., Zhang, J., Linden, M., & Sahlgren, C., 2016. Mesoporous silica nanoparticles in tissue engineering – a perspective. Nanomedicine 11, 391-402.

Sarparanta, M.P., Bimbo, L.M., Mäkilä, E.M., Salonen, J.J., Laaksonen, P.H., Helariutta, A.M.K., Linder, M.B., Hirvonen, J.T., Laaksonen, T.J., Santos, H.A., & Airaksinen, A.J., 2012. The mucoadhesive and gastroretentive properties of hydrophobin-coated porous silicon nanoparticle oral drug delivery systems. Biomaterials 33, 3353-3362.

Shrestha, N., Araújo, F., Shahbazi, M.-A., Mäkilä, E., Gomes, M.J., Herranz-Blanco, B., Lindgren, R., Granroth, S., Kukk, E., Salonen, J., Hirvonen, J., Sarmento, B., & Santos, H.A., 2016. Thiolation and cell-penetrating peptide surface functionalization of porous silicon nanoparticles for oral delivery of insulin. Advanced Functional Materials 26, 3405-3416.

Shrestha, N., Shahbazi, M.-A., Araújo, F., Mäkilä, E., Raula, J., Kauppinen, E.I., Salonen, J., Sarmento, B., Hirvonen, J., & Santos, H.A., 2015. Multistage pH-responsive mucoadhesive nanocarriers prepared by aerosol flow reactor technology: A controlled dual protein-drug delivery system. Biomaterials 68, 9-20.

Slowing, I.I., Vivero-Escoto, J.L., Wu, C.-W., & Lin, V.S.Y., 2008. Mesoporous silica nanoparticles as controlled release drug delivery and gene transfection carriers. Adv. Drug Del. Rev. 60, 1278-1288.

Stöber, W., Fink, A., & Bohn, E., 1968. Controlled growth of monodisperse silica spheres in the micron size range. J. Colloid Interface Sci. 26, 62-69.

Tang, F., Li, L., & Chen, D., 2012. Mesoporous silica nanoparticles: Synthesis, biocompatibility and drug delivery. Adv. Mater. 24, 1504-1534.

Tang, L., & Cheng, J., 2013. Nonporous silica nanoparticles for nanomedicine application. Nano today 8, 290-312.

Wang, T., Jiang, H., Zhao, Q., Wang, S., Zou, M., & Cheng, G., 2012. Enhanced mucosal and systemic immune responses obtained by porous silica nanoparticles used as an oral vaccine adjuvant: Effect of silica architecture on immunological properties. Int. J. Pharm. 436, 351-358.

Wani, A., Muthuswamy, E., Savithra, G.H.L., Mao, G., Brock, S., & Oupický, D., 2012. Surface functionalization of mesoporous silica nanoparticles controls loading and release behavior of mitoxantrone. Pharm. Res. 29, 2407-2418.

Watermann, A., & Brieger, J., 2017. Mesoporous silica nanoparticles as drug delivery vehicles in cancer. Nanomaterials 7, 189.

Yang, X., Li, Y., Liu, X., Huang, Q., Zhang, R., & Feng, Q., 2018. Incorporation of silica nanoparticles to PLGA electrospun fibers for osteogenic differentiation of human osteoblast-like cells. Regenerative Biomaterials 5, 229-238.

Yoshida, T., Yoshioka, Y., Takahashi, H., Misato, K., Mori, T., Hirai, T., Nagano, K., Abe, Y., Mukai, Y., Kamada, H., Tsunoda, S.-I., Nabeshi, H., Yoshikawa, T., Higashisaka,

K., & Tsutsumi, Y., 2014. Intestinal absorption and biological effects of orally administered amorphous silica particles. Nanoscale research letters 9, 532-532.

Yoshida, T., Yoshioka, Y., Tochigi, S., Hirai, T., Uji, M., Ichihashi, K.-i., Nagano, K., Abe, Y., Kamada, H., Tsunoda, S.-i., Nabeshi, H., Higashisaka, K., Yoshikawa, T., & Tsutsumi, Y., 2013. Intranasal exposure to amorphous nanosilica particles could activate intrinsic coagulation cascade and platelets in mice. Part. Fibre Toxicol. 10, 41.

Yu, T., Malugin, A., & Ghandehari, H., 2011. Impact of silica nanoparticle design on cellular toxicity and hemolytic activity. ACS Nano 5, 5717-5728.

Zhang, Q., Neoh, K.G., Xu, L., Lu, S., Kang, E.T., Mahendran, R., & Chiong, E., 2014. Functionalized mesoporous silica nanoparticles with mucoadhesive and sustained drug release properties for potential bladder cancer therapy. Langmuir 30, 6151-6161.

Zhao, Y., Wang, Y., Ran, F., Cui, Y., Liu, C., Zhao, Q., Gao, Y., Wang, D., & Wang, S., 2017. A comparison between sphere and rod nanoparticles regarding their *in vivo* biological behavior and pharmacokinetics. Sci. Rep. 7, 4131.

# Chapter 3: Synthesis of thiolated, PEGylated and POZylated silica nanoparticles and evaluation of their retention on rat intestinal mucosa *in vitro*

This chapter is published as:

M. Ways, T.M., Lau, W.M., Ng, K.W., & Khutoryanskiy, V.V., 2018. Synthesis of thiolated, PEGylated and POZylated silica nanoparticles and evaluation of their retention on rat intestinal mucosa *in vitro*. Eur. J. Pharm. Sci. 122, 230-238.

## Graphical abstract

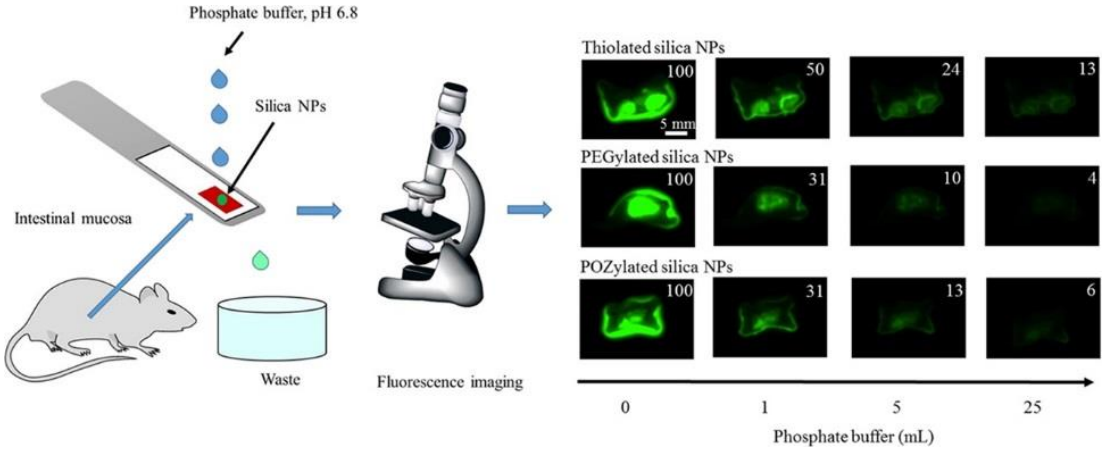



## Abstract

In this study, we synthesised thiolated silica nanoparticles using 3-mercaptopropyltrimethoxysilane and functionalised them with either 5 kDa methoxy polyethylene glycol maleimide (PEG) or 5 kDa alkyne-terminated poly(2-ethyl-2-oxazoline) (POZ). The main objectives of this study are to investigate the effects of pH on the size and ξ-potential of these nanoparticles and evaluate their mucoadhesive properties *ex vivo* using rat intestinal mucosa. The sizes of thiolated, PEGylated and POZylated silica nanoparticles were $53 \pm 1$, $68 \pm 1$ and $59 \pm 1$ nm, respectively. The size of both thiolated and POZylated nanoparticles significantly increased at $pH \leq 2$, whereas no size change was observed at pH 2.5–9 for both these two types of nanoparticles. On the other hand, the size of PEGylated nanoparticles did not change over the studied pH range (1.5–9). Moreover, thiolated nanoparticles were more mucoadhesive in the rat small intestine than both PEGylated and POZylated nanoparticles. After 12 cycles of washing (with a total of 20 mL of phosphate buffer solution pH 6.8), a significantly greater amount of thiolated nanoparticles remained on the intestinal mucosa than FITC-dextran (non-mucoadhesive polymer, $p < 0.005$) and both PEGylated and POZylated nanoparticles ($p < 0.05$ both). However, both PEGylated and POZylated nanoparticles showed similar retention to FITC-dextran ($p > 0.1$ for both). Thus, this study indicates that thiolated nanoparticles are mucoadhesive, whereas PEGylated and POZylated nanoparticles are non-mucoadhesive in the *ex vivo* rat intestinal mucosa model. Each of these nanoparticles has potential applications in mucosal drug delivery.

## 3.1 Introduction

Oral drug delivery is the preferred administration route for most drugs, as it has several advantages over other routes, including better patient adherence (especially for chronic diseases) and possibilities for flexible dosing (Date et al., 2016). In addition, oral dosage forms generally cost less to manufacture than other formulations (e.g. injectable, eye drops and inhalators) as they do not require sterilisation (Yun et al., 2013; Date et al., 2016) or use of complex delivery device. However, about 70% of new drugs do not reach pre-clinical development due to low bioavailability resulting from poor oral absorption (Gao et al., 2013). Drug absorption in the gastrointestinal tract (GIT) is hampered by a number of physiological barriers, including the mucus, the harsh pH and digestive environment of the GIT, tight junctions, epithelial cells and sub-epithelial tissues (Lundquist & Artursson, 2016).

Mucus is a viscous gel secreted by goblet cells, which are found in various organs, including the eye (Kessler & Dartt, 1994), the GIT (Deplancke & Gaskins, 2001) and the respiratory tract (Spicer et al., 1983). It consists mainly of water (~ 95%), alongside cross-linked and entangled mucin fibres, lipids, proteins, salts, cellular debris and bacteria (Moghissi et al., 1960; Bansil & Turner, 2006; Johansson et al., 2011; Leal et al., 2017)). Mucus can be targeted using mucoadhesive drug delivery systems that adhere to this layer to prolong the residence time of the dosage forms, leading to sustained release of the loaded drugs and enhanced bioavailability compared to conventional non-mucoadhesive formulations (Bernkop-Schnürch, 2005; Khutoryanskiy, 2011).

Several types of nanoparticles have been shown to have the potential as drug delivery systems (Nguyen et al., 2016; Hu et al., 2017; Davoudi et al., 2018). Siew et al. (2012) developed nanoparticles based on mucoadhesive quaternary ammonium palmitoyl glycol chitosan. These nanoparticles enhanced the oral absorption of both hydrophilic (ranitidine) and hydrophobic drugs (griseofulvin and cyclosporine A). In separate studies, Bernkop-Schnürch and co-workers have developed thiolated polymers and shown their potential in the design of mucoadhesive nanoparticulate drug delivery systems (Dünnhaupt et al., 2011; Bonengel & Bernkop-Schnürch, 2014). Prego et al. (2006) designed chitosan nanocapsules to enhance the absorption of salmon calcitonin from intestine and prolong its action as a

result of their mucoadhesive properties and strong interaction with the intestinal mucous membranes.

Previously, Khutoryanskiy et al. have developed thiolated silica nanoparticles and demonstrated their mucoadhesive properties on ocular (Irmukhametova et al., 2011) and urinary bladder mucosa (Mun et al., 2016). They also demonstrated that these nanoparticles could be easily functionalised via fluorescent labelling, PEGylation and POZylation (introduction of polyethylene glycols and polyoxazolines, respectively) (Irmukhametova et al., 2011; Irmukhametova et al., 2012; Mun et al., 2014a; Mansfield et al., 2015; Mansfield et al., 2016). PEGylation of thiolated silica nanoparticles was found to reduce the retention of thiolated silica nanoparticles on the ocular (Irmukhametova et al., 2011) and urinary bladder mucosal surfaces (Mun et al., 2016). More recently, Mansfield et al. (2015; 2016) demonstrated that POZylation of these nanoparticles could enhance their penetration into porcine gastric mucosa.

Clearly, the nature of the adhesion between two surfaces (here, the nanoparticles and the mucous membrane) is highly dependent on the properties of both (Smart, 2005; Varum et al., 2010; Khutoryanskiy, 2011). For example, we previously showed that thiolated and PEGylated silica nanoparticles were less retentive on the ocular surface compared to the urinary bladder mucosal surface (Irmukhametova et al., 2011; Mun et al., 2016). This difference in retention might be due to the rougher structure of the latter resulting in an increased contact area (Irmukhametova et al., 2011; Khutoryanskiy, 2011; Mun et al., 2016). The mucoadhesion of our POZylated silica nanoparticles has never been studied previously. Therefore, in the present work, we sought to investigate the retentive properties of these silica nanoparticles in the rat intestinal mucosa. We further analysed the physicochemical properties of these nanoparticles, particularly their pH-stability profiles.

## 3.2 Material and methods

### 3.2.1 Materials

3-mercaptopropyltrimethoxysilane (MPTS), maleimide terminated methoxy poly(ethylene glycol) (PEG) 5 kDa, alkyne terminated poly(2-ethyl-2-oxazoline) (POZ) 5 kDa (polydispersity index, PDI ≤ 1.2), 5,5′-dithiobis (2-nitrobenzoic acid) (DTNB), fluorescein isothiocyanate (FITC), medium molecular weight chitosan (degree of acetylation 26.1%,

124 kDa), FITC-dextran (3.5-5 kDa) and triethyl amine (TEA) were purchased from Sigma-Aldrich (Gillingham, UK). FITC-chitosan was made in house (Symonds et al., 2016a). Fluorescein-O-methacrylate (FMA), dimethyl sulfoxide (DMSO) and NaOH were purchased from Fisher Scientific (UK). Dialysis membrane with molecular cut-off 12-14 kDa was purchased from Medicell International Ltd., UK.

### 3.2.2 Synthesis of thiolated silica nanoparticles

Thiolated silica nanoparticles were synthesised according to a published method (Irmukhametova et al., 2011). In brief, 20 mL DMSO and 0.5 mL of 0.5 M NaOH solution were added to 0.75 mL MPTS. The mixture was continuously stirred and aerated for 24 hours at room temperature. Next, the nanoparticle suspensions were dialysed against deionised water (4 L, 8 changes of water over 2 days) using the dialysis membrane. The purified nanoparticle suspensions were refrigerated at 4 °C until use.

### 3.2.3 Synthesis of PEGylated and POZylated silica nanoparticles

Thiolated silica nanoparticles were functionalised using two different polymers; PEG and POZ. To synthesise PEGylated nanoparticles, 100 mg PEG was added to 10 mL thiolated nanoparticle suspension and the mixture was stirred for 24 hours at room temperature. To synthesise POZylated particles, 5 mL of thiolated nanoparticle suspension was diluted with 5 mL DMSO and then 100 mg POZ was added to the diluted thiolated nanoparticles. To this mixture, 200 µL TEA was added to enhance the thiol-yne click reaction (Mansfield et al., 2015). The reaction mixture was left for 24 hours with continuous stirring. The nanoparticles were purified by dialysis as described in section 3.2.2 and refrigerated at 4 °C until use.

### 3.2.4 Fluorescent labelling of nanoparticles

Each of the thiolated, PEGylated and POZylated silica nanoparticle suspensions (5 mL) were diluted with DMSO (5 mL). To this, 2 mL (3.59 µmol) of 1.8 mM fluorescein-O-methacrylate solution (in 1:1 deionised water: ethanol) and 200 µL TEA was added. The reaction mixture was stirred in the dark for 24 hours. Subsequently, the fluorescently labelled nanoparticles were purified (again in the dark) as described in section 3.2.2.

### 3.2.5 Characterisation of nanoparticles

The size and ξ-potential of the nanoparticles were measured using Zetasizer Nano-ZS (Malvern, UK). For the size measurements, the samples were diluted 1:100 with ultrapure water before analysis. A refractive index of 1.475 and an absorbance of 0.1 were used for all measurements. Measurements were conducted in triplicate for 10 seconds per run, with 12 runs per reading at 25 °C. ξ-potential values were measured using DTS-1070 folded capillary tube cuvettes (Malvern, UK). Samples were measured using 3 repeats of 20 sub-runs per reading. At least 3 samples were measured and processed using the Smoluchowski model (Fκa = 1.50).

Transmission electron microscopy (TEM) was conducted using a JEM-2100 PLUS Electron Microscope (JEOL, USA) at an accelerating voltage of 200 kV. Three drops of nanoparticle suspensions were placed on a carbon-coated copper grid and left for 1 minute before being loaded into the instrument. The morphology of the nanoparticles was investigated without any staining.

### 3.2.6 Determination of thiol content

Ellman's assay was used to quantify the free thiol groups available on the surface of the nanoparticles. Initially, the nanoparticles were lyophilised using the Heto Power Dry LL 3000 freeze-drier (Thermo Electron Corporation). The nanoparticles (3 mg) were suspended in 10 mL phosphate buffer solution (0.5 M, pH 8). Then, 0.5 mL aliquots of nanoparticle suspension was reacted with 0.5 mL DTNB (0.3 mg/mL) in the dark for 2 hours. Next, the product was centrifuged for 10 minutes at 13000 rpm (Sanyo, Micro Centaur, UK) and 200 µL aliquots of supernatant was loaded into a 96 well-plate. The light absorbance was measured at 420 nm using an Epoch microplate reader (BioTek Instruments, Inc.). In order to obtain a calibration curve, serial solutions of L-cysteine HCl over the concentration range of 0.634 to 0.004 µmol/mL were prepared and reacted with DTNB under the same conditions as the nanoparticles. Phosphate buffer solution (pH 8) was used as the blank control. Finally, the amount of free thiols per gram of the particles was calculated.

### 3.2.7 FTIR spectroscopy

FTIR spectra of the freeze-dried nanoparticles were recorded using a Spectrum 100 FTIR spectrophotometer (Perkin-Elmer, UK). The spectra were collected from an average of 4 scans, with a resolution of 4 $cm^{-1}$ over the range of 4000-650 $cm^{-1}$.

### 3.2.8 Thermogravimetric analysis

Freeze-dried samples were analysed for all three types of silica nanoparticles using the Q50 thermogravimetric analyser (TA Instruments, UK) equipped with nitrogen to provide an inert environment. The instrument was zeroed against an empty differential scanning calorimetry aluminium pan. The samples were placed in an aluminium pan and then in a platinum thermogravimetric analysis pan and loaded into the instrument. The initial temperature was set at 35 °C and the thermal decomposition of the samples was studied between 35 and 500 °C, at 5 °C /minute heating rate.

### 3.2.9 Fluorescence spectroscopy

Fluorescently labelled nanoparticle suspensions were diluted (1:400-1:12,800) with PBS (pH 7.4). The fluorescence emission spectra were measured between 500 -700 nm (emission wavelength) using a fluorescence spectrometer (Cary Eclipse, Varian Inc., US) at 490 nm excitation wavelength.

### 3.2.10 pH-stability study

Unlabelled nanoparticle suspensions were diluted with ultrapure water (1:100, 60 mL and 40 mL of the diluted nanoparticle suspensions were prepared for experiments of decreasing and increasing pH, respectively). The pH was adjusted using 1 M HCl or 1 M NaOH solutions. Then at each pH point, the size and ξ-potential of the nanoparticles were measured as described in section 3.2.5.

### 3.2.11 Determination of minimum detection limit of nanoparticles by fluorescence microscopy

The minimum detection limit of the nanoparticles was determined by first measuring the concentration of fluorescently labelled thiolated nanoparticles by gravimetry (1.15 ± 0.20 mg/mL; n = 3). This was performed by placing 1 mL of thiolated nanoparticles in a glass container and heating on a hotplate, initially at 100 °C for a few minutes, then at 75 °C. The

sample was weighed periodically and re-heated until a constant weight was obtained, indicating complete drying of the nanoparticles. Then, serial suspensions of fluorescently labelled thiolated nanoparticles were prepared in deionised water over the concentration range of 0.004–0.533 mg/mL. Diluted thiolated nanoparticle suspensions (20 µL) were applied on 0.8 × 1.2 $cm^2$ rat intestinal mucosa (tissues sample was used within 10 minutes of thawing). Fluorescent images were recorded using a fluorescence microscope (Leica Microsystems, UK) at 160 ms exposure time. The images were then analysed by ImageJ (National Institutes of Health, USA) and the coefficient of determination ($R^2$) was calculated.

### 3.2.12 Mucoadhesion study

Fluorescence microscopy was used to investigate the mucoadhesion of the synthesised nanoparticles. A Leica MZ10F fluorescence microscope (Leica Microsystems, UK) with ET-GFP filter, maximum excitation light intensity and 160 ms exposure time was used (in case of FITC-chitosan, however, 211 ms exposure time was used to compensate its poor fluorescence emission). In this study, freshly isolated small intestinal tissue from healthy 3 to 4 month-old Sprague Dawley female rats was used. The intestines were cut open to approximately 0.8 × 1.2 $cm^2$ and placed on a microscope slide. Fluorescence micrographs of the mucosal surface were taken as background fluorescence intensity. Thereafter, a 20 µL suspension of fluorescently labelled nanoparticles was placed on the intestinal mucosal surface and incubated for 5 minutes, before fluorescence micrographs were again recorded. The tissues were transferred to a sloped channel and washed with 1 mL or 5 mL of phosphate buffer solution (100 mM, pH 6.8, 37 ± 1 °C) for the total of 13 cycles. Fluorescence micrographs were recorded sequentially after each wash cycle. The images were analysed using the ImageJ software and normalised according to Equation 3.1:

$$Fluorescence\ intensity = \frac{I - I_b}{I_o - I_b} \times 100 \qquad \text{Equation 3.1}$$

where, $I$ is the fluorescence intensity of a given tissue sample nanoparticles after each wash cycle, $I_b$ is the background fluorescence intensity of that tissue sample, and $I_o$ is the initial fluorescence intensity of that sample (i.e. following nanoparticles incubation but preceding any wash cycle). Each tissue sample provided its own control for background fluorescence

intensity. The experiments were performed in triplicate using tissues obtained from 4 rats, and the order in which each nanoparticle type was studied in any individual experiment was randomised. FITC-chitosan (1 mg/mL in 0.1 M acetic acid) and FITC-dextran (1 mg/mL in deionised water) were used as positive and negative controls, respectively.

In addition, $WO_{50}$ (Mun et al., 2016) and $WO_{70}$ values were quantified. These values represent the amount of phosphate buffer solution necessary to attenuate the fluorescence intensity on the mucosal surface by 50% and 70%, respectively. The values were calculated by extrapolation of the average wash-off data using 6th order polynomial fitting and Wolfram Alpha (a computational knowledge engine).

### 3.2.13 Statistical analysis

Unless otherwise stated, all measurements were collected in triplicate and the data are expressed as mean ± standard deviation (SD). The data were analysed using the SPSS Statistics 21 program (IBM, US). The statistical significance of any difference between groups was determined using one-way analysis of variance (ANOVA) with the least significant difference (LSD) post-hoc test. Differences were considered statistically significant at $p < 0.05$.

## 3.3 Results and discussion

### 3.3.1 Nanoparticles synthesis and characterisation

Thiolated nanoparticles were synthesised via hydrolysis and subsequent condensation of the methoxysilane groups of MPTS, forming a cross-linked nanoparticle structure through Si-O-Si and disulfide bonds. All nanoparticle samples exhibited acceptable PDI (PDI < 0.2, as determined by DLS), with a single peak around the z-average of the particles (Figure 3.1 and Table 3.1). Particles with PDI < 0.05 are highly monodisperse but rarely seen unless with standard nanoparticles. Nanoparticles with PDI > 0.7 have generally very broad size distribution and not recommended to be sized using DLS technique. Thus, lower PDI indicates higher homogeneity of the nanoparticles and vice versa (Malvern Instruments Ltd., 2011). The particle size increased in the order of thiolated < POZylated < PEGylated nanoparticles (Figure 3.1 and Table 3.1).

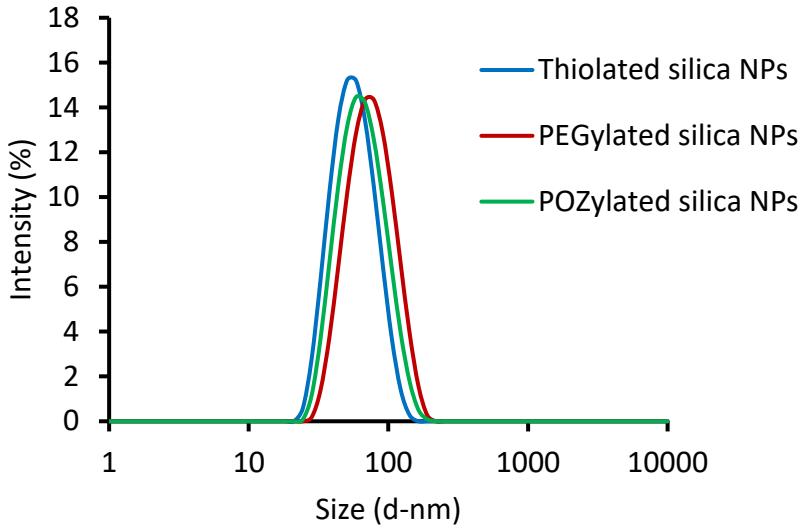


Figure 3.1 Exemplar dynamic light scattering size distribution of thiolated, PEGylated and POZylated silica nanoparticles.

Table 3.1 Characteristics of unlabelled thiolated, PEGylated and POZylated silica nanoparticles (mean ± SD, n = 3); for size and ξ-potential measurement, the nanoparticles suspensions were diluted with ultrapure water (1:100).

| Types of particles | Size (d-nm) | PDI | ξ-potential (mV) | Conc.[a] (mg/mL) | Free thiol content (µmol/g) |
|---|---|---|---|---|---|
| Thiolated | 53 ± 1 | 0.118 ± 0.012 | -42 ± 2 | 6 ± 2 | 368 ± 11 |
| PEGylated | 68 ± 1 | 0.128 ± 0.002 | -22 ± 3 | 13 ± 1 | 175 ± 2 |
| POZylated | 59 ± 1 | 0.134 ± 0.014 | -31 ± 4 | 5 ± 1 | 53 ± 18 |

[a] measured by freeze drying

The difference in particle size between each pair of nanoparticle type was statistically significant ($p < 0.05$). The larger PEGylated and POZylated nanoparticles indicate successful grafting of the polymers onto the thiolated nanoparticles core. PEG 5 kDa contains 113 repeating units of ethylene glycol (Mr= 44), whereas POZ 5 kDa consists of 50 repeating units of 2-ethyl-2-oxazoline (Mr=99). This means that the PEG chains were longer than the POZ chains, resulting in a thicker shell and thus larger particles (Mansfield, 2016).

Another possible reason for the size discrepancy between PEG and POZ nanoparticles is related to the different spatial arrangement of PEG and POZ around the core nanoparticles. Typically, PEG molecules form long-brush or mushroom configurations. The former happens when the density of PEG on the surface of nanoparticles is high, while the latter occurs in cases of low surface coverage (Owens & Peppas, 2006). In contrast, POZ forms star-shaped structures (Rossegger et al., 2013). Also, it can be hypothesised that different polymer chain folding and relaxation behaviour in water may also contribute to the difference in the size of the corresponding nanoparticles.

The concentration of the nanoparticles was estimated using freeze drying by determining the dry weight of the nanoparticles in 1 mL of suspensions. The results showed that PEGylated nanoparticles were more concentrated than both thiolated and POZylated nanoparticles (Table 3.1). These concentration estimates were used to quantify the free thiol contents of the nanoparticles.

In this study, all three types of silica nanoparticles (thiolated, PEGylated and POZylated) were labelled with a fluorescent marker, by reacting them with FMA (Figure 3.2 and Figure 3.3). The fluorescent molecules were covalently bound to the nanoparticles via thiol-ene click reaction between the thiol groups of the nanoparticles and the vinyl groups of FMA. Fluorescent labelling enabled facile quantification of the nanoparticles on the surface of rat intestinal mucosa, with virtually no change in the particle size (see Table 3.1 and Table 3.2). In addition, no signs of aggregation or flocculation was observed for both fluorescently labelled and unlabelled particles during the study (ca. 6 months). This indicates that FMA imparted a characteristic fluorescent signal to the particles without impairing the colloidal stability of the suspensions.

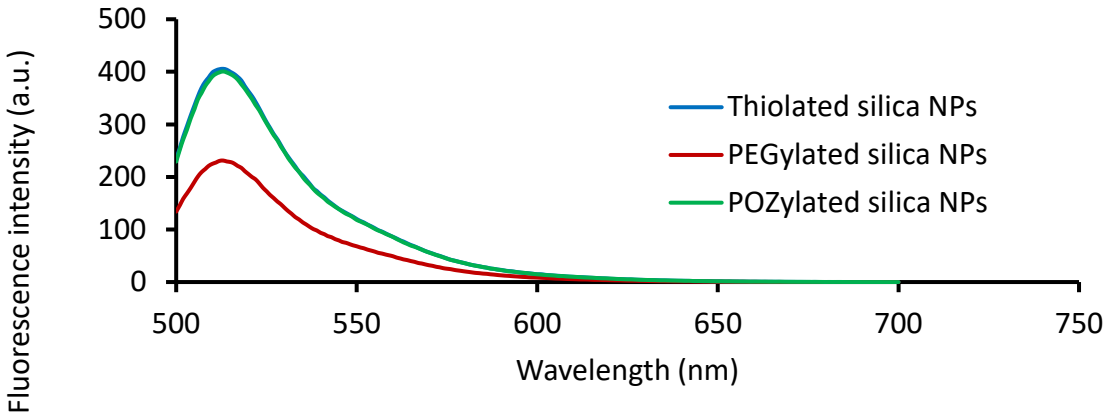


Figure 3.2 Fluorescence spectra of different types of silica nanoparticles diluted with PBS pH 7.4 (1:1600), mean, n = 3.

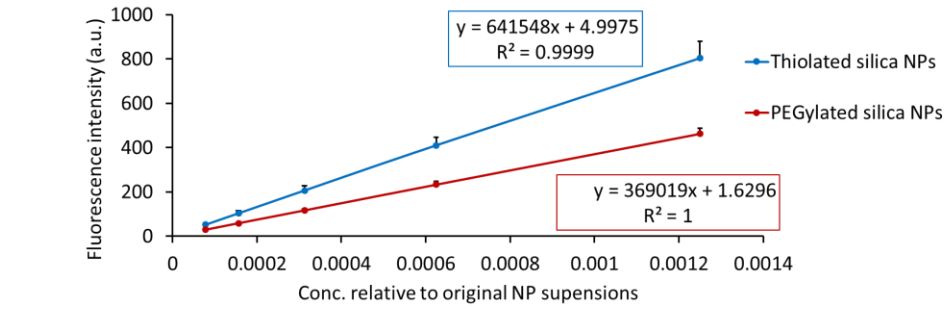


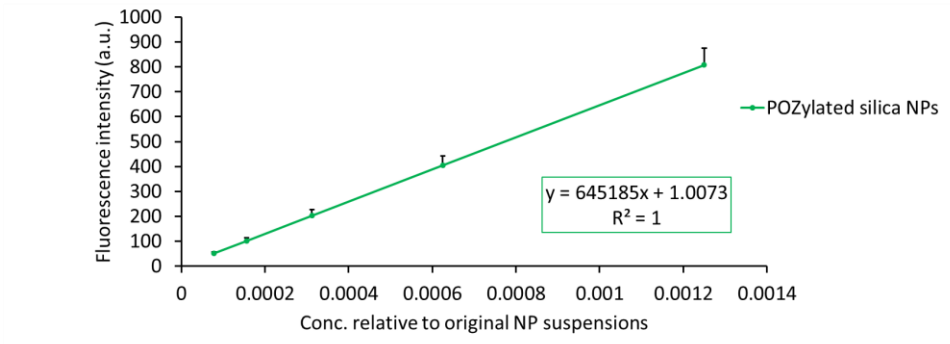


Figure 3.3 Calibration curves showing the linear relationships between fluorescence intensity and the concentration of FMA-labelled silica nanoparticles (mean ± SD, n = 3 for each nanoparticle type).

Ellman's assay showed a statistically significant difference in free thiol content among all three types of nanoparticles ($p < 0.05$). Free thiol content decreased in the order of thiolated > PEGylated > POZylated nanoparticles (Table 3.1). This result indicates successful functionalisation of both PEGylated and POZylated nanoparticles, since PEGylation and POZylation were expected to replace free thiol groups with the corresponding polymers. The calibration curve used in the Ellmans's assay is shown in Figure 3.4.

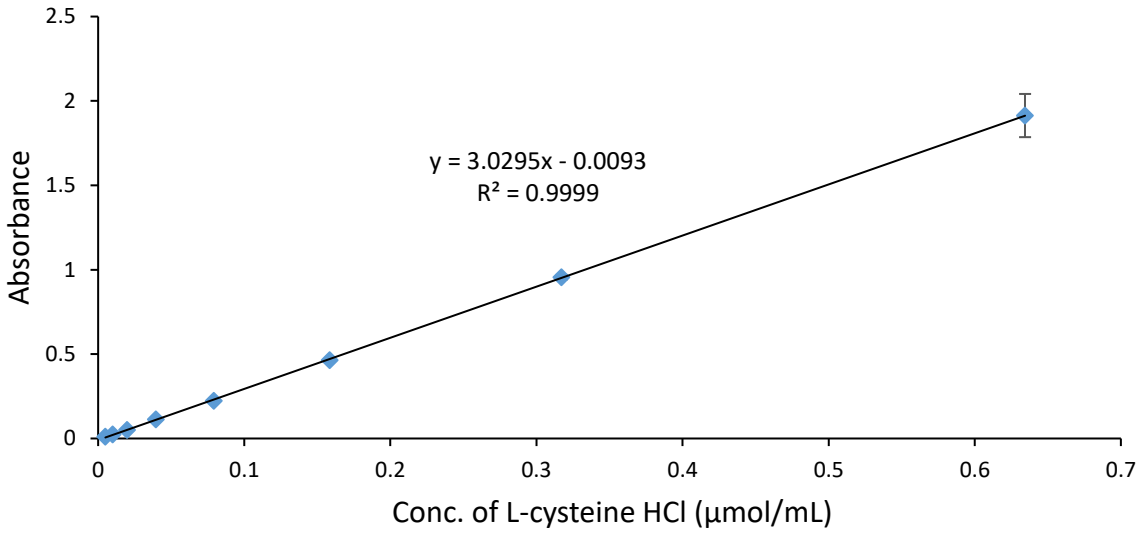


Figure 3.4 A calibration curve used to determine free thiol content of the silica nanoparticles (n = 3, mean ± SD).

Table 3.2 Properties of fluorescently labelled thiolated, PEGylated and POZylated silica nanoparticles (for fluorescence measurement, nanoparticles were diluted with PBS pH 7.4, 1:1,600), mean ± SD, n = 3.

| Types of particles | Size (d-nm) | PDI | Max. emission (nm) | Max. intensity (a.u.) |
|---|---|---|---|---|
| Thiolated | 51 ± 1 | 0.200 ± 0.018 | 512 | 411 ± 36 |
| PEGylated | 71 ± 2 | 0.106 ± 0.020 | 512 | 233 ± 14 |
| POZylated | 61 ± 3 | 0.117 ± 0.027 | 512 | 405 ± 38 |

In agreement with our previous study (Irmukhametova et al., 2011), TEM results show that thiolated nanoparticles aggregated and formed 'necklaces'(Figure 3.5). A possible reason for the aggregation is disulfide bond formation between the nanoparticles, facilitated by drying during TEM sample preparation. In contrast, TEM images of PEGylated and POZylated nanoparticles did not show any sign of aggregation. This observation, together with DLS data, confirm the presence of primarily non-aggregated PEGylated and POZylated particles in the samples. Thus, although the ξ-potential of both PEGylated and POZylated nanoparticles had significantly decreased compared to the parent thiolated nanoparticles (Table 3.1), their colloidal stability seemed to have dramatically improved. In addition to the overall reduction in reactive thiol groups in PEGylated and POZylated nanoparticles, steric hindrance (i.e. shielding of remaining thiol groups by the hydrophilic polymeric shells on the particle surface) is believed to be a major contributing factor to the improvement of colloidal stability.

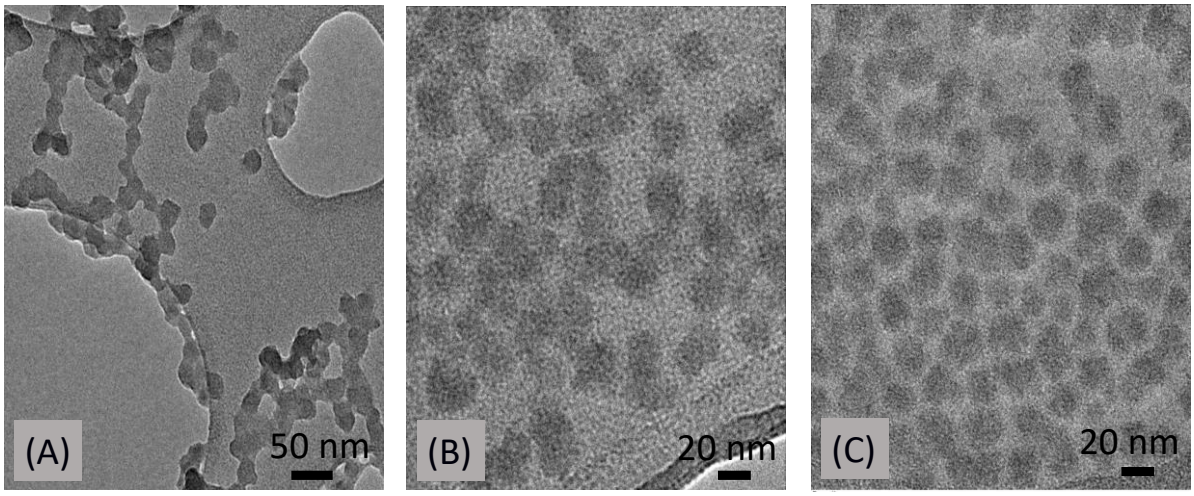


Figure 3.5 TEM images of unlabelled thiolated (A), PEGylated (B) and POZylated (C) silica nanoparticles. Thiolated nanoparticles formed necklace-like structure whereas both PEGylated and POZylated nanoparticles were mainly individually distributed.

The FTIR spectra of the silica nanoparticles are shown in Figure 3.6. Thiolated nanoparticles showed characteristic peaks of asymmetric $CH_2$ stretching, Si-O-Si asymmetric stretching and Si-O-Si bending vibration at 2933, 1103 and 1024 $cm^{-1}$, respectively. PEGylated nanoparticles showed a very specific peak at 1710 $cm^{-1}$, related to C=O of the maleimide part of PEG. POZylated nanoparticles demonstrated a peak at 1635 $cm^{-1}$, which is attributed to C=O stretching of POZ. In addition, asymmetric vibration of the $CH_3$ group in POZ resulted in the appearance of a characteristic peak at 1418 $cm^{-1}$.

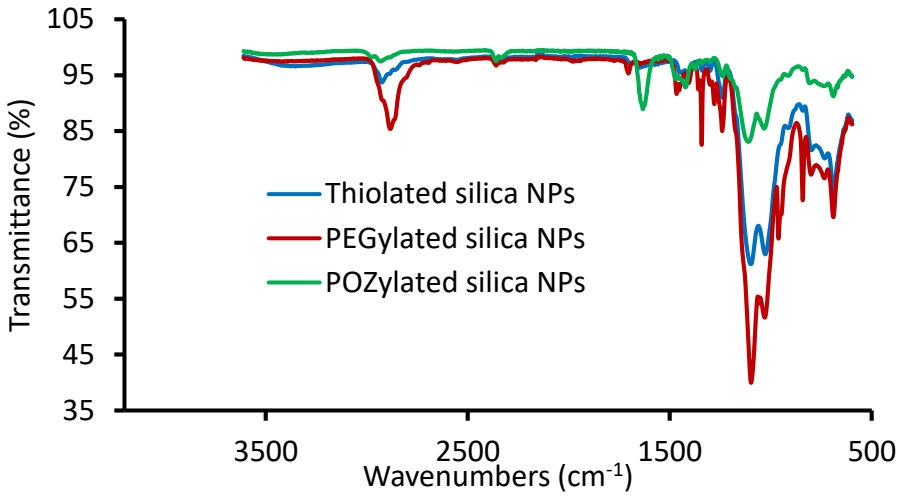


Figure 3.6 FTIR spectra of thiolated, PEGylated and POZylated silica nanoparticles.

Thermogravimetric analysis (Figure 3.7) indicate the successful grafting of both PEG and POZ to thiolated silica nanoparticles. A higher weight proportion of residues (62%) remained in thiolated nanoparticles compared to PEGylated and POZylated nanoparticles (44 and 36%, respectively). In other words, thiolated nanoparticles had lost just 38% of weight while PEGylated and POZylated nanoparticles had lost 56 and 64%, respectively. The greater percentage weight loss (% $w_{loss}$) in the PEGylated and POZylated nanoparticles was assumed to be due to thermal decomposition of PEG and POZ moieties, which were absent from the thiolated nanoparticles. The nanoparticles core, synthesised from MPTS, was composed of inorganic $SiO_2$ which would have been resistant to thermal decomposition within the temperature range used in the thermogravimetric analysis study (35 to 500 °C) (Mun, 2014). By subtracting the % $w_{loss}$ of thiolated nanoparticles from that of PEGylated and POZylated nanoparticles, the amount of each polymer in the functionalised nanoparticles was calculated. It was found that PEGylated nanoparticles had 18% w/w bound PEG whereas POZylated nanoparticles had 26% w/w bound POZ.

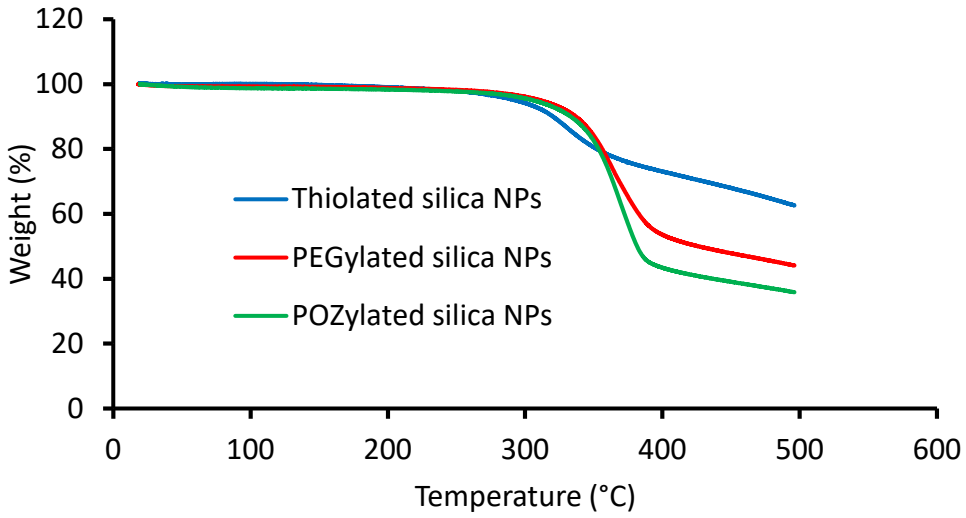


Figure 3.7 Thermogravimetric analysis of thiolated, PEGylated and POZylated silica nanoparticles.

As shown in Figure 3.2, Figure 3.3 and Table 3.2, PEGylated nanoparticles fluoresced less intensely ($p < 0.05$) than thiolated particles. This is most likely due to the screening effect of non-fluorescent PEG on the surface of these PEGylated nanoparticles. However, POZylated nanoparticles showed similar fluorescence intensity compared to thiolated nanoparticles ($p > 0.05$), which was significantly higher ($p < 0.05$) than that of PEGylated nanoparticles. The shorter POZ chain length (50 repeating units) compared to PEG (113 repeating units) (Mansfield et al., 2015) potentially led to less fluorescence screening resulting in a higher fluorescence signal in the POZylated nanoparticles.

### 3.3.2 pH-stability study

The dosage form administered orally is expected to pass through regions of GIT with different pH values. The pH along the GIT ranges from around 2 in the stomach, to 6-7 in the small intestine and about 8 in the colon. We therefore evaluated the stability of thiolated, PEGylated and POZylated silica nanoparticles over the pH range of 1.5–9, in terms of particle size, PDI and ξ-potential. The initial pH of the diluted thiolated, PEGylated and POZylated silica nanoparticle suspensions were 5.93, 5.67 and 6.08, respectively. Thiolated and POZylated nanoparticles were stable over the pH range of 2.5-9 as no change in their z-average size was observed. However, they aggregated at pH ≤ 2, resulting in a significant increase in particle size (z-average: 4.29 ± 0.78 µm for thiolated and 6.84 ± 0.52 µm for POZylated nanoparticles) and a polydisperse system (Figure 3.8-A, B and C). This aggregation was irreversible as particle size was not reduced when higher pH was restored. The aggregation of the particles at pH < 2 could be a result of Si-O-Si covalent bond formation between the nanoparticles, owing to the availability of ≡SiOH groups on the surface of the particles (Irmukhametova et al., 2012). The instability of thiolated and POZylated nanoparticles at pH ≤ 2 may potentially limit their application for oral drug delivery; however, this limitation could potentially be overcome by encapsulating these particles into a vehicle protected with pH-sensitive enteric coating such as Eudragits or their complexes with other polymers (Moustafine et al., 2011; Mustafin, 2011). In contrast, PEGylated nanoparticles were stable over the entire pH range investigated (1.5-9), as they showed neither aggregation nor dissociation.

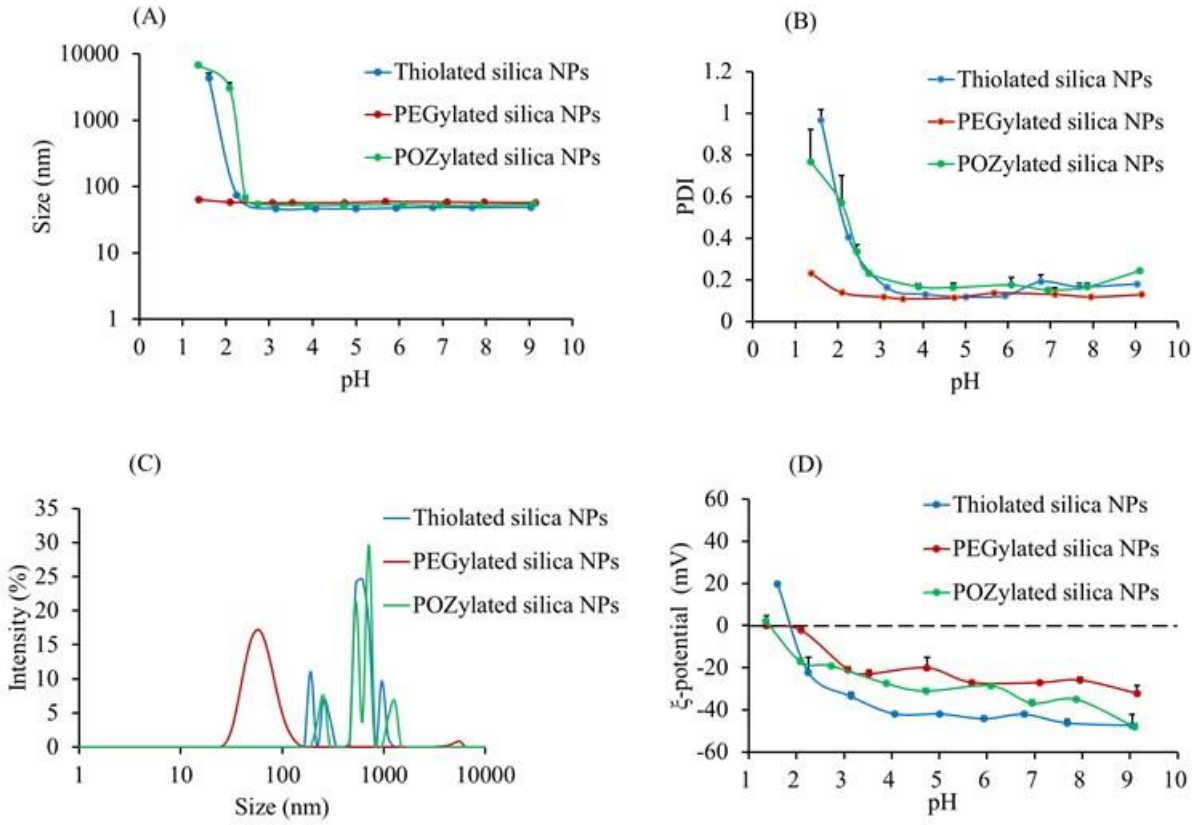


Figure 3.8 (A) DLS average size, (B) PDI at different pH environments, (C) particle size distribution at pH 1.5 and (D) ξ-potential of thiolated, PEGylated and POZylated silica nanoparticles in different pH environments, mean ± SD, n = 3. No error bars shown in (C).

The ξ-potential of the nanoparticles was lower at low pH than at high pH (Figure 3.8-D). Thiolated nanoparticles, however, had a more positive value (20 ± 1 mV) compared to PEGylated and POZylated nanoparticles (-0.17 ± 5 mV and 2 ± 1 mV, respectively). The reduction in the ξ-potential could be due to the association of the negatively charged $SiO^-$ and $S^-$ ions with positively charged $H^+$ ions, resulting in neutral SiOH or SH (Dyab, 2012). Interestingly, at low pH (~1.5) both PEGylated and POZylated nanoparticles showed a lower ξ-potential than thiolated nanoparticles. This could be explained by the fact that a significant number of SH groups were already substituted with PEG or POZ.

### 3.3.3 *Ex vivo* mucoadhesion study

In order to conduct the evaluation of mucoadhesive properties of the nanoparticles, the minimal detectable concentration of fluorescently labelled particles on the surface of rat intestinal mucosa was determined. The fluorescence of labelled particles was detectable even upon dilution by nearly 60-fold (Figure 3.9). This result is also important for future studies involving the monitoring of these fluorescent nanoparticles in the GIT following oral administration, as the particles are likely to be diluted by GI fluids. As shown in Figure 3.9, there is a linear relationship ($R^2$ = 0.9968) between the concentration of thiolated nanoparticles and their fluorescence intensity.

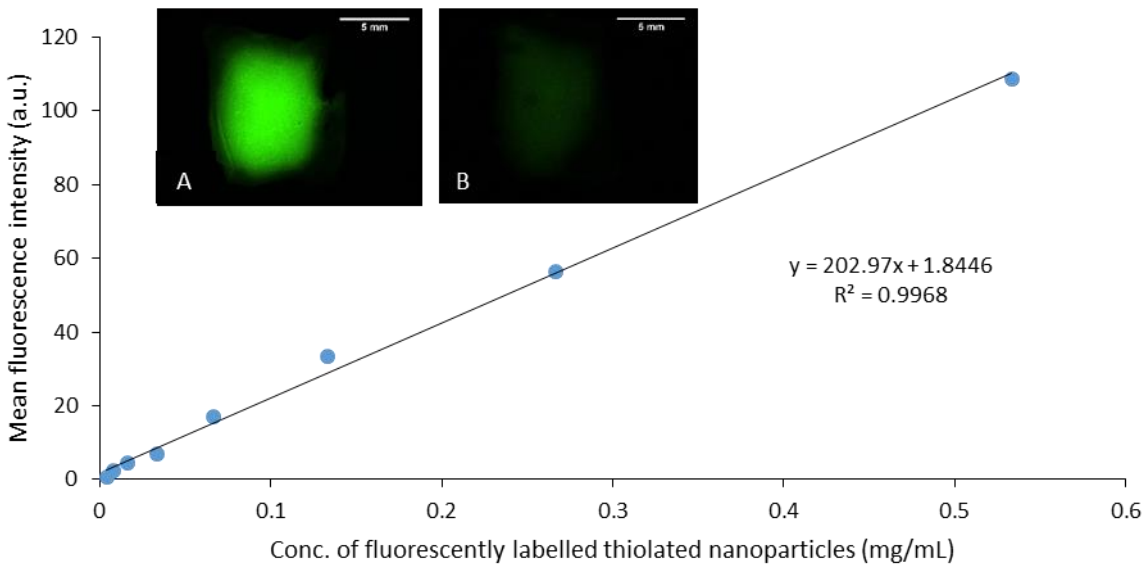


Figure 3.9 Fluorescence level of serial suspensions of thiolated silica nanoparticles applied on the rat intestinal mucosa. Inset: fluorescence micrographs showing 0.533 (A) and 0.066 (B) mg/mL thiolated nanoparticles on the rat intestinal mucosa, scale bar = 5 mm.

Using a wash-off technique (Ranga Rao & Buri, 1989; Nielsen et al., 1998) in combination with fluorescence microscopy, the retention of fluorescently labelled nanoparticles on the surface of rat intestinal mucosa was studied. This technique has been previously used to study the retention of various materials on different surfaces including animal tissues and plant leaves (Irmukhametova et al., 2011; Štorha et al., 2013; Cook et al., 2015; Mun et al., 2016; Symonds et al., 2016b; Tonglairoum et al., 2016).

Samples were applied on the surface of rat intestinal mucosa and then washed with phosphate buffer pH 6.8 over several cycles. The fluorescence intensity on the mucosa was monitored following each wash cycle (Figure 3.10). Based on the linear relationship established between nanoparticles concentration and fluorescence intensity (Figure 3.9), the amount of fluorescent nanoparticles remaining on the tissue was estimated. As both fluorophores (FMA and FITC) were covalently bound to the materials used in this study (nanoparticles, chitosan and dextran), it can be assumed that the fluorescence intensity was directly proportional to the percentage of the materials retained on the mucosal surface. However, this method is likely to underestimate the amount of labelled nanoparticles/macromolecules as they are diluted by phosphate buffer solution during the wash cycles. In addition, a portion of the nanoparticles/macromolecules may diffuse into the mucus layer, resulting in attenuation or even obliteration of the fluorescent signal. However, both these factors were excluded in this particular study and the % remaining of all nanoparticles, FITC-chitosan and FITC-dextran (positive and negative controls) were calculated as described in section 3.2.12.

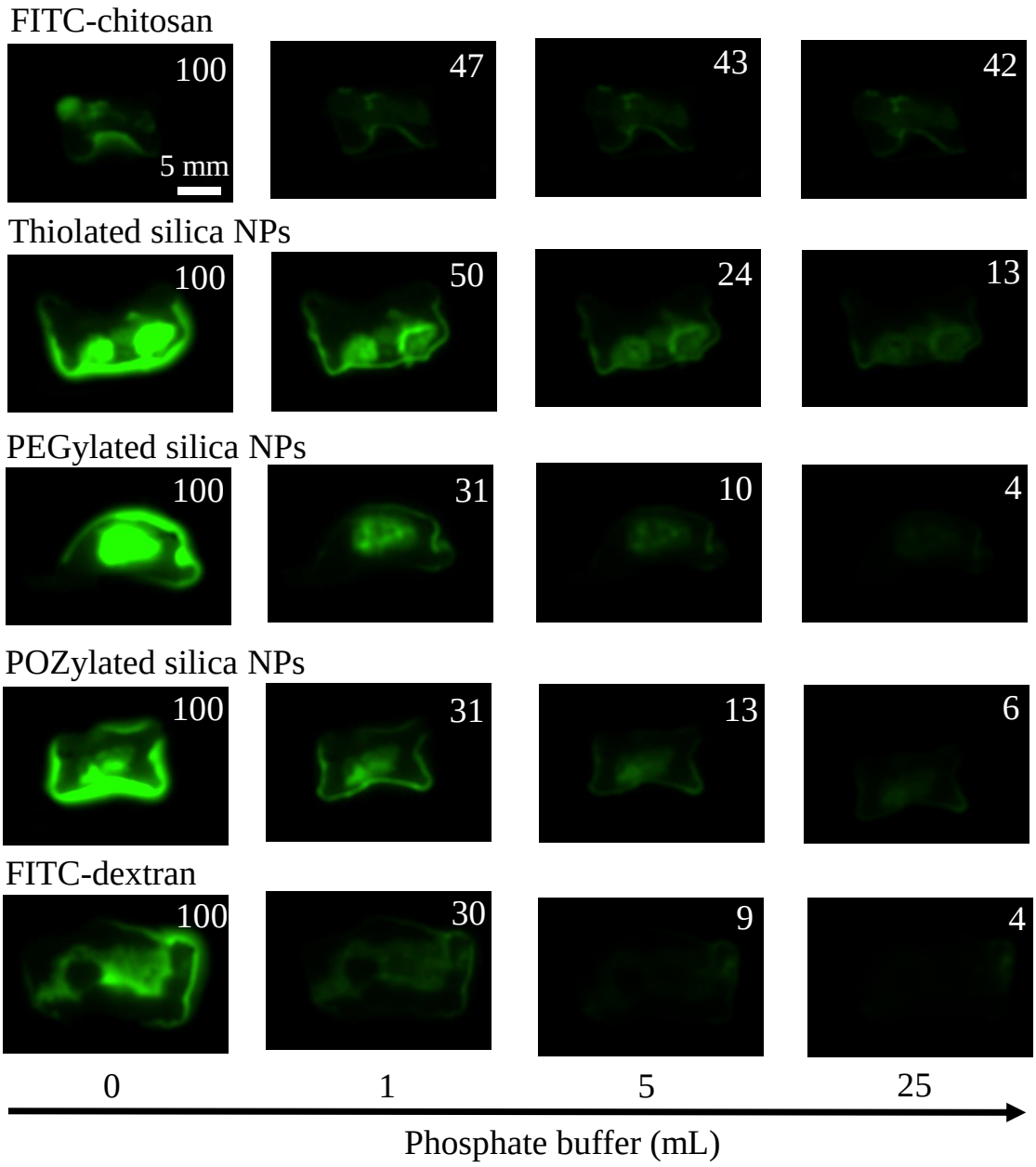


Figure 3.10 Exemplar fluorescence microphotographs showing retention of FITC-chitosan (postive control used as a mucoadhesive material), thiolated, PEGylated and POZylated silica nanoparticles and FITC-dextran (negative control used as a non-mucoadhesive material) on rat intestinal mucosa following wash-out with phosphate buffer solution at pH 6.8. The values of the normalised fluorescence intensity were inserted into the top right corners of the representative images (a.u.). After washing the fluorescent nanoparticles by certain amounts of phosphate buffer solution, the fluorescence intensity from thiolated nanoparticles were greater than both PEGylated and POZylated nanoparticles. The scale bar is 5 mm.

At the end of each wash cycle, the % of thiolated nanoparticles remaining was significantly greater ($p < 0.05$) than FITC-dextran, which was used as a non-mucoadhesive material (negative control) (Figure 3.11). Several studies have reported the non-mucoadhesive nature of dextran, which is likely due to its non-ionic character leading to muco-inertness instead of mucoadhesion (Khutoryanskiy, 2011; Withers et al., 2013; Mun et al., 2016). Thiolated nanoparticles also showed better retention than both PEGylated and POZylated nanoparticles ($p < 0.05$) (Figure 3.11).

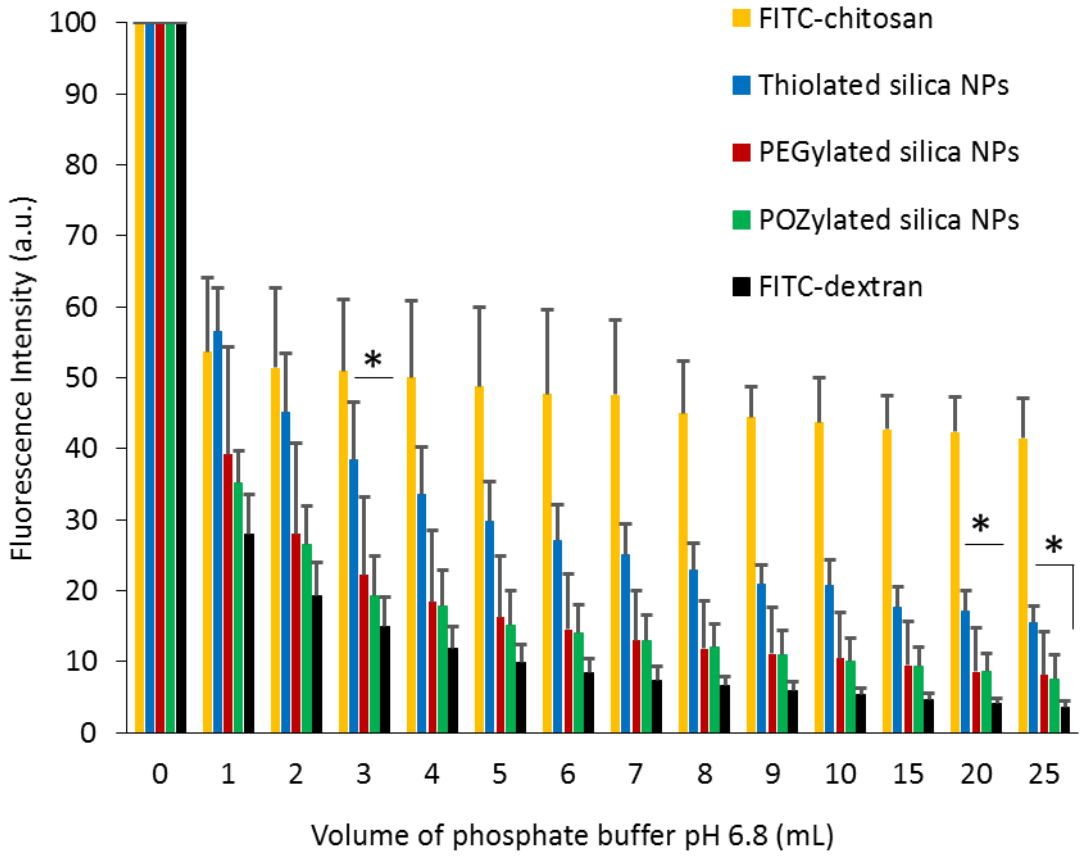


Figure 3.11 Fluorescence level of rat intestinal mucosa exposed to FITC-chitosan , thiolated, PEGylated and POZylated silica nanoparticles and FITC-dextran washed by phosphate buffer solution (100 mM, pH 6.8) (n = 3 using 4 rats, mean ± SD, "*" represents $p < 0.05$).

FITC-chitosan (positive control) showed remarkably higher retention than FITC-dextran (Figure 3.11). Many studies have confirmed the adhesion of chitosan to the mucus layers of various surfaces, including the eye, stomach and urinary bladder, owing to its cationic nature and ability to form electrostatic and hydrogen bonds with mucus components (Sogias et al., 2008; Mun et al., 2016; Tonglairoum et al., 2016). Over the first 3 wash cycles, thiolated nanoparticles showed a similar retention profile to FITC-chitosan ($p > 0.05$). However, at the end of each wash cycle, neither PEGylated nor POZylated nanoparticles showed any statistically significant difference compared to FITC-dextran ($p > 0.05$). This similarity of PEGylated and POZylated nanoparticles with FITC-dextran was persistent until the end of all wash cycles. In contrast, POZylated and PEGylated nanoparticles showed significantly less mucoadhesion than FITC-chitosan starting from the first and second wash cycle, respectively ($p < 0.05$ for both POZylated and PEGylated nanoparticles) (Figure 3.11).

Mun et al. (2016) showed that about 80% of thiolated silica nanoparticles, and only about 40% of PEGylated nanoparticles, remained on the surface of bladder mucosal tissues after washing with 10 mL artificial urine. In comparison, we found less retention for all three types of nanoparticles (thiolated: 21%, PEGylated: 11%, POZylated: 10%) after washing with the same volume of the bio-relevant fluid (Figure 3.11). The reason for this difference is not clear yet, but it could be related to the differences in the structure, chemical compositions, concentration and types of mucin on the mucosal surfaces.

In addition to the method developed by Mun et al. (2016) to determine $WO_{50}$, we propose to calculate $WO_{70}$ of the formulations. $WO_{50}$ and $WO_{70}$ represent the volume of phosphate buffer solution required to wash out 50% and 70%, respectively, of the formulations from the rat intestinal mucosa. Calculation of $WO_{70}$ is important as generally a greater amount of both thiolated and PEGylated nanoparticles were washed off from rat intestinal mucosa compared to urinary bladder mucosa (Mun et al., 2016). Similar differences in mucosal retention have also been reported by Irmukhametova et al. (2011), Mun et al. (2016) and Štorha et al. (2013) on bovine corneal and porcine urinary bladder tissues. A few studies reported the similarity of the thickness and the structure of the mucus of human GIT to that of porcine and showed some resemblance of the two (Varum et al., 2010, 2012). However, rat intestinal mucosa is an *ex vivo* model widely used to measure the oral absorption of drugs and evaluate the mucoadhesion and/or mucus-penetration of various drug delivery systems

including nanoparticles (Lehr et al., 1992; Keely et al., 2005; Dünnhaupt et al., 2011; Merchant et al., 2014; Maisel et al., 2015; Oltra-Noguera et al., 2015; Lozoya-Agullo et al., 2016).

Therefore, using $WO_{70}$ allows the comparison of different nanoparticles in terms of their wash-off profiles. Table 3.3 shows that $WO_{50}$ values for FITC-chitosan (1.9 mL) and thiolated nanoparticles (1.58 mL) are nearly double to those for PEGylated (0.95 mL) and POZylated nanoparticles (0.88 mL). The $WO_{70}$ for FITC-chitosan could not be determined since a sizeable proportion (> 40%) of the formulation remained tenaciously on the intestinal mucosa withstanding the multiple washing cycles (Figure 3.10 and Figure 3.11). On the other hand, the $WO_{70}$ for thiolated nanoparticles was approximately 3-fold higher than PEGylated and POZylated nanoparticles. This indicates that thiolated nanoparticles resisted a greater amount of wash buffer than both PEGylated and POZylated nanoparticles. $WO_{50}$ and $WO_{70}$ of both PEGylated and POZylated nanoparticles were close to that of FITC-dextran denoting the non-mucoadhesive nature of these two types of nanoparticles (Table 3.3).

Table 3.3 Values of $WO_{50}$ and $WO_{70}$ for FITC-chitosan, thiolated, PEGylated and POZylated silica nanoparticles, as well as FITC-dextran in rat intestinal mucosa.

| Types of materials | $WO_{50}$ (mL) | $WO_{70}$ (mL) |
|---|---|---|
| FITC-chitosan | 1.90 | NA |
| Thiolated silica nanoparticles | 1.58 | 5.26 |
| PEGylated silica nanoparticles | 0.95 | 1.73 |
| POZylated silica nanoparticles | 0.88 | 1.58 |
| FITC-dextran | 0.76 | 1.32 |

Polynomial fitting ($6^{th}$ order) was used to calculate $WO_{50}$ and $WO_{70}$, the values of $R^2$ were between 0.94-0.98, $WO_{50}$ and $WO_{70}$: volume of phosphate buffer solution required to wash out 50% and 70% of the formulations, respectively, NA: not applicable.

The reason for the better retention of thiolated nanoparticles compared to PEGylated and POZylated nanoparticles was most likely the formation of disulfide bridges between the thiolated nanoparticles and cysteine-rich domains of mucosal layers, since these nanoparticles had a greater free thiol content than PEGylated and POZylated nanoparticles. Conversely, PEGylated and POZylated nanoparticles were effectively removed after a few wash cycles probably due to less disulfide bridge formation by virtue of their lower thiol contents.

As all 3 types of the nanoparticles used in this study were negatively charged, the discrepancy in their mucoadhesive properties is unlikely to be related to the difference in charge. According to the electronic theory of mucoadhesion, anionic particles do not show any signs of adhesion to mucosal surfaces, which are also negatively charged, as like charges repel each other. However, mucoadhesion can be the result of one or more mechanisms, including ionic interaction, covalent bonding, hydrogen bonding, hydrophobic interaction, wetting, adsorption, diffusion and entanglement (Smart, 2005). Additionally, as the particles are dispersed in water, the effect of dispersion media on the mucoadhesive properties of the particles was excluded. Finally, the mucoadhesion was studied at pH 6.8, which was close to the pH of the ultrapure water used to dilute the nanoparticles for DLS size measurement. From the DLS data (Table 3.1 and Table 3.2 and Figure 3.1 and Figure 3.8), it is clearly seen that the nanoparticles were stable at neutral pH and did not show any sign of aggregation. Therefore, their retention would not be due to their deposition on the mucosal surfaces and rather was due to their ability to form disulfide bonds with cysteine residues in mucus.

Several studies have shown that decorating nanoparticles with PEG facilitates their diffusion or penetration through mucus barriers (Lai et al., 2007; Mun et al., 2014b; Maisel et al., 2015). Lai et al. (2007) reported that PEGylation of conventional large polystyrene nanoparticles (200 and 500 nm) led to their rapid transport through fresh human cervicovaginal mucus (CVM) and their diffusion coefficient ($D_c$) in mucus was just 4 to 6-fold smaller than in water. In contrast, the $D_c$ of uncoated polystyrene nanoparticles in CVM was 2400 to 40000-fold lower than in water. POZ has been studied as an alternative to PEG for the development of mucus-penetrating nanomaterials (Khutoryanskiy, 2018). For instance, Mansfield et al. (2015) showed that POZylated silica nanoparticles diffused rapidly

through porcine gastric mucosa. Similarly, in this study, the PEGylated and POZylated nanoparticles showed less mucoadhesion than thiolated nanoparticles. Based on these and our previous findings, we postulate that the PEGylated and POZylated nanoparticles may diffuse through rat intestinal mucus and thus be mucus-penetrating, which is a desirable property in some drug delivery applications. In other words, the fact that the PEGylated and POZylated nanoparticles exhibited less mucosal retention may not diminish their importance as a drug delivery system relative to the more mucoadhesive thiolated nanoparticles. The selection of either mucoadhesive or mucus-penetrating carriers depends on the drug being delivered, the mucosal surface being targeted, the mucus turnover rate, the presence of water, the disease state and the intended release profile. Generally, mucoadhesive nanoparticles are advantageous for ocular and intravesical drug delivery where lacrimation in the eye and urine voiding from bladder remove a substantial amount of the drug at the site of application/absorption. Mucus-penetrating carriers, on the other hand, are desirable in the design of oral drug delivery where deeper mucus gel penetration and a broader particle distribution through the absorptive epithelia are required (Mun et al., 2014b; Maisel et al., 2015; Mun et al., 2016; Netsomboon & Bernkop-Schnürch, 2016).

### 3.4 Conclusions

In this study, we have investigated the pH-stability profiles of thiolated, PEGylated and POZylated silica nanoparticles and evaluated their mucoadhesive properties in rat intestinal mucosa. PEGylated nanoparticles showed similar size over a broad pH range (1.5-9). Also, in case of thiolated and POZylated nanoparticles, no change in size was observed at pH 2.5-9. Thiolated nanoparticles were mucoadhesive in rat intestinal mucosa *ex vivo* but to a lesser extent than to urinary bladder mucosa as reported in our previous study. These mucoadhesive nanoparticles can potentially be used to prolong drug release. PEGylated and POZylated nanoparticles showed less mucoadhesion which suggests better permeability through the mucus layer compared to thiolated nanoparticles. This property may allow the particles to diffuse more easily through the mucus barrier to the deeper absorptive epithelia, leading to better absorption of the drugs.

### 3.5 Acknowledgements

We are thankful to HCED-Iraq for funding this research. We acknowledge the assistance of staff at the Chemical Analysis Facility (CAF), University of Reading, in FTIR, fluorescence spectroscopy and TEM experiments. We are grateful to Mr. Andrew Cripps for his assistance in obtaining the animal tissues used in this study.

### 3.6 References

Bansil, R., & Turner, B.S., 2006. Mucin structure, aggregation, physiological functions and biomedical applications. Curr. Opin. Colloid Interface Sci. 11, 164-170.

Bernkop-Schnürch, A., 2005. Mucoadhesive systems in oral drug delivery. Drug Discovery Today: Technol. 2, 83-87.

Bonengel, S., & Bernkop-Schnürch, A., 2014. Thiomers-from bench to market. J. Control. Release 195, 120-129.

Cook, M.T., Schmidt, S.A., Lee, E., Samprasit, W., Opanasopit, P., & Khutoryanskiy, V.V., 2015. Synthesis of mucoadhesive thiol-bearing microgels from 2-(acetylthio)ethylacrylate and 2-hydroxyethylmethacrylate: Novel drug delivery systems for chemotherapeutic agents to the bladder. J. Mater. Chem. B 3, 6599-6604.

Date, A.A., Hanes, J., & Ensign, L.M., 2016. Nanoparticles for oral delivery: Design, evaluation and state-of-the-art. J. Control. Release 240, 504-526.

Davoudi, Z., Peroutka-Bigus, N., Bellaire, B., Wannemuehler, M., Barrett, T.A., Narasimhan, B., & Wang, Q., 2018. Intestinal organoids containing poly(lactic-co-glycolic acid) nanoparticles for the treatment of inflammatory bowel diseases. J Biomed Mater Res A 106, 876-886.

Deplancke, B., & Gaskins, H.R., 2001. Microbial modulation of innate defense: Goblet cells and the intestinal mucus layer. Am. J. Clin. Nutr. 73, 1131S–1141S.

Dünnhaupt, S., Barthelmes, J., Hombach, J., Sakloetsakun, D., Arkhipova, V., & Bernkop-Schnürch, A., 2011. Distribution of thiolated mucoadhesive nanoparticles on intestinal mucosa. Int. J. Pharm. 408, 191-199.

Dyab, A.K.F., 2012. Destabilisation of Pickering emulsions using pH. Colloids Surf. Physicochem. Eng. Aspects 402, 2-12.

Gao, L., Liu, G., Ma, J., Wang, X., Zhou, L., Li, X., & Wang, F., 2013. Application of drug nanocrystal technologies on oral drug delivery of poorly soluble drugs. Pharm. Res. 30, 307-324.

Hu, R., Zheng, H., Cao, J., Davoudi, Z., & Wang, Q., 2017. Synthesis and *in vitro* characterization of carboxymethyl chitosan-CBA-doxorubicin conjugate nanoparticles as pH-sensitive drug delivery systems. Journal of Biomedical Nanotechnology 13, 1097-1105.

Irmukhametova, G.S., Fraser, B.J., Keddie, J.L., Mun, G.A., & Khutoryanskiy, V.V., 2012. Hydrogen-bonding-driven self-assembly of PEGylated organosilica nanoparticles with poly(acrylic acid) in aqueous solutions and in layer-by-layer deposition at solid surfaces. Langmuir 28, 299-306.

Irmukhametova, G.S., Mun, G.A., & Khutoryanskiy, V.V., 2011. Thiolated mucoadhesive and PEGylated nonmucoadhesive organosilica nanoparticles from 3-mercaptopropyltrimethoxysilane. Langmuir 27, 9551-9556.

Johansson, M.E.V., Ambort, D., Pelaseyed, T., Schütte, A., Gustafsson, J.K., Ermund, A., Subramani, D.B., Holmén-Larsson, J.M., Thomsson, K.A., Bergström, J.H., van der Post, S., Rodriguez-Piñeiro, A.M., Sjövall, H., Bäckström, M., & Hansson, G.C., 2011. Composition and functional role of the mucus layers in the intestine. Cell. Mol. Life Sci. 68, 3635-3641.

Keely, S., Rullay, A., Wilson, C., Carmichael, A., Carrington, S., Corfield, A., Haddleton, D.M., & Brayden, D.J., 2005. *In vitro* and *ex vivo* intestinal tissue models to measure mucoadhesion of poly (methacrylate) and N-trimethylated chitosan polymers. Pharm. Res. 22, 38-49.

Kessler, T.L., & Dartt, D.A. (1994). Neural stimulation of conjunctival goblet cell mucous secretion in rats, in: D. A. Sullivan (Ed.), Lacrimal gland, tear film, and dry eye syndromes: Basic science and clinical relevance. Springer US, Boston, MA, pp. 393-398.

Khutoryanskiy, V.V., 2011. Advances in mucoadhesion and mucoadhesive polymers. Macromol. Biosci. 11, 748-764.

Khutoryanskiy, V.V., 2018. Beyond PEGylation: Alternative surface-modification of nanoparticles with mucus-inert biomaterials. Adv. Drug Del. Rev. 124, 140-149.

Lai, S.K., O'Hanlon, D.E., Harrold, S., Man, S.T., Wang, Y.-Y., Cone, R., & Hanes, J., 2007. Rapid transport of large polymeric nanoparticles in fresh undiluted human mucus. Proc. Natl. Acad. Sci. U. S. A. 104, 1482-1487.

Leal, J., Smyth, H.D.C., & Ghosh, D., 2017. Physicochemical properties of mucus and their impact on transmucosal drug delivery. Int. J. Pharm. 532, 555-572.

Lehr, C.-M., Bouwstra, J.A., Kok, W., De Boer, A.G., Tukker, J.J., Verhoef, J.C., Breimer, D.D., & Junginger, H.E., 1992. Effects of the mucoadhesive polymer polycarbophil on the intestinal absorption of a peptide drug in the rat. J. Pharm. Pharmacol. 44, 402-407.

Lozoya-Agullo, I., Zur, M., Beig, A., Fine, N., Cohen, Y., González-Álvarez, M., Merino-Sanjuán, M., González-Álvarez, I., Bermejo, M., & Dahan, A., 2016. Segmental-dependent permeability throughout the small intestine following oral drug administration: Single-pass vs. Doluisio approach to in-situ rat perfusion. Int. J. Pharm. 515, 201-208.

Lundquist, P., & Artursson, P., 2016. Oral absorption of peptides and nanoparticles across the human intestine: Opportunities, limitations and studies in human tissues. Adv Drug Deliv Rev 106, 256-276.

Maisel, K., Ensign, L., Reddy, M., Cone, R., & Hanes, J., 2015. Effect of surface chemistry on nanoparticle interaction with gastrointestinal mucus and distribution in the gastrointestinal tract following oral and rectal administration in the mouse. J. Control. Release 197, 48-57.

Malvern Instruments Ltd., 2011. Dynamic light scattering-common terms defined. https://www.malvern.com/en/support/resourcecenter/Whitepapers/WP111214DLS TermsDefined.html (accessed 23 January 2018).

Mansfield, E.D. (2016). Synthesis, characterisation, and diffusive properties of functionalised nanomaterials. (PhD), University of Reading.

Mansfield, E.D., de la Rosa, V.R., Kowalczyk, R.M., Grillo, I., Hoogenboom, R., Sillence, K., Hole, P., Williams, A.C., & Khutoryanskiy, V.V., 2016. Side chain variations radically alter the diffusion of poly(2-alkyl-2-oxazoline) functionalised nanoparticles through a mucosal barrier. Biomaterials Science 4, 1318-1327.

Mansfield, E.D., Sillence, K., Hole, P., Williams, A.C., & Khutoryanskiy, V.V., 2015. POZylation: A new approach to enhance nanoparticle diffusion through mucosal barriers. Nanoscale 7, 13671-13679.

Merchant, H.A., Rabbie, S.C., Varum, F.J., Afonso-Pereira, F., & Basit, A.W., 2014. Influence of ageing on the gastrointestinal environment of the rat and its implications for drug delivery. Eur. J. Pharm. Sci. 62, 76-85.

Moghissi, K., Neuhaus, O.W., & Stevenson, C.S., 1960. Composition and properties of human cervical mucus. I. Electrophoretic separation and identification of proteins. The Journal of Clinical Investigation 39, 1358-1363.

Moustafine, R.I., Bobyleva, V.L., Bukhovets, A.V., Garipova, V.R., Kabanova, T.V., Kemenova, V.A., & Van Den Mooter, G., 2011. Structural transformations during swelling of polycomplex matrices based on countercharged (meth)acrylate copolymers (Eudragit® EPO/Eudragit® L 100-55). J. Pharm. Sci. 100, 874-885.

Mun, E.A. (2014). Functionalised organosilica nanoparticles: Synthesis, mucoadhesion and diffusion. (PhD), University of Reading.

Mun, E.A., Hannell, C., Rogers, S.E., Hole, P., Williams, A.C., & Khutoryanskiy, V.V., 2014a. On the role of specific interactions in the diffusion of nanoparticles in aqueous polymer solutions. Langmuir 30, 308-317.

Mun, E.A., Morrison, P.W., Williams, A.C., & Khutoryanskiy, V.V., 2014b. On the barrier properties of the cornea: A microscopy study of the penetration of fluorescently labeled nanoparticles, polymers, and sodium fluorescein. Mol. Pharm. 11, 3556-3564.

Mun, E.A., Williams, A.C., & Khutoryanskiy, V.V., 2016. Adhesion of thiolated silica nanoparticles to urinary bladder mucosa: Effects of PEGylation, thiol content and particle size. Int. J. Pharm. 512, 32-38.

Mustafin, R.I., 2011. Interpolymer combinations of chemically complementary grades of Eudragit copolymers: A new direction in the design of peroral solid dosage forms of drug delivery systems with controlled release (review). Pharm. Chem. J. 45, 285.

Netsomboon, K., & Bernkop-Schnürch, A., 2016. Mucoadhesive vs. mucopenetrating particulate drug delivery. Eur. J. Pharm. Biopharm. 98, 76-89.

Nguyen, T.X., Huang, L., Gauthier, M., Yang, G., & Wang, Q., 2016. Recent advances in liposome surface modification for oral drug delivery. Nanomedicine (Lond). 11, 1169-1185.

Nielsen, L.S., Schubert, L., & Hansen, J., 1998. Bioadhesive drug delivery systems I. Characterisation of mucoadhesive properties of systems based on glyceryl mono-oleate and glyceryl monolinoleate. Eur. J. Pharm. Sci. 6, 231–239.

Oltra-Noguera, D., Mangas-Sanjuan, V., González-Álvarez, I., Colon-Useche, S., González-Álvarez, M., & Bermejo, M., 2015. Drug gastrointestinal absorption in rat: Strain and gender differences. Eur. J. Pharm. Sci. 78, 198-203.

Owens, D.E., & Peppas, N.A., 2006. Opsonization, biodistribution and pharmacokinetics of polymeric nanoparticles. Int. J. Pharm. 307, 93-102.

Prego, C., Fabre, M., Torres, D., & Alonso, M.J., 2006. Efficacy and mechanism of action of chitosan nanocapsules for oral peptide delivery. Pharm. Res. 23, 549-556.

Ranga Rao, K.V., & Buri, P., 1989. A novel in situ method to test polymers and coated microparticles for bioadhesion. Int. J. Pharm. 52, 265-270.

Siew, A., Le, H., Thiovolet, M., Gellert, P., Schatzlein, A., & Uchegbu, I., 2012. Enhanced oral absorption of hydrophobic and hydrophilic drugs using quaternary ammonium palmitoyl glycol chitosan nanoparticles. Mol. Pharm. 9, 14-28.

Smart, J.D., 2005. The basics and underlying mechanisms of mucoadhesion. Adv. Drug Del. Rev. 57, 1556-1568.

Sogias, I.A., Williams, A.C., & Khutoryanskiy, V.V., 2008. Why is chitosan mucoadhesive? Biomacromolecules 9, 1837–1842.

Spicer, S.S., Schulte, B.A., & Chakrin, L.W., 1983. Ultrastructural and histochemical observations of respiratory epithelium and gland. Exp. Lung Res. 4, 137-156.

Štorha, A., Mun, E.A., & Khutoryanskiy, V.V., 2013. Synthesis of thiolated and acrylated nanoparticles using thiol-ene click chemistry: Towards novel mucoadhesive materials for drug delivery. RSC Adv. 3, 12275–12279.

Symonds, B.L., Lindsay, C.I., Thomson, N.R., & Khutoryanskiy, V.V., 2016a. Chitosan as a rainfastness adjuvant for agrochemicals. RSC Adv. 6, 102206-102213.

Symonds, B.L., Thomson, N.R., Lindsay, C.I., & Khutoryanskiy, V.V., 2016b. Rainfastness of poly(vinyl alcohol) deposits on Vicia faba leaf surfaces: From laboratory-scale washing to simulated rain. ACS Appl. Mater. Interfaces 8, 14220-14230.

Tonglairoum, P., Brannigan, R.P., Opanasopit, P., & Khutoryanskiy, V.V., 2016. Maleimide-bearing nanogels as novel mucoadhesive materials for drug delivery. J. Mater. Chem. B 4, 6581-6587.

Varum, F.J.O., Veiga, F., Sousa, J.S., & Basit, A.W., 2010. An investigation into the role of mucus thickness on mucoadhesion in the gastrointestinal tract of pig. Eur. J. Pharm. Sci. 40, 335-341.

Varum, F.J.O., Veiga, F., Sousa, J.S., & Basit, A.W., 2012. Mucus thickness in the gastrointestinal tract of laboratory animals. J. Pharm. Pharmacol. 64, 218-227.

Withers, C.A., Cook, M.T., Methven, L., Gosney, M.A., & Khutoryanskiy, V.V., 2013. Investigation of milk proteins binding to the oral mucosa. Food Funct. 4, 1668-1674.

Yun, Y., Cho, Y.W., & Park, K., 2013. Nanoparticles for oral delivery: Targeted nanoparticles with peptidic ligands for oral protein delivery. Adv. Drug Del. Rev. 65, 822-832.

# Chapter 4: Synthesis of POZylated and PEGylated chitosan as potential materials for mucosal drug delivery

**Abstract**

In this chapter, we contrast and compare various approaches for the synthesis of POZylated and PEGylated chitosan. The final aim of this study was to prepare nanoparticles using the unmodified and modified chitosan for mucosal drug delivery. Using turbidimetry, it was found that the dispersion of PEGylated chitosan in 1% v/v acetic acid showed less turbidity than the POZylated, thiolated and the unmodified chitosan counterparts at neutral and basic pH. However, none of these modified chitosan were fully soluble at any pH. It is believed that oxidation of thiol groups of thiolated, POZylated and PEGylated chitosan and the subsequent formation of disulfide bonds were responsible for their incomplete solubilisation in water.

## 4.1 Introduction

Chitosan is a natural cationic polysaccharide which has been widely used in the design of mucosal drug delivery systems (MDDS) including nanoparticles (Illum et al., 1994; Illum et al., 2001; Issa et al., 2005). However, poor aqueous solubility of chitosan at pH > 6 limits its applications. Additionally, the mucoadhesive strength of chitosan is limited only to a certain degree which is often not satisfactory and justifies investigating approaches to enhance chitosan mucoadhesive properties. One such approach is the chemical modifications of chitosan. For example, thiolated chitosan was first investigated by Bernkop-Schnürch and co-workers (2003) and showed better mucoadhesive properties than the unmodified chitosan *in vitro* and *in vivo* rat models for oral (Dünnhaupt et al., 2011; Dünnhaupt et al., 2012) and nasal (Krauland et al., 2006) route of administration. Whereas, our group demonstrated that methacrylated chitosan showed an enhanced mucoadhesive properties compared to unmodified chitosan using excised porcine bladder mucosa (Kolawole et al., 2018).

For certain applications, for example when a deeper mucus-penetration is required as in the case of oral and respiratory drug delivery, mucus-penetrating nanoparticles are more useful compared to mucoadhesive nanoparticles. Mucus-penetrating nanoparticles can be prepared via surface modification of nanoparticles using certain hydrophilic polymers including polyethylene glycol (PEG) and poly-2-ethyl-2-oxazoline (POZ). For example, Lai et al. (2007) showed that coating polystyrene nanoparticles with dense PEG (2 kDa) resulted in a rapid transport of the nanoparticles through human cervicovaginal mucus. Maisel et al. (2015) showed that, when carboxylate-modified polystyrene nanoparticles were orally administered to mice, they aggregated in the mucus layer of mice intestinal lumen and could not reach the highly folded absorptive surfaces of villi. In contrast, PEG-coated carboxylate-modified polystyrene nanoparticles diffused freely in the intestinal mucus gel and distributed evenly throughout the intestinal epithelial tissues. Mansfield et al. (2015) demonstrated that the coating of thiolated silica nanoparticles with either PEG or POZ led to an increase in their diffusivity in mucin dispersion and enhanced penetration into the freshly excised porcine gastric mucosa.

In this study an attempt has been made to synthesise thiolated chitosan by reacting chitosan with 2-iminothiolane HCl which was then further modified by reacting it with POZ or PEG using thiol-yne and thiol-ene click reactions to form POZylated and PEGylated chitosan,

respectively. The main aim of this study was to prepare nanoparticles using unmodified and each of thiolated, POZylated and PEGylated chitosan and evaluate their mucus-penetrating properties. It has been hypothesised that both unmodified and thiolated chitosan nanoparticles would potentially be mucoadhesive (thiolated chitosan > unmodified chitosan) whereas both POZylated and PEGylated counterparts mucus-penetrating.

## 4.2 Materials and methods

### 4.2.1 Materials

Medium molecular weight chitosan (190-310 kDa based on viscosity, 75-85% degree of deacetylation), 2-iminothiolane hydrochloride, 5,5′-dithiobis-2-nitrobenzoic acid (DTNB, Ellman's reagent), anhydrous L-cysteine hydrochloride, maleimide-terminated methoxy polyethylene glycol (PEG) 5 kDa, alkyne-terminated-poly-2-ethyl-2-oxazoline (POZ) 5 kDa (PDI ≤ 1.2) and triethyl amine (TEA) were purchased from Sigma-Aldrich (Gillingham, UK). Dialysis tubing with molecular weight cut off 12-14 kDa was purchased from Medicell International Ltd., UK. All other reagents were of analytical grade.

### 4.2.2 Synthesis of thiolated chitosan

The original chitosan was modified according to the method described by Bernkop-Schnürch et al. (2003) with minor modification. Briefly, 500 mg chitosan (1% w/v) was dissolved in 50 mL of 1% v/v acetic acid. Then, the pH was increased to 5 using 5 M NaOH. After that, 200 mg 2-iminothiolane HCl (0.4% w/v) was added and stirred for 24 hours at room temperature. Then, the reaction mixture was dialysed using 5 mM HCl (once), then 5 mM HCl containing 1% w/v NaCl (twice), followed by 5 mM HCl and finally 0.4 mM HCl (once) (each with 4 L over 72 hours). Finally the product was lyophilised and stored at 4 °C until further use.

### 4.2.3 Determination of thiol content

Ellman's assay was used to quantify the immobilised thiol groups on the modified polymers. The polymers were hydrated in ultrapure water (at 1 or 2 mg/mL) for 1 hour. Then, 0.25 mL of the polymer solution was mixed with 0.25 mL phosphate buffer solution (0.5 M, pH 8) and this was reacted with 0.5 mL Ellman's reagent (0.3 mg/mL) in the dark for 2 hours, then centrifuged for 10 minutes at 13000 rpm (Sanyo, Micro Centaur, UK) and 200 µL aliquots

of the supernatant were loaded into a 96 well plate. The absorbance was measured at 420 nm using a BioTek Epoch plate reader. Serial standard solutions of L-cysteine HCl over the concentration range of 0.004 to 0.634 µmol/mL were prepared and reacted under the same condition of the modified chitosan. Finally, the amount of free thiols per one gram of the polymer was calculated.

### 4.2.4 Synthesis of POZylated chitosan

Thiolated chitosan (100 mg) was dispersed in 50 mL deionized water. Then, 200 µL of TEA and 100 mg POZ were added and stirred for 18 hours. Thereafter, the pH was lowered to 5 using 1% v/v acetic acid and the reaction mixture was stirred for 5 hours. The product was dialysed against deionised water (4 L, 5 times, over 24 hours) using 12-14 kDa dialysis membrane (Medicell International Ltd., UK,). The product was freeze dried and stored at 4 °C until further studies.

### 4.2.5 NMR spectroscopy

$^{1}$H NMR spectra were recorded using a Bruker Nanobay 400 MHz NMR spectrometer. Unmodified chitosan (5 mg) was dissolved in $D_2O$ (1 mL) with 10 µL of trifluoroacetic acid (TFA). $D_2O$ was used as a solvent for thiolated and POZylated chitosan (2.5 mg/mL) and PEGylated chitosan (10 mg/mL). The degree of acetylation (DA) of the unmodified chitosan was calculated according to Equation 4.1 (Sogias et al., 2008):

$$DA = \frac{\mathrm{I\,CH_3/3}}{\mathrm{I\,H_2 - H_6/6}} \times 100 \qquad \text{Equation 4.1}$$

Where $\mathrm{I\,CH_3}$ is the intergral intesity of N-acetylated proton and $\mathrm{I\,H_2 - H_6}$ is the summation of the integral intesity of proton number 2, 3, 4, 5 and 6.

### 4.2.6 FTIR spectroscopy

The FTIR spectra of unmodified chitosan and freeze dried modified chitosan were recorded using a spectrum 100 FTIR spectrophotometer (Perkin-Elmer, UK). The spectra were collected from an average of 4 scans, with a resolution of 4 $cm^{-1}$ over the range of 4000-650 $cm^{-1}$.

### 4.2.7 Synthesis of PEGylated and POZylated chitosan; Optimisation study

Since poor water solubility of the resultant POZylated chitosan was observed, another approach was used to synthesise POZylated chitosan. Here, thiolated chitosan was used before freeze drying (i.e. just after the dialysis) as it was expected that the insolubility of the POZylated chitosan was originated from the cross-linking of the precursor thiolated chitosan which could have happened during the freeze drying process of the thiolated chitosan aqueous solution. This approach was also used to synthesise PEGylated chitosan. It should be noted that for this purpose, similar method (section 4.2.2) was used to synthesise thiolated chitosan except the concentration of chitosan and 2-iminothiolane HCl was reduced to 0.5% w/v and 0.2% w/v, respectively.

Table 4.1 shows the composition of the reaction mixtures of PEGylated and POZylated chitosan. Thiolated chitosan was diluted with deionised water before PEG or POZ was added with or without TEA. Then, the reaction mixtures were left at room temperature for 24 hours under continuous stirring. Following this, the resulting products were dialysed against deionised water (4 L, 8 times, over 4 days) using 12-14 kDa dialysis membrane. The products were characterised in terms of particle size by dynamic light scattering (DLS), ξ-potential using Zetasizer Nano-ZS (Malvern, UK) and concentration by freeze drying. The freeze-dried products were used for Ellman's assay and NMR spectroscopy. Thiolated chitosan reacted under the same condition of PEGylated and POZylated chitosan but without PEG or POZ was used as a control.

Table 4.1 Composition of reaction mixtures of PEGylated and POZylated chitosan

| Types of polymers | Thiolated chitosan solution (mL) | DI water (mL) | PEG (mg) | POZ (mg) | TEA (µL) |
|---|---|---|---|---|---|
| Control | 5 | 20 | - | - | - |
| PEG-chitosan 1 | 5 | 20 | 50 | - | - |
| PEG-chitosan 2 | 5 | 20 | 100 | - | - |
| PEG-chitosan 3 | 5 | 20 | 50 | | 10 (pH 6) |
| POZ-chitosan 1 | 5 | 20 | - | 50 | - |
| POZ-chitosan 2 | 5 | 20 | - | 100 | - |
| POZ-chitosan 3 | 5 | 20 | - | 50 | 5 (pH 5) |

### 4.2.8 pH-solubility profile

Solubility of the unmodified and modified chitosan was measured at different pH at room temperature using turbidimetric technique. The polymers were dissolved/dispersed (0.5 mg/mL) in 1% v/v acetic acid and left stirring for 24 hours. The turbidity (absorbance) of the systems was measured with a Jenway 7315 UV-visible spectrophotometer at 400 nm using 1% v/v acetic acid as a blank. The pH was adjusted using 1 M NaOH solution.

## 4.3 Results and discussion

Thiolated chitosan was synthesised according to the method described by Bernkop-Schnürch et al. (2003) (Figure 4.1). The method involves the covalent attachment of 2-iminothiolane HCl to chitosan leading to the immobilisation of thiol groups (-SH) on chitosan as a result of amidine bond formation. In this method, reaction mediators including 1-ethyl-3-(3-dimethylaminopropyl)-carbodiimide hydrochloride (EDAC)/N-hydroxysuccinimide (NHS)

are not required. In contrast, the methods based on amide bond formation require these mediators (Kast & Bernkop-Schnürch, 2001; Roldo et al., 2004; Hintzen et al., 2013).

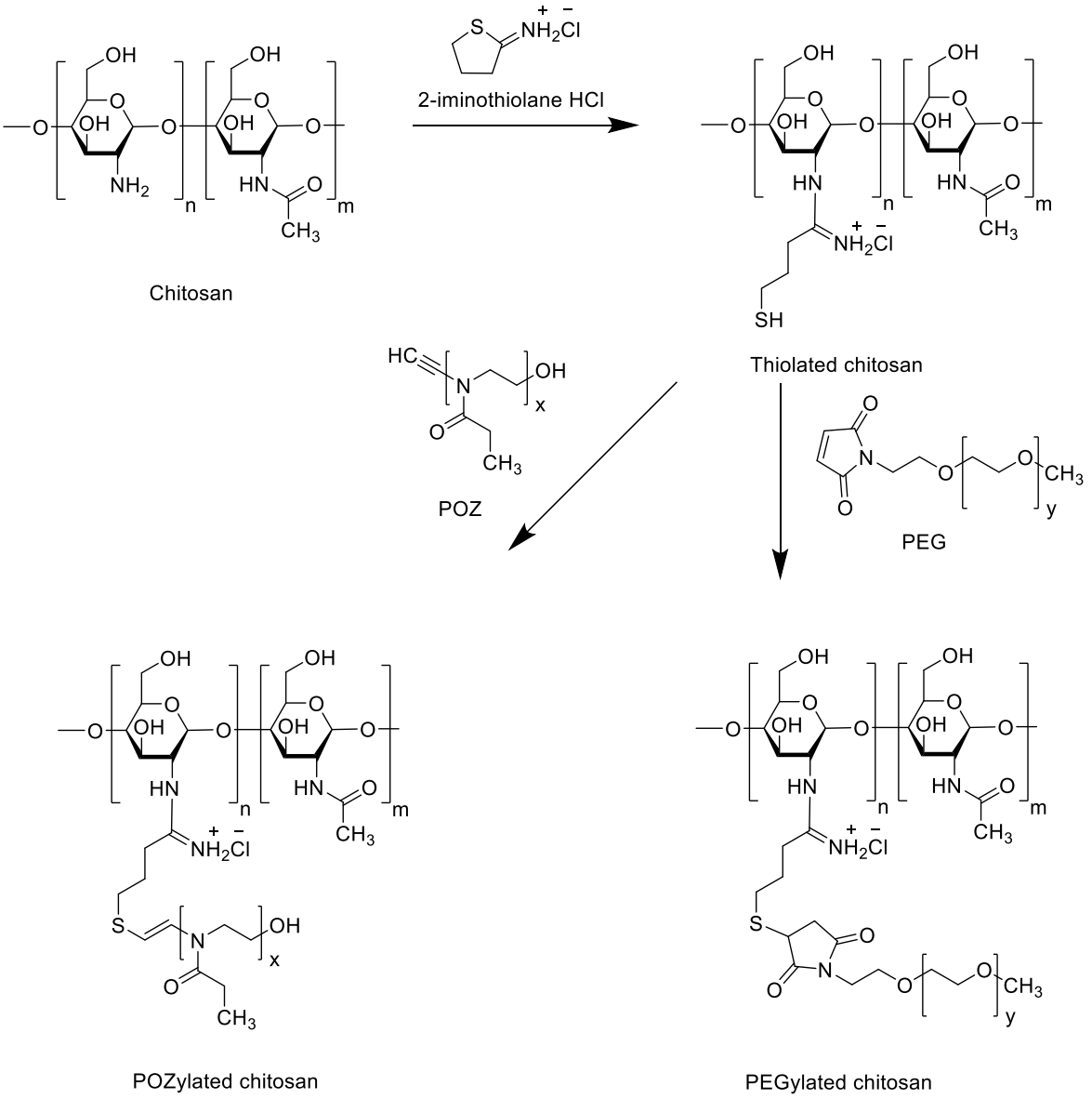


Figure 4.1 Synthetic pathways of thiolated, POZylated and PEGylated chitosan.

The thiolated chitosan synthesised in this study had a white-faint yellow colour with a fibrous structure. Using Ellman's assay, it was found that the thiolated chitosan had 432 ± 28 µmol/g free thiol groups. Also, the reaction showed a high yield (69.8%). These results were in agreement with the results reported by Bernkop-Schnürch et al. (2003). For instance, their thiolated chitosan had a free thiol groups of 408.9 ± 49.8 µmol/g and had a white appearance with a fibrous structure. However, compared to thiolated chitosan synthesised by Roldo et al. (2004) (263.8 ± 47.4 µmol/g), thiolated chitosan synthesised in the current study (432 ± 28 µmol/g) showed a higher amount of free thiol groups. Nevertheless, the weight ratio of chitosan/2-iminothiolane HCl, the pH of the reaction mixture and the molecular weight of the chitosan seem to influence the thiol content of the resultant thiolated chitosan (Bernkop-Schnürch et al., 2003; Roldo et al., 2004). A higher free thiol content would potentially lead to better mucoadhesive properties. Also, these free thiol groups can potentially react with alkyne and alkene groups via thiol-yne and thiol-ene click reactions. Therefore, POZylated chitosan was synthesised by reacting thiolated chitosan with alkyne terminated POZ (Figure 4.1). The product yield was 78% and it had a white colour with a soft structure.

As shown in Figure 4.2, the $^{1}$H NMR assignments of unmodified chitosan were as follows; chemical shift (δ) = 3.06 ppm (H2), δ = 3.57-3.80 ppm (H3-H6) and δ = 1.97 ppm ($NHCOCH_3$). The peak of H1 was not observed. The degree of acetylation was 25%. No difference between the $^{1}$H NMR spectrum of unmodified and thiolated chitosan was observed (Figure 4.2). We believe that the peaks of H7, H8 and H9 were overlapped in δ =3.61-3.80 ppm (H3-H8) and δ = 3.07 ppm (H2 and H9). The POZylated chitosan, however, showed very characteristic peaks at δ = 1 ppm (H12) and δ = 2.29 ppm (H11), in addition to the peaks of thiolated chitosan (Figure 4.2). From the NMR spectra of pure POZ (Figure 4.2), it was revealed that theses peaks are related to POZ.

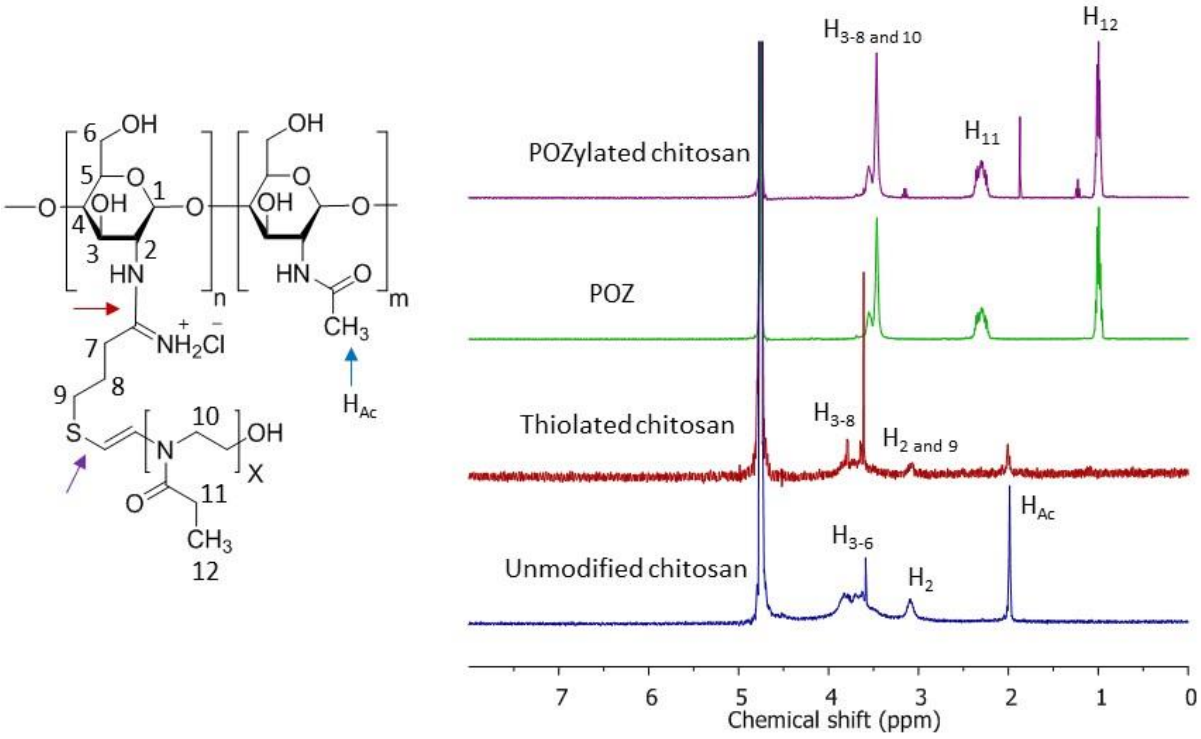


Figure 4.2 $^{1}H$ NMR spectra of unmodified, thiolated and POZylated chitosan, $H_{Ac}$ = acetylated hydrogen. The proposed molecular structure of POZylated chitosan is shown. The red arrow indicates the possible bond formed leading to thiolated chitosan, whereas the purple arrow shows the possible bond formed leading to POZylated chitosan.

The FTIR spectra of unmodified, thiolated and POZylated chitosan are shown in Figure 4.3. As noted, a characteristic broad peak appeared at 3362 $cm^{-1}$ related to the stretching vibration of both –OH and $NH_2$ groups of the unmodified chitosan. In case of thiolated chitosan, these peaks were also observed, but with a slight change in their intensities which is believed to be due to the reduction in the number of $–NH_2$ group upon thiolation. Amide bond peaks were observed at 1650 and 1630 $cm^{-1}$ for unmodified and thiolated chitosan, respectively. Additionally, in the spectrum of thiolated chitosan, a new peak was observed at 1523 $cm^{-1}$ which can be associated with the stretching vibration of C=N of amidine groups. These results are in agreement with the study of Sakloetsakun et al. (2010). POZylated chitosan showed a sharp strong peak at 1631 $cm^{-1}$ due to the stretching vibration of C=O of POZ. In addition, a medium peak at 1470 $cm^{-1}$ appeared which belongs to the bending vibration of $CH_3$ group of POZ.

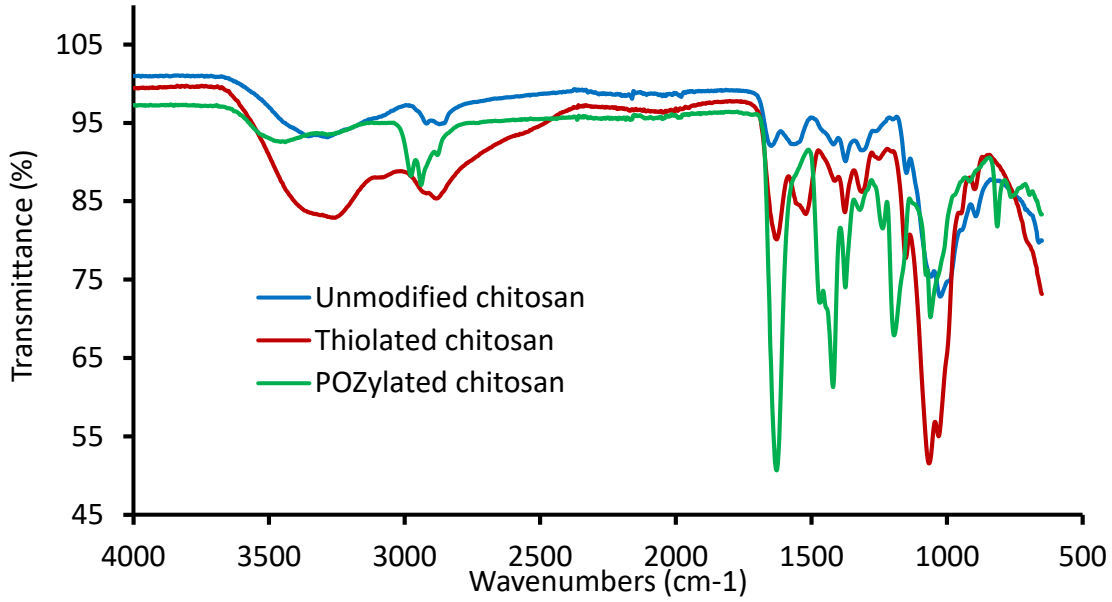


Figure 4.3 FTIR spectra of unmodified, thiolated and POZylated chitosan

### 4.3.1 Optimisation study

The DLS study revealed the presence of some large particles (few μm, Table 4.2) in the aqueous dispersions of all types of the modified chitosan. This means the systems were not molecularly dispersed in water and rather aggregates of some macromolecules were formed. Their polydispersity index (PDI) was high, which indicated high polydispersity of the products. Both PEGylated and POZylated chitosan had lower ξ-potential than thiolated chitosan which could be due to the grafting of PEG or POZ to thiolated chitosan. Moreover, the concentration of both PEGylated and POZylated chitosan dispersions were higher than the control due to the incorporation of PEG or POZ. This was further increased with increasing the amount of PEG or POZ in the reaction mixture but did not significantly change with the addition of TEA (Table 4.2).

Table 4.2 Characteristics of PEGylated and POZylated chitosan dispersions just after the dialysis; samples were diluted with ultrapure water (1:100) before the measurement (mean ± SD, n = 3). PEG-chitosan 1, 2, 3 and POZ-chitosan 1, 2, 3 refer to the products synthesised according to conditions described in Table 4.1.

| Types of polymers | Z-average (nm, DLS) | PDI | ξ-potential (mV) | Conc. (mg/mL) |
|---|---|---|---|---|
| Thiolated chitosan | 3319 ± 170 | 0.384 ± 0.227 | 50.85 ± 8.29 | 11.51 ± 2.82 |
| Control thiolated chitosan | 6748 ± 6063 | 0.759 ± 0.182 | 36.17 ± 1.50 | 1.23 ± 0.01 |
| PEG-chitosan 1 | 2329 ± 220 | 0.703 ± 0.102 | 20.77 ± 4.15 | 2.79 ± 0.01 |
| PEG-chitosan 2 | 2105 ± 842 | 0.790 ± 0.127 | 27.68 ± 3.01 | 4.32 ± 0.01 |
| PEG-chitosan 3 | 2888 ± 432 | 0.685 ± 0.075 | 23.22 ± 5.38 | 3.01 ± 0.01 |
| POZ-chitosan 1 | 2611 ± 665 | 0.540 ± 0.167 | 30.10 ± 7.10 | 2.45 ± 0.03 |
| POZ-chitosan 2 | 3272 ± 643 | 0.757 ± 0.174 | 34.14 ± 2.42 | 3.44 ± 0.05 |
| POZ-chitosan 3 | 2988 ± 969 | 0.906 ± 0.125 | 29.30 ± 2.06 | 2.46 ± 0.04 |

Ellman's assay showed that all three PEG-chitosan conjugates did not contain any free thiol groups. This suggested that all free thiol groups of thiolated chitosan were reacted with maleimide double bonds of PEG. However, in case of POZ-chitosan conjugates, only POZ-chitosan 2 exhibited complete consumption of all free thiol groups, whereas both POZ-chitosan 1 and POZ-chitosan 3 showed 43.2 ± 5.5 and 47.0 ± 14.1 µmol/g of free thiol groups, respectively (Figure 4.4). This indicated that an increase in the concentration of POZ resulted in a higher degree of substitution (DS). On the other hand, the addition of TEA to the reaction mixture did not increase the DS of POZylated chitosan. Although some studies showed that TEA could facilitate thiol-yne click reaction (Ganivada et al., 2015; Mansfield et al., 2015), no improvement in the DS was achieved upon addition of TEA. This could be attributed to the small amount of TEA (5 µL**)** which was less than the amount used by Mansfield et al. (2015) (200 µL**)**. It should be noted that, the increase in the amount of TEA,

leads to the precipitation of thiolated chitosan and formation of disulfide bonds which leads to the reduction of free thiol groups. Thus, in our study, minimum amount of TEA was used. Based on these results, PEG-chitosan 2 and POZ-chitosan 2 were selected for $^{1}$H NMR spectroscopy and pH-solubility studies which will be discussed further.

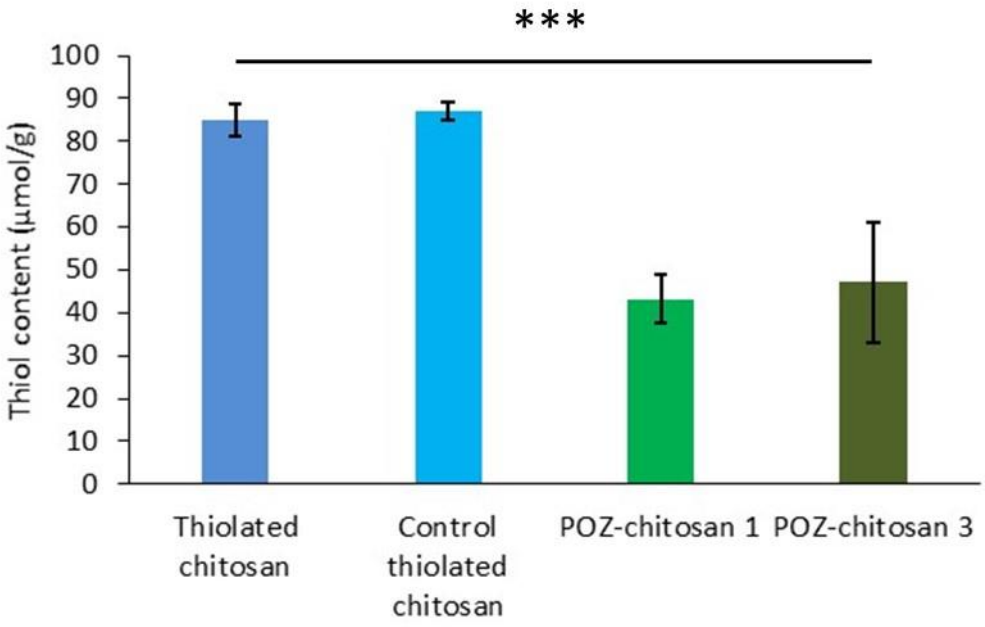


Figure 4.4 Thiol content of thiolated and POZylated chitosan; *** denotes $p < 0.001$; no significant difference between thiolated chitosan and control thiolated chitosan ($p = 0.689$) and also between POZ-chitosan 1 and POZ-chitosan 3 ($p = 0.507$) was observed (one way ANOVA).

The $^{1}$H NMR spectrum of pure PEG showed peaks at 3.34, 3.47-3.84 and 6.84 ppm related to protons a, b, c, d and e, respectively which are highlighted in Figure 4.5 (Luo et al., 2016; Ananda K. et al., 2008). The $^{1}$H NMR spectrum of PEG-chitosan 2 (Figure 4.5) also showed all these peaks except the maleimide-related peak at 6.84 ppm which confirmed the disappearance of the double bond of maleimide and subsequent formation of C-S single bond. Chitosan-related peaks were also observed. The $^{1}$H NMR spectrum of POZ-chitosan 2 showed peaks related to POZ, however, peaks related to chitosan were not clearly visible (data not shown).

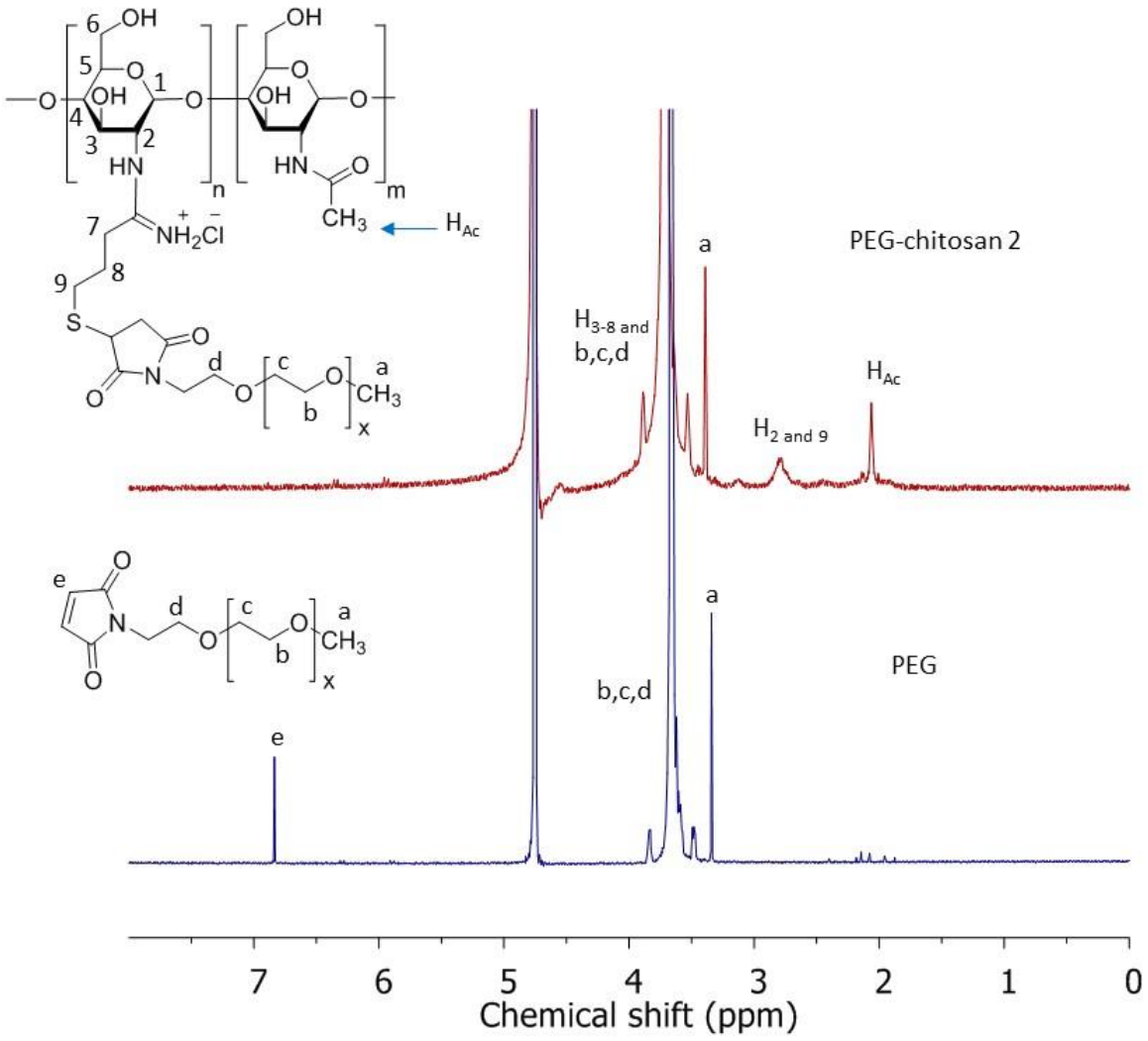


Figure 4.5 $^{1}H$ NMR spectra of PEG and PEG-chitosan 2 in $D_2O$ (10 mg/mL), $H_{Ac}$ = acetylated hydrogen.

Since the main challenge with chitosan is its poor aqueous solubility (especially when pH is higher than its pKa (pH 5.5–6.5)) (Casettari et al., 2012), the turbidimetric technique was used to determine the pH-solubility profiles of unmodified and modified chitosan (Figure 4.6). It was found that the unmodified chitosan was soluble at acidic pH ranges. However, it underwent rapid precipitation at pH higher than 7.3. Thiolated and POZylated chitosan dispersions, however, showed more turbidity than unmodified chitosan at acidic pH, whereas at basic pH, they were less turbid than the unmodified chitosan. In contrast, PEGylated

chitosan showed better dispersibility (illustrated by its low turbidity, about 0.04 a.u.) at acidic pH than both thiolated and POZylated chitosan. Interestingly, its turbidity did not change after the pH was increased to 11 but it still was not completely soluble. This result could be due to the grafting of PEG on chitosan macromolecules which could reduce the crystallinity of chitosan by reducing intra and inter-molecular hydrogen bonding, leading to enhanced solubility (Sogias et al., 2010). Nevertheless, the incomplete solubilisation of thiolated, POZylated and PEGylated chitosan could be due to the formation of disulfide bonds upon oxidation of thiol groups which eventually leads to the formation of insoluble crosslinked structure (Bernkop-Schnürch et al., 2003). Decreasing the number of free amino groups due to their substitution with 2-iminothiolane HCl can also be another possible reason for the poor solubility of thiolated, POZylated and PEGylated chitosan. The amino groups are essential for complete dissolution of chitosan as they undergo protonation and enhance the solubility of chitosan (Saito et al., 1997; Mao et al., 2005; Casettari et al., 2012).

Some other studies also reported the incomplete solubilisation of thiolated chitosan synthesised from chitosan with the molecular weights of 50, 100 and 400 kDa in 0.2 M nitric acid even at pH 1 (Bravo-Osuna et al., 2006; Bravo-Osuna et al., 2007a; Bravo-Osuna et al., 2007b). Also it has been observed that aqueous solution of thiolated chitosan with thiol content of 46.59 ± 15.04 µmol/g was slightly viscous, however a higher thiol content made the polymer insoluble in the aqueous media (Maculotti et al., 2005). Conversely, Masuko et al. (2005) suggested that even the solution of thiolated chitosan with 913 µmol/g in 1% v/v acetic acid was completely soluble over the pH range of 7-10 indicated by a very low absorbance at 650 nm. Masuko et al. (2005) performed the thiolation reaction at a higher temperature (55 °C), for a short time (4-10 hours) and using a high molar ratio of 2-iminothiolane/$NH_2$ group of chitosan (64:1).

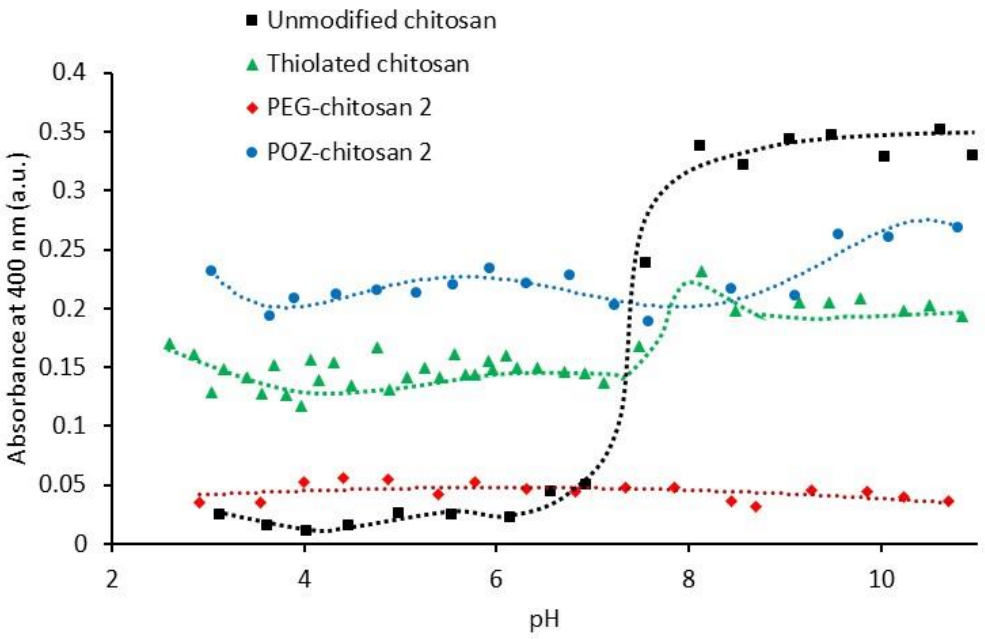


Figure 4.6 pH-solubility profiles of unmodified, thiolated, PEGylated and POZylated chitosan using turbidimetry.

Several studies have reported the effect of PEGylation on water solubility of chitosan and suggested that the solubility of the PEGylated chitosan is largely dependent on the molecular weight and the type of the parent chitosan and the DS of the PEGylated chitosan. Casettari et al. (2010) demonstrated that PEGylated chitosan was fully soluble in aqueous buffer at pH 2 to 9.6. Jeong et al. (2008) conjugated PEG to low molecular weight chitosan (10 kDa) and found that the PEGylated chitosan did not only show good transparency (higher than 90%) in aqueous buffers but was also soluble in common organic solvents including DMSO and DMF. Chitosan used in our study was larger than the chitosan used by Jeong et al. (2008) (medium molecular weight versus 10 kDa). On the other hand, Mao et al. (2005) synthesised PEGylated trimethyl chitosan (PEG-TMC) where TMC with 40% degree of quaternisation was prepared, then native chitosan and TMC was PEGylated. The results showed that solutions of PEG-native chitosan, even with high DS, were not clear at pH 7. However, solutions of PEG-TMC were clear over the entire pH ranges regardless of PEG molecular weight and DS. The authors believed that the lower water solubility of PEG-native chitosan compared to PEG-TMC is due to the strong interaction between PEG and native chitosan

which was also confirmed by the decrease in melting temperature ($T_{m)}$. In addition, Saito et al. (1997) found that PEGylated chitosan with DS of 78.5 and 92.7 %w/w were soluble up to pH 6.5. However, when the pH was increased to 6.8, PEGylated chitosan with DS of 78.5% w/w showed a cloudy solution while PEGylated chitosan with DS of 92.7% w/w remained clear.

In the current study, Ellman's data indirectly showed that PEGylated and POZylated chitosan had similar DS (as in both cases no free thiol content was detected). However, PEGylated chitosan dispersion was less turbid compared to POZylated chitosan counterpart.

### 4.4 Conclusion

In the present study, thiolated chitosan was synthesised by reacting unmodified chitosan with 2-iminothiolane HCl. Then, the thiolated chitosan has been reacted with alkyne-terminated POZ and maleimide-terminated PEG to synthesise POZylated and PEGylated chitosan, respectively. Generally, all the modified chitosans showed incomplete solubilisation in water discouraging the subsequent formation of the nanoparticles using these modified chitosan. Studies towards improving the solubility of thiolated chitosan could potentially result in better solubility of both POZylated and PEGylated chitosan which could lead to some interesting materials for mucosal drug delivery. It seems the main cause of insolubility of thiolated chitosan is the oxidation of its free thiol groups (-SH) and formation of disulfide bonds (S-S) leading to a crosslinked structure. Although this seems to be an unavoidable issue, performing the thiolation reaction under inert condition (e.g. nitrogen) and dark could potentially improve the solubility of thiolated chitosan. If any thiol groups of thiolated chitosan oxidised to form disulfide bonds, these bonds would possibly remain in the POZylated and PEGylated chitosan and would potentially make these two products only partially soluble in water.

## 4.5 References

Ananda K., Nacharaju, P., Smith, P.K., Acharya, S.A., & Manjula, B.N., 2008. Analysis of functionalization of methoxy–PEG as maleimide–PEG. Anal. Biochem. 374, 231–242.

Bernkop-Schnürch, A., Hornof, M., & Zoidl, T., 2003. Thiolated polymers—thiomers: Synthesis and in vitro evaluation of chitosan–2-iminothiolane conjugates. Int. J. Pharm. 260, 229-237.

Bravo-Osuna, I., Millotti, G., Vauthier, C., & Ponchel, G., 2007a. In vitro evaluation of calcium binding capacity of chitosan and thiolated chitosan poly(isobutyl cyanoacrylate) core–shell nanoparticles. Int. J. Pharm. 338, 284-290.

Bravo-Osuna, I., Schmitz, T., Bernkop-Schnürch, A., Vauthier, C., & Ponchel, G., 2006. Elaboration and characterization of thiolated chitosan-coated acrylic nanoparticles. Int. J. Pharm. 316, 170-175.

Bravo-Osuna, I., Vauthier, C., Farabollini, A., Palmieri, G.F., & Ponchel, G., 2007b. Mucoadhesion mechanism of chitosan and thiolated chitosan-poly(isobutyl cyanoacrylate) core-shell nanoparticles. Biomaterials 28, 2233-2243.

Casettari, L., Vllasaliu, D., Castagnino, E., Stolnik, S., Howdle, S., & Illum, L., 2012. PEGylated chitosan derivatives: Synthesis, characterisations and pharmaceutical applications. Prog. Polym. Sci. 37, 659-685.

Casettari, L., Vllasaliu, D., Stolnik, S., Mantovani, G., Illum, L., & Howdle, M.S., 2010. Effect of PEGylation on the toxicity and permeability enhancement of chitosan. Biomacromolecules 11, 2854–2865.

Dünnhaupt, S., Barthelmes, J., Hombach, J., Sakloetsakun, D., Arkhipova, V., & Bernkop-Schnürch, A., 2011. Distribution of thiolated mucoadhesive nanoparticles on intestinal mucosa. Int. J. Pharm. 408, 191-199.

Dünnhaupt, S., Barthelmes, J., Iqbal, J., Perera, G., Thurner, C.C., Friedl, H., & Bernkop-Schnürch, A., 2012. In vivo evaluation of an oral drug delivery system for peptides based on S-protected thiolated chitosan. J. Control. Release 160, 477-485.

Ganivada, M.N., Kumar, P., & Shunmugam, R., 2015. A unique polymeric gel by thiol–alkyne click chemistry. RSC Adv. 5, 50001-50004.

Hintzen, F., Hauptstein, S., Perera, G., & Bernkop-Schnürch, A., 2013. Synthesis and in vitro characterisation of entirely S-protected thiolated pectin for drug delivery. Eur. J. Pharm. Biopharm. 85, 1266-1273.

Illum, L., Farraj, N.F., & Davis, S.S., 1994. Chitosan as a novel nasal delivery system for peptide drugs. Pharmaceutical Research 11, 1186-1189.

Illum, L., Jabbal-Gill, I., Hinchcliffe, M., Fisher, A.N., & Davis, S.S., 2001. Chitosan as a novel nasal delivery system for vaccines. Adv. Drug Del. Rev. 51, 81-96.

Issa, M.M., Köping-Höggård, M., & Artursson, P., 2005. Chitosan and the mucosal delivery of biotechnology drugs. Drug Discovery Today: Technol. 2, 1-6.

Jeong, Y., Kim, D., Jang, M., & Nah, J., 2008. Preparation and spectroscopic characterization of methoxy poly(ethylene glycol)-grafted water-soluble chitosan. Carbohydrate Research 343 282–289.

Kast, C., & Bernkop-Schnürch, A., 2001. Thiolated polymers-thiomers: development and in vitro evaluation of chitosan-thioglycolic acid conjugates. Biomaterials 22, 2345-2352.

Kolawole, O.M., Lau, W.M., & Khutoryanskiy, V.V., 2018. Methacrylated chitosan as a polymer with enhanced mucoadhesive properties for transmucosal drug delivery. Int. J. Pharm. 550, 123-129.

Krauland, A.H., Leitner, V.M., Grabovac, V., & Bernkop-Schnürch, A., 2006. In vivo evaluation of a nasal insulin delivery system based on thiolated chitosan. J. Pharm. Sci. 95, 2463-2472.

Lai, S.K., O'Hanlon, D.E., Harrold, S., Man, S.T., Wang, Y.Y., Cone, R., & Hanes, J., 2007. Rapid transport of large polymeric nanoparticles in fresh undiluted human mucus. Proceedings of the National Academy of Sciences of the United States of America 104, 1482-1487.

Luo, Q., Gao, H., Peng, L., Liu, G., & Zhang, Z., 2016. Synthesis of PEGylated chitosan copolymers as efficiently antimicrobial coatings for leather. J. Appl. Polym. Sci., 43465-43472.

Maculotti, K., Genta, I., Perugini, P., Imam, M., Bernkop-Schnürch, A., & Pavanetto, F., 2005. Preparation and in vitro evaluation of thiolated chitosan microparticles. J. Microencapsul. 22, 459-470.

Maisel, K., Ensign, L., Reddy, M., Cone, R., & Hanes, J., 2015. Effect of surface chemistry on nanoparticle interaction with gastrointestinal mucus and distribution in the gastrointestinal tract following oral and rectal administration in the mouse. J. Control. Release 197, 48-57.

Mansfield, E.D., Sillence, K., Hole, P., Williams, A.C., & Khutoryanskiy, V.V., 2015. POZylation: A new approach to enhance nanoparticle diffusion through mucosal barriers. Nanoscale 7, 13671-13679.

Mao, S., Shuaia, X., Ungera, F., Wittmara, M., Xiec, X., & Kissela, T., 2005. Synthesis, characterization and cytotoxicity of poly(ethylene glycol)-graft-trimethyl chitosan block copolymers. Biomaterials 26, 6343–6356.

Masuko, T., Minami, A., Iwasaki, N., Majima, T., Nishimura, S.-I., & Lee, Y.C., 2005. Thiolation of Chitosan. Attachment of Proteins via Thioether Formation. Biomacromolecules 6, 880-884.

Roldo, M., Hornof, M., Caliceti, P., & Bernkop-Schnürch, A., 2004. Mucoadhesive thiolated chitosans as platforms for oral controlled drug delivery: Synthesis and in vitro evaluation. Eur. J. Pharm. Biopharm. 57, 115-121.

Saito, H., Wu, X., Harris, J.M., & Hoffman, A.S., 1997. Graft copolymers of poly(ethylene glycol) (PEG) and chitosan. Macromol. Rapid Commun 18, 547-550.

Sakloetsakun, D., Perera, G., Hombach, J., Millotti, G., & Bernkop-Schnürch, A., 2010. The impact of vehicles on the mucoadhesive properties of orally administrated nanoparticles: A case study with chitosan-4-thiobutylamidine conjugate. AAPS PharmSciTech 11, 1185-1192.

Sogias, I.A., Khutoryanskiy, V.V., & Williams, A.C., 2010. Exploring the factors affecting the solubility of chitosan in water. Macromol. Chem. Phys. 211, 426-433.

Sogias, I.A., Williams, A.C., & Khutoryanskiy, V.V., 2008. Why is chitosan mucoadhesive? Biomacromolecules 9, 1837–1842.

# Chapter 5: Developing mucus-penetrating chitosan nanoparticles for nasal drug delivery

This chapter is planned to be published in Nanoscale as:

M. Ways, T.M., Lau, W.M., Hoogenboom, R., Maji S., Glassner, M., Cegłowski M., Filippov S. K. & Khutoryanskiy, V.V., Developing mucus-penetrating chitosan nanoparticles for nasal drug delivery.

**Abstract**

The administration of drugs via the nasal route offers the benefits of avoiding pre-systemic metabolism, rapid absorption, the possibility of accessing the brain and a better patient compliance. However, the nasal route also includes the presence of a highly viscous mucus and mucociliary clearance mechanism, which normally protect the human body by preventing the entrance of harmful chemicals and microorganisms, but often generate obstacles in the absorption of drugs and nanoformulations leading to poor efficacy. The design of mucus-penetrating nanoparticles can overcome the barrier function of mucus and mucociliary clearance which may lead to better therapeutic outcomes. Thus, in this study, unmodified and modified chitosan (grafted with 5 kDa polyethylene glycol (PEG)-, polyhydroxyethyl acrylate (PHEA)-, poly-2-ethyl-2-oxazoline (POZ)- and polyvinyl pyrrolidone (PVP)-CO-NH-chitosan) nanoparticles were prepared by an ionic gelation method using sodium tripolyphosphate. The nanoparticles were characterised using DLS, TEM and NTA. A method to evaluate the diffusion of chitosan nanoparticles in bovine submaxillary mucin (BSM) solution using NTA has been developed. It was found that modified chitosan nanoparticles diffuse faster in BSM solution than unmodified chitosan nanoparticles. The penetration into the sheep nasal mucosa study corroborated the diffusion data. Our findings in this study, encourage researchers to use these mucus-penetrating chitosan nanoparticles in nasal drug delivery.

## 5.1 Introduction

Nasal route of drug administration is advantageous as it avoids first pass metabolism, provides rapid onset of action and is non-invasive (Ugwoke et al., 2005). It is also considered as a potential direct transport route of drugs from the nasal cavity to the brain useful for the treatment of various central nervous system diseases including epilepsy, schizophrenia, migraine, Alzheimer's and meningitis which require the delivery of the drugs to the brain (Mistry et al., 2009; Kozlovskaya et al., 2014). The nasal mucosa is covered by a viscoelastic mucus gel layer similar to other mucosal surfaces, e.g. the gastrointestinal tract, eyes and respiratory system. The mucus layer acts as a protective barrier preventing the entrance of harmful substances into the human tissues. However, the protective function of mucus also inhibits the diffusion of lipophilic drugs and nanoformulations and can result in a significant reduction of their efficacy (Lai et al., 2009; Sigurdsson et al., 2013).

Human nasal cavity and upper airways produce about 1.5-2 L of nasal mucus daily which forms a 5 μm thick mucus bilayer (lower sol and upper gel layer) (Ugwoke et al., 2005). However, in the case of respiratory diseases including chronic rhinitis, asthma and chronic obstructive pulmonary disease, excessive mucus production and mucosal hyper-responsiveness lead to the formation of thick and tenacious mucus layer (Baraniuk, 1997; Rogers & Barnes, 2006; Sin & Togias, 2011; Ramos et al., 2014). It is known that the mucus layer is continuously renewed during mucus turnover within various times depending on the type of mucosal surfaces. The rapid movement of cilia propels the nasal respiratory mucus (known as mucociliary clearance) from the interior toward the posterior part of the nasal cavity resulting in a short mucus turnover time (15-20 minutes, in human) (Illum, 2003). In rats, the mucus turnover time of nasal respiratory mucosa is about 10 minutes (Harkema et al., 2006). The mucociliary clearance and the mucus turnover significantly decrease the residence time of both conventional (e.g. simple solution) and mucoadhesive drug delivery systems at the nasal mucosa (Lai et al., 2009). Due to the protective mechanism of the mucus barrier, alternative drug delivery systems that allow rapid penetration through the mucus layer and overcome the mucociliary clearance must be sought.

It has been shown that mucoadhesive chitosan-based nanoemulsion could improve the nose to brain transport of small molecular weight drugs including risperidone in rats compared to the uncoated nanoemulsion and the simple resperidone solution (Kumar et al., 2008). Thiolated chitosan nanoparticles enhanced the permeation of leuprolide through freshly

excised porcine respiratory mucosa compared to unmodified chitosan nanoparticles and leuprolide solution (Shahnaz et al., 2012). Also, thiolated chitosan nanoparticles improved the bioavailability of leuprolide after nasal administration to Sprague–Dawley rats compared to the unmodified chitosan nanoparticles and leuprolide solution. These effects could be due to the mucoadhesive properties of thiolated chitosan, the ability of thiolated chitosan to open the tight junctions (the hydrophilic channels between the epithelial cells) and protect leuprolide against enzymatic degradation (Shahnaz et al., 2012).

Surface modification has been shown to enhance the penetration of nanoparticles into the nasal mucosa (Sonvico et al., 2018). For example, Vila et al. (2004) demonstrated an enhanced nasal mucosal penetration of high density polyethylene glycol coated polylactic acid (PEG-coated PLA) nanoparticles compared to low density PEG-coated and non-coated PLA nanoparticles in rat. Lai et al. (2011) showed that 200 nm PEG-coated polystyrene nanoparticles diffused significantly faster than 200 nm uncoated polystyrene nanoparticles in human chronic rhinosinusitis mucus which was collected from maxillary sinus cavities. In the same study, they also showed the enhanced diffusivity of 188 nm Pluronic-F127-coated polylactide-co-glycolide (PLGA) nanoparticles compared to 129 nm uncoated PLGA nanoparticles. In an *ex vivo* porcine model, Mistry et al. (2015) found that chitosan-coated polystyrene nanoparticles entrapped in the mucus layer and could not reach the epithelial layer of olfactory mucosa. However, the polysorbate-80-coated polystyrene nanoparticles showed some degree of penetration into the epithelial cells. Nevertheless none of these two types of nanoparticles were able to cross the excised porcine olfactory mucosa in significant quantity.

PEG has been used as a gold standard polymer with stealth properties, however, its efficiency as a coating material in the mucus penetrating nanoparticles is controversial. For example, using atomic force microscopy, Kirch et al. (2012) showed that PEG-coated dextran-iron oxide magnetic composite nanoparticles (500 nm) are less mucoadhesive than their chitosan-coated counterpart when 1% w/v mucin solution was used as a substrate. However, upon conducting capillary penetration experiment using mucus from the distal part of horse bronchia, no difference in the mucus penetration ability between the two types of nanoparticles was observed. On the other hand, Schneider et al. (2017) demonstrated that PEG coating significantly improved the mobility of both polystyrene and PLGA nanoparticles in the mouse lung mucus *in vivo* compared to non-coated polystyrene and

PLGA nanoparticles. In a mouse model of acute lung inflammation, they also showed that inhalation of dexamethasone sodium phosphate loaded PEG-coated PLGA nanoparticles enhanced the anti-inflammatory effect compared to free dexamethasone sodium phosphate and dexamethasone sodium phosphate loaded non-coated PLGA nanoparticles (Schneider et al., 2017).

Previously, we showed that PEGylated and poly-2-ethyl-2-oxazoline (POZ)ylated silica nanoparticles had a greater diffusivity in porcine gastric mucin (PGM) dispersion and porcine gastric mucosa compared to their thiolated counterpart (Mansfield et al., 2015). Later, we demonstrated that nanoparticles coated with a more hydrophilic polyoxazoline derivative (poly-2-methyl-2-oxazoline) penetrated deeper into the porcine gastric mucosa compared to the nanoparticles coated with a less hydrophilic polyoxazoline derivatives (POZ and poly-2-n-propyl-2-oxazoline) (Mansfield et al., 2016). Considering the above aspects, in this study, we sought to determine the potential of some hydrophilic polymers in the design of mucus-penetrating chitosan nanoparticles for nasal drug delivery. Thus, we prepared 4 types of nanoparticles (PEG-, polyhydroxyethyl acrylate(PHEA)-, POZ- and polyvinyl pyrrolidone(PVP)-CO-NH-chitosan-TPP) (hereinafter refer to PEG-, PHEA-, POZ- and PVP-chitosan nanoparticles) and compared their diffusivity in mucin solution and sheep nasal mucosa against unmodified chitosan nanoparticles.

## 5.2 Materials and methods

### 5.2.1 Materials

Medium molecular weight chitosan (degree of deacetylation 75-85%), trifluoroacetic acid (TFA), $D_2O$, methoxy-PEG-COOH (5 kDa), 1-ethyl-3-(3-dimethylaminopropyl)-carbodiimide hydrochloride (EDAC), N-hydroxysuccinimide (NHS), mucin from bovine submaxillary glands Type I-S (BSM), sodium tripolyphosphate (TPP), 4′,6-diamidino-2-phenylindole dihydrochloride (DAPI), ninhydrin and D-(+) glucosamine hydrochloride were purchased from Sigma-Aldrich (Gillingham, UK). Uranyl acetate dihydrate was purchased from Agar Scientific (UK). Sodium acetate trihydrate, Molecular Probes™ Alexa Fluor™ 546 NHS ester (Alexa Fluor™ 546), glacial acetic acid, dimethyl sulfoxide (DMSO), sodium hydroxide (NaOH) and Cellpath™ OCT embedding matrix (OCT) were purchased from Fisher Scientific (UK). Dialysis membrane with molecular cut-off 12–14 kDa was purchased from Medicell International Ltd., UK. Phosphotungstic acid hydrate was purchased from Fluca (UK). Hydroxyethyl acrylate (HEA, 96%, Aldrich) was

destabilized by passing the monomer through a basic aluminum oxide column prior to polymerization. *N*-Vinylpyrrolidone (NVP, 99%, Acros) was purified by vacuum distillation. 2,2'-Azobis(isobutyronitrile) (AIBN), potassium ethyl xanthogenate and 2-bromopropionic acid 99% were obtained from Sigma-Aldrich. AIBN was purified by recrystallization twice in methanol before use. HPLC grade solvents *N,N*-dimethylacetamide (DMA), diethyl ether and dichloromethane were obtained from Sigma Aldrich, *N,N*-dimethylformamide (DMF) from Biosolve and n-hexane from Fischer Scientific. 2-(butylthiocarbonothioylthio)propanoic acid (BTTCP) was synthesized as described by Ferguson et al. (2005). Xanthate CTA (2-((ethoxycarbonothioyl)thio)propanoic acid) (ECTTPA) was synthesized by a general procedure described previously by Pound et al. (2008). Acetonitrile (Aldrich) was dried in a solvent purification system (J. C. Meyer). 2-Ethyl-2-oxazoline (EtOx; Aldrich), methyl 2-bromoacetate and piperidine were distilled over barium oxide and stored under argon. All other chemicals were purchased from Sigma-Aldrich or Acros Organics and used as received.

**The synthetic method presented in sections 5.2.2, 5.2.3, 5.2.4 and 5.2.5 were carried out in Prof Richard Hoogenboom research group at University of Ghent, Belgium.**

### 5.2.2 Synthesis of PHEA-COOH

The RAFT polymerization of HEA was performed in a 25 mL Schlenk tube under an argon atmosphere. An example of RAFT polymerization with BTTCP was as follows. HEA (4.0 g, 34.4 mmol), 2-(butylthiocarbonothioylthio)propanoic acid (BTTCP) (82.0 mg, 0.35 mmol) and AIBN (5.7 mg, 0.035 mmol) were dissolved in 9.6 mL DMF in a 25 ml Schlenk vial. The solution was then degassed by bubbling with argon over 50 min, immersing in ice bath, after which the Schlenk vial was filled with argon and immersed in an oil bath preheated at 70 $^{o}$C while stirring. The polymerization was performed for 20 min and stopped by immersing the Schlenk vial into a dry ice/isopropanol bath. Polymeric product was then isolated by manual precipitation in a cold 50/50 mixture of diethyl ether and hexane and dried under vacuum to yield PHEA-COOH. By determining the monomer conversion via gas chromatography, a theoretical molecular weight, $M_{n,th}$, of 4.3 kDa was measured. Size exclusion chromatography (SEC) in dimethylacetamide (DMA) showed $M_{n,SEC}$ = 10.1 kDa against PMMA standards and a dispersity (Đ) of 1.20.

### 5.2.3 Synthesis of POZ-COOH

A solution of EtOx (4.7582 g, 48.00 mmol), methyl 2-bromoacetate (90.9 µL, 0.96 mmol) and potassium iodide (0.1753 g, 1.06 mmol) in acetonitrile with an initial monomer concentration of 4 M was prepared in a microwave vial and closed with a crimp cap under argon. The polymerization mixture was heated to 140 °C for 7 min 45 sec under microwave irradiation and subsequently cooled to ambient temperature. To the polymer solution piperidine (378.6 µL, 3.83 mmol) was added and the obtained mixture was stirred overnight. The solution was concentrated under reduced pressure, and the residue was dissolved in water. Lithium hydroxide (230 mg, 9.6 mmol) was added to the solution and the mixture was stirred overnight. The solution was acidified using hydrochloric acid (10%) until pH 2 was obtained. The solution was dialyzed (Spectra/Por CE membrane, MWCO 500 – 1000 D) against water until neutral pH was obtained. POZ-COOH was obtained after freeze-drying. DMA-SEC: $M_n$ = 6.8 kDa, Đ = 1.06.

### 5.2.4 Synthesis of PVP-COOH

The MADIX/RAFT polymerization of NVP was performed in a 25 mL Schlenk tube under argon atmosphere. NVP (4 g, 36.0 mmol), ECTTPA (46.6 mg, 0.24 mmol), AIBN (3.94 mg, 2.4 x $10^{-2}$ mmol) and 7.8 mL anisole were added to the Schlenk flask at a molar ratio of monomer/CTA/AIBN of 150/1/0.1. After degassing by 3 freeze-pump thaw cycles the Schenk flask was placed in an oil bath set at 60 °C for 12 h. The polymer was isolated by precipitation in hexane. Further, the polymer was dissolved in dichloromethane (DCM) and re-precipitated in hexane three times and were recovered as a white powder. By determining the monomer conversion via gas chromatography a theoretical molecular weight, $M_{n,th}$, of 6.7 kDa was measured. SEC in DMA showed $M_{n,SEC}$ = 4.9 kDa against PMMA standards and a dispersity (Đ) of 1.21.

### 5.2.5 Characterization of PHEA-, POZ- and PVP-COOH

A Bruker Avance 300 MHz Ultrashield was used to measure the $^1$H-nuclear magnetic resonance ($^1$H NMR) spectra at room temperature, the chemical shifts are given in parts per million (δ) relative to tetramethylsilane (TMS).

Size-exclusion chromatography (SEC) was performed on an Agilent 1260-series HPLC system equipped with a 1260 online degasser, a 1260 ISO-pump, a 1260 automatic liquid sampler (ALS), a thermostatted column compartment (TCC) at 50°C equipped with two

PLgel 5 µm mixed-D columns and a guard column in series, a 1260 diode array detector (DAD) and a 1260 refractive index detector (RID). The used eluent was *N*,*N*-dimethylacetamide DMA containing 50 mM of LiCl at a flow rate of 0.593 mL/min. The spectra were analyzed using the Agilent Chemstation software with the GPC add-on. Molar mass and Đ values were calculated against POZ (for POZ-COOH) and PMMA (for PHEA- and PVP-COOH) standards.

### 5.2.6 Synthesis of PEG-, PHEA-, POZ- and PVP-CO-NH-chitosan

Four modified chitosan (PEG-, PHEA-, POZ- and PVP-CO-NH-chitosan, hereinafter refer to PEG-, PHEA-, POZ- and PVP-chitosan) were synthesised as follows. To 80 mg medium molecular weight chitosan, 11.5 mL acetic acid (1% v/v) was added. The mixture was continuously stirred for 20 hours at room temperature. The pH of chitosan solutions was increased to 6 using 5 M NaOH solution. PEG-COOH (117 mg), PHEA-COOH (117 mg dissolved in 5 mL deionised water) and POZ-COOH (117 mg) and PVP-COOH (100 mg) was added to the chitosan solutions. Then after 5 minutes stirring, NHS (13.5 mg) was added to each and stirred for 30 minutes. EDAC (22.4 mg) was then added and stirred for 24 hours. The products were dialysed against deionised water (4 L, 8 total changes, 12-14 kDa) at room temperature for at least 3 days. The products were recovered by lyophilisation using Heto Power Dry LL 3000 freeze-drier (Thermo Electron Corporation). The % of yield was calculated according to Equation 5.1.

$$\text{Yield } \% = \frac{W_1}{W_2 + W_3} \times 100 \qquad \text{Equation 5.1}$$

$W_1$ is the weight of the freeze dried modified chitosan.

$W_2$ and $W_3$ are the weight of unmodified chitosan and modifying polymers (PEG-, PHEA-, POZ- and PVP-COOH) in the reaction mixture, respectively.

The percentage of grafting in weight (GW %) was calculated according to the method reported by Bhattarai et al. (2005) (Equation 5.2).

$$GW\ \% = \frac{W_g - W_n}{W_g} \times 100 \qquad \text{Equation 5.2}$$

Where $W_g$ is the weight of the freeze dried grafted polymer and $W_n$ is the weight of native chitosan in the reaction mixture.

### 5.2.7 NMR spectroscopy

$^1$H NMR spectra were recorded using a Bruker Nanobay 400 MHz NMR spectrometer. The polymers were added to acidified $D_2O$ (made from 1 mL $D_2O$ with 10 µL of TFA) and stirred for 16 hours at room temperature. The degree of acetylation (DA) of the unmodified chitosan was calculated using Equation 5.3 (Sogias et al., 2008):

$$DA = \frac{I_{CH3}/3}{I_{H2\text{-}H6}/6} \times 100 \qquad \text{Equation 5.3}$$

Where $I_{CH3}$ is the integral intensity of N-acetylated proton and $I_{H2\text{-}H6}$ is the sum of the integral intensity of proton number 2, 3, 4, 5 and 6.

The degree of substitution (DS) of the modified chitosan was calculated using $^1$H NMR spectroscopy by integrating related peaks of the grafted polymers against specific chitosan peak in the modified chitosan. The related peaks were marked in Figure 5.1, Figure 5.2, Figure 5.4 and Figure 5.6.

### 5.2.8 FTIR spectroscopy

FTIR spectra of the polymers were recorded using a NICOLET iS5 FTIR spectrophotometer (ThermoScientific, UK). The spectra were collected from an average of 16 scans, with a resolution of 4 $cm^{-1}$ over the range of 4000-400 $cm^{-1}$.

### 5.2.9 pH-solubility profile

Solubility of the modified and unmodified chitosan was measured at different pHs at room temperature using turbidimetric technique. The polymers were dissolved (0.5 mg/mL, 20 mL) in 1% v/v acetic acid and left stirring for 24 hours. The turbidity (absorbance) of the systems was measured at room temperature using a BioTek Epoch plate reader at 400 nm using 1% v/v acetic acid as a blank. 200 µL aliquots were used. The pH was adjusted by the addition of either 1 M NaOH solution or 1% v/v acetic acid. The results are reported as the average of the turbidity of 3 samples at each pH point ± standard deviation.

### 5.2.10 Ninhydrin assay

Ninhydrin assay was performed to determine free amino groups to find out the DA of unmodified chitosan and the DS of modified chitosan. Ninhydrin reagent was prepared by dissolving ninhydrin powder in DMSO (2% w/v, stirred for 1 hour) at room temperature in the dark. Solutions of glucosamine (standard) and the polymers were prepared by dissolving the calculated amounts of the materials in 1% v/v acetic acid (glucosamine 0.3 to 0.125% w/v, unmodified chitosan 0.5 to 0.15% w/v and modified chitosan 0.6 to 0.25% w/v). 100 µL of each solution was mixed with 250 µL of 0.5 M sodium acetate buffer solution (pH 5.4) and 1 mL of ninhydrin reagent. The final mixtures were incubated in a 95 °C water bath for 40 minutes. The mixtures were then allowed to cool down for 15 minutes. Then, 200 µL aliquots from each mixture were analysed using a BioTek Epoch plate reader at a wavelength of 570 nm. The curve of concentration versus absorbance was plotted. Then the DA of unmodified chitosan and the DS of modified chitosan were calculated according the published method (Shitrit & Bianco-Peled, 2017) with some modifications using Equation 5.4 and Equation 5.5, respectively.

$$DA = [1- (\frac{m_{\text{unmodified chitosan}}}{m_{\text{glucosamine}}})]\times 100 \qquad \text{Equation 5.4}$$

$$DS = [1- (\frac{m_{\text{modified chitosan}}}{m_{\text{unmodified chitosan}}})]\times 100 \qquad \text{Equation 5.5}$$

Where m is the gradient of the trendlines (Figure 5.8).

### 5.2.11 Unmodified and modified chitosan Alexa Fluor™ 546 labelling

Chitosan was dissolved in acetic acid (1% v/v, 5 mg/mL, 9.66 mL). The pH was increased to 6 using 5 M NaOH solution. Alexa Fluor™ 546 was dissolved in DMSO (5 mg/mL), vortexed for 2 minutes then 138 µL Alexa Fluor™ 546 solution (equivalent to 0.69 mg Alexa Fluor™ 546) was added to chitosan solution and the reaction mixture was stirred for 4 hours at room temperature in the dark. Then the product was dialysed against deionised water in the dark using 12-14 kDa MWCO dialysis membrane (for 96 hours, 1 L for 5 changes). To determine Alexa Fluor™ 546 content, chitosan solutions (0.2 mg/mL in 1% v/v acetic acid) were prepared by stirring overnight in the dark. Then the solutions were diluted according to the calibration curve with ultrapure water in the dark. The pH was adjusted to 6 using 0.5 M NaOH solution. The fluorescence intensity of three separate samples was measured using a fluorescence spectrometer (Cary Eclipse, Varian Inc., US). In order to establish a calibration curve, serial dilutions of Alexa Fluor™ 546 in ultrapure water (50, 25, 12.5, 6.25 and 3.125 ng/mL) were prepared by diluting Alexa Fluor™ 546 stock solution (5 mg/mL in DMSO). Finally, Alexa Fluor™ 546 content was calculated with reference to the calibration curve.

### 5.2.12 Preparation of chitosan nanoparticles

Unmodified chitosan and modified chitosan nanoparticles were prepared using an ionic gelation method according to Calvo et al. (1997) but with some modifications. After, optimisation steps, where various factors including the concentration of chitosan solution, chitosan/TPP weight ratio, the pH of chitosan and TPP solutions, the concentration of acetic acid and the temperature of crosslinking, a protocol was selected. Briefly, to prepare unlabelled chitosan nanoparticles, chitosan solutions (1 mg/mL in 1% v/v acetic acid) were prepared and the pH was increased to 5.5 using 5 M NaOH solution. 1 mg/mL TPP solution was prepared by dissolving calculated amount of TPP in deionised water. Before mixing, both TPP and chitosan solutions (pH 5.5) were filtered through 0.2 µm syringe filter. Then, 4 mL TPP solution was added dropwise to the chitosan solutions (8 mL) over the period of 5 minutes. The suspensions were stirred for another 30 minutes at room temperature. Alexa Fluor™ 546-labelled unmodified chitosan and PEG-chitosan nanoparticles were also prepared as mentioned for unlabelled chitosan nanoparticles. However, for Alexa Fluor™ 546-labelled PHEA-, POZ- and PVP-chitosan nanoparticles, 2 mL TPP solution was added to 4 mL Alexa Fluor™ 546-labelled chitosan solutions and the rest was performed as

described for the unlabelled chitosan nanoparticles. In case of Alexa Fluor™ 546-labelled nanoparticles, the experiments were conducted in the dark.

### 5.2.13 Characterisation of the nanoparticles

#### 5.2.13.1 Dynamic light scattering (DLS)

The size and ξ-potential of the nanoparticles were measured using a Zetasizer Nano-ZS (Model: ZEN3600, Malvern, UK). For the size measurements, the samples were diluted (1:100 for unlabelled nanoparticles and 1:20 for Alexa Fluor™ 546-labelled nanoparticles) with ultrapure water before analysis. A refractive index of 1.59 and an absorbance of 0.01 were used for all measurements. Viscosity (0.8872 cP) and refractive index (1.33) of water were used as dispersant parameters. The samples were incubated for 60 seconds and the measurements were conducted in triplicate for 10 seconds per run, with 12 runs per reading at 25 °C. The measurement angle was set to 173° backscatter. For the data processing, the normal resolution analysis model was selected. ξ-potential values were measured using DTS-1070 folded capillary tube cuvettes (Malvern, UK). Samples were diluted with ultrapure water (1:10) before analysis. Samples were measured using 3 repeats of 20 sub-runs per reading. For ξ-potential, data was processed using auto mode analysis model. At least 3 samples were measured and processed using the Smoluchowski model (Fκa = 1.50).

#### 5.2.13.2 Nanoparticle tracking analysis (NTA)

The nanoparticles were also characterised by NTA using NanoSight instrument (LM10 system, LM14 laser module, top plate and green 532 nm laser, Malvern, UK). For the NTA measurements, Alexa Fluor™ 546-labelled nanoparticles suspensions were diluted (1:10,000) with ultrapure water (pH 5.5, acidified with 1% v/v acetic acid). Fluorescence mode was used for the NTA measurement of the nanoparticles. 1 mL diluted sample was taken using a 1 mL syringe and the syringe was loaded onto an NTA syringe pump. A sCMOS camera and an NTA 3.2 software were used to capture and process the motion of the nanoparticles. The camera level was set to 16 and the detection thresholds were 5. The syringe pump speed of 50 AU was selected to minimise the settlement and the subsequent adhesion of the nanoparticles to the surface of the instrument chamber. The viscosity of water was used as the diluent viscosity. Automatic maximum jump mode, blur and minimum track length were used for all NTA measurements. The temperature was fixed at 25 °C. For each sample, 6 videos of 60 seconds were recorded and for each nanoparticle type, three

separate samples were analysed. Finally, the mean and the mode of size and the mean diffusion coefficient were reported. 100 nm nonfluorescent polystyrene latex (diluted 1:150,000 with ultrapure water) was used as a standard, however, the scatter mode was used to measure the size of this standard nanoparticles.

5.2.13.3 Transmission electron microscopy (TEM)

TEM was conducted using a JEM-2100 PLUS Electron Microscope (JEOL, USA) at an accelerating voltage of 200 kV. One drop of nanoparticles suspensions were placed on a piece of parafilm. A carbon-coated copper grid was dipped into the nanoparticles suspensions and left for 1 minute. The excess nanoparticles suspensions were then removed by a filter paper. Then a drop of 2% w/v phosphotungstic acid solution was placed on the parafilm. The grid was then immersed in the stain solution for 30 seconds and any excess stain was removed using a filter paper. The samples were then air dried and analysed. At least 3 images were taken and the size of the nanoparticles were measured using ImageJ software (Version 1.50b, National Institutes of Health, USA).

5.2.13.4 Fluorescence spectroscopy

Fluorescence emission spectra of Alexa Fluor™ 546-labelled chitosan nanoparticles and 0.5% w/v BSM solution were obtained between 560-750 nm at excitation wavelength of 554 nm using a fluorescence spectrometer (Cary Eclipse, Varian Inc., US). For the measurement, the nanoparticles were diluted (1:50) with ultrapure water, whereas the mucin solution was measured without dilution. The experiments were conducted in triplicate.

**5.2.14 Viscosity measurement of BSM solution**

0.5% w/v BSM solutions (3 × 25 mL) were prepared by dissolving the required amount of BSM in ultrapure water. The samples were stirred overnight at room temperature. After complete hydration, the pH of the solutions was decreased to 5.5 using 1% v/v acetic acid. Rheological analysis was performed using an AR 2000ex rheometer (TA Instruments, UK) with a 40 mm parallel plate. First, 0.5 mL sample was measured to find the linear visco-elastic region of BSM. This measurement was conducted at 25 °C and the solvent trap was placed. Thus, at a constant frequency of 1 Hz, strain sweep was performed between 0.01-10%. Then, at a constant strain of 4% a frequency sweep between 0.01-10 Hz was performed. Then, it was found that frequency of 1 Hz and strain of 4% is optimum as it provided a linear visco-elastic region. Thus, the temperature ramp experiments (at 1 °C/minute, between 20

to 40 °C) were performed at frequency of 1 Hz and strain of 4%. Then values of viscosity was plotted as a function of temperature. Finally, viscosity of the mucin solution at 25 °C was calculated using the trendline equation which was later used in the NTA diffusion study of the nanoparticles in BSM solution.

### 5.2.15 Evaluation of diffusion of chitosan nanoparticles in BSM solution

NTA was used to evaluate the diffusion of chitosan nanoparticles in BSM solution. Initially, four different concentrations of BSM solution (0.1, 0.25, 0.5 and 1% w/v) were evaluated for their background fluorescence noise and their consistency. Alexa Fluor™ 546-labelled chitosan nanoparticles were first diluted in ultrapure water (pH 5.5, 1:100) and then mixed with 0.5% w/v BSM solution (pH 5.5, 1:100). 1 mL of the mixture was injected into the NTA system with flow rate set at 50 AU. The diffusion of the nanoparticles in mucin solution was visualised at 25 °C. The videos were recorded through a 565 nm cut-on filter. Each individual mucin solution (0.5% w/v, 3 separate samples) was mixed 3 times with each of the nanoparticles type and thus generated 9 × 6 × 60 second videos (n = 9). The measured viscosity of 0.5% w/v BSM solution (3.05 cP, which was found from the rheological analysis) was used for processing the diffusion data. The other parameters were set as described for size measurement of the nanoparticles using NTA in section 5.2.13.2.

### 5.2.16 Penetration of chitosan nanoparticles into sheep nasal mucosa

The penetration of chitosan nanoparticles was studied using whole thickness sheep nasal septum mucosa. The tissues were used immediately after obtained from a local abattoir (P.C. Turner Abattoirs, Farnborough, UK). The nasal septum mucosa was segmented into 1 × 1.5 $cm^2$ and placed in a plastic Petri dish and transferred to a temperature controlled incubator (32 °C). 20 µL Alexa Fluor™ 546-labelled chitosan nanoparticles were added onto the nasal mucosal tissues and incubated at 32 °C for 5, 15 and 30 minutes. After each time point, tissues were transferred and covered with OCT and placed on dry ice for overnight storage. The rectangular frozen tissue blocks were then stored in sealed bags at -80 °C freezer until processing.

To prepare tissue slices, the tissues were cross-sectioned using a Bright 5040 cryostat (Bright Instrument Co. Ltd., UK) which was loaded with an MB35 Premier Disposable Microtome blade (34° cutting angle, length × width × thickness: 80 × 8 × 0.25 mm, Thermo Scientific, UK ). The blade angle and thickness was set to 2.5° and 20 µm, respectively. The

specimen and chamber temperature was -20 and -25 °C, respectively. The slices were cut upward through the mucosal layer and transferred to SuperFrost Plus™ Adhesion slides (Thermo Scientific, UK) and air dried for 30 minutes before storage. At least 10 slices were prepared for each time point. Sheep nasal mucosa without any exposed nanoparticles was used as a background control.

The fluorescence microscopy was performed using a Leica MZ10F fluorescence stereomicroscope (Leica Microsystems, UK). The images were taken at exposure time 344 ms, gain 3X, gamma 1, pseudocolour 565 nm, maximum intensity, magnification of 3.2 and ET CY3 filter. At least 10 images were recorded for each time point.

The images were analysed using ImageJ software (National Institutes of Health, USA) and the depth of penetration was measured according to Mansfield et al. (2015) with some modifications. The images were opened using the software and the scale was set. A line was drawn along the mucosal layer and the fluorescence intensity profile of the line was plotted. The plot showed the fluorescence peak width which indicates the depth of penetration of the nanoparticles into the nasal mucosa. The graphical profile was converted into numbers using list option. The depth of penetration was calculated by subtracting the value of the start point from the value of the end point of the peak. For each image, this procedure was repeated 5 times at random regions of mucosal barrier and thus for each sample at each time point, 50 profiles were generated.

Additionally, to investigate how far the nanoparticles penetrated into the nasal mucosa, 75 µL DAPI solution (1.5 µg/mL in deionised water) was added to stain the cross sections and incubated overnight in the dark at room temperature. At least 6 slices were stained. DAPI solution was kept at 4 °C in the fridge and used within 1 week of preparation. Fluorescence microscopy was performed in the following day in the dark using Zeiss Axio Imager.A1 upright epifluorescent microscope with AxioVision Rel. 4.8 software. At least 3 images for each time point were taken. Each image was taken first with Alexa 546 (yellow) and then with DAPI (blue) filters. The images were then merged and exported as composite images using AxioVision Rel. 4.8 software.

### 5.2.17 Statistical analysis

Unless otherwise stated, all measurements were collected in triplicate and the data are expressed as mean ± standard deviation (SD). The data were analysed using the SPSS

Statistics 21 program (IBM, US). The statistical significance of any difference between groups was determined using one-way analysis of variance (ANOVA) with the least significant difference (LSD) post-hoc test. Independent sample t-test was performed to compare each pair of data sets. Differences were considered statistically significant at $p < 0.05$.

## 5.3 Results and discussion

### 5.3.1 Characterisation of unmodified and modified chitosan

Chitosan is a cationic mucoadhesive polysaccharide having free amino and hyroxyl groups. The presence of these groups in chitosan allows possible chemical modifications (M. Ways et al., 2018a). We hypothesised that modification of chitosan into a more hydrophilic derivative can impart stealth properties to the modified chitosan which can be used in formulating mucus penetrating nanoparticles. In this study, four chitosan derivatives have been synthesised by reacting chitosan with water soluble polymers (carboxyl terminated-PEG, PHEA, POZ and PVP) using EDAC/NHS chemistry. The DA of unmodified chitosan was determined using $^{1}$H NMR (Figure 5.1) and ninhydrin assay and was found to be 25.03% and 71.73 ± 1.60%, respectively. The synthetic procedure provided high yield (Table 5.1). The DS of modified chitosan was determined using NMR and ninhydrin test (Table 5.1).

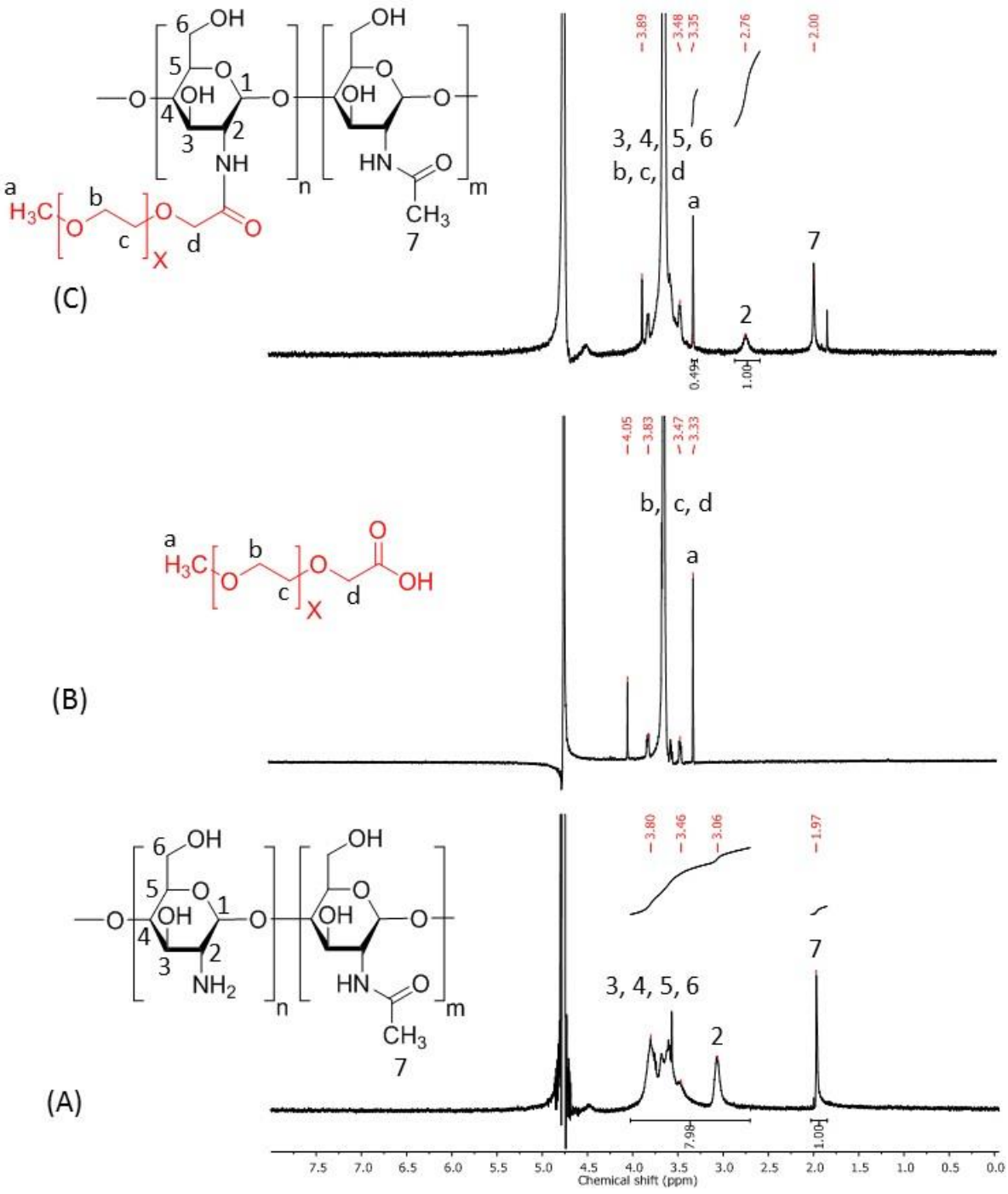


Figure 5.1 $^{1}$H NMR spectrum of (A) unmodified chitosan in acidified $D_2O$, (B) PEG-COOH in $D_2O$ and (C) PEG-chitosan in acidified $D_2O$.

Table 5.1 Characterisation of the synthesised modified chitosan.

| Types of materials | Yield (%) | GW (%) | DS[a] (%, NMR) | DS (%, ninhydrin) |
|---|---|---|---|---|
| PEG-chitosan | 77.15 | 47.36 | 16.33 | 50.05 ± 2.22 |
| PHEA-chitosan | 63.05 | 36.36 | 6.39 | 64.70 ± 1.64 |
| POZ-chitosan | 65.48 | 37.98 | 15.97 | 34.58 ± 1.86 |
| PVP-chitosan | 80.00 | 44.44 | NA | 38.99 ± 2.57 |

[a] Degree of substitution (DS) was calculated using $^{1}$H NMR spectroscopy by integrating related peaks of the grafted polymers against specific chitosan peak in the modified chitosan as marked in Figure 5.1, Figure 5.2, Figure 5.4 and Figure 5.6.

As shown in Figure 5.1, the $^{1}$H NMR spectrum of unmodified chitosan contains peaks at 3.06, 3.57-3.80 and 1.97 ppm corresponding to H2, H3-6 and $NHCOCH_3$, respectively. H1 was not observed and this is consistent with the literature claiming that H1 can only be determined at a temperature higher than 25 °C (Wu et al., 2007).

The NMR spectrum of PEG-chitosan showed a peak at 3.33 ppm due to the $OCH_3$ group of PEG-COOH and the peaks related to H3, H4, H5 and H6 were overlapped with the peaks of the $OCH_2CH_2$ and $OCH_2$ groups (b, c and d) (3.35-3.89 ppm) (Figure 5.1). The appearance of the peaks of PEG-COOH and PEG-chitosan were identified and compared as highlighted in the literature (Luo et al., 2016). The DS (DPEG %) was calculated according to Equation 5.6.

$$\text{DPEG \%} = \frac{\text{I (OCH}_3\text{)/3}}{\text{I (H}_2\text{)}} \times 100 \qquad \text{Equation 5.6}$$

The NMR spectrum of PHEA-chitosan showed additional peaks related to PHEA (most notably the peak at 4.10 ppm (b), Figure 5.2). The NMR spectrum of PHEA-COOH is also shown in Figure 5.3. The DS (DPHEA %) was calculated using our proposed method according to Equation 5.7.

$$\text{DPHEA \%} = \frac{\frac{I(b)PHEA}{2\times 43}}{I(H_2)} \times 100 \qquad \text{Equation 5.7}$$

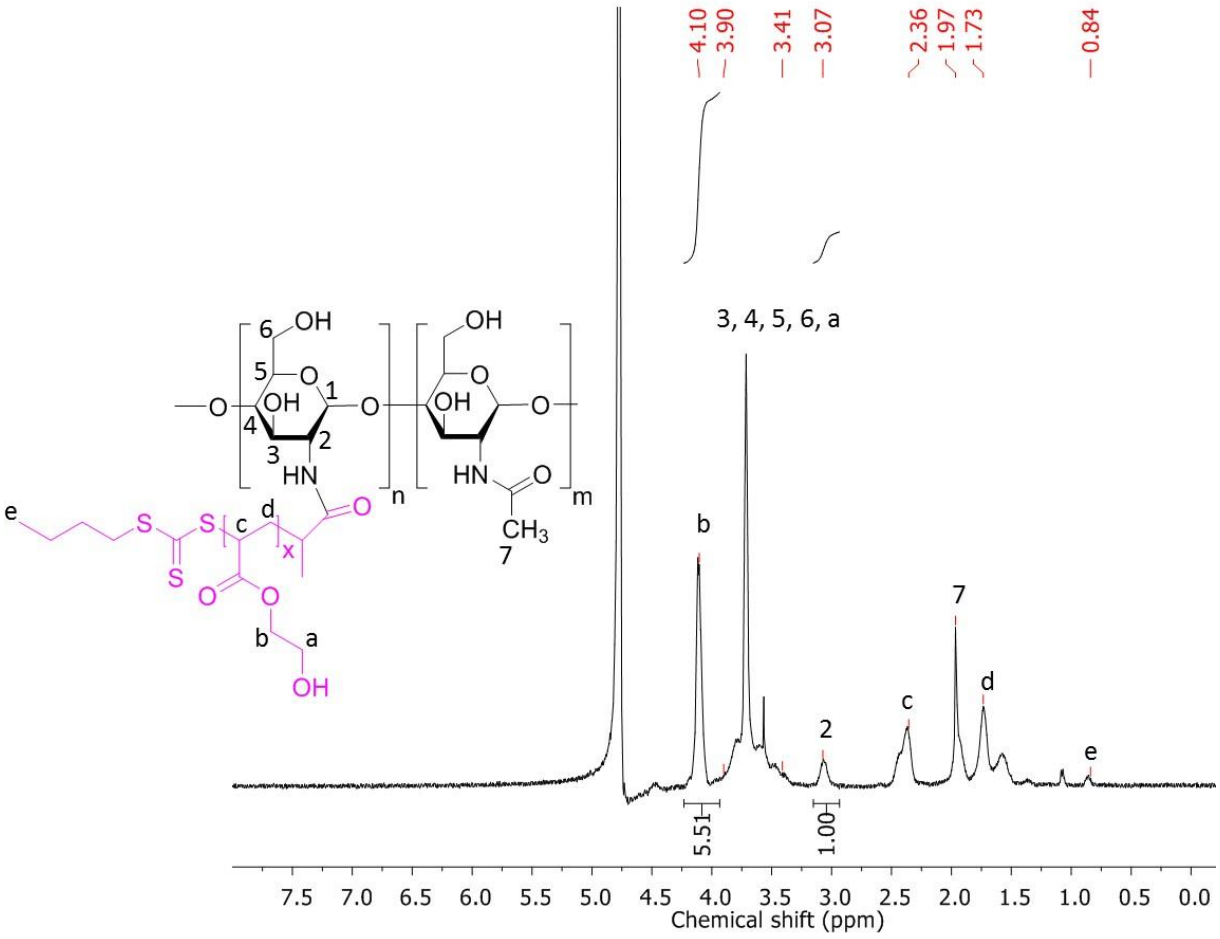


Figure 5.2 $^{1}$H NMR of PHEA-chitosan measured in acidified $D_2O$.

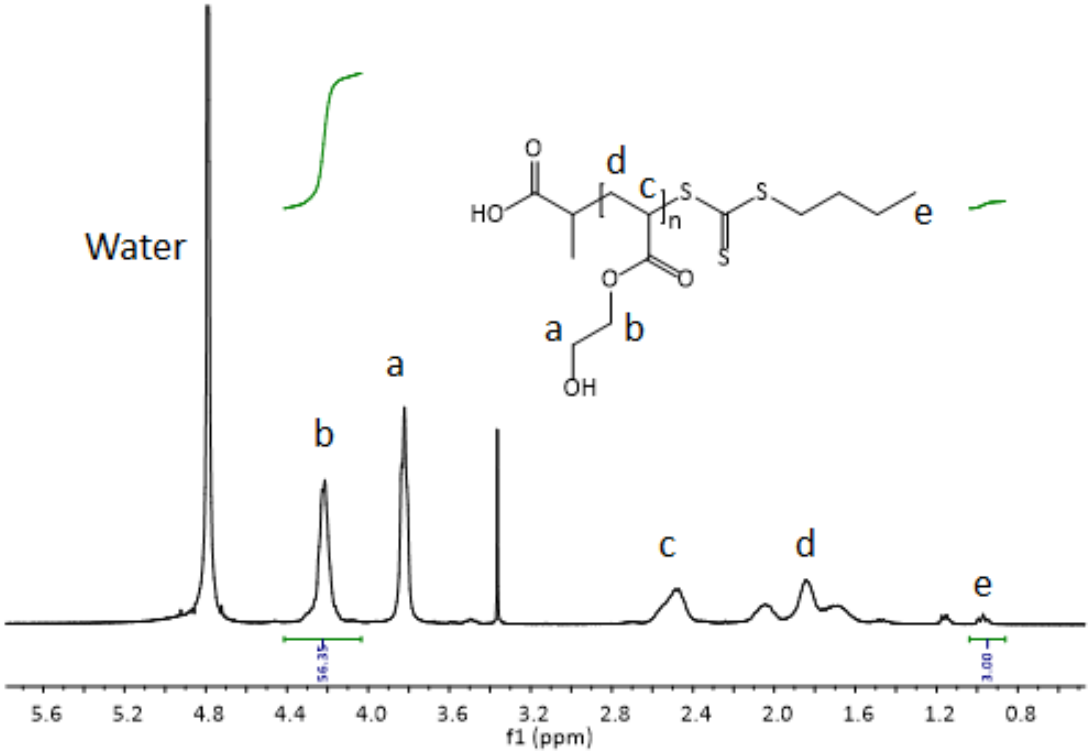


Figure 5.3 $^{1}$H NMR spectrum of PHEA-COOH measured in $D_2O$ **(this data was recorded, analysed and provided by Prof Richard Hoogenboom research group)**.

The NMR spectrum of POZ-chitosan showed 2 new characteristic peaks related to POZ appeared at 0.96 ppm ($CH_3$ of side chain i.e. 3 H) and 2.27 ppm ($CH_2$ of side chain i.e. 2 H and N-$CH_2$ of the end group). 4 H of $CH_2$ of main chain were overlapped with H2-H6 peaks of chitosan (Figure 5.4). The NMR spectrum of POZ-COOH is also shown in Figure 5.5. The DS (DPOZ %) was calculated according to Equation 5.8 .

$$\text{DPOZ }\% = \frac{\frac{I_{CH_3}\ POZ}{3\times 50}}{I(CH_3)/3} \times 100 \qquad \text{Equation 5.8}$$

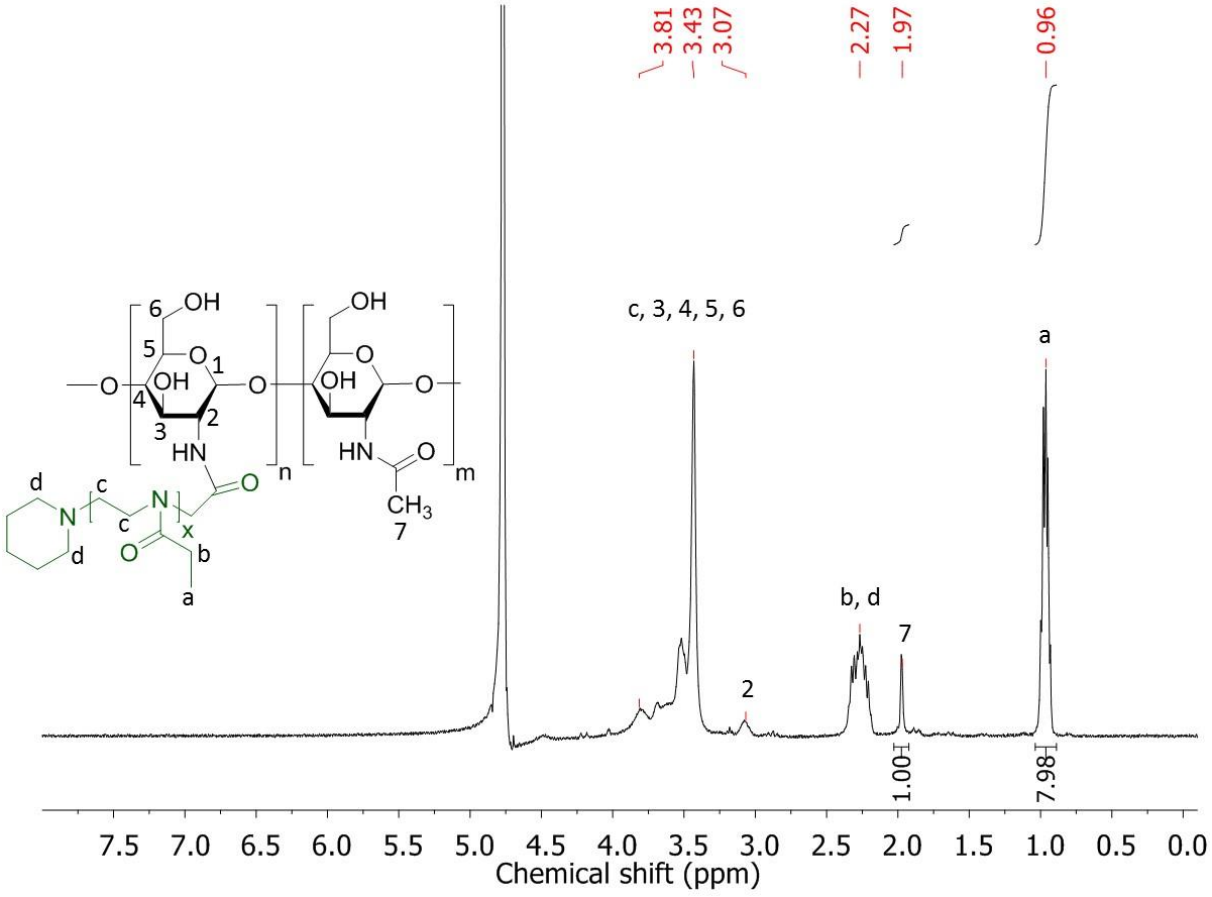


Figure 5.4 $^1$H NMR spectrum of POZ-chitosan measured in acidified $D_2O$.

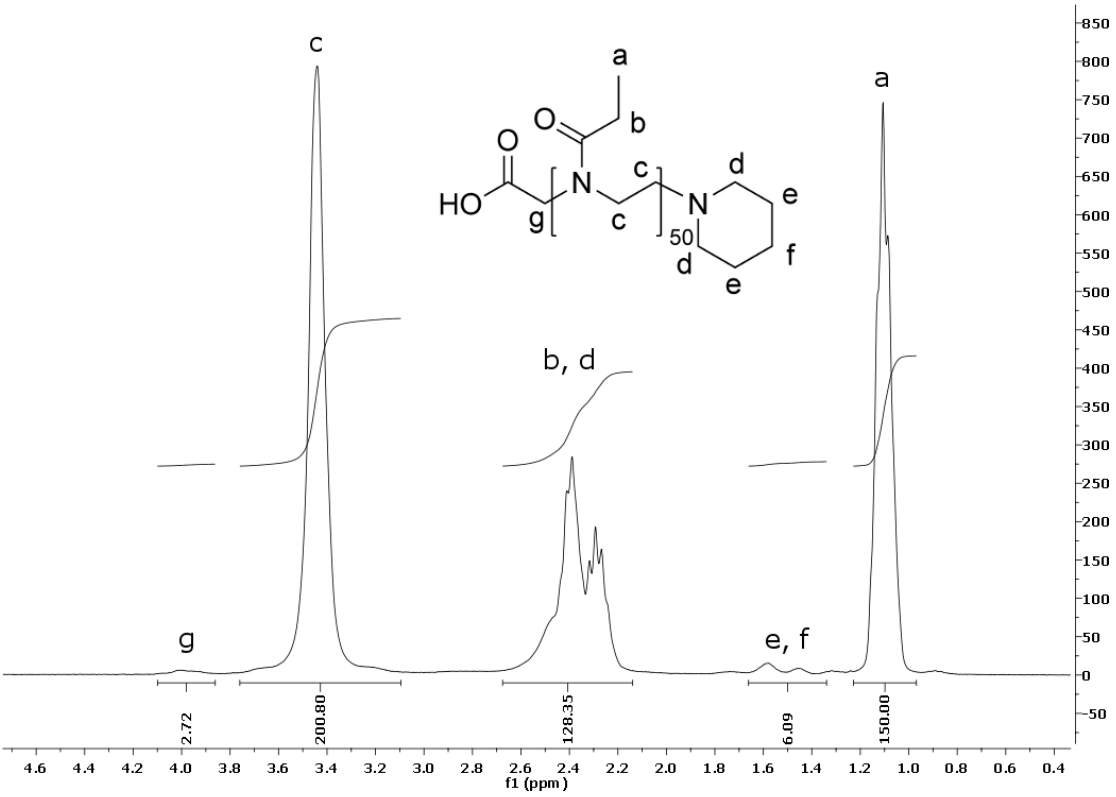


Figure 5.5 $^{1}H$ NMR spectrum of POZ-COOH measured in $CDCl_3$ **(this data was recorded, analysed and provided by Prof Richard Hoogenboom research group)**.

The NMR spectrum of PVP-chitosan also showed peaks related to PVP, however, the DS of PVP-chitosan could not be determined by NMR as the peaks of PVP and chitosan were overlapped (Figure 5.6). The NMR spectrum of PVP-COOH is also shown in Figure 5.7. Instead, ninhydrin assay was used to determine the DS of PVP-chitosan, which will be discussed in the next section.

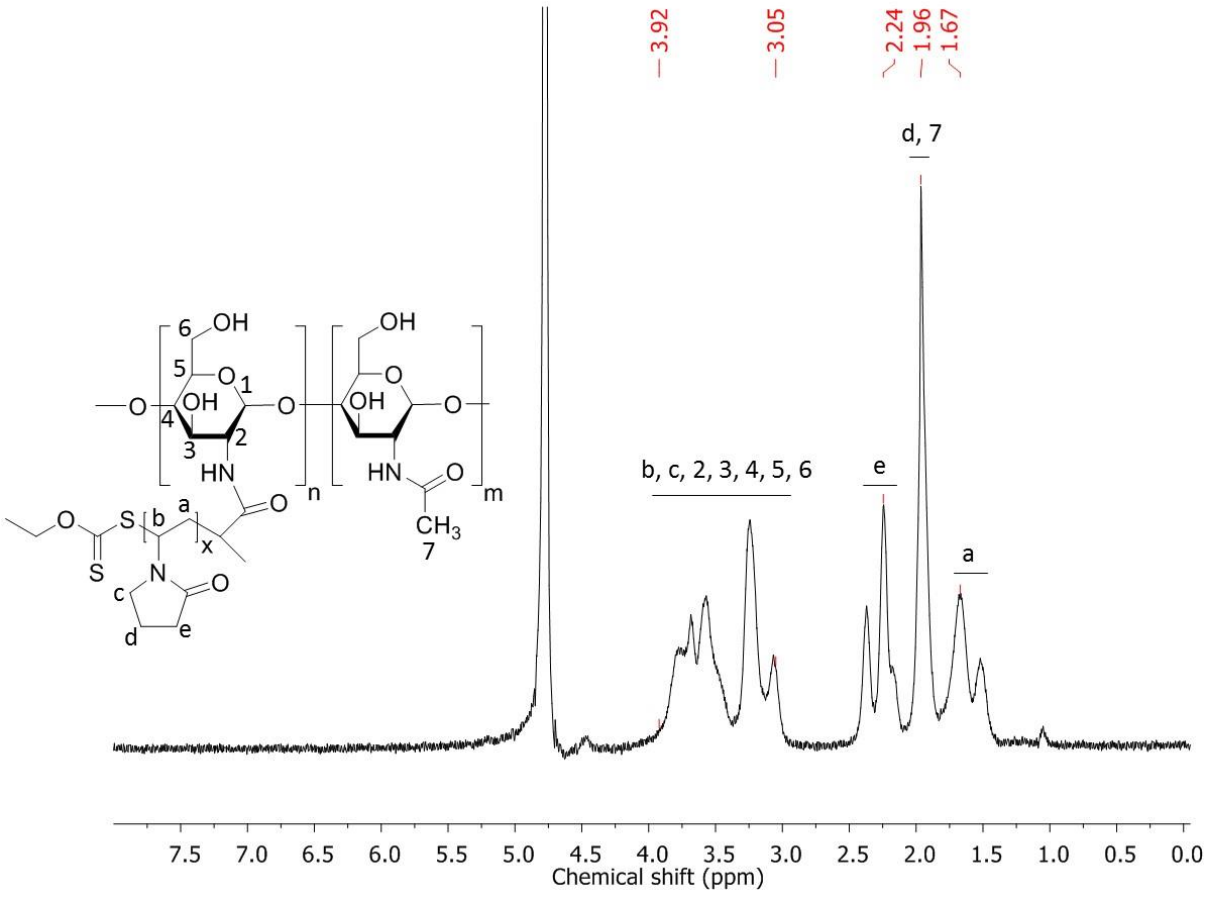


Figure 5.6 $^{1}H$ NMR of PVP-chitosan measured in acidified $D_2O$.

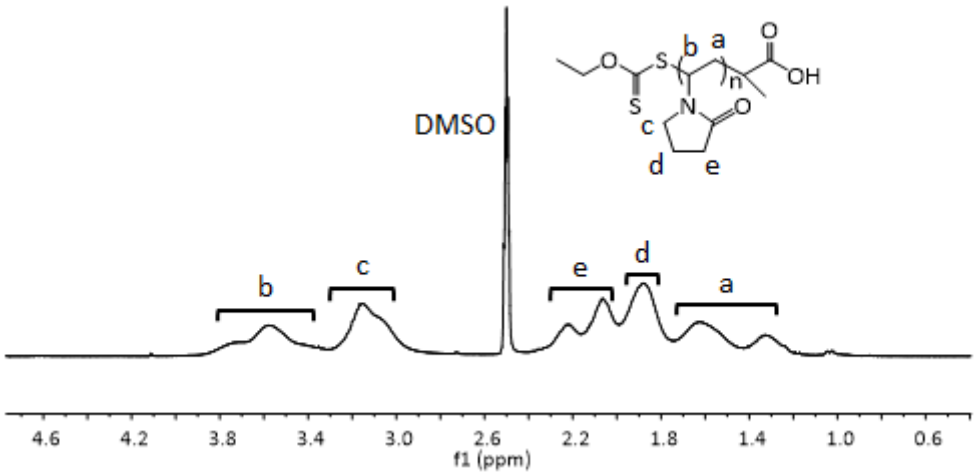


Figure 5.7 $^{1}$H NMR spectrum of PVP-COOH measured in DMSO-$d_6$ **(this data was recorded, analysed and provided by Prof Richard Hoogenboom research group)**.

Ninhydrin assay showed a higher DS than NMR data (Table 5.1), which is in agreement with literature (Kolawole et al., 2018). This could be due to the fact that different solvent environment (most notably pH, ionic strength and polarity) has been used in the two methods. This in turn could lead to different conformations of the polymers and the availability of free amino groups to react with the ninhydrin reagent (Kolawole et al., 2018). Additionally, it can be argued that ninhydrin assay is less precise than the NMR technique as the intensity of the colour of the blue product is not exactly linearly dependent on the concentration of the amino groups in the analyte. This was indicated by a relatively low $R^2$ value (Figure 5.8). This could be due to the non-stoichiometric nature of the ninhydrin reaction and is consistent with the literature (Prochazkova et al., 1999; Friedman, 2004).

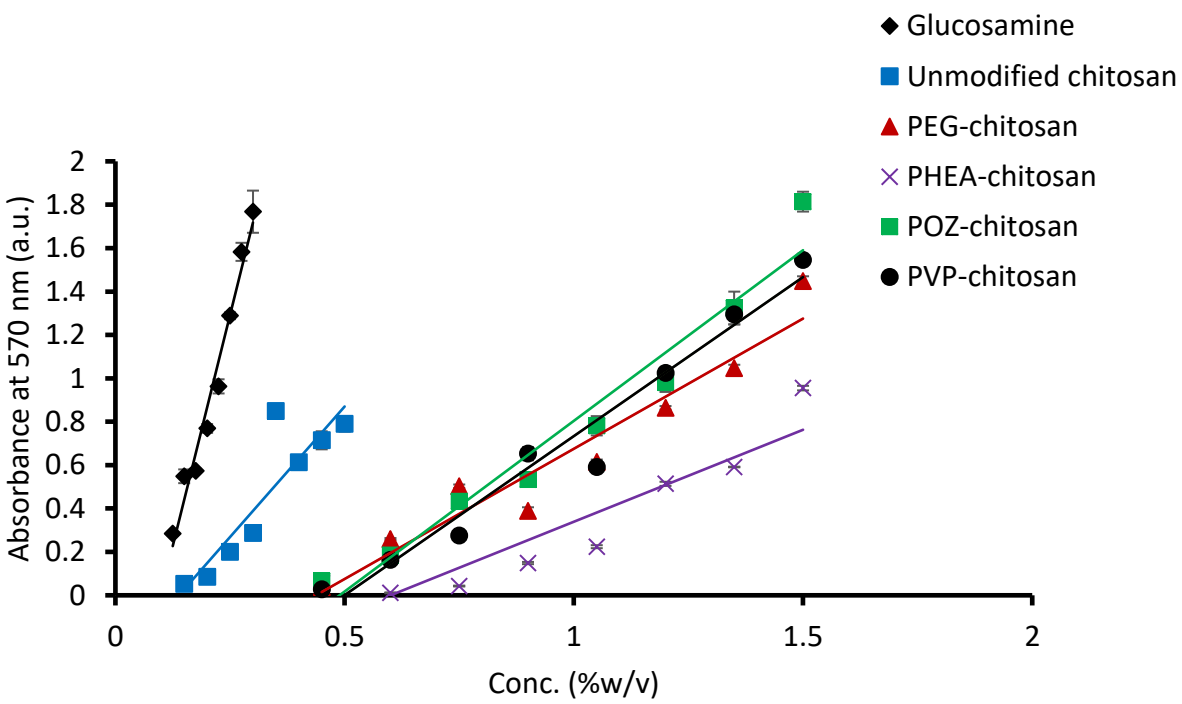


Figure 5.8 Calibration curves used for the ninhydrin assay of glucosamine (y = 8.5211x - 0.8384, $R^2$ = 0.973), unmodified chitosan (y = 2.4063x - 0.3331, $R^2$ = 0.8094), PEG-chitosan (y = 1.2002x - 0.525, $R^2$ = 0.9328), PHEA-chitosan (y = 0.8479x - 0.5089, $R^2$ = 0.8547), POZ-chitosan (y = 1.5731x - 0.7691, $R^2$ = 0.955) and PVP-chitosan (y = 1.4659x - 0.7322, $R^2$ = 0.963). Data represent mean ± SD, n = 3.

The FTIR spectra of the unmodified and modified chitosan are shown in Figure 5.9. The FTIR spectrum of unmodified chitosan showed peaks at 3000-3600 $cm^{-1}$ due to stretching vibration of O-H and N-H bonds and 1649 $cm^{-1}$ due to amide group (N-C=O) stretching. For PEG-chitosan, characteristic peaks due to PEG backbone at 842, 961 and 2882 $cm^{-1}$ were observed. The peak at 1654 $cm^{-1}$ was believed to be due to amide groups in the linker between PEG and chitosan. A very weak ester peak at 1746 $cm^{-1}$ was also observed (Casettari et al., 2010). The FTIR spectrum of PHEA-chitosan showed a characteristic carbonyl peak (C=O stretching) at 1724 $cm^{-1}$, the aliphatic C-H stretching peak at 2929 $cm^{-1}$, $CH_2$ stretching at 1447 $cm^{-1}$ and O-H stretching at 3357 $cm^{-1}$. POZ-chitosan showed peaks related to POZ at 1633 $cm^{-1}$ (C=O stretching), 1471 $cm^{-1}$ (C-H deformation), 1423 $cm^{-1}$ ($CH_3$ symmetrical deformation/$CH_2$ bending) and 1239 $cm^{-1}$ (C-N stretch). The FTIR spectrum of PVP-chitosan showed peaks at 3370 $cm^{-1}$ (O-H stretching), 2921 $cm^{-1}$ (symmetric stretching $CH_2$ ring), 1654 $cm^{-1}$ (C═O stretching), 1288 $cm^{-1}$ ($CH_2$ wag), 1152 $cm^{-1}$ (C-N stretch), 845 $cm^{-1}$ (C-C ring) and 642 $cm^{-1}$ (N-C=O bend).

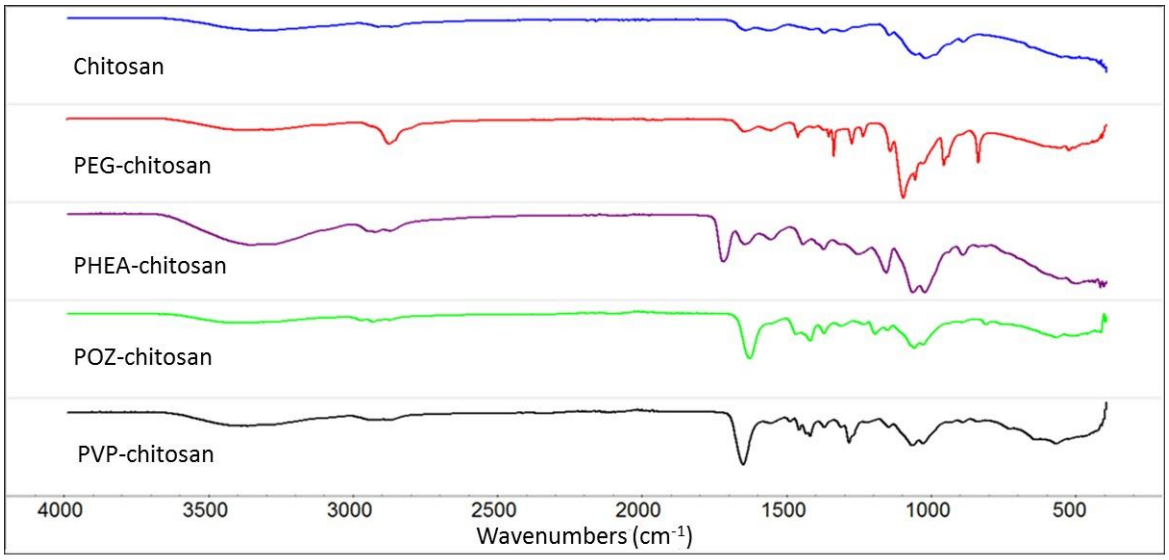


Figure 5.9 FTIR of unmodified chitosan, PEG-chitosan, PHEA-chitosan, POZ-chitosan and PVP-chitosan.

The main problem of chitosan is its poor aqueous solubility, especially when the pH is higher than its pKa (pKa is ~ 6.5, depending on factors such as DA and the molecular weight of chitosan) (Wang et al., 2006). A turbidimetric technique was used to determine the pH-solubility profiles of unmodified and modified chitosan. Figure 5.10 shows that unmodified chitosan was soluble (illustrated by low turbidity or absorbance) at acidic pH ranges. However, it underwent rapid precipitation (indicated by high turbidity or absorbance) at pH higher than 7.38. This result was expected, because at acidic pH, the amino groups of chitosan undergo protonation, whereas at near neutral pH, they become deprotonated (Rinaudo, 2006). All the modified chitosan, however, showed full aqueous solubility (illustrated by low turbidity) at the studied pH ranges (3-10). This result could be due to the grafting of the polymers to the chitosan macromolecules which reduced the crystallinity of chitosan by reducing intra- and inter-molecular hydrogen bonding, leading to enhanced hydrophilicity (Sogias et al., 2010).

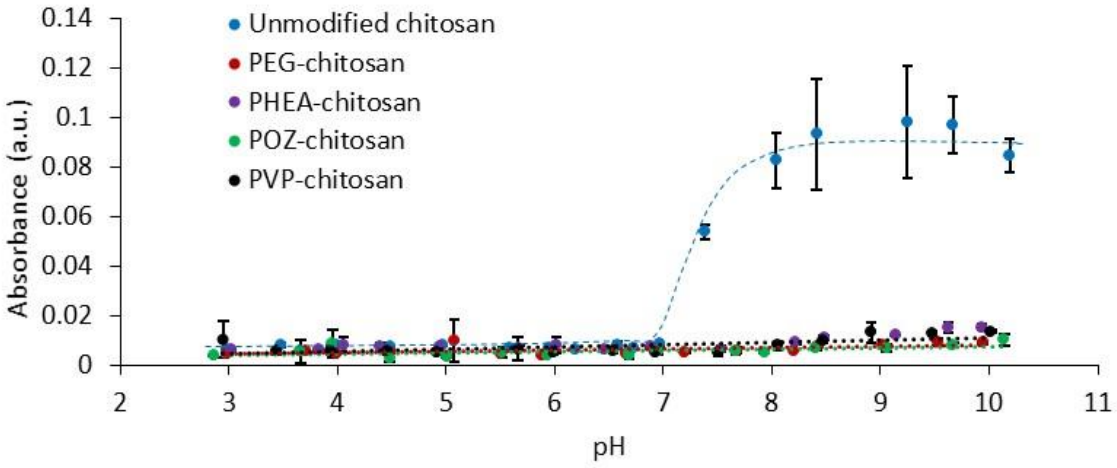


Figure 5.10 pH-solubility profiles of unmodified and modified chitosan (mean ± SD, n = 3).

### 5.3.2 Characterisation of unmodified and modified chitosan nanoparticles

The improved water-solubility of modified chitosan is a highly important step towards the preparation of modified chitosan nanoparticles as solubilisation of chitosan is necessary prior to ionic gelation. Chitosan nanoparticles can be prepared via electrostatic attractive interactions between positively charged chitosan and negatively charged TPP (Figure 5.11). Although several studies have reported the formation of chitosan nanoparticles using TPP, the variation in the source of chitosan which in turn leads to the variation in the molecular weight, the DA, the viscosity and other properties requires a full optimisation study to prepare chitosan nanoparticles. Some studies reported that there is no clear correlation between the mass ratio of chitosan/TPP and the size of chitosan nanoparticles (Zhang et al., 2018). Thus, several attempts have been tried to obtain nanoparticles aiming to determine the smallest size with acceptable polydispersity index (PDI) (Table 5.2). This was achieved by changing the concentration of chitosan solution, weight ratio of chitosan/TPP, concentration of acetic acid, temperature of crosslinking and pH of chitosan and TPP solutions. CS16 (Table 5.2) was selected as the optimum formula of unmodified chitosan nanoparticles. The same condition was used to prepare modified chitosan nanoparticles. The DLS study showed that unlabelled unmodified and modified chitosan nanoparticles were

130-152 nm with a PDI of 0.24-0.29 ( Table 5.3 and Figure 5.12). However, the ξ-potential of each of the unlabelled modified chitosan nanoparticles was lower than the unmodified chitosan nanoparticles (Table 5.3). This may be attributed to the decrease in the number of protonated amino groups upon modification or the presence of a polymeric shell in modified chitosan nanoparticles which can mask the positive charges of chitosan. The ξ-potential of all the chitosan nanoparticles are generally low (< 30 mV), but taking into account the effect of pH and ionic strength, these values are acceptable (Zhang et al., 2018).

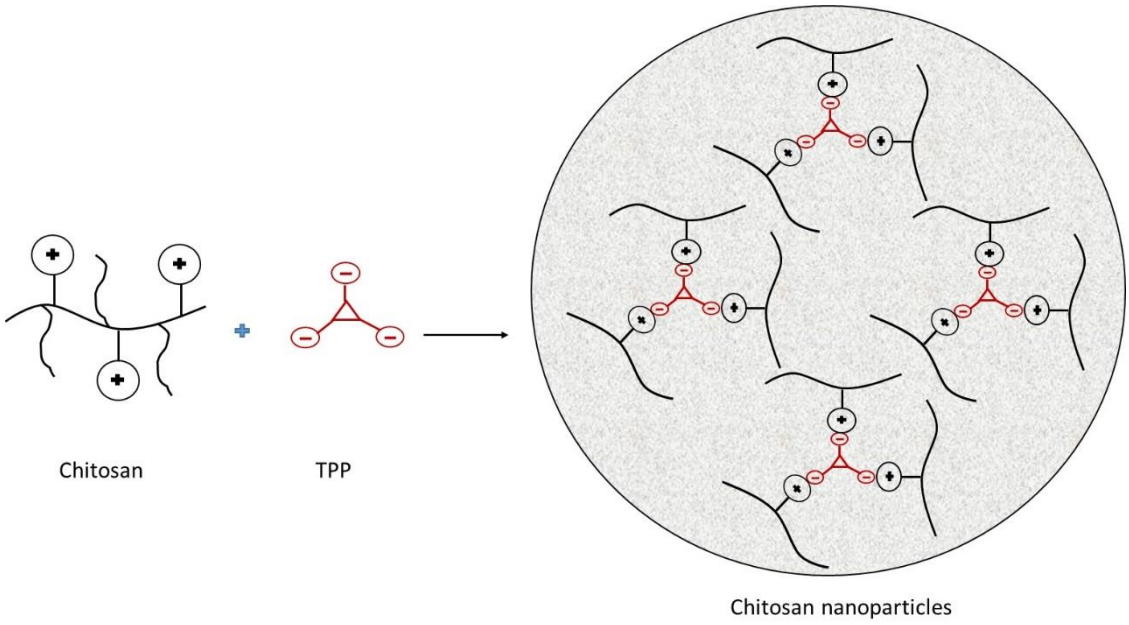


Figure 5.11 Structure diagram of the prepared chitosan nanoparticles.

Table 5.2 Optimisation of preparation of unmodified chitosan nanoparticles. The size of chitosan coils in solution without addition of TPP was also measured. The nanoparticles were prepared at room temperature.

| Formulations | CS [a] conc. (mg/mL) | TPP conc. (mg/mL) | CS/TPP weight ratio | Acetic acid conc. (% v/v) | CS solution pH | TPP solution pH | Z-average (nm) | PDI |
|---|---|---|---|---|---|---|---|---|
| CS solution | 1 | 0 | - | 1 | 3 | - | 956 ± 124 | 0.197 ± 0.233 |
| CS solution [b] | 1 | 0 | - | 1 | 3 | - | 361 ± 332 | 0.846 ± 0.263 |
| CS1 | 2 | 1 | 3:1 | 1 | 4.9 | 9 | 554 ± 191 | 0.600 ± 0.109 |
| CS2 | 2 | 1 | 5:1 | 1 | 4.9 | 9 | 577 ± 68 | 0.427 ± 0.030 |
| CS3 | 2 | 1 | 6:1 | 1 | 4.9 | 9 | 602 ± 46 | 0.260 ± 0.048 |
| CS4 | 2 | 1 | 7:1 | 1 | 4.9 | 9 | 601 ± 23 | 0.447 ± 0.061 |
| CS5 | 1.5 | 1 | 6:1 | 1 | 4.9 | 9 | 758 ± 501 | 0.612 ± 0.336 |
| CS6 | 1 | 1 | 1:1 | 1 | 4.9 | 9 | 225 ± 16 | 0.339 ± 0.089 |
| CS7 | 1 | 1 | 2:1 | 1 | 4.9 | 9 | 169 ± 8 | 0.384 ± 0.014 |
| CS8 | 1 | 1 | 3:1 | 1 | 4.9 | 9 | 256 ± 11 | 0.380 ± 0.028 |
| CS9 | 1 | 1 | 6:1 | 1 | 4.9 | 9 | 893 ± 857 | 0.614 ± 0.334 |
| CS10 [c] | 2 | 1 | 5:1 | 1 | 4.9 | 9 | 397 ± 38 | 0.587± 0.138 |
| CS11 | 1 | 1 | 2:1 | 0.175 | 4.9 | 9 | 266 ± 15 | 0.366 ± 0.047 |
| CS12 | 1 | 1 | 2:1 | 0.175 | 4.15 | 9 | 205 ± 42 | 0.298 ± 0.013 |
| CS13 | 1 | 1 | 2:1 | 1 | 3.6 | 2 | 187 ± 48 | 0.315 ± 0.083 |
| CS14 | 1 | 1 | 2:1 | 1 | 3.6 | 5 | 162 ± 21 | 0.442 ± 0.046 |
| CS15 | 1 | 1 | 2:1 | 1 | 4.5 | 9 | 214 ± 9 | 0.387 ± 0.049 |
| CS16 | 1 | 1 | 2:1 | 1 | 5.5 | 9 | 152 ± 13 | 0.242 ± 0.016 |
| CS17 | 1 | 1 | 2:1 | 1 | 6 | 9 | 151 ± 13 | 0.255 ± 0.031 |
| CS18 | 1 | 1 | 1:1 | 1 | 5.5 | 9 | 367 ± 4 | 0.323 ± 0.016 |
| CS19 | 0.5 | 1 | 2:1 | 1 | 5.5 | 9 | 125 ± 8 | 0.317 ± 0.022 |

[a] CS: chitosan

[b] chitosan solution filtered through 0.2 µm syringe filter

[c] Prepared at 35 °C

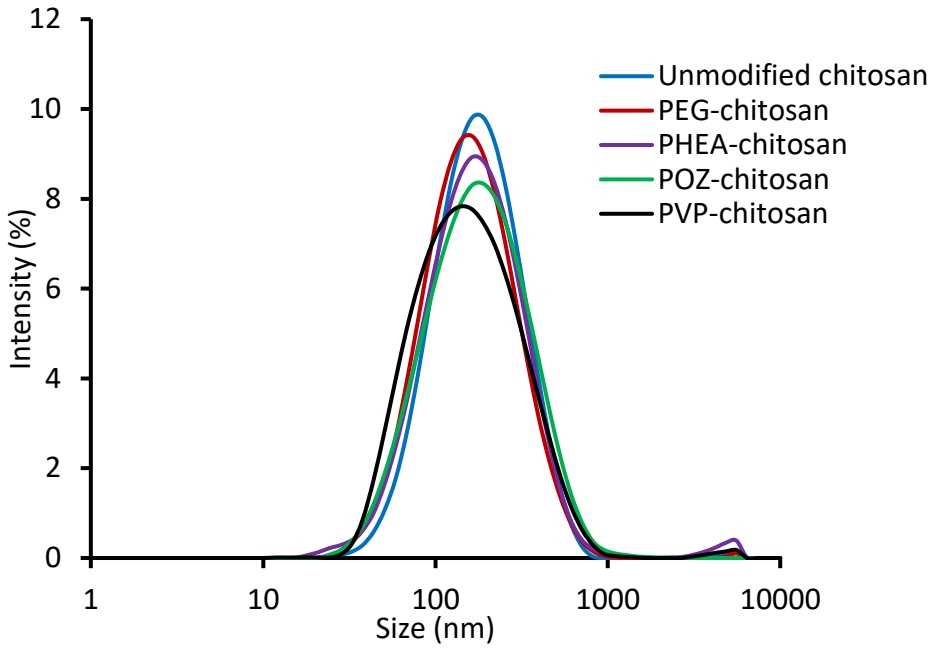


Figure 5.12 DLS size distribution of different unlabelled chitosan nanoparticles.

Initial TEM analysis was performed without staining and also with staining using uranyl acetate dihydrate solution (1% w/v in distilled water) and this resulted in images with poor contrast (data not shown). However, using phosphotungstic acid hydrate solution (2% w/v in deionised water) the particles were clearly visible (Figure 5.13). The size of all unmodified and modified chitosan nanoparticles measured by TEM was smaller than the size measured by DLS. This discrepancy can be due to the presence of a hydration shell around the nanoparticles, as in DLS, particles are measured in the aqueous suspension form. The thickness of this shell can be significantly decreased during TEM sample preparation upon drying. The discrepancy in the size using DLS and TEM has also been discussed in other studies on silica nanoparticles (Mun et al., 2014; Mansfield et al., 2018). However, the difference observed in this study is greater (Table 5.3) than the previous publications (Mun et al., 2014; Mansfield et al., 2018) which could be due to the highly hydrophilic nature and the swelling capacity of chitosan nanoparticles compared to silica nanoparticles.

Table 5.3 Physicochemical properties of unlabelled chitosan nanoparticles (mean ± SD, n = 3).

| Types of nanoparticles | Z-average (nm) | PDI | ξ-potential (mV) | Size (nm, TEM)[a] |
|---|---|---|---|---|
| Unmodified chitosan | 152 ± 13 | 0.242 ± 0.016 | 25.54 ± 1.25 | 43 ± 15 |
| PEG-chitosan | 137 ± 23 | 0.253 ± 0.028 | 13.38 ± 0.08 | 55 ± 15 |
| PHEA-chitosan | 142 ± 11 | 0.292 ± 0.035 | 13.66 ± 0.13 | 41 ± 9 |
| POZ-chitosan | 145 ± 21 | 0.277 ± 0.017 | 15.01 ± 0.28 | 31 ± 9 |
| PVP-chitosan | 130 ± 19 | 0.280 ± 0.037 | 12.29 ± 1.62 | 33 ± 10 |

[a] For size measurement by TEM, 20 values from 20 individual nanoparticles from 3 different TEM images were used. Note: only individual particles were measured and fused particles were excluded.

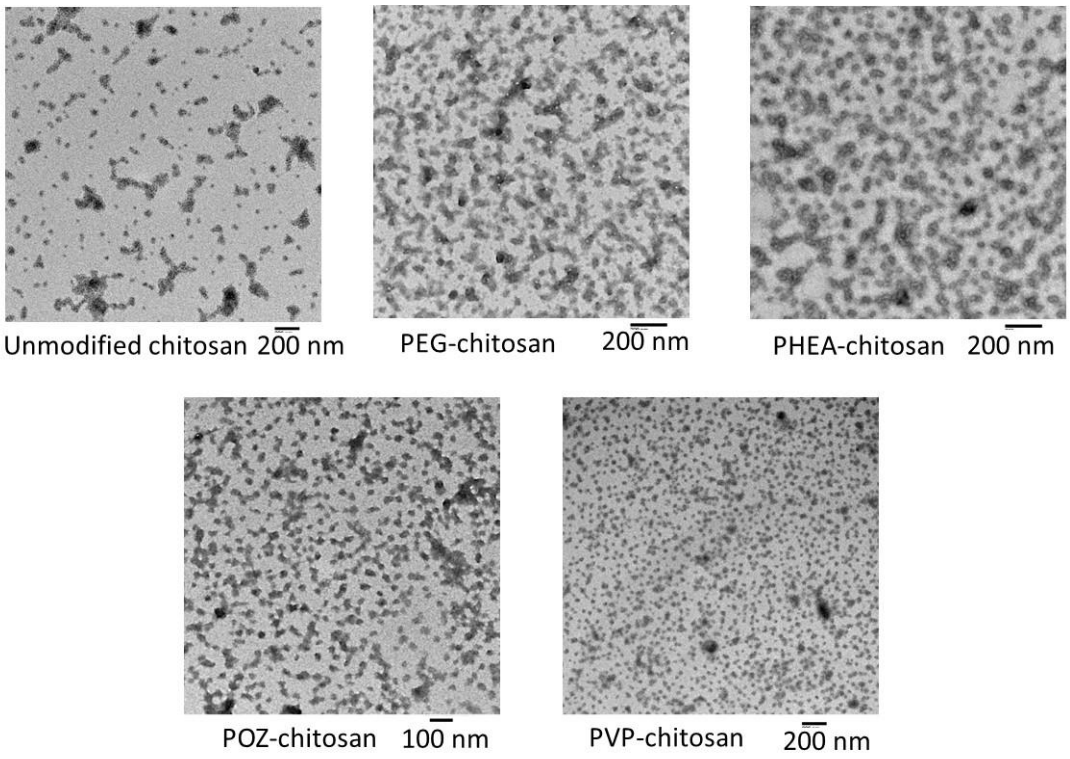


Figure 5.13 TEM images of unmodified and modified chitosan nanoparticles.

To prepare fluorescent chitosan nanoparticles, unmodified and modified chitosan were first fluorescently labelled using Alexa Fluor™ 546 according to Figure 5.14-A. The fluorescence labelling is essential for the later diffusion study in BSM solution and penetration through nasal mucosa. The freeze dried Alexa Fluor™ 546-labelled unmodified and modified chitosan had a bright pink colour. Analysis of the dialysis media showed that there was no free Alexa Fluor™ 546 in the labelled polymers (Figure 5.15). The calibration curve which was used to calculate the Alexa Fluor™ 546 content of chitosan is shown in Figure 5.16. Unmodified and modified chitosan showed similar Alexa Fluor™ 546 content (Table 5.4). However, the fluorescence intensity of the Alexa Fluor™ 546-labelled unmodified chitosan nanoparticles was less than modified chitosan nanoparticles (Figure 5.14-B and Table 5.4), which could be due to the stronger interaction between the amino groups of the unmodified chitosan and TPP resulting in a partial fluorescence quenching. In case of modified chitosan, this interaction could be decreased as a significant number of amino groups have been replaced by the correspondent polymers resulting in a higher fluorescence intensity of modified chitosan nanoparticles compared to unmodified chitosan nanoparticles (Table 5.4).

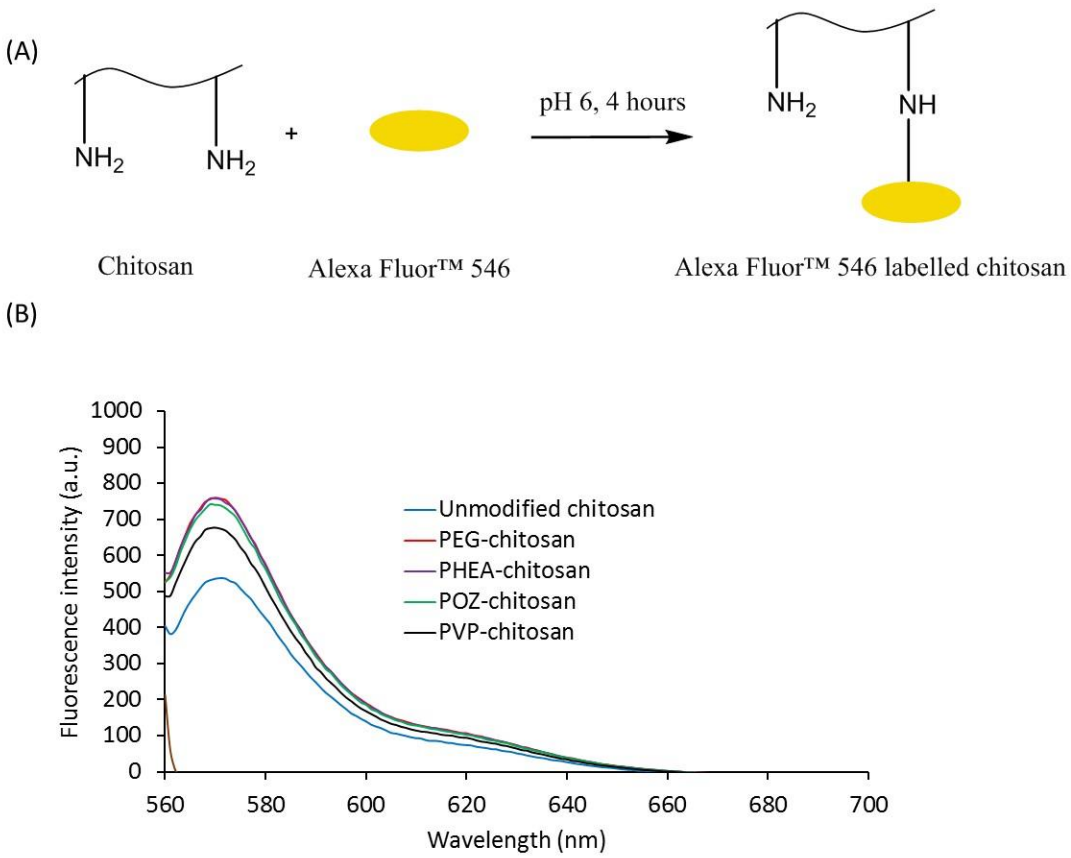


Figure 5.14 (A) Scheme of fluorescent labelling of chitosan with Alexa Fluor™ 546 and (B) fluorescence emission spectra of the unmodified and modified chitosan nanoparticles, with 0.5% w/v bovine submaxillary mucin (BSM) solution as background control at 554 nm. The nanoparticles were diluted (1:50) with ultrapure water, whereas the BSM was measured without dilution, n=3.

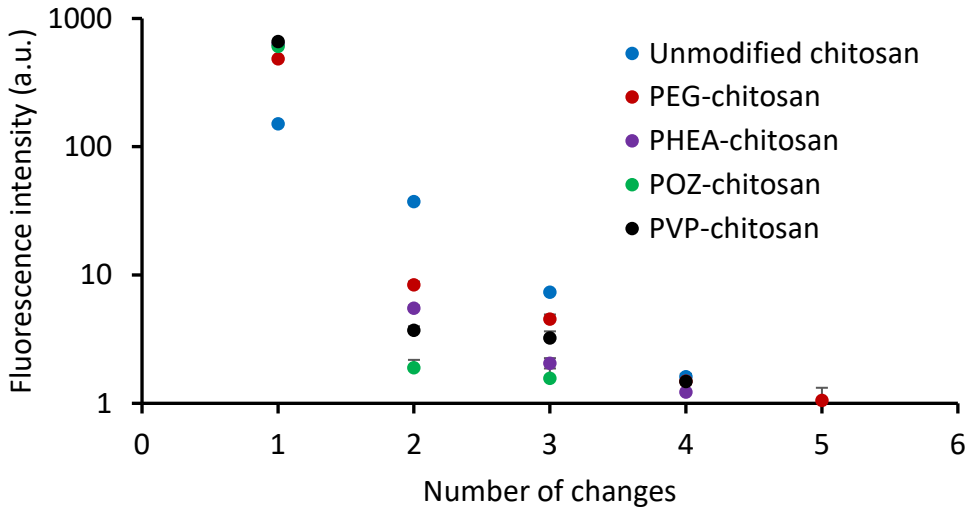


Figure 5.15 Washing after dialysis for Alexa Fluor™ 546-labelling of unmodified and modified chitosan.

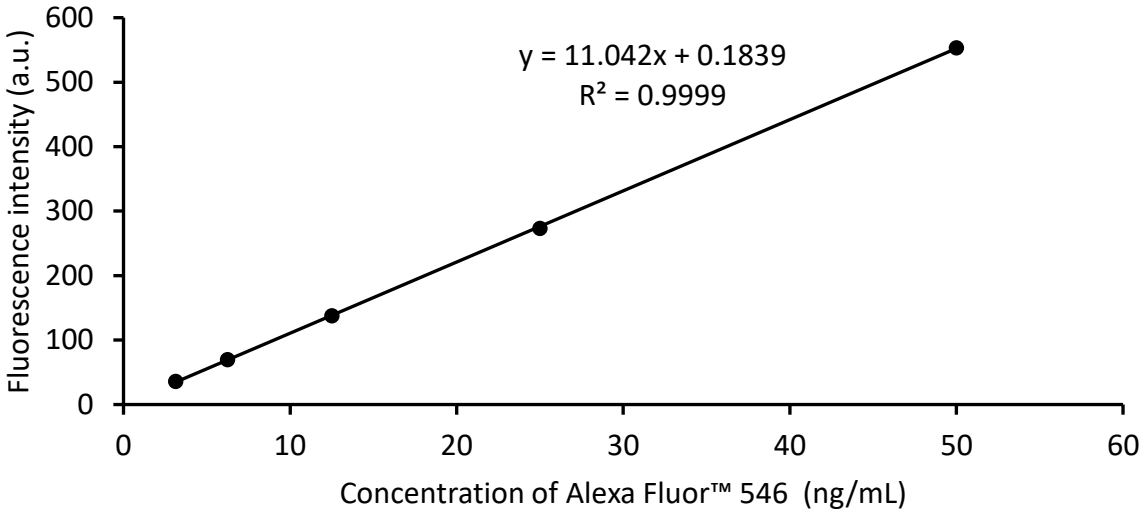


Figure 5.16 A calibration curve used to calculate the degree of Alexa Fluor™ 546-labelling of unmodified and modified chitosan.

Table 5.4 Characterisation of Alexa Fluor™ 546 labelled polymers and nanoparticles (mean ± SD, n = 3).

| Materials | Alexa Fluor™ 546 content | | Z-average (nm, DLS) | Modal size (nm, NTA) | Mean size (nm, NTA) | PDI (DLS) | ξ-potential (mV) | Diffusion coefficient in $H_2O$ ($\times 10^4$ $nm^2/s$) | Maximal fluorescence intensity (a.u.) |
|---|---|---|---|---|---|---|---|---|---|
| | µmol/g of polymer | W% of polymer | | | | | | | |
| Unmodified chitosan | 9.319 ± 0.023 | 1.080 ± 0.002 | 144 ± 1 | 142 ± 14 | 187 ± 8 | 0.174 ± 0.014 | 18.40 ± 1.82 | 306 ± 20 | 539 ± 1 |
| PEG-chitosan | 8.721± 0.050 | 1.011 ± 0.005 | 107 ± 1 | 109 ± 11 | 131 ± 6 | 0.098 ± 0.011 | 11.93 ± 0.47 | 436 ± 27 | 761 ± 10 |
| PHEA-chitosan | 10.103 ± 0.029 | 1.171 ± 0.003 | 134 ± 3 | 128 ± 4 | 151 ± 6 | 0.067 ± 0.022 | 11.84 ± 0.16 | 366 ± 11 | 760 ± 3 |
| POZ-chitosan | 9.603 ± 0.046 | 1.113 ± 0.005 | 119 ± 2 | 110 ± 5 | 134 ± 3 | 0.091 ± 0.015 | 12.48 ± 0.17 | 412 ± 6 | 743 ± 3 |
| PVP-chitosan | 8.889 ± 0.070 | 1.030 ± 0.008 | 112 ± 1 | 108 ± 8 | 155 ± 2 | 0.106 ± 0.003 | 12.03 ± 0.49 | 391 ± 7 | 677 ± 4 |

It was possible to measure the size of the Alexa Fluor™ 546-labelled chitosan nanoparticles using DLS. This was because the excitation wavelength (absorption maxima, 554 nm) of Alexa Fluor™ 546-labelled chitosan nanoparticles is significantly lower than the wavelength used by the Zetasizer (633 nm, red laser) and thus no interference in light scattering would be expected. This hypothesis is also supported by Geißler et al. (2015) who showed that fluorescent-labelling does not have a significant impact on the size data of the polymeric nanoparticles from DLS and small angle X-ray scattering especially when absorption maxima of the nanoparticles are different from the wavelength of the laser used and the degree of fluorescent-labelling is not extremely high. Nevertheless our data showed that the Alexa Fluor™ 546-labelled chitosan nanoparticles have a slightly lower PDI than the unlabelled nanoparticles (Table 5.3 and Table 5.4).

NTA can be used to measure the size, the concentration (particles/mL) and also the diffusion coefficient of the nanoparticles dispersed in liquid media (Mansfield et al., 2018). Compared

to DLS, it is a more accurate technique for the measurement of the size of the polydispersed nanoparticles (Filipe et al., 2010; Gross et al., 2016). The NTA analysis of size was in agreement with the DLS data (Table 5.4). The particle size distribution measured by NTA (Figure 5.17) indicated that the prepared unmodified and modified chitosan nanoparticles were relatively monodispersed. This was also evident from the relatively low standard deviation measured by NTA (99 ± 13, 85 ± 12, 81 ± 16, 78 ± 10 and 106 ± 4 nm for unmodified, PEG-, PHEA-, POZ- and PVP-chitosan nanoparticles, respectively).

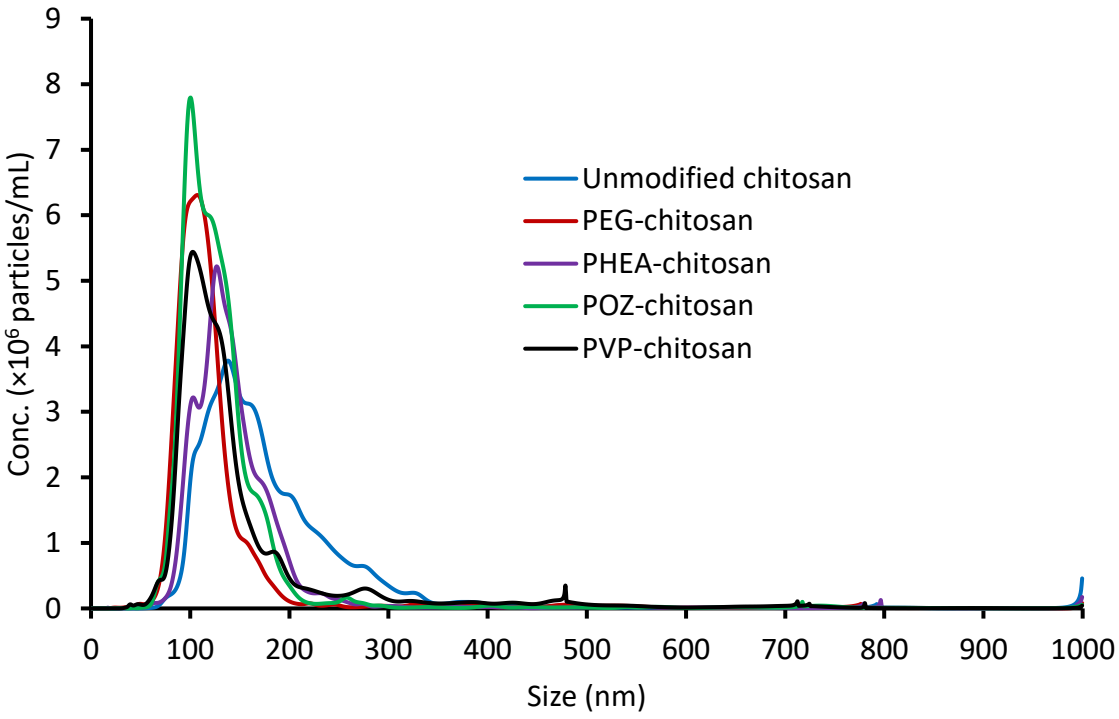


Figure 5.17 Size distribution of Alexa Fluor™ 546-labelled unmodified and modified chitosan nanoparticles measured by NTA (mean, n = 3).

### 5.3.3 Chitosan nanoparticles' diffusion in BSM solution and penetration into sheep nasal mucosa

NTA can be used to measure the mean diffusion of nanoparticles in polymeric solutions (Mun et al., 2014) and mucin dispersion (Mansfield et al., 2015). To conduct diffusion studies, NanoSight should be under the fluorescent mode instead of light scattering mode enabling the visualisation of only the fluorescent nanoparticles. BSM solution (2% w/v, in pH 5 phosphate buffer solution) has previously been used to study mucoadhesive properties of polymeric microparticles (L. Achar & Peppas, 1994). As BSM solution has intrinsic fluorescence properties, a preliminary study was required to find the optimum concentration of BSM solution that gives minimal interference. It was found that 0.5% w/v BSM solution had negligible interference with the visualisation of the nanoparticles compared to 1% w/v BSM solution, and therefore 1% w/v BSM solution was excluded. We preferred 0.5% w/v BSM solution over each of 0.1 or 0.25% w/v BSM solution as the higher concentration may provide a higher opportunities of the interaction of the particles with the mucin macromolecules. It is worth mentioning that the concentration of mucin solution in this study is lower than the nasal mucosa (2% w/v) (Mistry et al., 2009), however, it is significantly higher than the concentration used in some studies involving polymers- and nanoparticles-mucin interactions (0.1% w/v and even 0.001% w/v) (Fefelova et al., 2007; Chuah et al., 2014; Albarkah et al., 2015). Additionally it is not recommended to use 2% w/v mucin solution as its high viscosity could limit the NanoSight's application range which work optimally when the viscosity of the media is between 0 to 10 cP (Mansfield, 2016). The viscosity of 0.5% w/v BSM solution used in this study was 3.05 ± 0.37 cP at 25 °C. This value was calculated using the trendline equation of the temperature-viscosity plot (Figure 5.18). The reason for using BSM and not PGM was mainly related to the stronger auto fluorescence and the higher viscosity of PGM compared to BSM which hindered the precise detection of the nanoparticles. Our diffusion study was conducted at pH 5.5 which is in the range of human nasal mucosa pH (5.3–7.0) (England et al., 1999; Ireson et al., 2001; Aderibigbe, 2018). The NTA analysis revealed that the modified chitosan nanoparticles diffuse significantly faster in BSM solution ($p < 0.001$) compared to unmodified chitosan nanoparticles (Figure 5.19). This was evident from the higher normalised mean diffusion coefficient of the modified chitosan nanoparticles in 0.5% w/v BSM solution compared to unmodified chitosan nanoparticles. In addition to the mean diffusion coefficient, the distribution of diffusion coefficient of the nanoparticles in 0.5% w/v BSM solution was

determined (Figure 5.20), which also indicated higher diffusivity of the modified chitosan nanoparticles compared to unmodified chitosan nanoparticles.

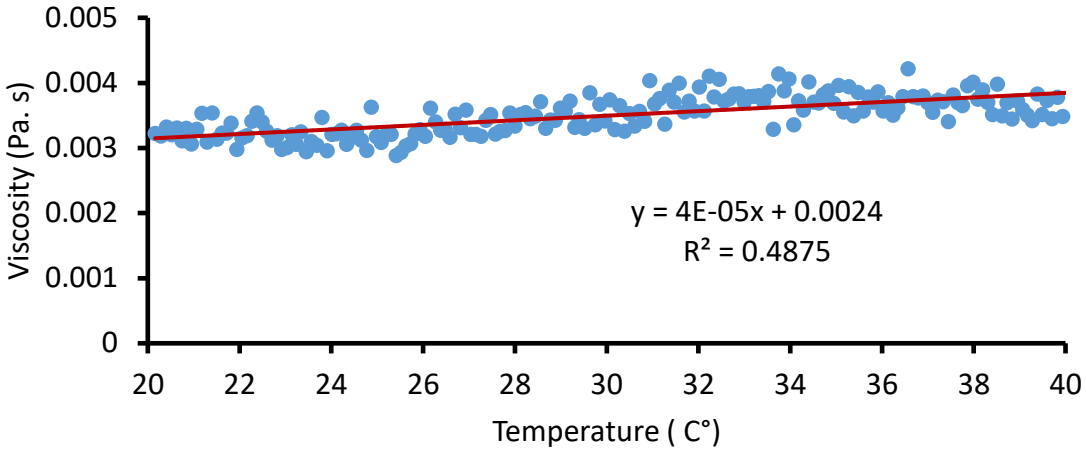


Figure 5.18 Temperature versus viscosity profile of 0.5% w/v bovine submaxillary mucin (BSM) solution, the calculated value of viscosity of BSM solution was 3.05 ± 0.37 and 3.21 ± 0.80 cP at 25 and 32 °C, respectively, n = 3.

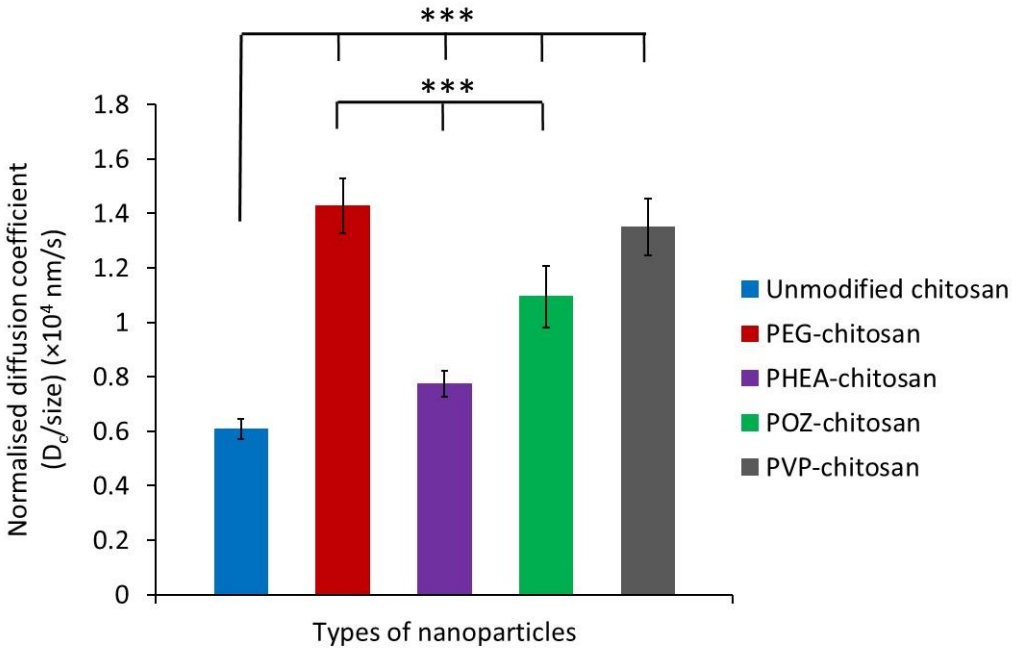


Figure 5.19 Normalised experimentally determined mean diffusion coefficient of Alexa Fluor™ 546-labelled unmodified and modified chitosan nanoparticles in 0.5% w/v BSM solution. One way ANOVA between chitosan and each of modified chitosan nanoparticles, and also between PEG- and each of PHEA, POZ- and PVP-chitosan nanoparticles was performed; there is no significant difference ($p = 0.063$) between PEG- and PVP-chitosan nanoparticles, *** denotes $p < 0.001$ (mean ± SD, $n = 9$).

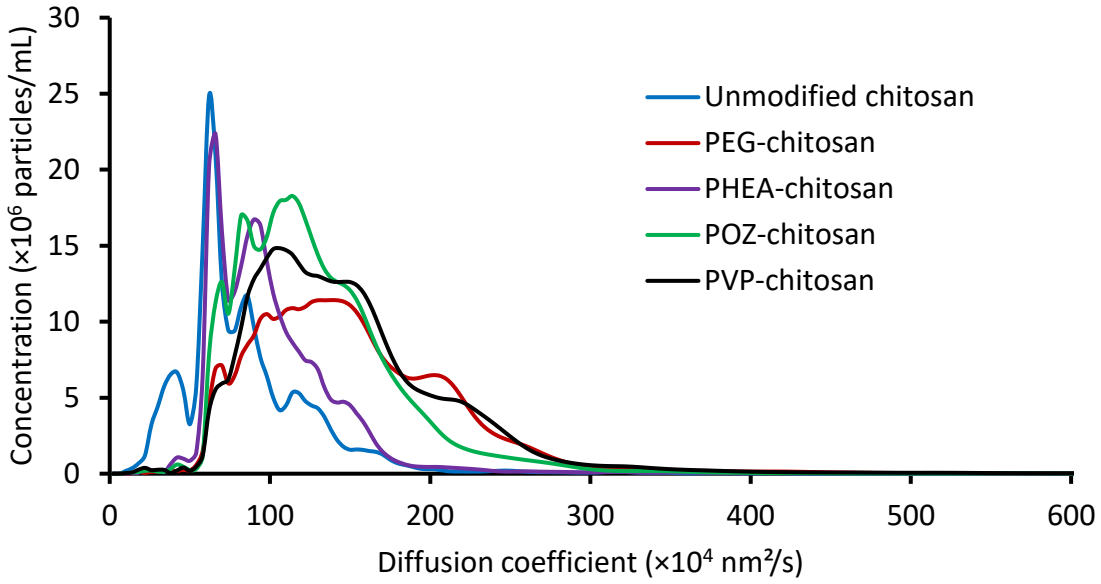


Figure 5.20 Distribution of diffusion coefficient for Alexa Fluor™ 546-labelled unmodified and modified chitosan nanoparticles in 0.5% w/v BSM solution measured at 25 °C using NTA (mean, n = 9).

The enhanced diffusivity of the modified chitosan nanoparticles can be related to the presence of PEG, PHEA, POZ or PVP in the modified chitosan nanoparticles. Lai et al. (2007) showed that PEG coating of the polystyrene nanoparticles facilitates their penetration in fresh undiluted human cervicovaginal mucus. We also showed that PEGylation and POZylation of thiolated silica nanoparticles enhanced their diffusivity in PGM dispersion and through porcine gastric mucosa (Mansfield et al., 2015) and also reduced their mucoadhesiveness with regard to rat intestinal mucosa (M. Ways et al., 2018b). Casettari et al. (2010) showed that PEGylated chitosan does not significantly enhance the permeability of fluorescein isothiocyanate-dextran macromolecules across Calu-3 cell monolayer at pH 7.4, whereas they observed a dramatic permeability enhancement when the polymer was tested at pH 6. Casettari et al. (2010) did not report any possible reasons for the difference in the permeability at these two different pH. However, they claimed that the enhancement could be due to the higher equivalent concentration of chitosan in PEGylated chitosan compared to unmodified chitosan and also the enhanced diffusivity of the PEGylated chitosan compared to unmodified chitosan. The latter reason was also indirectly supported by Prego et al. (2006) who observed that calcitonin loaded PEGylated chitosan nanocapsules

with 1% degree of PEGylation had significantly less hypocalcaemic effect than those with 0.5% degree of PEGylation when orally administered to rats. They postulated that an increase in the degree of PEGylation might result in a decrease in the mucoadhesive properties of chitosan. Thus, a weak interaction between PEGylated chitosan nanocapusles (with 1% degree of PEGylation) and the negatively charged components of the gastrointestinal mucosa was expected. Zhang et al. (2018) claimed that they were the first research group who reported the ability of PEGylated chitosan/DNA nanocomplexes to enhance the transport of DNA through artificial mucus using a Transwell mucus permeation assay. However, to our knowledge no studies on the diffusion of PEGylated chitosan nanoparticles in mucin solution using NTA have been reported.

The NTA data showed the rank of diffusivity in BSM solution as PEG-=PVP->POZ->PHEA-chitosan>unmodified chitosan nanoparticles (Figure 5.19). To compare the NTA analysis to nasal mucosal tissues, a penetration study was conducted using sheep nasal mucosa. Sheep model was selected mainly due to its large nares and anatomical similarity of the nasal cavity with human nose (Illum, 1996; Tas et al., 2009; Barrios et al., 2014; Macias-Valle et al., 2018). The chitosan nanoparticles showed different degrees of penetration into sheep nasal mucosa (Figure 5.21 and Figure 5.22). After 5 minutes of incubation, modified chitosan penetrated significantly ($p < 0.001$) deeper into the nasal mucosa compared to unmodified chitosan. From Figure 5.21 and Figure 5.22, it is clear that all nanoparticles gradually diffused thorough the nasal mucosa. After 15 minutes incubation, modified chitosan nanoparticles still penetrated deeper than the unmodified nanoparticles significantly. However, at 30 minutes no statistical significant difference ($p = 0.08$) was found between unmodified and PEGylated chitosan nanoparticles. On the contrary, PHEA-, POZ- and PVP-chitosan nanoparticles showed significantly greater penetration compared to unmodified chitosan. The distance between the nanoparticles and the nasal epithelial cells are shown in Figure 5.23 and Figure 5.24. It is clear that an agreement exists between the diffusion study using NTA and sheep nasal mucosa, where generally, modified chitosan showed a greater diffusivity than the unmodified chitosan nanoparticles. However, the potential differences in the barrier properties, the pH and the biochemical composition of the media in the NTA study using BSM solution compared to ex *vivo* penetration study with sheep nasal mucosa could explain the lack of difference between the penetration depth of unmodified chitosan and PEG-chitosan nanoparticles at the longer incubation time (30 minutes). The pH of the BSM solution used in our study was 5.5 but no literature reported

the pH of sheep nasal mucosa, nevertheless studies suggested the presence of acidic and neutral polysaccharides in the sheep nasal mucosa (Ibrahim et al., 2014).

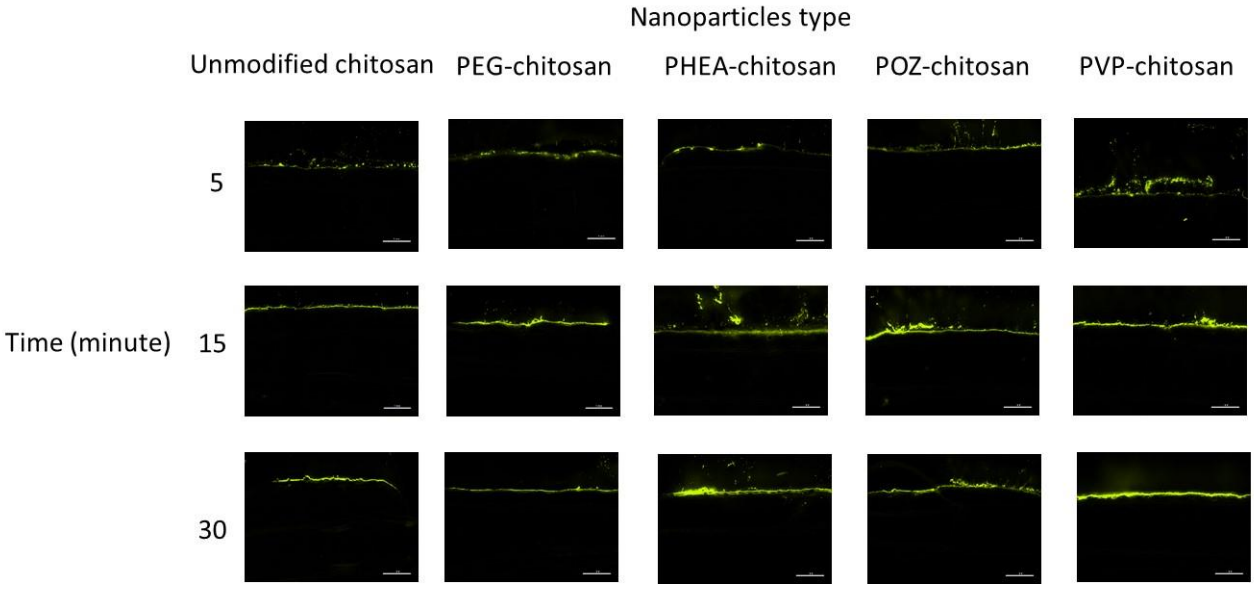


Figure 5.21 Exemplary fluorescent images showing penetration of Alexa Fluor™ 546-labelled (yellow) unmodified and modified chitosan nanoparticles into sheep nasal mucosa after 5, 15 and 30 minutes of incubation. The scale bars are 1 mm in all images.

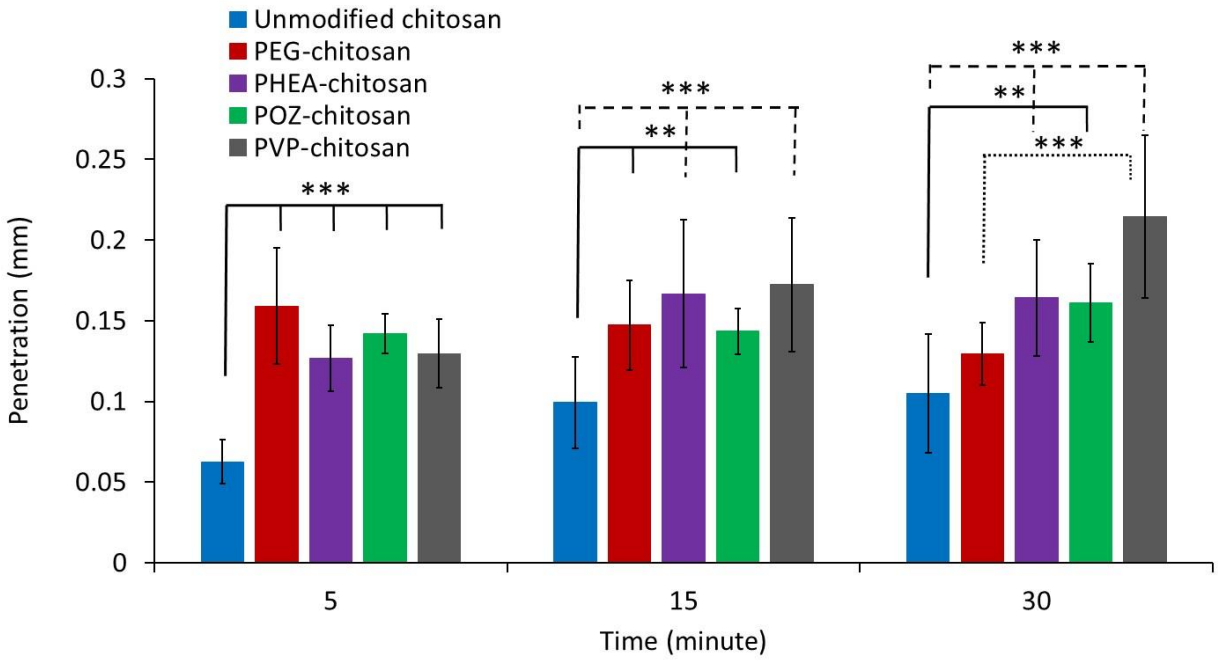


Figure 5.22 Comparison of penetration depth of unmodified and modified chitosan nanoparticles into the freshly excised sheep nasal mucosa after 5, 15 and 30 minutes of incubation. Values represent the mean penetration across 10 separate tissue sections ± standard deviation. *** denotes $p < 0.001$, ** denotes $p < 0.01$.

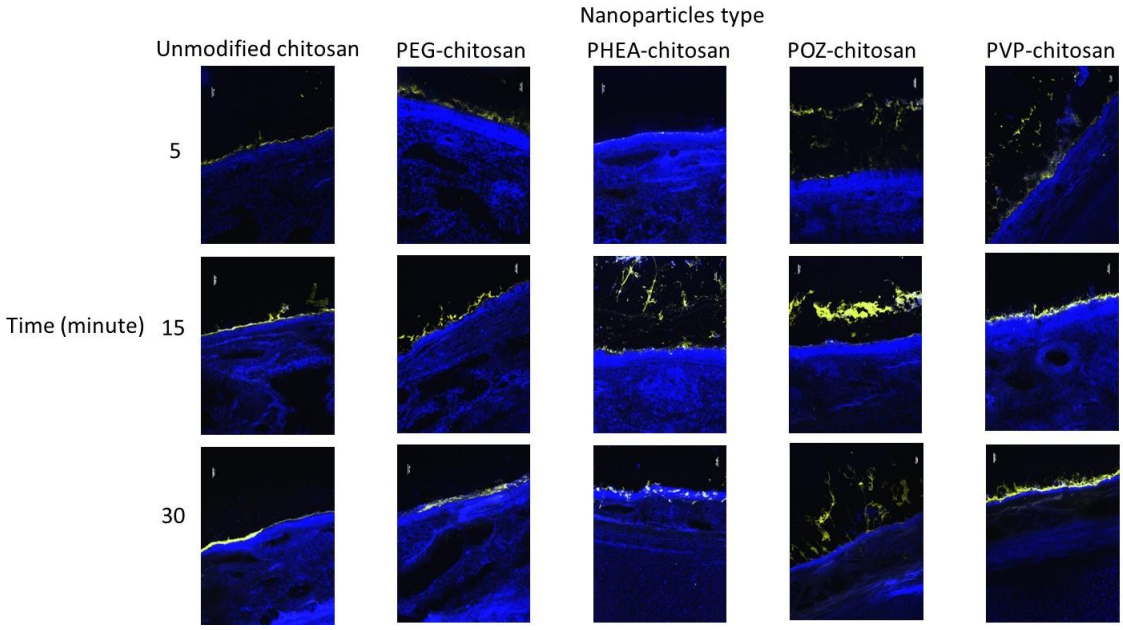


Figure 5.23 Exemplary fluorescent images showing penetration of Alexa Fluor™ 546-labelled (yellow) unmodified and modified chitosan nanoparticles into sheep nasal mucosa after 5, 15 and 30 minutes of incubation at 10x magnification (except for PVP-chitosan 5 minutes and POZ-chitosan 30 minutes, which are at 5x magnification). The nuclei of the epithelial cells were stained (blue) with DAPI solution. The scale bars are 50 µm in all images.

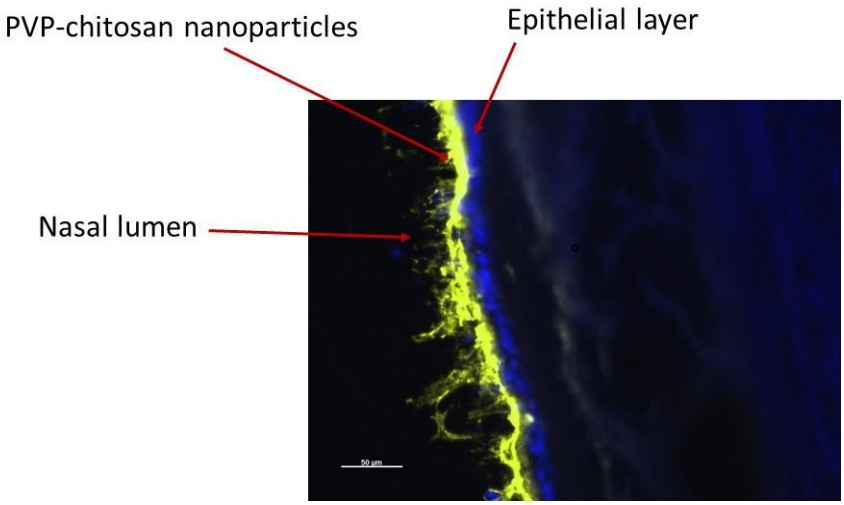


Figure 5.24 Exemplary fluorescent images showing the penetration of Alexa Fluor™ 546-labelled (yellow) PVP-chitosan nanoparticles into sheep nasal mucosa after 30 minutes of incubation with sheep nasal mucosa at 20x magnification. The nuclei of the epithelial cells were stained (blue) with DAPI solution. The scale bar is 50 µm.

The nasal mucosa of both human and sheep is mainly divided into olfactory and respiratory regions. The olfactory mucosa is a small area of the caudal roof of the nasal cavity which covers ethmoturbinates and the caudal parts of the dorsal and middle nasal conchae. It consists of the olfactory mucosa and the underlying connective tissue lamina propria. The olfactory mucosa consists of specialised ciliated cells which their main function is the detection of smell (Ugwoke et al., 2005; Ibrahim et al., 2014). This layer has a direct access to the central nervous system (Ugwoke et al., 2005). The respiratory mucosa composed of respiratory epithelium and the connective tissue laminar propria. The respiratory epithelium is a pseudostratified ciliated and non-ciliated columnar type cells distributed alongside with basal cells, ciliated cells, goblet cells and the opening of the seromucus glands (Ugwoke et al., 2005; Ibrahim et al., 2014). The goblet cells consist of an apical part which contains mucin polysaccharides (Ibrahim et al., 2014) which swell in the nasal fluid as a component of the mucus layer (Ugwoke et al., 2005). Although, due to technical limitations, we have used the respiratory mucosa, studies reported some similarities in the mucin expression between the olfactory and the respiratory mucosa (Ibrahim et al., 2014). Nevertheless, in contrast to respiratory mucosa, cilia in olfactory region are non-motile as they lack dynein arms which contain the $Mg^{2+}$-ATPase required to generate the force for the ciliary movement (Mistry et al., 2009). Thus, there is no mucociliary clearance mechanism in the olfactory mucosa. However, mucus can still be cleared due to gravity when the human head is at upright position (Charlton et al., 2007). Therefore, mucus penetrating nanoparticles may have a great potential applications in nasal drug delivery via both respiratory and olfactory mucosa.

PHEA is a polymer with hydroxyl side groups which has been used in drug delivery due to its hydrophilicity and biocompatibility (Arun & Reddy, 2005; Khutoryanskaya et al., 2008; Steinhauer et al., 2010; Lin et al., 2012). PHEA has FDA approval for indirect additives used in food contact substances as an adhesive and a component of coatings (FDA, 2018). Polymers with hydroxyl side groups including poly-*N*-2-hydroxypropyl methacrylamide (PHPMA) were found to have stealth properties (Talelli et al., 2010; Du et al., 2016). PHPMA is even superior to PEG in decreasing the accelerated blood clearance phenomenon of poly-D,L-lactic acid-PHPMA nanoparticles (Du et al., 2016). In contrast to poly-2-hydroxyethylmethacrylate (PHEMA) (the closest analogue to PHEA), PHEA is completely soluble in water, a property which could potentially make the polymer muco-inert

(Khutoryanskiy, 2018). To the best of our knowledge, no studies have reported the use of PHEA in designing the mucus-penetrating nanoparticles.

Peppas and colleagues (1995 ; 1996) showed the mucoadhesive capacity of PHEMA microparticles in Sprague Dawley rat jejunum and found that the presence of free short chain PEG (1 kDa) in the PHEMA microparticles significantly increased their mucoadhesive capacity. However, longer chain PEG (100 kDa) had a detrimental effect on the mucoadhesive capacity. In the light of Peppas et al. study (1995 ) and as mentioned earlier that PHEA is more water soluble than PHEMA, we can hypothesise that PHEA is less mucoadhesive than PHEMA. An outcome which we indirectly showed by the enhanced mucus penetrating capacity of PHEA-chitosan nanoparticles compared to unmodified chitosan nanoparticles.

POZ belongs to polyoxazolines which are a class of polymers with polypeptide isomeric structures. They have recently attracted a considerable attention in biomedical applications (Gaertner et al., 2007; Hoogenboom, 2009; Sedlacek et al., 2012). They were found to have some similar properties to PEG in terms of blood circulation time, their uptake by liver and spleen (Adams & Schubert, 2007), the biodegradability (Ulbricht et al., 2014; Hoogenboom & Schlaad, 2017), the biocompatibility and non-toxicity (Lava et al., 2015). Nevertheless, polyoxazolines have some advantages over PEG and these include the possibility in the variation of the monomer composition and the versatility of the side chain functionalities. This feature can result in polymers with various physicochemical properties and a broad range of applications (Hoogenboom, 2009; Tim R Dargaville et al., 2014; Hoogenboom & Schlaad, 2017). POZ currently lacks FDA approval, however, SER-214 (rotigotine-POZ conjugate) is currently under clinical trial for the treatment of Parkinsonism as an injectable formulation administered subcutaneously once a week (ClinicalTrials.gov Identifier: NCT02579473). Our current study clearly demonstrates the mucus-penetrating capacity of POZ-chitosan nanoparticles.

PVP has a wide range of applications as a biomaterial in various medical areas such as dosage forms design including tablets, granules, soft shell capsules and injectables as well as non-medicals including optical, electric, ceramics, papers, coating and inks (Teodorescu & Bercea, 2015). This is due to its solubility in water and several organic solvents, biocompatibility, lack of toxicity, wetting and binding properties (Teodorescu & Bercea, 2015). It is also frequently used as an alternative to PEG as a polymer with stealth properties

(Benahmed et al., 2001; Hadjesfandiari & Parambath, 2018), but again no literature on the mucus penetration ability of PVP exists. However, several publications indicated that PVP has poor mucoadhesive properties (J. D. Smart et al., 1984; Solomonidou et al., 2001; Mishra & Mishra, 2012; Russo et al., 2016). Indeed, Smart et al. (1984) found that PVP (44 kDa) and PEG (6 kDa) were less mucoadhesive compared to other studied materials (75P sodium carboxy methylcellulose, Carbopol 934, tragacanth, Gantrez® AN, sodium alginate (high viscosity), hydroxypropylmethyl cellulose (medium viscosity), gelatin and pectin) with regard to partially purified mucus obtained from guinea-pig intestine. Additionally, Ivarsson & Wahlgren (2012) reported that PVP has poor or no mucoadhesive properties when studied using ellipsometry, tensile strength and rheological methods in respect to PGM. These observations indirectly indicate the mucus-penetrating ability of PVP and PEG and is in agreement with our results. Another possible explanation for the better mucus penetration ability of PVP could be due to its amphiphilic properties (having both polar and apolar groups) (Benahmed et al., 2001), which allows easier diffusion through mucus gel via hydrogen bonding and interacting with the lipophilic cellular surfaces via hydrophobic interactions.

## 5.4 Conclusions

We synthesised four derivatives of chitosan using EDAC/NHS chemistry by reacting carboxyl-terminated PEG, PHEA, POZ and PVP with unmodified chitosan. The modified chitosan showed full solubility at any pH whereas unmodified chitosan precipitated at pH 7.3. This improvement in the solubility can dramatically broaden the range of chitosan applications. Methods to prepare, characterise and evaluate different unmodified and modified chitosan nanoparticles were developed. The modified chitosan nanoparticles showed an enhanced diffusivity in BSM solution compared to unmodified chitosan nanoparticles. They also penetrated deeper into the sheep nasal mucosa compared to unmodified chitosan nanoparticles. The modified chitosan nanoparticles have potential applications in the nasal drug delivery for the treatment of various local and systemic diseases including central nervous system disorders.

## 5.5 Conflicts of interest

There are no conflicts to declare.

## 5.6 Acknowledgements

We are thankful to HCED-Iraq for funding this research. We acknowledge the assistance of staff at the Chemical Analysis Facility (CAF), University of Reading, in NMR, FTIR, fluorescence spectroscopy and TEM experiments. We are grateful to P.C. Turner Abattoirs (Farnborough, UK) for supplying the sheep heads used in this study.

## 5.7 References

Adams, N., & Schubert, U.S., 2007. Poly(2-oxazolines) in biological and biomedical application contexts. Adv. Drug Del. Rev. 59, 1504-1520.

Aderibigbe, B.A., 2018. In situ-based gels for nose to brain delivery for the treatment of neurological diseases. Pharmaceutics 10, 40.

Albarkah, Y.A., Green, R.J., & Khutoryanskiy, V.V., 2015. Probing the mucoadhesive interactions between porcine gastric mucin and some water-soluble polymers. Macromol. Biosci. 15, 1546-1553.

Alessia De Ascentiis, Janet L. deGrazia , Christopher N. Bowman , Paolo Colombo , & Peppas, N.A., 1995 Mucoadhesion of poly(2-hydroxyethyl methacrylate) is improved when linear poly(ethylene oxide) chains are added to the polymer network. J. Control. Release 33, 197-201.

Arun, A., & Reddy, B.S., 2005. *In vitro* drug release studies of 2-hydroxyethyl acrylate or 2-hydroxypropyl methacrylate-4-{(1E,4E)-5-[4-(acryloyloxy)phenyl]-3-oxopenta-1,4-dienyl}phenyl acrylate copolymer beads. J. Biomed. Mater. Res. B Appl. Biomater. 73, 291-300.

Baraniuk, J.N., 1997. Pathogenesis of allergic rhinitis. J. Allergy Clin. Immunol. 99, S763-S772.

Barrios, A.W., Sanchez Quinteiro, P., & Salazar, I., 2014. The nasal cavity of the sheep and its olfactory sensory epithelium. Microsc Res Tech 77, 1052-1059.

Benahmed, A., Ranger, M., & Leroux, J.-C., 2001. Novel polymeric micelles based on the amphiphilic diblock copolymer poly(N-vinyl-2-pyrrolidone)-block-poly(D,L-lactide). Pharm. Res. 18, 323-328.

Bhattarai, N., Ramay, H.R., Gunn, J., Matsen, F.A., & Zhang, M., 2005. PEG-grafted chitosan as an injectable thermosensitive hydrogel for sustained protein release. J. Control. Release 103, 609-624.

Calvo, P., Remuñán-López, C., Vila-Jato, J.L., & Alonso, M.J., 1997. Novel hydrophilic chitosan-polyethylene oxide nanoparticles as protein carriers. J. Appl. Polym. Sci. 63, 125-132.

Casettari, L., Vllasaliu, D., Mantovani, G., Howdle, S.M., Stolnik, S., & Illum, L., 2010. Effect of PEGylation on the toxicity and permeability enhancement of chitosan. Biomacromolecules 11, 2854–2865.

Charlton, S., Jones, N.S., Davis, S.S., & Illum, L., 2007. Distribution and clearance of bioadhesive formulations from the olfactory region in man: Effect of polymer type and nasal delivery device. Eur. J. Pharm. Sci. 30, 295-302.

Chuah, L.H., Roberts, C.J., Billa, N., Abdullah, S., Rosli, R., & Manickam, S., 2014. Using nanoparticle tracking analysis (NTA) to decipher mucoadhesion propensity of curcumin-containing chitosan nanoparticles and curcumin release. J. Dispersion Sci. Technol. 35, 1201-1207.

Du, N., Guo, W., Yu, Q., Guan, S., Guo, L., Shen, T., Tang, H., & Gan, Z., 2016. Poly(d,l-lactic acid)-block-poly(N-(2-hydroxypropyl)methacrylamide) nanoparticles for overcoming accelerated blood clearance and achieving efficient anti-tumor therapy. Polymer Chemistry 7, 5719-5729.

England, R.J.A., Homer, J.J., Knight, L.C., & Ell, S.R., 1999. Nasal pH measurement: A reliable and repeatable parameter. Clin. Otolaryngol. 24, 67-68.

FDA, 2018. CFR - Code of Federal Regulations Title 21. https://www.accessdata.fda.gov/scripts/cdrh/cfdocs/cfCFR/CFRSearch.cfm?fr=175.105 (10/12/2018).

Fefelova, N.A., Nurkeeva, Z.S., Mun, G.A., & Khutoryanskiy, V.V., 2007. Mucoadhesive interactions of amphiphilic cationic copolymers based on [2-(methacryloyloxy)ethyl]trimethylammonium chloride. Int. J. Pharm. 339, 25-32.

Ferguson, C.J., Hughes, R.J., Nguyen, D., Pham, B.T.T., Gilbert, R.G., Serelis, A.K., Such, C.H., & Hawkett, B.S., 2005. Ab initio emulsion polymerization by RAFT-controlled self-assembly. Macromolecules 38, 2191-2204.

Filipe, V., Hawe, A., & Jiskoot, W., 2010. Critical evaluation of nanoparticle tracking analysis (NTA) by nanosight for the measurement of nanoparticles and protein aggregates. Pharm. Res. 27, 796-810.

Friedman, M., 2004. Applications of the ninhydrin reaction for analysis of amino acids, peptides, and proteins to agricultural and biomedical sciences. J. Agric. Food Chem. 52, 385-406.

Gaertner, F.C., Luxenhofer, R., Blechert, B., Jordan, R., & Essler, M., 2007. Synthesis, biodistribution and excretion of radiolabeled poly(2-alkyl-2-oxazoline)s. J. Control. Release 119, 291-300.

Geißler, D., Gollwitzer, C., Sikora, A., Minelli, C., Krumrey, M., & Resch-Genger, U., 2015. Effect of fluorescent staining on size measurements of polymeric nanoparticles using DLS and SAXS. Analytical Methods 7, 9785-9790.

Gross, J., Sayle, S., Karow, A.R., Bakowsky, U., & Garidel, P., 2016. Nanoparticle tracking analysis of particle size and concentration detection in suspensions of polymer and protein samples: Influence of experimental and data evaluation parameters. Eur. J. Pharm. Biopharm. 104, 30-41.

Hadjesfandiari, N., & Parambath, A. (2018). 13 - Stealth coatings for nanoparticles: Polyethylene glycol alternatives, in: A. Parambath (Ed.), Engineering of Biomaterials for Drug Delivery Systems. Woodhead Publishingpp. 345-361.

Harkema, J.R., Carey, S.A., & Wagner, J.G., 2006. The nose revisited: A brief review of the comparative structure, function, and toxicologic pathology of the nasal epithelium. Toxicol. Pathol. 34, 252-269.

Hoogenboom, R., 2009. Poly(2-oxazoline)s: A polymer class with numerous potential applications. Angew. Chem. Int. Ed. 48, 7978-7994.

Hoogenboom, R., & Schlaad, H., 2017. Thermoresponsive poly(2-oxazoline)s, polypeptoids, and polypeptides. Polymer Chemistry 8, 24-40.

Ibrahim, D., Nakamuta, N., Taniguchi, K., Yamamoto, Y., & Taniguchi, K., 2014. Histological and lectin histochemical studies on the olfactory and respiratory mucosae of the sheep. J Vet Med Sci. 76, 339–346.

Illum, L., 1996. Nasal delivery. The use of animal models to predict performance in man. J. Drug Target. 3, 427-442.

Illum, L., 2003. Nasal drug delivery—possibilities, problems and solutions. J. Control. Release 87, 187-198.

Ireson, N.J., Tait, J.S., MacGregor, G.A., & Baker, E.H., 2001. Comparison of nasal pH values in black and white individuals with normal and high blood pressure. Clin. Sci. 100, 327–333.

Ivarsson, D., & Wahlgren, M., 2012. Comparison of *in vitro* methods of measuring mucoadhesion: Ellipsometry, tensile strength and rheological measurements. Colloids Surf. B. Biointerfaces 92, 353-359.

J. D. Smart, Kellaway, I.W., & Worthington, H.E.C., 1984. An *in-vitro* investigation of mucosa-adhesive materials for use in controlled drug delivery. J. Pharm. Pharmacol. 36, 295-299.

Khutoryanskaya, O.V., Mayeva, Z.A., Mun, G.A., & Khutoryanskiy, V.V., 2008. Designing temperature-responsive biocompatible copolymers and hydrogels based on 2-hydroxyethyl(meth)acrylates. Biomacromolecules 9, 3353-3361.

Khutoryanskiy, V.V., 2018. Beyond PEGylation: Alternative surface-modification of nanoparticles with mucus-inert biomaterials. Adv. Drug Del. Rev. 124, 140-149.

Kirch, J., Schneider, A., Abou, B., Hopf, A., Schaefer, U.F., Schneider, M., Schall, C., Wagner, C., & Lehr, C.-M., 2012. Optical tweezers reveal relationship between microstructure and nanoparticle penetration of pulmonary mucus. Proceedings of the National Academy of Sciences 109, 18355-18360.

Kolawole, O.M., Lau, W.M., & Khutoryanskiy, V.V., 2018. Methacrylated chitosan as a polymer with enhanced mucoadhesive properties for transmucosal drug delivery. Int. J. Pharm. 550, 123-129.

Kozlovskaya, L., Abou-Kaoud, M., & Stepensky, D., 2014. Quantitative analysis of drug delivery to the brain via nasal route. J. Control. Release 189, 133-140.

Kumar, M., Misra, A., Babbar, A.K., Mishra, A.K., Mishra, P., & Pathak, K., 2008. Intranasal nanoemulsion based brain targeting drug delivery system of risperidone. Int. J. Pharm. 358, 285-291.

L. Achar, & Peppas, N.A., 1994. Preparation, characterisation and mucoadhesive interactions of poly ( methacrylic acid) copolymers with rat mucosa. J. Control. Release 31, 271-276.

Lai, S.K., O'Hanlon, D.E., Harrold, S., Man, S.T., Wang, Y.-Y., Cone, R., & Hanes, J., 2007. Rapid transport of large polymeric nanoparticles in fresh undiluted human mucus. Proc. Natl. Acad. Sci. U. S. A. 104, 1482-1487.

Lai, S.K., Suk, J.S., Pace, A., Wang, Y.-Y., Yang, M., Mert, O., Chen, J., Kim, J., & Hanes, J., 2011. Drug carrier nanoparticles that penetrate human chronic rhinosinusitis mucus. Biomaterials 32, 6285-6290.

Lai, S.K., Wang, Y.Y., & Hanes, J., 2009. Mucus-penetrating nanoparticles for drug and gene delivery to mucosal tissues. Adv. Drug Del. Rev. 61, 158-171.

Lava, K., Verbraeken, B., & Hoogenboom, R., 2015. Poly(2-oxazoline)s and click chemistry: A versatile toolbox toward multi-functional polymers. Eur. Polym. J. 65, 98-111.

Lin, M., Xu, P., & Zhong, W., 2012. Preparation, characterization, and release behavior of aspirin-loaded poly(2-hydroxyethyl acrylate)/silica hydrogels. J. Biomed. Mater. Res. B Appl. Biomater. 100, 1114-1120.

Luo, Q., Gao, H., Peng, L., Liu, G., & Zhang, Z., 2016. Synthesis of PEGylated chitosan copolymers as efficiently antimicrobial coatings for leather. J. Appl. Polym. Sci. 133, 43465-43472.

M. Ways, T.M., Lau, W.M., & Khutoryanskiy, V.V., 2018a. Chitosan and its derivatives for application in mucoadhesive drug delivery systems. Polymers 10, 267.

M. Ways, T.M., Lau, W.M., Ng, K.W., & Khutoryanskiy, V.V., 2018b. Synthesis of thiolated, PEGylated and POZylated silica nanoparticles and evaluation of their retention on rat intestinal mucosa *in vitro*. Eur. J. Pharm. Sci. 122, 230-238.

Macias-Valle, L., Finkelstein-Kulka, A., Manji, J., Okpaleke, C., Al-Salihi, S., & Javer, A.R., 2018. Evaluation of sheep sinonasal endoscopic anatomy as a model for rhinologic research. World Journal of Otorhinolaryngology - Head and Neck Surgery 4, 268-272.

Mansfield, E.D. (2016). Synthesis, characterisation, and diffusive properties of functionalised nanomaterials. (PhD), University of Reading.

Mansfield, E.D., de la Rosa, V.R., Kowalczyk, R.M., Grillo, I., Hoogenboom, R., Sillence, K., Hole, P., Williams, A.C., & Khutoryanskiy, V.V., 2016. Side chain variations radically alter the diffusion of poly(2-alkyl-2-oxazoline) functionalised nanoparticles through a mucosal barrier. Biomaterials Science 4, 1318-1327.

Mansfield, E.D., Sillence, K., Hole, P., Williams, A.C., & Khutoryanskiy, V.V., 2015. POZylation: A new approach to enhance nanoparticle diffusion through mucosal barriers. Nanoscale 7, 13671-13679.

Mansfield, E.D.H., Pandya, Y., Mun, E.A., Rogers, S.E., Abutbul-Ionita, I., Danino, D., Williams, A.C., & Khutoryanskiy, V.V., 2018. Structure and characterisation of hydroxyethylcellulose–silica nanoparticles. RSC Adv. 8, 6471-6478.

Mishra, M., & Mishra, B., 2012. Mucoadhesive microparticles as potential carriers in inhalation delivery of doxycycline hyclate: A comparative study. Acta Pharmaceutica Sinica B 2, 518-526.

Mistry, A., Stolnik, S., & Illum, L., 2009. Nanoparticles for direct nose-to-brain delivery of drugs. Int. J. Pharm. 379, 146-157.

Mistry, A., Stolnik, S., & Illum, L., 2015. Nose-to-brain delivery: Investigation of the transport of nanoparticles with different surface characteristics and sizes in excised porcine olfactory epithelium. Mol. Pharm. 12, 2755-2766.

Mun, E.A., Hannell, C., Rogers, S.E., Hole, P., Williams, A.C., & Khutoryanskiy, V.V., 2014. On the role of specific interactions in the diffusion of nanoparticles in aqueous polymer solutions. Langmuir 30, 308-317.

Peppas, N.A., & Sahlin, J.J., 1996. Hydrogels as mucoadhesive and bioadhesive materials: A review. Biomaterials 17, 1553-1561.

Pound, G., Eksteen, Z., Pfukwa, R., McKenzie, J.M., Lange, R.F.M., & Klumperman, B., 2008. Unexpected reactions associated with the xanthate-mediated polymerization of N-vinylpyrrolidone. Journal of Polymer Science Part A: Polymer Chemistry 46, 6575-6593.

Prego, C., Torres, D., Fernandez-Megia, E., Novoa-Carballal, R., Quinoa, E., & Alonso, M.J., 2006. Chitosan-PEG nanocapsules as new carriers for oral peptide delivery: Effect of chitosan pegylation degree. J. Control. Release 111, 299-308.

Prochazkova, S., Vårum, K.M., & Ostgaard, K., 1999. Quantitative determination of chitosans by ninhydrin. Carbohydr. Polym. 38, 115-122.

Ramos, F.L., Krahnke, J.S., & Kim, V., 2014. Clinical issues of mucus accumulation in COPD. Int. J. Chron. Obstruct. Pulmon. Dis. 9, 139-150.

Rinaudo, M., 2006. Chitin and chitosan: Properties and applications. Prog. Polym. Sci. 31, 603-632.

Rogers, D.F., & Barnes, P.J., 2006. Treatment of airway mucus hypersecretion. Ann Med 38, 116-125.

Russo, E., Selmin, F., Baldassari, S., Gennari, C.G.M., Caviglioli, G., Cilurzo, F., Minghetti, P., & Parodi, B., 2016. A focus on mucoadhesive polymers and their application in buccal dosage forms. J. Drug Deliv. Sci. Technol. 32, 113-125.

Schneider, C.S., Xu, Q., Boylan, N.J., Chisholm, J., Tang, B.C., Schuster, B.S., Henning, A., Ensign, L.M., Lee, E., Adstamongkonkul, P., Simons, B.W., Wang, S.-Y.S., Gong, X., Yu, T., Boyle, M.P., Suk, J.S., & Hanes, J., 2017. Nanoparticles that do not adhere to mucus provide uniform and long-lasting drug delivery to airways following inhalation. Science Advances 3, e1601556.

Sedlacek, O., Monnery, B.D., Filippov, S.K., Hoogenboom, R., & Hruby, M., 2012. Poly(2-oxazoline)s – are they more advantageous for biomedical applications than other polymers? Macromol. Rapid Commun. 33, 1648-1662.

Shahnaz, G., Vetter, A., Barthelmes, J., Rahmat, D., Laffleur, F., Iqbal, J., Perera, G., Schlocker, W., Dünnhaput, S., Augustijns, P., & Bernkop-Schnürch, A., 2012. Thiolated chitosan nanoparticles for the nasal administration of leuprolide: Bioavailability and pharmacokinetic characterization. Int. J. Pharm. 428, 164-170.

Shitrit, Y., & Bianco-Peled, H., 2017. Acrylated chitosan for mucoadhesive drug delivery systems. Int. J. Pharm. 517, 247-255.

Sigurdsson, H.H., Kirch, J., & Lehr, C.-M., 2013. Mucus as a barrier to lipophilic drugs. Int. J. Pharm. 453, 56-64.

Sin, B., & Togias, A., 2011. Pathophysiology of allergic and nonallergic rhinitis. Proc. Am. Thorac. Soc. 8, 106-114.

Sogias, I.A., Khutoryanskiy, V.V., & Williams, A.C., 2010. Exploring the factors affecting the solubility of chitosan in water. Macromol. Chem. Phys. 211, 426-433.

Sogias, I.A., Williams, A.C., & Khutoryanskiy, V.V., 2008. Why is chitosan mucoadhesive? Biomacromolecules 9, 1837–1842.

Solomonidou, D., Cremer, K., Krumme, M., & Kreuter, J., 2001. Effect of carbomer concentration and degree of neutralization on the mucoadhesive properties of polymer J. Biomater. Sci. Polymer 12, 1191–1205.

Sonvico, F., Clementino, A., Buttini, F., Colombo, G., Pescina, S., Stanisçuaski Guterres, S., Raffin Pohlmann, A., & Nicoli, S., 2018. Surface-modified nanocarriers for nose-to-brain delivery: From bioadhesion to targeting. Pharmaceutics 10, 34.

Steinhauer, W., Hoogenboom, R., Keul, H., & Moeller, M., 2010. Copolymerization of 2-hydroxyethyl acrylate and 2-methoxyethyl acrylate via RAFT: Kinetics and thermoresponsive properties. Macromolecules 43, 7041-7047.

Talelli, M., Rijcken, C.J.F., van Nostrum, C.F., Storm, G., & Hennink, W.E., 2010. Micelles based on HPMA copolymers. Adv. Drug Del. Rev. 62, 231-239.

Tas, C., Ozkan, C.K., Savaser, A., Ozkan, Y., Tasdemir, U., & Altunay, H., 2009. Nasal administration of metoclopramide from different dosage forms: *In vitro*, *ex vivo*, and *in vivo* evaluation. Drug Deliv. 16, 167-175.

Teodorescu, M., & Bercea, M., 2015. Poly(vinylpyrrolidone) – a versatile polymer for biomedical and beyond medical applications. PPTEn 54, 923-943.

Tim R Dargaville, Hollier, B.G., Shokoohmand, A., & Hoogenboom, R., 2014. Poly(2-oxazoline) hydrogels as next generation three-dimensional cell supports. Cell Adhesion & Migration 8, 88–93.

Ugwoke, M.I., Agu, R.U., Verbeke, N., & Kinget, R., 2005. Nasal mucoadhesive drug delivery: Background, applications, trends and future perspectives. Adv Drug Deliv Rev 57, 1640-1665.

Ulbricht, J., Jordan, R., & Luxenhofer, R., 2014. On the biodegradability of polyethylene glycol, polypeptoids and poly(2-oxazoline)s. Biomaterials 35, 4848-4861.

Vila, A., Gill, H., McCallion, O., & Alonso, M.a.J., 2004. Transport of PLA-PEG particles across the nasal mucosa: Effect of particle size and PEG coating density. J. Control. Release 98, 231-244.

Wang, Q.Z., Chen, X.G., Liu, N., Wang, S.X., Liu, C.S., Meng, X.H., & Liu, C.G., 2006. Protonation constants of chitosan with different molecular weight and degree of deacetylation. Carbohydr. Polym. 65, 194-201.

Wu, J., Wang, X., Keum, J.K., Zhou, H., Gelfer, M., Avila-Orta, C.A., Pan, H., Chen, W., Chiao, S.M., Hsiao, B.S., & Chu, B., 2007. Water soluble complexes of chitosan-g-MPEG and hyaluronic acid. J Biomed Mater Res A 80, 800-812.

Zhang, H., Bahamondez-Canas, T.F., Zhang, Y., Leal, J., & Smyth, H.D.C., 2018. Pegylated chitosan for nonviral aerosol and mucosal delivery of the CRISPR/Cas9 system *in vitro*. Mol. Pharm. 15, 4814-4826.

# Chapter 6: Haloperidol- and phenobarbital-loaded unmodified chitosan and PVP-chitosan nanoparticles for nasal drug delivery

**Abstract**

Study in the area of nasal drug delivery is becoming one of the focal points of pharmaceutics research groups in both academia and industry. This is due to the several advantages of the nasal route of drug administration including the avoidance of pre-systemic metabolism, rapidity of onset of action, its non-invasive nature and the possibility of a direct access to the central nervous system. Chitosan-based formulations have been used to enhance the efficacy of nasal formulations. However, this effect can be further enhanced using formulations based on hydrophilically modified chitosan. In this study, we have formulated haloperidol unmodified chitosan-sodium tripolyphosphate (TPP) nanoparticles and phenobarbital unmodified and polyvinyl pyrrolidone (PVP)-chitosan-TPP nanoparticles. These two drugs were selected to allow future *in vivo* experiment of the nanoformulations using behavioural studies. With haloperidol loaded unmodified chitosan nanoparticles, a relatively low drug loading capacity was found. On the other hand, phenobarbital loaded unmodified and PVP-chitosan nanoparticles demonstrated a high drug loading capacity and a sustained drug release. Our findings provide an important insight into some of the aspects of the chitosan-based nasal nanoformulations.

## 6.1 Introduction

The nasal route of drug administration has attracted a lot of attention due to avoidance of first pass metabolism, the presence of highly vascularised nasal mucosa with large surface area and its non-invasive nature (Ugwoke et al., 2005). It has been extensively used for systemic delivery of various peptide-based drugs and indeed a number of products including Synarel™ and Miacalcic™ (for nasal administration of nafarelin and calcitonin, respectively) are currently available (Rohrer et al., 2018). However, the barrier properties of mucus, the mucociliary clearance, the tight junctions and degradation of drugs by the nasal mucosal enzymes often resulted in low bioavailability of hydrophilic peptide-based drugs larger than 1 kDa (Rohrer et al., 2018). The nasal route has showed some potential for direct transport of drugs (mainly hydrophilic) to the central nervous system (CNS) in animals and humans, due to the presence of olfactory epithelium and trigeminal nerves in the olfactory and respiratory epithelia. However, evident from animal studies, the CNS bioavailability of drugs directly via the nasal route is often very low (< 0.12% of the administered dose) (Illum, 2000, 2004; Wang et al., 2008; Mistry et al., 2015).

The use of mucoadhesive polymers, permeation enhancers, enzyme inhibitors and nanoparticles are considered as potential strategies to enhance the systemic and CNS bioavailability of drugs (Mistry et al., 2009; Rohrer et al., 2018). In this regard, chitosan has been frequently used due to its mucoadhesive, permeation enhancing effect and nontoxicity (Bernkop-Schnürch & Dunnhaupt, 2012; Casettari & Illum, 2014; M. Ways et al., 2018). We previously showed that modification of chitosan with hydrophilic polymers including polyethylene glycol (PEG), polyhydroxyethyl acrylate (PHEA), poly-2-ethyl-2-oxazoline (POZ) and polyvinyl pyrrolidone (PVP) enhanced the diffusion of modified chitosan nanoparticles in mucin solution and their nasal mucosa penetration capacity compared to unmodified chitosan nanoparticles (Chapter 5). In the current study, we explored the possibilities of incorporating two CNS active drugs (haloperidol and phenobarbital sodium) into unmodified and modified chitosan nanoparticles. Haloperidol is a dopamine $D_2$ receptor antagonist which is prescribed for the treatment of nausea and vomiting, schizophrenia, bipolar disorder and some other CNS disorders (Joint Formulary Committee, 2018). Its administration to rats results in catalepsy and such behavioural responses can be used to test certain formulations (Piazza et al., 2014). Phenobarbital is a barbiturate and is used in the treatment of all forms of epilepsy except typical absence seizures (Joint Formulary Committee, 2018). It can cause drowsiness which can also be monitored in behavioural study

by clinical observation of the subjects. Figure 6.1 shows the chemical structure of both haloperidol and phenobarbital.

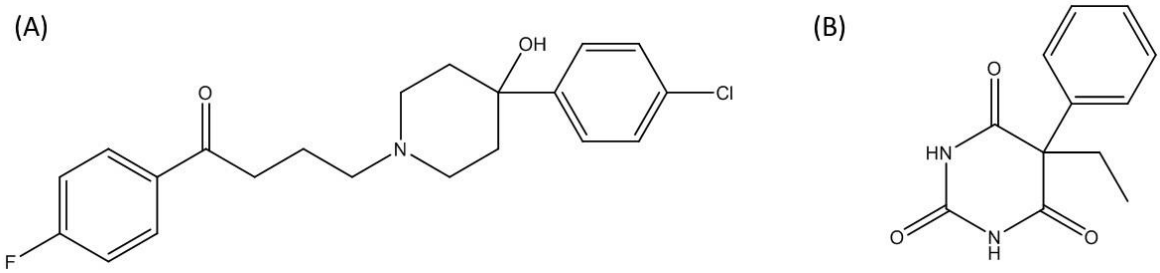


Figure 6.1 (A) Chemical structure of haloperidol and (B) phenobarbital.

There are a small number of studies that looked at the nasal route for delivering haloperidol (El-Setouhy et al., 2016) and phenobarbital (Czapp et al., 2008) using nanoemulsions and gels, respectively, to enhance the drug efficacy and to reduce systemic side effects. Chitosan-sodium tripolyphosphate (TPP) nanoparticles are promising drug carriers and they can be prepared via ionic interaction between cationic chitosan and anionic TPP. This method requires only a few excipients and does not need a high temperature, allowing the incorporation of temperature-sensitive drugs (Calvo et al., 1997). Unmodified chitosan-TPP nanoparticles enhanced the systemic bioavailability of insulin in rabbits (Fernández-Urrusuno et al., 1999) and leuprolide in rats (Shahnaz et al., 2012) via nasal route. However, to our knowledge, no unmodified- and PVP-chitosan-TPP nanoparticles were studied as a potential nasal delivery system for both haloperidol and phenobarbital. The main aim of this study is to develop unmodified and PVP-chitosan-TPP nanoparticles as a potential nasal drug delivery for haloperidol and phenobarbital.

## 6.2 Materials and methods

### 6.2.1 Materials

Medium molecular weight chitosan (degree of deacetylation 75-85%), 1-ethyl-3-3-dimethylaminopropyl-carbodiimide hydrochloride (EDAC), N-hydroxysuccinimide (NHS), sodium tripolyphosphate (TPP), phenobarbital sodium, methoxy-PEG-COOH and D-(+)-trehalose dihydrate were purchased from Sigma-Aldrich (Gillingham, UK). Glacial acetic acid, dimethyl sulfoxide (DMSO), sodium hydroxide (NaOH), sodium phosphate monobasic

dihydrate ($NaH_2PO_4.2H_2O$), sodium phosphate dibasic anhydrous ($Na_2HPO_4$) were purchased from Fisher Scientific (UK). Haloperidol was purchased from Alfa Aesar (Lancashire, UK). PVP-COOH was synthesised by Prof Richard Hoogenboom research group at University of Ghent, Belgium as described in Chapter 5. Dialysis membrane with molecular cut-off 12–14 kDa was purchased from Medicell International Ltd., UK. All other chemicals were of analytical grade and were used as received.

### 6.2.2 Synthesis of PEG- and PVP-CO-NH-chitosan

PEG-CO-NH chitosan and PVP-CO-NH-chitosan were synthesised according to the method described in Chapter 5. Briefly, 11.5 mL acetic acid (1% v/v) was added to 80 mg medium molecular weight chitosan. The mixture was continuously stirred for 20 hours at room temperature. The pH of the chitosan solutions was increased to 6 using 5 M NaOH solution. 117 mg of methoxy-PEG-COOH or 100 mg of PVP-COOH was added to the chitosan solution. Then after 5 minutes stirring, NHS (13.5 mg) was added and stirred for 30 minutes. EDC (22.4 mg) was then added and stirred for 24 hours. The products were dialysed against deionised water (4 L, 8 total changes, 12-14 kDa) at room temperature for 3 days. The products were recovered by lyophilisation using Heto Power Dry LL 3000 freeze-drier (Thermo Electron Corporation) and characterised as described in Chapter 5.

### 6.2.3 Preparation of haloperidol loaded unmodified chitosan-TPP nanoparticles

Haloperidol loaded unmodified chitosan-TPP nanoparticles (hereinafter referred to haloperidol-chitosan nanoparticles) were prepared using an ionic gelation method. Chitosan solution (1 mg/mL in 1% v/v acetic acid) was prepared and the pH was adjusted to 5.5 using 5 M NaOH solution. TPP (1 mg/mL in deionised water) and the chitosan solutions were filtered through 0.2 µm syringe filter. 1 mL Haloperidol solution (initial conc. 5 mg/mL in 1% v/v acetic acid) was added to 4 mL of the filtered chitosan solution. Then, 2 mL TPP solution was added dropwise to 5 mL of chitosan-haloperidol mixture over 5 minutes. The nanoparticles suspension (pH 5.06) were stirred for another 30 minutes at room temperature. The nanoparticle suspension were then centrifuged using Amicon Ultra™ centrifugal filter unit (0.5 mL capacity, 3 kDa MWCO, Millipore, UK Limited) for 90 minutes at 10000 rpm (Sanyo, Micro Centaur, UK). The retentates were reverse spun at 1000 rpm for 2 minutes and the nanoparticles were re-suspended with 200 µL ultrapure water. The pH of the nanoparticle suspension was 5.06. The particles were freeze dried using Heto Power Dry LL 3000 freeze-drier (Thermo Electron Corporation) after addition of trehalose (5% w/v). At

each step of preparation (before and after centrifugation and after freeze drying), the particles size was measured using dynamic light scattering (DLS).

### 6.2.4 Preparation of phenobarbital loaded unmodified, PEG- and PVP-chitosan-TPP nanoparticles

Unmodified, PEG-CO-NH- and PVP-CO-NH-chitosan solutions (1 mg/mL in 1% v/v acetic acid) were prepared and the pH was adjusted to 5.5 using 5 M NaOH solution. Phenobarbital sodium (at the final concentration of 4 or 2 mg/mL) was added to TPP solution (1 mg/mL in deionised water). Both TPP-phenobarbital mixture and chitosan solutions were filtered through 0.2 μm syringe filter. Then, TPP-phenobarbital mixture was added dropwise to chitosan solution (1:2) over 5 minutes. The suspensions were stirred for another 30 minutes at room temperature. Based on the size analysis by DLS, the optimised nanoparticle types were selected and were lyophilised using Heto Power Dry LL 3000 freeze-drier (Thermo Electron Corporation) after addition of trehalose (5% w/v) to produce the phenobarbital loaded unmodified, PEG-CO-NH- and PVP-CO-NH-chitosan-TPP nanoparticles (hereinafter referred to phenobarbital-unmodified chitosan, PEG-chitosan and PVP-chitosan nanoparticles, respectively).

### 6.2.5 Characterisation of the nanoparticles

The size, polydispersity index (PDI) and ξ-potential of the nanoparticles were measured using a Zetasizer Nano-ZS (Model: ZEN3600, Malvern, UK). For the size measurement, the samples were diluted (1:20) with ultrapure water before analysis. A refractive index of 1.59 and an absorbance of 0.01 were used for all measurements. Viscosity (0.8872 cP) and refractive index (1.33) of water were used as dispersant parameters. The samples were incubated for 60 seconds and the measurements were conducted in triplicate for 10 seconds per run, with 12 runs per reading at 25 °C. The measurement angle was set to 173° backscatter. For the data processing, the normal resolution analysis model was selected. In case of the freeze dried nanoparticles, the nanoparticles were first redispersed in ultrapure water (at a concentration of 108.5 and 100 mg/mL of haloperidol- and phenobarbital-chitosan nanoparticles, respectively) and then diluted (1:20) with ultrapure water. ξ-potential values were measured using DTS-1070 folded capillary tube cuvettes (Malvern, UK). Samples were diluted (1:10) with ultrapure water before analysis. Samples were measured using 3 repeats of 20 sub-runs per reading. The ξ-potential data were processed using auto

mode analysis model. At least 3 samples were measured and processed using the Smoluchowski model (Fκa = 1.50).

### 6.2.6 High performance liquid chromatography (HPLC) analysis of haloperidol

The HPLC analysis of haloperidol was carried out using an Agilent 1100 Series automated system. Chemstation software was used for the acquisition and processing of the data. The HPLC instrument was coupled with a binary pump and a VWD UV detector. Chromatographic separations were carried out using a Phenomenex® HPLC column (5 µm C18 (2), 100 Å, 250 × 4.6 mm, P/NO: 00G-4252-E0). The mobile phase consisted of 0.05 M $NaH_2PO_4.2H_2O$ solution: acetonitrile (70:30, pH 5) with flow rate set at 1 mL/minute in isocratic mode, injection volume of 100 µL and detection at 254 nm with each run lasted 30 minutes at 25 °C. Freshly prepared mobile phase was used and degassed for 20 minutes prior to HPLC experiments. The calibration curve was constructed from serial solutions of haloperidol in the mobile phase in the concentration range of 5-30 µg/mL.

### 6.2.7 HPLC analysis of phenobarbital

For phenobarbital, the HPLC system and method were performed as section 6.2.6 with some modifications. Briefly, the mobile phase consisted of 0.05 M $NaH_2PO_4.2H_2O$ solution: acetonitrile (65:35, pH 5.2). The detection was at the wavelength of 220 nm and each run lasted 20 minutes. The calibration curve was constructed from serial solutions of phenobarbital in the mobile phase in the concentration range of 1.25-160 µg/mL.

### 6.2.8 Drug loading capacity of haloperidol-chitosan nanoparticles

The freeze dried haloperidol-chitosan nanoparticles were redispersed in DMSO (1 mg/mL). The mixture was stirred overnight at room temperature to extract the haloperidol content. The samples were filtered through 0.22 µm syringe filter prior to HPLC analysis. The haloperidol association efficiency and loading capacity were calculated according to Equation 6.1 and Equation 6.2, respectively.

$$\text{Association efficiency} = \frac{\text{Amount of associated haloperidol in freeze dried nanoparticles}}{\text{Total amount of haloperidol}} \times 100 \quad \text{Equation 6.1}$$

$$\text{Drug loading capacity} = \frac{\text{Amount of associated haloperidol}}{\text{Weight of freeze dried nanoparticles}} \times 100 \quad \text{Equation 6.2}$$

### 6.2.9 Determination of association efficiency of phenobarbital-unmodified and PVP-chitosan nanoparticles

The filtration and extraction methods were used in calculating association efficiency of phenobarbital-unmodified and PVP-chitosan nanoparticles. First, nanoparticles suspension (12 × 0.5 mL) was centrifuged at 10000 rpm for 1 hour. For the filtration method, the filtrate was collected and the volume was measured. Then, 0.25 mL filtrate was diluted with 4.75 mL mobile phase and phenobarbital content was quantified by HPLC. For the extraction method, retentate was recovered by reverse spinning at 1000 rpm for 2 minutes. Then, 9 mL of 50% v/v ethanol in deionised water was added to the retentate (1 mL) to extract phenobarbital from the nanoparticles and stirred for 20 hours at room temperature. Then 2.5 mL extract was diluted with 2.5 mL of the mobile phase. The solutions were filtered through 0.22 µm syringe filter before HPLC analysis. The phenobarbital calibration curve was plotted in the concentration range of 1.25 to 160 µg/mL using stock solution (5 mg/mL in the mobile phase stirred for 18 hours at room temperature). The mobile phase was used as blank. The phenobarbital association efficiency was calculated according to Equation 6.3 .

$$\text{Association efficiency} = \frac{\text{Amount of associated phenobarbital in nanoparticles retentate}}{\text{Total amount of phenobarbital}} \times 100 \qquad \text{Equation 6.3}$$

### 6.2.10 Drug loading capacity of phenobarbital-unmodified and PVP-chitosan nanoparticles

50 mg of freeze dried phenobarbital-unmodified and PVP-chitosan nanoparticles were redispersed in 10 mL of 50% v/v ethanol in deionised water and stirred at room temperature for 20 hours. Then, 2.5 mL extract was diluted with 2.5 mL of the mobile phase, filtered through 0.22 µm syringe and analysed by HPLC as described in section 6.2.9. The drug loading capacity of phenobarbital-unmodified and PVP-chitosan nanoparticles was calculated using Equation 6.4.

$$\text{Drug loading capacity} = \frac{\text{Total amount of phenobarbital (associated+free) in freeze dried nanoparticles}}{\text{Weight of freeze dried nanoparticles}} \times 100$$

Equation 6.4

### 6.2.11 Phenobarbital drug release

78 and 81 mg of freeze-dried phenobarbital-unmodified and PVP-chitosan nanoparticles (equivalent to 1 mg phenobarbital sodium) were redispersed in 1 mL 0.05 M phosphate buffer solution pH 6.4 (PBS). A Spectra-Por® Float-A-Lyzer® (G2 black, 1 mL, MWCO 3.5-5 kDa) was rinsed 3 times with deionised water and equilibrated with 2 mL deionised water at room temperature for 10 minutes. Then, it was conditioned with 2 mL PBS twice. The Float-A-Lyzer® submerged in 20 mL PBS and was placed in a 50 mL centrifuge tube. 1 mL aliquot was taken and this was considered as time zero sample. Then, 1 mL redispersed nanoparticle suspensions was placed in the Float-A-Lyzer® and the system was returned to the centrifuge tube. At pre-determined time intervals, 1 mL aliquot was taken and the phenobarbital content was quantified by HPLC. Phenobarbital sodium solution (1 mg/mL in PBS) was used as a control. The experiment was performed at 32 °C. The data were expressed as mean ± SD of three independent experiments. Duplicate injections were performed for both samples and the standard at each time and concentration point. The phenobarbital calibration curve was established in the concentration range of 1.25 to 160 µg/mL from 3 independent 1 mg/mL stock solutions in PBS prepared at room temperature.

### 6.2.12 Statistical analysis

Unless otherwise stated, all measurements were collected in triplicate and the data are expressed as mean ± standard deviation (SD). The data were analysed using the SPSS Statistics 21 program (IBM, US). The statistical significance of any difference between groups was determined using one-way analysis of variance (ANOVA) with the least significant difference (LSD) post-hoc test. Differences were considered statistically significant at $p < 0.05$.

## 6.3 Results and discussion

Incorporation of drugs (especially lipophilic drugs) into chitosan nanoparticles has always been challenging due to the hydrophilic nature of chitosan and the lack of drug-chitosan interactions (De Campos et al., 2001). In this study, the poor aqueous solubility of haloperidol provided an additional formulation challenge. Haloperidol is only soluble in organic solvents and dilute acids. Thus, haloperidol was dissolved in 1% v/v acetic acid and added dropwise to the acidic chitosan solution to prevent precipitation. The pH of chitosan solution was adjusted to 5.5 which favours the formation of nanoparticles with small particle size and with acceptable PDI as shown in Chapter 5. Addition of TPP solution resulted in

the formation of nanoparticle suspensions due to the electrostatic interactions between the positively charged chitosan macromolecules and the negatively charged TPP molecules (Calvo et al., 1997). As shown in Table 6.1, the haloperidol-chitosan nanoparticles had size of 117 ± 1 nm and low PDI (0.198 ± 0.018). Centrifugation was used as a method for the analysis of association efficiency to separate the free drug from the drug-loaded nanoparticles. The nanoparticles were centrifuged and their size and PDI before and after centrifugation was compared. As shown in Table 6.1, at the optimised centrifugation condition, it was possible to retain the size of the nanoparticles close to their original size. The pH of the nanoparticles suspensions before and also after centrifugation was 5.06 at which haloperidol is still soluble. The use of trehalose (5% w/v) resulted in the preservation of the nanoparticles size and PDI after freeze drying (Table 6.1 and Figure 6.2).

Table 6.1 DLS data of haloperidol-chitosan nanoparticles at different stages of preparation (mean ± SD, n = 3).

| Conditions | Z-average (nm, DLS) | PDI |
|---|---|---|
| Before centrifugation | 117 ± 1 | 0.198 ± 0.018 |
| After centrifugation | 95 ± 2 | 0.289 ± 0.029 |
| After redispersion of the freeze dried nanoparticles | 94 ± 4 | 0.247 ± 0.020 |

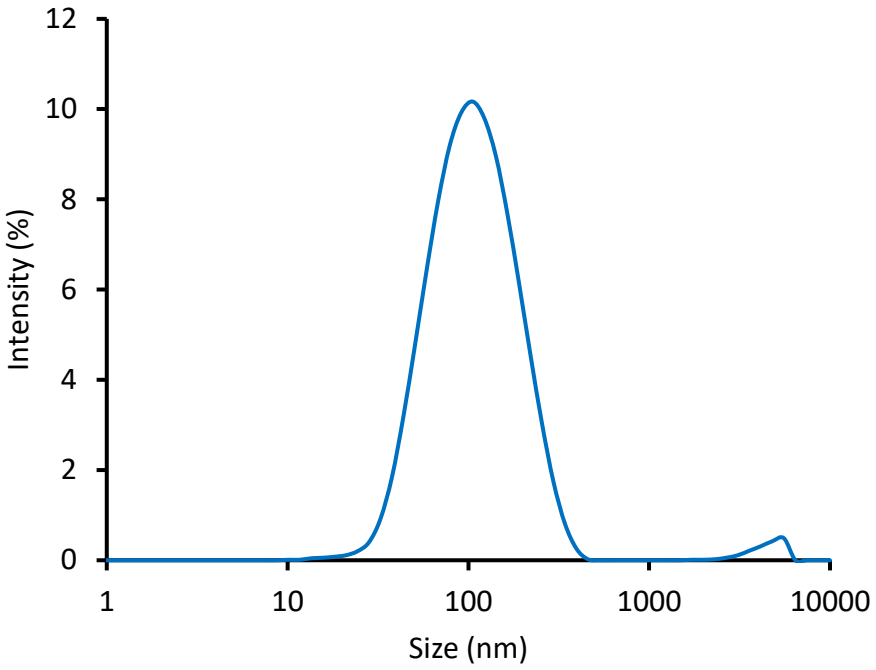


Figure 6.2 DLS size distribution of haloperidol-chitosan nanoparticles after redispersion of freeze dried nanoparticles (108.5 mg/mL ultrapure water), n=3.

Figure 6.3 and Figure 6.4 shows the HPLC chromatogram of haloperidol and the calibration curve used to calculate the haloperidol content, respectively. The loading capacity and the association efficiency of haloperidol-chitosan nanoparticles were 0.204 ± 0.001% w/w and 4.78 ± 0.039% w/w, respectively. The haloperidol content was quantified using HPLC. These values are relatively low, which could be due to the lipophilic nature of haloperidol and the hydrophilic nature of chitosan. This resulted in the poor affinity of haloperidol to the unmodified chitosan nanoparticles.

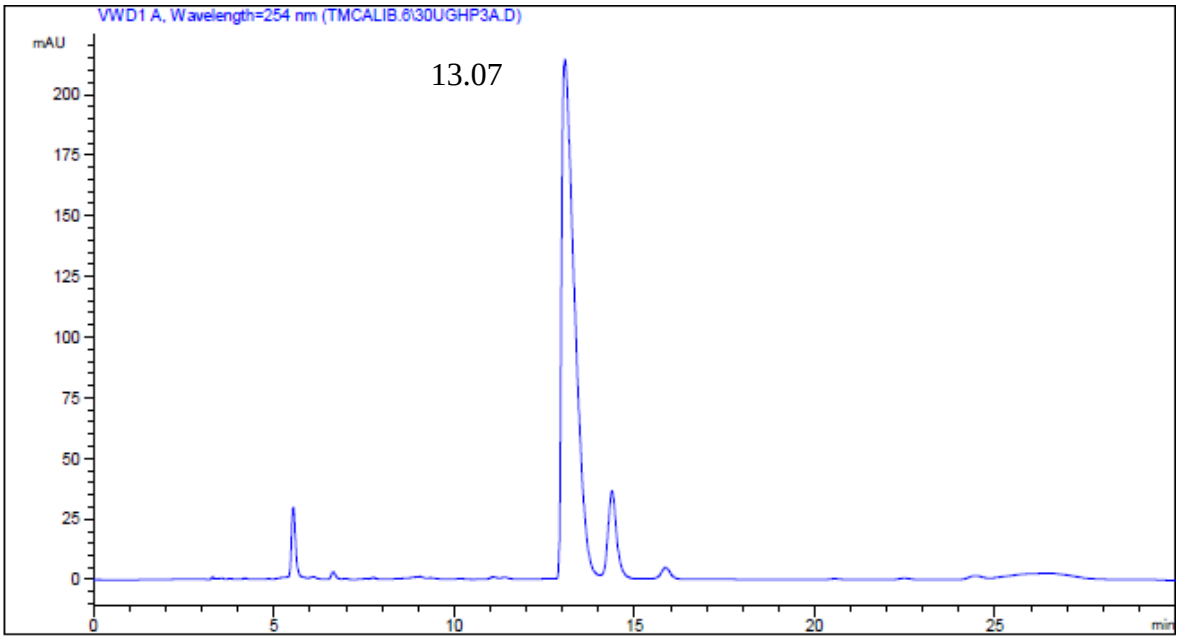


Figure 6.3 An example of chromatogram of 30 µg/mL haloperidol solution in the mobile phase; the peak at retention time of 13.07 minutes is related to haloperidol. The mobile phase composed of 0.05 M $NaH_2PO_4$:$2H_2O$ solution: acetonitrile (70:30, pH 5).

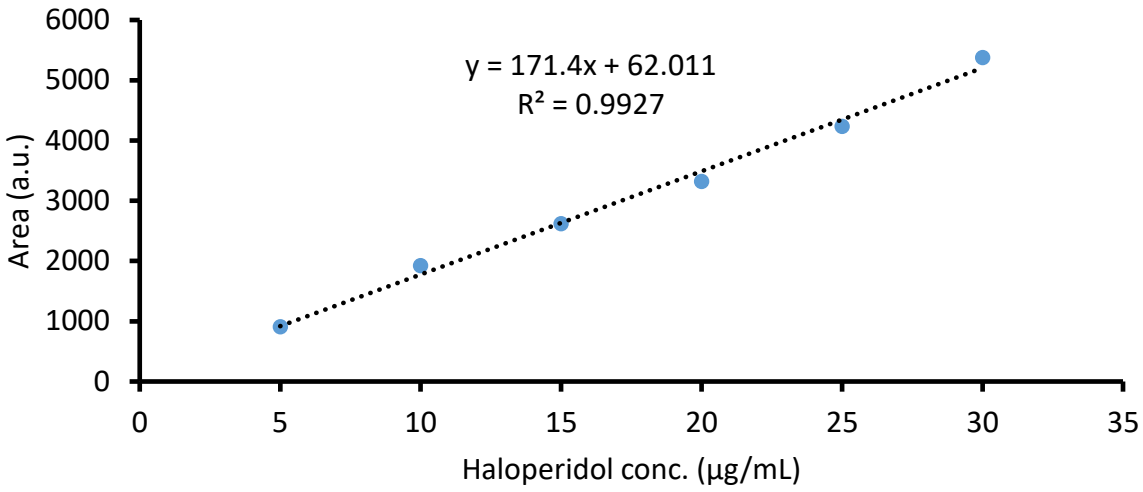


Figure 6.4 An HPLC calibration curve of haloperidol in the mobile phase. The mobile phase composed of 0.05 M $NaH_2PO_4.2H_2O$ solution: acetonitrile (70:30, pH 5).

Phenobarbital-unmodified chitosan nanoparticles were prepared using an incorporation technique prior to the ionic gelation. As phenobarbital is soluble at basic pH, it was first added to the basic TPP solution (pH 9) prior to the addition to chitosan solution. At 4 mg/mL phenobarbital, it was possible to produce unmodified chitosan nanoparticles (Table 6.2 and Figure 6.5), however, these nanoparticles could not be redispersed (Table 6.3). On the other hand, at 2 mg/mL, it could be redispersed readily in ultrapure water and PBS (Table 6.2, Table 6.3, Figure 6.5 and Figure 6.6).

To explore the possibilities of incorporating phenobarbital into modified chitosan nanoparticles, initially, PEG-chitosan was investigated as a model example of modified chitosan. At 4 mg/mL phenobarbital sodium solution, large aggregates of PEG-chitosan were observed. DLS study of the supernatant of these aggregates revealed the presence of nanoparticles with size of 106 ± 2 nm. However, due to the presence of excessive amount of visible large aggregates, further experiments on these particles were not performed. At 2 mg/mL phenobarbital sodium solution, PEG-chitosan nanoparticles produced can be readily redispersed in both ultrapure water and PBS. Thus, 2 mg/mL phenobarbital sodium solution was also used to prepare PVP-chitosan nanoparticles (Table 6.2, Table 6.3, Figure 6.5 and Figure 6.6). The final pH (before freeze drying) of 2 mg/mL phenobarbital-unmodified and PVP-chitosan nanoparticles suspensions was 5.57 and 5.58, respectively.

Table 6.2 DLS data of phenobarbital-chitosan nanoparticles suspensions before freeze drying (mean ± SD, n = 3).

| Types of nanoparticles | Initial conc. of phenobarbital in TPP solution (mg/mL) | Z-average (nm, DLS) | PDI | Zeta potential (mV) |
|---|---|---|---|---|
| Unmodified chitosan | 4 | 159 ± 5 | 0.264 ± 0.005 | 17.11 ± 0.05 |
| Unmodified chitosan | 2 | 173 ± 4 | 0.265 ± 0.029 | 16.65 ± 0.97 |
| PEG-chitosan | 4 | 106 ± 2* | 0.128 ± 0.023 | 8.04 ± 0.85* |
| PEG-chitosan | 2 | 99 ± 4 | 0.115 ± 0.021 | 11.41 ± 0.84 |
| PVP-chitosan | 2 | 93 ± 3 | 0.102 ± 0.030 | 10.59 ± 1.50 |

*samples from supernatant portion were taken for analysis as large aggregates was observed.

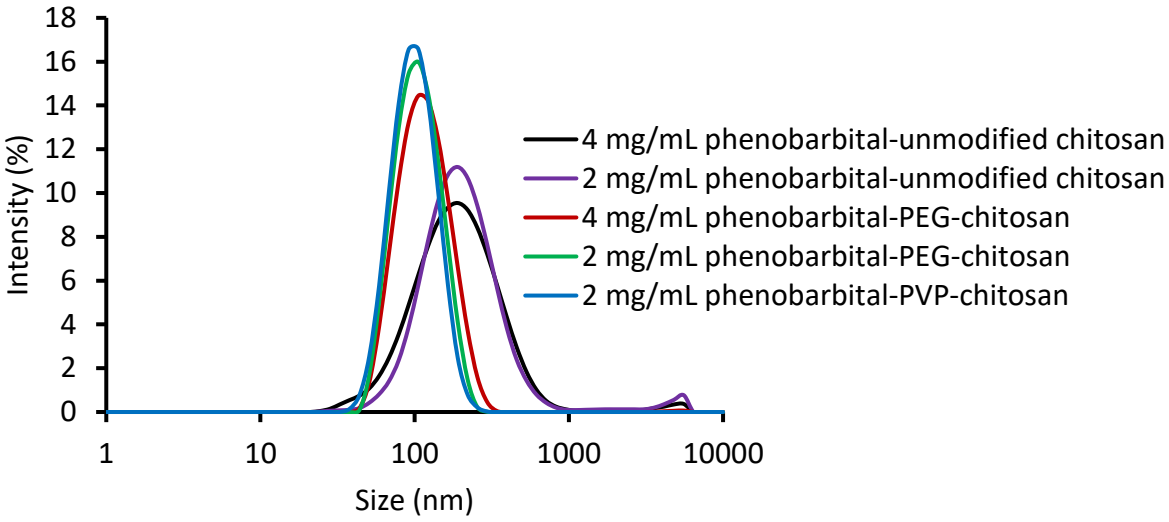


Figure 6.5 DLS size distribution of phenobarbital-chitosan nanoparticles suspensions before freeze drying, n=3.

Table 6.3 Properties of phenobarbital-chitosan nanoparticles suspensions after redispersion of the freeze dried products with ultrapure water and PBS.

| Types of nanoparticles | Initial conc. of phenobarbital in TPP solution (mg/mL) | Notes | Z-average (nm, DLS) | PDI |
|---|---|---|---|---|
| Unmodified chitosan | 4 | After redispersion with ultrapure water, transparent solution with large aggregates were observed which did not disintegrate after overnight stirring at room temperature | 814 ± 211 | 0.652 ± 0.116 |
| Unmodified chitosan | 2 | Redispersed rapidly in deionised water and PBS | 193 ± 9 | 0.311 ± 0.017 |
| PEG-chitosan | 2 | Small white particles observed after redispersion but easily dissolved upon further dilution with water | 147 ± 3 | 0.190 ± 0.037 |
| PVP-chitosan | 2 | Redispered fully in deionised water and PBS | 156 ± 4 | 0.213 ± 0.015 |

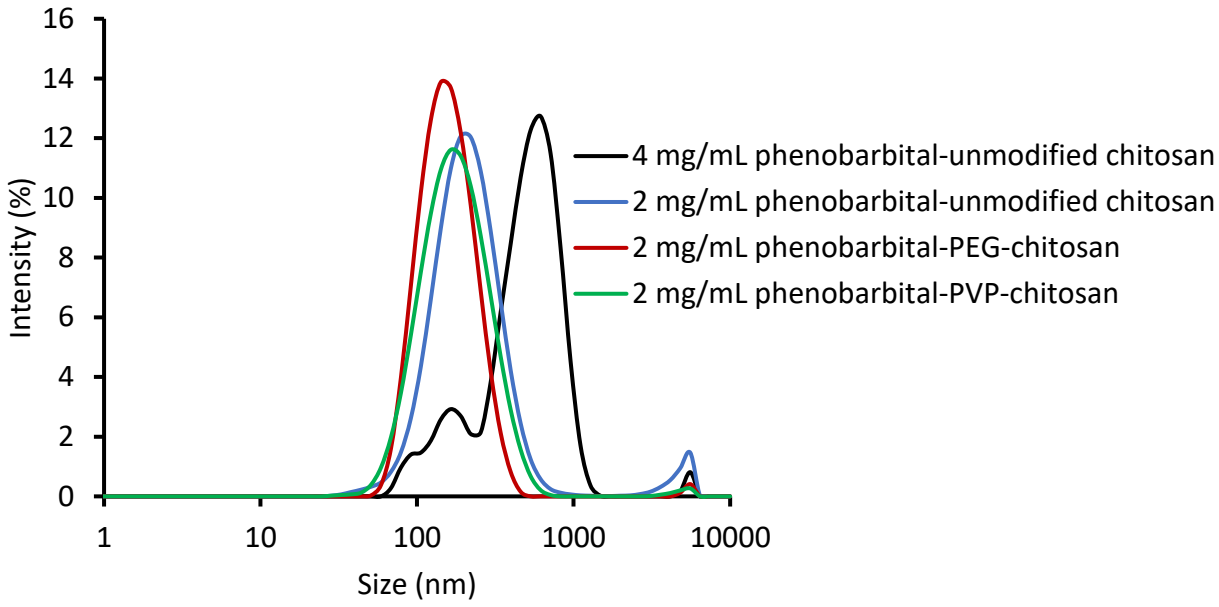


Figure 6.6 DLS size distribution of phenobarbital loaded nanoparticles suspensions after redispersion of the freeze dried products, n=3.

Phenobarbital- PEG- and PVP-chitosan nanoparticles had a lower zeta potential than their unmodified chitosan counterparts (Table 6.2). This could be due to the presence of PEG and PVP shells in the structure of phenobarbital- PEG- and PVP-chitosan nanoparticles.

Figure 6.7 and Figure 6.8 show the HPLC chromatogram of phenobarbital and the calibration curve used to calculate the phenobarbital content of the chitosan nanoparticles, respectively. Using filtration method, it was found that phenobarbital-unmodified and PVP-chitosan nanoparticles displayed an association efficiency of 25.13 ± 0.04 and 26.00 ± 0.05% w/w, respectively. The association efficiency of phenobarbital-unmodified and PVP-chitosan nanoparticles found by extraction method was 36.73 ± 0.03 and 32.01 ± 0.03% w/w, respectively. Although phenobarbital is poorly water soluble (Jelveghari & Nokhodchi, 2008), both phenobarbital-unmodified and PVP-chitosan nanoparticles had a high association efficiency which could be due to the fact that phenobarbital is negatively charged (Cheng et al., 2008) and thus it is postulated that phenobarbital can associate with the positively charged chitosan via electrostatic interactions. The drug loading capacity of phenobarbital-unmodified and PVP-chitosan nanoparticles found by HPLC was 1.2718 ± 0.0004 and 1.2299 ± 0.0001% w/w, respectively.

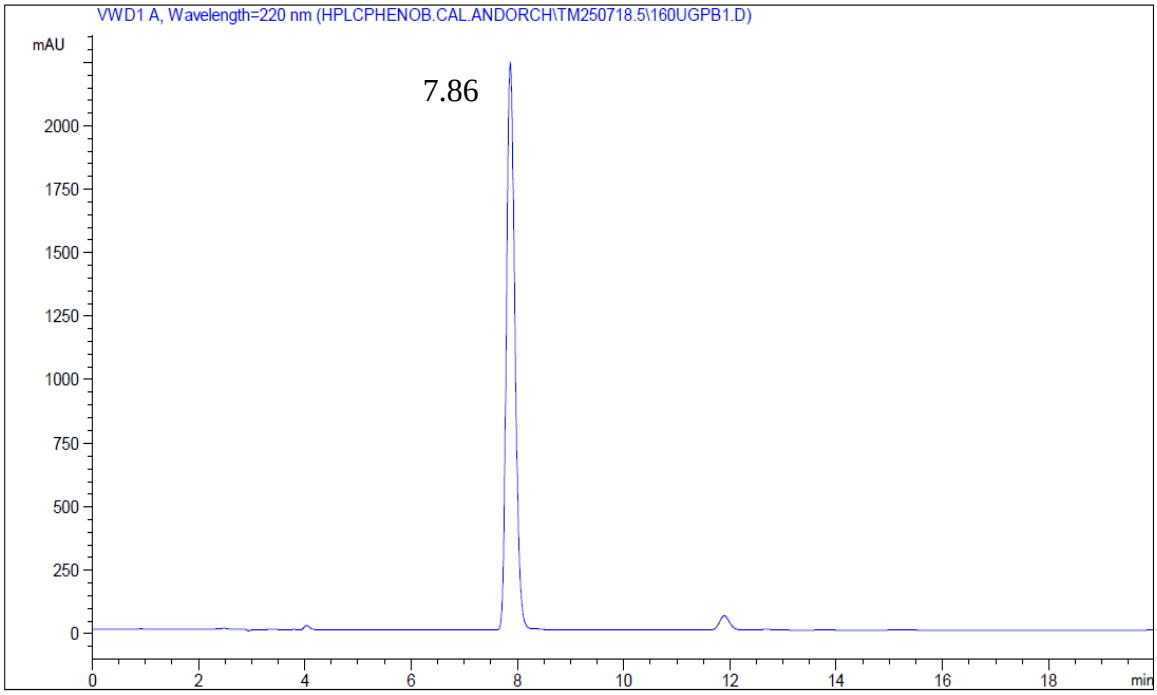


Figure 6.7 An example of chromatogram of 160 µg/mL phenobarbital sodium solution in the mobile phase; the peak at retention time of 7.86 minutes is related to phenobarbital. The mobile phase composed of 0.05 M $NaH_2PO_4.2H_2O$ solution: acetonitrile (65:35, pH 5.2).

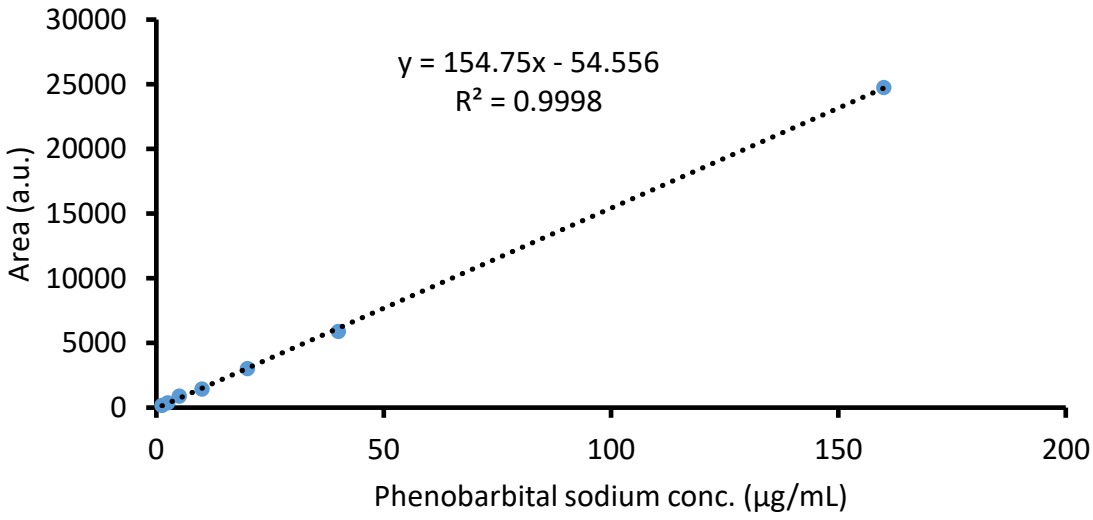


Figure 6.8 An HPLC calibration curve used for the analysis of phenobarbital loading capacity of the unmodified and PVP-chitosan nanoparticles. The mobile phase composed 0.05 M $NaH_2PO_4.2H_2O$ solution: acetonitrile (65:35, pH 5.2) (mean ± SD, n = 3).

As phenobarbital is a negatively charged drug (Cheng et al., 2008), we investigated the possibility of any crosslinking between phenobarbital and unmodified chitosan. As shown in Table 6.4 and Figure 6.9, no such crosslinking happened at the studied conditions.

Table 6.4 Properties of phenobarbital-unmodified chitosan without addition of TPP solution (mean ± SD, n = 3).

| Types of material | Notes | Z-average (nm, DLS) | PDI |
|---|---|---|---|
| Phenobarbital-unmodified chitosan without TPP | No translucence observed and the solution was clear | 153 ± 4 | 0.626 ± 0.017 |

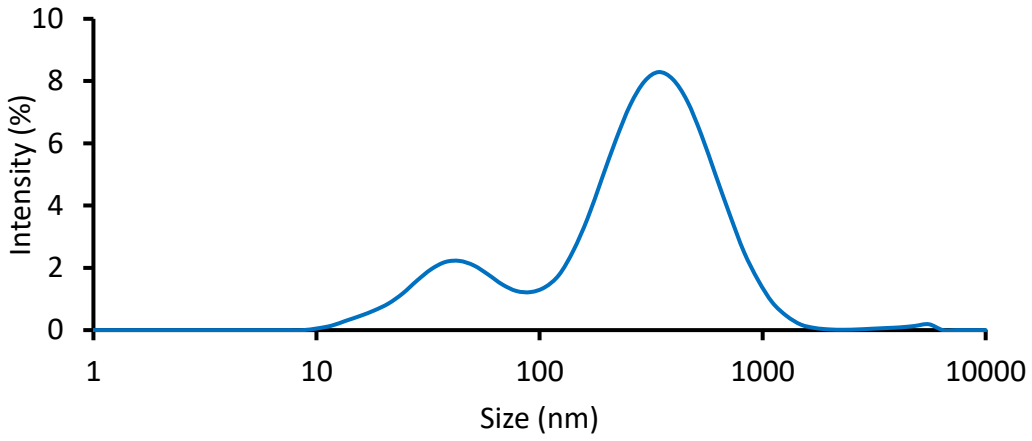


Figure 6.9 DLS size distribution of phenobarbital-unmodified chitosan without addition of TPP solution.

Trehalose was used as a cryoprotectant as nanoparticles generally do not redisperse readily after freeze drying. Some studies reported that PVP itself can be used as a cryoprotectant in nanoparticle formulations (Abdelwahed et al., 2006a; Abdelwahed et al., 2006b), however, our results showed that without using trehalose, phenobarbital-PVP-chitosan nanoparticles (which contain PVP) could not be redispersed in water (Table 6.5 and Figure 6.10).

Table 6.5 Properties of phenobarbital-PVP-chitosan after redispersion of the freeze dried product without addition of trehalose (mean ± SD, n = 3).

| Types of material | Notes | Z-average (nm, DLS) | PDI |
|---|---|---|---|
| Phenobarbital-PVP-chitosan without trehalose | Formation of thread-like gel which could not be redispersed easily | 720 ± 875 | 0.591 ± 0.326 |

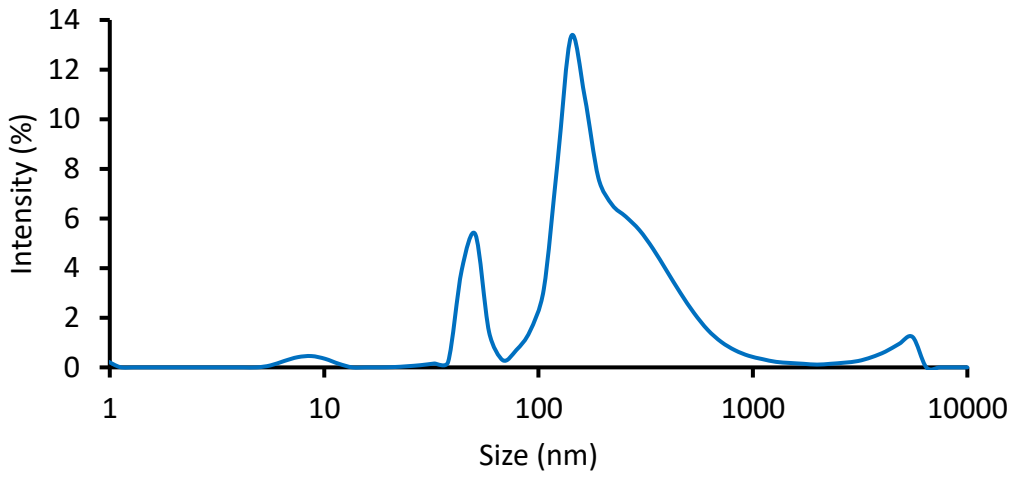


Figure 6.10 DLS size distribution of PVP-chitosan after redispersion of the freeze dried product without addition of trehalose.

The phenobarbital release study was performed at pH 6.4 to mimic the human nasal mucosa pH which shown to be in the range of 5.3–7.0 (England et al., 1999; Ireson et al., 2001; Aderibigbe, 2018). Figure 6.11 shows the calibration curve used in the calculation of phenobarbital release. The nanoparticles provided a sustained release of the drug (Figure 6.12). Focusing on the initial release (Figure 6.13), it is clear that both unmodified chitosan and PVP-chitosan nanoparticles provided a slower initial drug release compared to the free phenobarbital solution (control). The cumulative drug release from the nanoparticles at time

points between 20-60 minutes was significantly lower from the control phenobarbital sodium solution (Figure 6.13). This could be due to the association of phenobarbital to the surface of the nanoparticles or its entrapment within the nanoparticles internal structure.

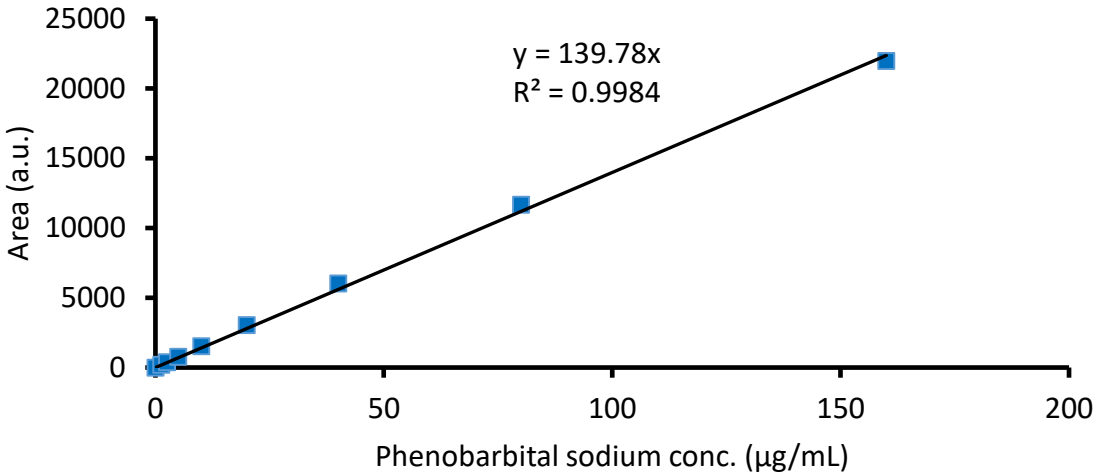


Figure 6.11 An HPLC calibration curve used for the analysis of phenobarbital in 0.05 M PBS (pH 6.4, composed of both $NaH_2PO_4.2H_2O$ and $Na_2HPO_4$) for the release study of the unmodified and PVP-chitosan nanoparticles. The mobile phase composed 0.05 M $NaH_2PO_4.2H_2O$ solution: acetonitrile (65:35, pH 5.2) (mean ± SD, n = 3).

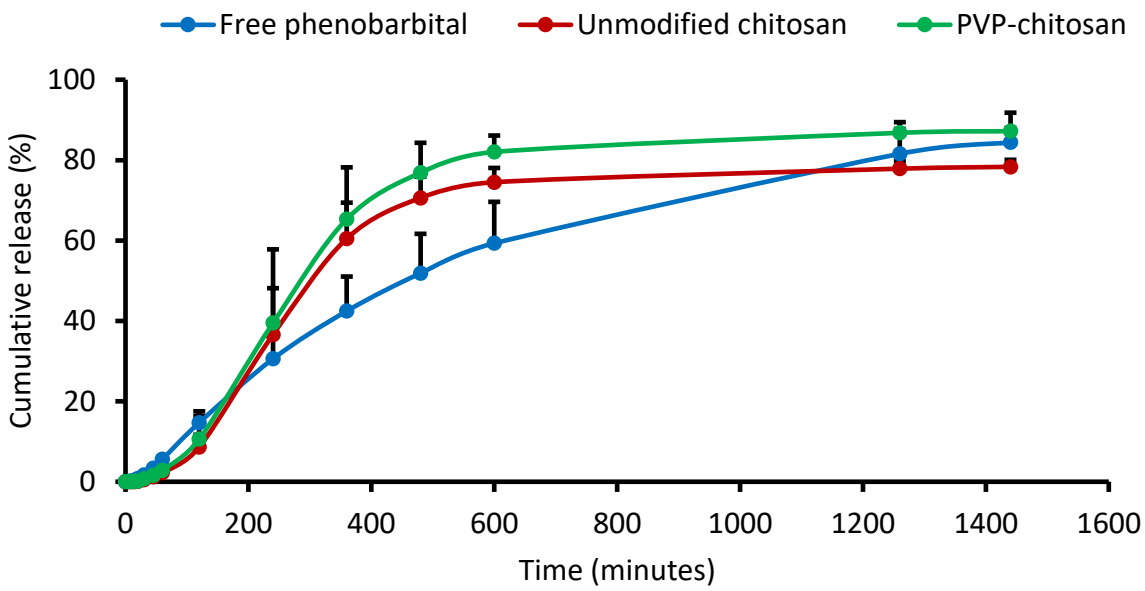


Figure 6.12 Release profiles of phenobarbital from phenobarbital sodium solution, phenobarbital-unmodified chitosan and PVP-chitosan nanoparticles at 32 °C. Data represent mean ± SD, n= 3.

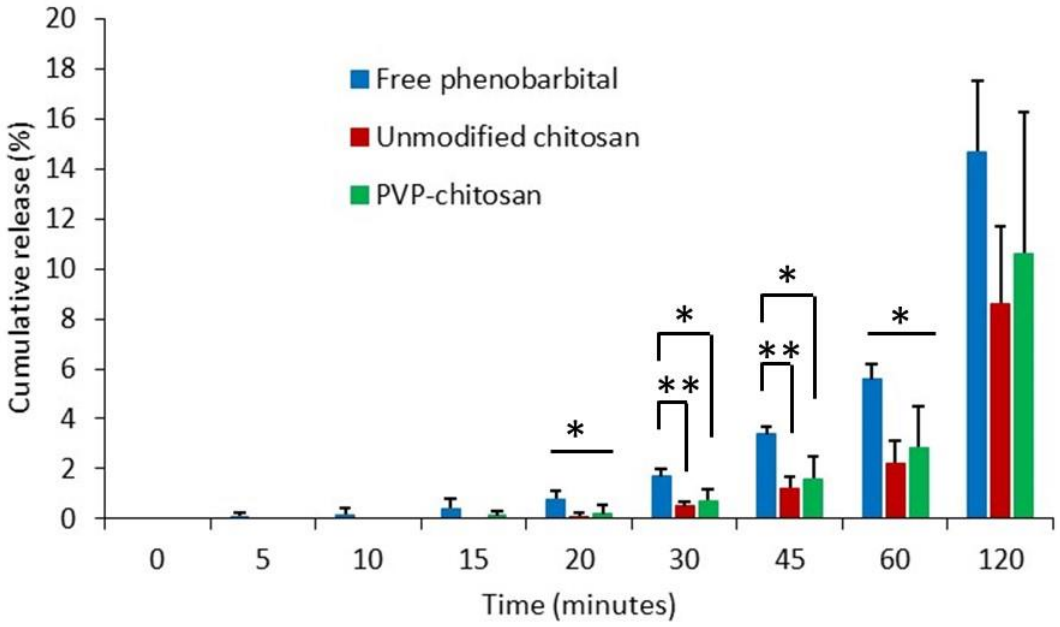


Figure 6.13 Comparison of the release profiles of phenobarbital from phenobarbital sodium solution, phenobarbital-unmodified chitosan and PVP-chitosan nanoparticles at 32 °C over the first 120 minutes. Data represent mean ± SD, n= 3; * denotes $p < 0.05$, ** denotes $p < 0.01$.

Although the initial release from unmodified chitosan and PVP-chitosan nanoparticles was slower than the control, once released, the release was rapid as higher % release can be seen at earlier time (e.g. at 360 minutes) and then reached a plateau at 480 minutes. This could be due to the potential enhancement of the water solubility of phenobarbital by chitosan and PVP-chitosan present in the structure of both unmodified chitosan and PVP-chitosan nanoparticles, respectively. It has been shown that polyamidoamine dendrimers enhanced the water solubility of phenobarbital possibly due to the electrostatic interaction between positively charged polyamidoamine and negatively charged phenobarbital (Cheng et al., 2008). Also, Portero et al. (1998) revealed that chitosan enhanced the dissolution rate of other poorly water soluble drugs (nifedipine) when used in nifedipine-chitosan co-ground and/or solid dispersion. They related this to a decrease in the drug's crystallinity (changed from a crystalline form to a more water soluble amorphous form) and an increase in the drug wettability. Similarly, in the current study, chitosan and PVP-chitosan could enhance the dissolution rate of phenobarbital, which eventually led to a higher % phenobarbital release at earlier time (e.g. at 360 minutes) from unmodified and PVP-chitosan nanoparticles compared to the control. On the other hand, the control provided a relatively constant release throughout the time frame.

## 6.4 Conclusion

In this study, we have demonstrated a method of incorporating a drug, haloperidol, into unmodified chitosan nanoparticles and phenobarbital into unmodified and PVP-chitosan nanoparticles. Both phenobarbital- unmodified and PVP-chitosan nanoparticles showed a relatively high drug loading capacity and a sustained drug release. The *in vivo* performance of these nanoparticles can be explored using behavioural studies in rats following their nasal administration.

## 6.5 Acknowledgements

We are thankful to HCED-Iraq for funding this research. We acknowledge the assistance of staff of University of Reading, especially Chemical Analysis Facility (CAF) laboratory in HPLC experiments.

## 6.6 References

Abdelwahed, W., Degobert, G., & Fessi, H., 2006a. Investigation of nanocapsules stabilization by amorphous excipients during freeze-drying and storage. Eur. J. Pharm. Biopharm. 63, 87-94.

Abdelwahed, W., Degobert, G., Stainmesse, S., & Fessi, H., 2006b. Freeze-drying of nanoparticles: Formulation, process and storage considerations. Adv. Drug Del. Rev. 58, 1688-1713.

Aderibigbe, B.A., 2018. In situ-based gels for nose to brain delivery for the treatment of neurological diseases. Pharmaceutics 10, 40.

Bernkop-Schnürch, A., & Dunnhaupt, S., 2012. Chitosan-based drug delivery systems. Eur. J. Pharm. Biopharm. 81, 463-469.

Calvo, P., Remuñán-López, C., Vila-Jato, J.L., & Alonso, M.J., 1997. Novel hydrophilic chitosan-polyethylene oxide nanoparticles as protein carriers. J. Appl. Polym. Sci. 63, 125-132.

Casettari, L., & Illum, L., 2014. Chitosan in nasal delivery systems for therapeutic drugs. J. Control. Release 190, 189-200.

Cheng, Y., Wu, Q., Li, Y., & Xu, T., 2008. External electrostatic interaction versus internal encapsulation between cationic dendrimers and negatively charged drugs: Which contributes more to solubility enhancement of the drugs? The Journal of Physical Chemistry B 112, 8884-8890.

Czapp, M., Bankstahl, J.P., Zibell, G., & Potschka, H., 2008. Brain penetration and anticonvulsant efficacy of intranasal phenobarbital in rats. Epilepsia 49, 1142-1150.

De Campos, A.M., Sánchez, A., & Alonso, M.a.J., 2001. Chitosan nanoparticles: A new vehicle for the improvement of the delivery of drugs to the ocular surface. Application to cyclosporin A. Int. J. Pharm. 224, 159-168.

El-Setouhy, D.A., Ibrahim, A.B., Amin, M.M., Khowessah, O.M., & Elzanfaly, E.S., 2016. Intranasal haloperidol-loaded miniemulsions for brain targeting: Evaluation of locomotor suppression and in-vivo biodistribution. Eur. J. Pharm. Sci. 92, 244-254.

England, R.J.A., Homer, J.J., Knight, L.C., & Ell, S.R., 1999. Nasal pH measurement: A reliable and repeatable parameter. Clin. Otolaryngol. 24, 67-68.

Fernández-Urrusuno, R., Calvo, P., Remuñán-López, C., Vila-Jato, J.L., & José Alonso, M., 1999. Enhancement of nasal absorption of insulin using chitosan nanoparticles. Pharm. Res. 16, 1576-1581.

Illum, L., 2000. Transport of drugs from the nasal cavity to the central nervous system. Eur. J. Pharm. Sci. 11, 1-18.

Illum, L., 2004. Is nose-to-brain transport of drugs in man a reality? J. Pharm. Pharmacol. 56, 3-17.

Ireson, N.J., Tait, J.S., MacGregor, G.A., & Baker, E.H., 2001. Comparison of nasal pH values in black and white individuals with normal and high blood pressure. Clin. Sci. 100, 327–333.

Jelveghari, M., & Nokhodchi, A., 2008. Development and chemical stability studies of alcohol-free phenobarbital solution for use in pediatrics: A technical note. AAPS PharmSciTech 9, 939-943.

Joint Formulary Committee, 2018. British National Formulary. Available from https://www.medicinescomplete.com

M. Ways, T.M., Lau, W.M., & Khutoryanskiy, V.V., 2018. Chitosan and its derivatives for application in mucoadhesive drug delivery systems. Polymers 10, 267.

Mistry, A., Stolnik, S., & Illum, L., 2009. Nanoparticles for direct nose-to-brain delivery of drugs. Int. J. Pharm. 379, 146-157.

Mistry, A., Stolnik, S., & Illum, L., 2015. Nose-to-brain delivery: Investigation of the transport of nanoparticles with different surface characteristics and sizes in excised porcine olfactory epithelium. Mol. Pharm. 12, 2755-2766.

Piazza, J., Hoare, T., Molinaro, L., Terpstra, K., Bhandari, J., Selvaganapathy, P.R., Gupta, B., & Mishra, R.K., 2014. Haloperidol-loaded intranasally administered lectin functionalized poly(ethylene glycol)-block-poly(D,L)-lactic-co-glycolic acid (PEG-PLGA) nanoparticles for the treatment of schizophrenia. Eur. J. Pharm. Biopharm. 87, 30-39.

Portero, A., Remuñán-López, C., & Vila-Jato, J.L., 1998. Effect of chitosan and chitosan glutamate enhancing the dissolution properties of the poorly water soluble drug nifedipine. Int. J. Pharm. 175, 75-84.

Rohrer, J., Lupo, N., & Bernkop-Schnürch, A., 2018. Advanced formulations for intranasal delivery of biologics. Int. J. Pharm. 553, 8-20.

Shahnaz, G., Vetter, A., Barthelmes, J., Rahmat, D., Laffleur, F., Iqbal, J., Perera, G., Schlocker, W., Dünnhaput, S., Augustijns, P., & Bernkop-Schnürch, A., 2012. Thiolated chitosan nanoparticles for the nasal administration of leuprolide: Bioavailability and pharmacokinetic characterization. Int. J. Pharm. 428, 164-170.

Ugwoke, M.I., Agu, R.U., Verbeke, N., & Kinget, R., 2005. Nasal mucoadhesive drug delivery: background, applications, trends and future perspectives. Adv Drug Deliv Rev 57, 1640-1665.

Wang, X., Chi, N., & Tang, X., 2008. Preparation of estradiol chitosan nanoparticles for improving nasal absorption and brain targeting. Eur. J. Pharm. Biopharm. 70, 735-740.

# Chapter 7: Concluding remarks and recommendation for future studies

## 7.1 Conclusion and future studies

Mucosal drug delivery refers to drug administration via the mucosal membranes such as oral, nasal, pulmonary, ocular and vaginal mucosa. The oral and nasal routes of drugs administration offer several advantages including the ease of administration and the presence of large absorptive surface area. For oral route, the presence of gastric acid, the digestive enzymes as well as the mucus layer potentially may lead to poor drug bioavailability. For the nasal route, in addition to the presence of metabolising enzymes in the human nasal mucosa (Rohrer et al., 2018), the mucociliary clearance can entrap drug molecules, prevent their penetration into the mucus and significantly decrease their absorption via the nasal mucosa. The pore size of mucus gel, its viscosity, pH, ionic strength, binding capacity, and turnover rate are some of the factors which determine the barrier properties of the mucus (Leal et al., 2017; Murgia et al., 2018). These properties vary depending on the type of mucosal tissues. Nanoparticles can overcome the mucosal barriers due to their unique properties including small size, large surface area, providing protection for drugs, the possibilities of functionalisation and targeted drug delivery. Among various nanoparticles, organosilica nanoparticles are interesting candidates as a drug delivery system due to the relatively simple method for their preparation and the possibility of their surface functionalisation with fluorescent dyes (for facile detection and analysis in biological tissues) and various polymers (to make them either mucoadhesive or mucus-penetrating, depending on the type of the polymers). Polymeric nanoparticles (such as chitosan nanoparticles) are also desirable due to their biocompatibility, biodegradability and a relatively high drug loading capacity. Nanoparticles with an ability to adhere to (trapped in) or penetrate into (diffuse rapidly in) the mucus layer are known as mucoadhesive or mucus-penetrating nanoparticles, respectively. In this thesis, both types of nanoparticles were considered. Several key parameters govern whether the nanoparticles are mucoadhesive or mucus-penetrating and these include the particle size, hydrophilicity, chemical structure and charges (Lai et al., 2007; Mansfield et al., 2015; Menzel et al., 2016). However, so far, no simple relationship between these parameters and the resultant nature of the nanoparticles'-mucus interactions exists, and rather sophisticated phenomena are involved (Lai et al., 2007; Nordgård and Draget, 2018).

The aim of this thesis was to prepare and characterise silica and chitosan nanoparticles for oral and nasal mucosal drug delivery, respectively. The studies presented in this thesis, showed that functionalisation of silica and chitosan nanoparticles with certain hydrophilic

polymers resulted in a dramatic change in their physicochemical properties. Studies were then conducted to understand how these changes affect the mucoadhesive and mucus-penetration abilities of the prepared nanoparticles with regards to intestinal and nasal mucosa.

In the first instance, additional physicochemical characterisation was performed in order to fully understand the behaviour of thiolated, PEGylated and POZylated silica nanoparticles at various pH. It was demonstrated that the size of both thiolated and POZylated silica nanoparticles significantly increased at $pH \leq 2$, whereas no size change was observed at pH 2.5–9 for these two types of nanoparticles. On the other hand, the size of PEGylated silica nanoparticles did not change over the pH range of 1.5–9. These indicate that all three types of silica nanoparticles can be used in studies involving mucosal surfaces with pH ranging 2.5–9. However, care should be taken when thiolated and POZylated silica nanoparticles are used in studies involving mucosal surfaces with highly acidic pH ($pH \leq 2$ e.g. adhesion to gastric mucosa). Despite this, it is possible to protect both thiolated and POZylated silica nanoparticles using enteric coated capsules and study their *in vivo* performances (Chapter 3).

The retention of thiolated silica nanoparticles in rat intestinal mucosa was significantly greater compared to both PEGylated and POZylated nanoparticles (Chapter 3). This could be due to the greater thiol content of thiolated silica nanoparticles compared to both the PEGylated and POZylated counterparts. The poor retention of PEGylated and POZylated silica nanoparticles could also be due to the stealth properties of both PEG and POZ. This could minimise the entrapment of PEGylated and POZylated silica nanoparticles in the mucus gel layer of rat intestinal mucosa and therefore they only adhered to the superficial layer of the mucus gel which could be washed off relatively easily with the bio-relevant media.

In the second instance, a novel method to prepare PEG- and POZ-chitosan (using thiol-ene and thiol-yne click chemistry, respectively) from thiolated chitosan was shown in Chapter 4. However, both PEG- and POZ-chitosan showed poor aqueous solubility possibly due to the formation of disulfide bonds which could be originated from the precursor thiolated chitosan. Further attempts to improve the solubility of thiolated chitosan (via minimising the oxidation of thiol groups or reduction in the number of immobilised thiol groups) may significantly improve the solubility of both PEG- and POZ-chitosan. This led us to seek an

alternative approach to synthesise not only PEG- and POZ-chitosan but also two other hydrophilic chitosans namely PHEA- and PVP-chitosan using EDAC/NHS chemistry. These modified chitosans exhibited a complete solubility at a broad range of pH (3-10). This finding will widen the potential applications of chitosan in mucosal drug delivery as those formulations often encounter pH changes after their administration into the human body and yet should not affect its solubility.

Until the current studies were carried out, very little was known about the penetration ability of chitosan nanoparticles in mucus gel. Methods were developed to prepare and characterise unlabelled and fluorescently labelled chitosan nanoparticles with different functionalities, and study their diffusion in mucus model. Nanoparticle tracking analysis was used to study the diffusive properties of the chitosan nanoparticles in bovine submaxillary mucin solution. It was revealed that modified chitosan nanoparticles diffused significantly faster than unmodified chitosan nanoparticles in mucin solution. Fluorescence microscopy was used to study the penetration of the chitosan nanoparticles into sheep nasal mucosa and showed that modified chitosan nanoparticles generally penetrated deeper into the nasal mucosa (Chapter 5).

Finally, the possibilities of loading unmodified and PVP-chitosan nanoparticles with two psychoactive drugs (haloperidol and phenobarbital) was investigated in Chapter 6. It was possible to load haloperidol into unmodified chitosan nanoparticles, however, the loading capacity was 0.2% w/w, which is considered to be relatively low taking into account the dose of this drug necessary for *in vivo* studies in rats. On the other hand, both phenobarbital-unmodified and PVP-chitosan nanoparticles, had relatively high loading capacities (1.271 and 1.229 %w/w, respectively), which is highly promising for *in vivo* studies of these novel nanoparticles.

Throughout this thesis, we showed that using non-ionic hydrophilic polymers, it is possible to reduce the mucoadhesive properties of thiolated silica nanoparticles in rat intestinal mucosa and enhance the diffusive properties of chitosan nanoparticles in mucus gel either in mucin solution or sheep nasal mucosa. Other types of silica nanoparticles are generally synthesised using TEOS as a silica source. However, the resultant TEOS-silica nanoparticles do not contain reactive functional groups and thus an additional step (e.g. covalent attachment of 3-aminopropytriethoxysilane) is often needed before their functionalisation with fluorescent dyes or polymers (Gao et al., 2009). On the other hand, due to the presence

of free thiol groups on the surface of our thiolated silica nanoparticles (synthesised from MPTS, Chapter 3), they can be easily functionalised with fluorescent dyes or polymers using common click chemistry approaches e.g. thiol-ene reactions. One of the disadvantages of our thiolated silica nanoparticles is their nonporous nature (and thus potentially low drug loading capacity), which limits their applications in drug delivery. However, they are considered as an excellent model to study mucoadhesion and mucus-penetration. Alternatively, using surfactants, it is possible to synthesise mesoporous thiolated silica nanoparticles with potentially high drug loading capacity (Mun, 2014). The use of cetyltrimethylammonium bromide as a cationic surfactant during the synthesis has resulted in the formation of large, porous and hollow thiolated silica particles. These particles were also polydisperse and had a relatively low yield (Mun, 2014). Therefore, optimisation studies are needed to maintain the size of the thiolated silica nanoparticles as small as possible while imparting some degree of porosity to the thiolated silica nanoparticles. For example, these could be achieved by using different types and concentrations of surfactants during the synthesis of the nanoparticles.

Chitosan nanoparticles can be relatively easily prepared by cross-linking cationic chitosan with anionic molecules such as TPP using an ionic gelation method (Calvo et al., 1997). Chitosan-TPP nanoparticles are advantageous as no heat and organic solvents are needed for their preparation. Consequently, it is possible to load labile drugs including peptides into chitosan-TPP nanoparticles (Rampino et al., 2013). Due to the highly hydrophilic nature, swelling capacity, potentially porous nature, biocompatibility and biodegradability of chitosan and each of PEG, PHEA, POZ and PVP, the developed chitosan nanoparticles are interesting candidates for mucosal drug delivery. The behavioural study of phenobarbital-loaded unmodified and PVP-chitosan nanoparticles in rats would be an interesting approach to investigate their performances *in vivo*. It is also possible to orally load these nanoparticles with various small and large molecular weight drugs (especially peptide-based drugs such as insulin) and study their pharmacokinetics parameters as an indirect method of their performances. Alternatively, Alexa-labelled chitosan nanoparticles can be administered nasally or orally *in vivo* and fluorescence microscopy imaging can be used to study the kinetics of the nanoparticles.

## 7.2 Future perspective

The challenges associated with the transmucosal routes of drug administration include the presence of the harsh environments in the mucosal lumen, the mucus layer and the epithelial barriers. The use of mucoadhesive materials has already been proved as an effective strategy to improve the mucosal drug delivery. This can be due to the abilities of the mucoadhesive polymers to protect the labile drugs against degradation in the mucosal lumen and the enhancement of the retention of drugs on the mucosal surfaces. Recently, the use of mucus-penetrating nanoparticles has become an alternative approach to minimise the barriers associated with transmucosal drug delivery. In this case, mucus-inert materials are used to modify the surface chemistry of the nanoparticles and thus they decrease the nanoparticles-mucus interactions. So far, only few polymers (namely PEG and POZ) have shown their abilities to enhance the penetration of nanoparticles into the mucus (Khutoryanskiy, 2018). In addition to PEG and POZ, in this thesis, we also showed that PHEA and PVP could enhance the penetration of chitosan nanoparticles into the mucus. There are conflicting data on the abilities of other materials to enhance the nanoparticles' penetration into the mucus gel. This could be related to the differences in the evaluation methods of mucoadhesion and mucus-penetration of these systems. This means that there is an urgent need to develop a standard method for evaluation of mucoadhesion and mucus-penetration. Due to the differences in the properties of mucus in various mucosal surfaces, it is conceivable that a method developed to evaluate the mucoadhesion and mucus-penetration in a particular type of mucosa may not be used in another type of mucosa. Care should be taken to mimic several factors including pH, ionic strength, mucus turnover rate, and the mucin concentration. The more resemblance of a method to the *in vivo* situation, the better *in vitro*/*in vivo* correlation can be achieved. Considering the reduction in the number of animals in mucoadhesive evaluation, several attempts have been made to mimic the mucosal surfaces using polymeric materials (Khutoryanskiy, 2011). However, as mucus is a complex biological gel, further studies is needed to mimic its biochemical properties. The next step will be the development of novel materials with either mucoadhesive or mucus-penetrating properties, which can be used in the formulation of nanoparticles for mucosal drug delivery. Theoretically, cationic high molecular weight polymers and those with abilities to form covalent and hydrogen bonds with mucus can be mucoadhesive. However, non-ionic or zwitterionic low molecular weight hydrophilic polymers can be mucus-penetrating (Khutoryanskiy, 2018). The toxicity of any newly developed materials should be investigated prior to pre-clinical studies.

Mucoadhesive and/or mucus-penetrating nanoparticles are highly promising drug delivery systems and can significantly improve the therapeutic drug efficacy.

## 7.3 References

Calvo, P., Remuñán-López, C., Vila-Jato, J.L., Alonso, M.J., 1997. Novel hydrophilic chitosan-polyethylene oxide nanoparticles as protein carriers. J. Appl. Polym. Sci. 63, 125-132.

Gao, X., He, J., Deng, L., Cao, H., 2009. Synthesis and characterization of functionalized rhodamine B-doped silica nanoparticles. Opt. Mater. 31, 1715-1719.

Khutoryanskiy, V.V., 2011. Advances in mucoadhesion and mucoadhesive polymers. Macromol. Biosci. 11, 748-764.

Khutoryanskiy, V.V., 2018. Beyond PEGylation: Alternative surface-modification of nanoparticles with mucus-inert biomaterials. Adv. Drug Del. Rev. 124, 140-149.

Lai, S.K., O'Hanlon, D.E., Harrold, S., Man, S.T., Wang, Y.-Y., Cone, R., Hanes, J., 2007. Rapid transport of large polymeric nanoparticles in fresh undiluted human mucus. Proc. Natl. Acad. Sci. U. S. A. 104, 1482-1487.

Leal, J., Smyth, H.D.C., Ghosh, D., 2017. Physicochemical properties of mucus and their impact on transmucosal drug delivery. Int. J. Pharm. 532, 555-572.

Mansfield, E.D., Sillence, K., Hole, P., Williams, A.C., Khutoryanskiy, V.V., 2015. POZylation: A new approach to enhance nanoparticle diffusion through mucosal barriers. Nanoscale 7, 13671-13679.

Menzel, C., Bonengel, S., de Sousa, I.P., Laffleur, F., Prüfert, F., Bernkop-Schnürch, A., 2016. Preactivated thiolated nanoparticles: A novel mucoadhesive dosage form. Int. J. Pharm. 497, 123-128.

Mun, E.A., 2014. Functionalised organosilica nanoparticles: Synthesis, mucoadhesion and diffusion, Pharmacy. University of Reading.

Murgia, X., Loretz, B., Hartwig, O., Hittinger, M., Lehr, C.-M., 2018. The role of mucus on drug transport and its potential to affect therapeutic outcomes. Adv. Drug Del. Rev. 124, 82-97.

Nordgård, C.T., Draget, K.I., 2018. Co association of mucus modulating agents and nanoparticles for mucosal drug delivery. Adv. Drug Del. Rev. 124, 175-183.

Rampino, A., Borgogna, M., Blasi, P., Bellich, B., Cesaro, A., 2013. Chitosan nanoparticles: Preparation, size evolution and stability. Int. J. Pharm. 455, 219-228.

Rohrer, J., Lupo, N., Bernkop-Schnürch, A., 2018. Advanced formulations for intranasal delivery of biologics. Int. J. Pharm. 553, 8-20.